

The role of FoxO1 in neurodegenerative diseases

Inaugural-Dissertation
zur
Erlangung des Doktorgrades
der Mathematisch-Naturwissenschaftlichen Fakultät
der Universität zu Köln

vorgelegt von
Lorna Moll

aus Frechen
Köln 2012

Berichtersteller:

Prof. Dr. Jens C. Brüning

Prof. Dr. Wilhelm Krone

Tag der letzten mündlichen Prüfung: 31.01.2012

1.	Introduction	1
1.1.	The Insulin and Insulin-like growth factor-1 signaling pathway	2
1.1.1.	Insulin- and Insulin-like growth factor-1 receptors	2
1.1.2.	Insulin receptor substrates	4
1.1.3.	Phosphatidylinositide(PI)3 kinase signaling	6
1.1.4.	Forkhead box O transcription factors	8
1.1.4.1.	Regulation of FoxO mediated transcription	10
1.1.5.	Function of FoxOs	11
1.1.5.	MAPK signaling	12
1.2.	Alzheimer's disease	12
1.2.1.	Pathology of Alzheimer's disease	13
1.2.2.	Hyperphosphorylation of tau	13
1.2.3.	Generation of amyloid- β	14
1.2.4.	Degradation and clearance of amyloid- β	16
1.2.5.	Genetic risk factors of Alzheimer's disease	16
1.2.6.	IR/IGF-1R signaling in Alzheimer's disease	17
1.2.7.	FoxO action in Alzheimer's disease	18
1.3.	Mouse models	19
1.3.1.	Constitutive active and dominant negative forms of FoxO1	20
1.3.2.	Synapsin 1 promoter driven expression of the Cre recombinase	21
1.3.3.	Tg2576, a model for Alzheimer's disease	22
1.4.	Aims of the present thesis	22
2.	Material and Methodes	23
2.1.	Chemicals	24
2.2.	Enzymes	25
2.3.	Vectors, Primer and supplies	26
2.4.	Buffer and solution	26
2.5.	Cells and bacteria	28
2.6.	Kits	28
2.7.	Primary Antibodies	28
2.8.	Secondary Antibodies	31
2.9.	Material	31
2.10.	Methods	33
2.10.1.	Mice breeding	33
2.10.2.	Isolation of genomic DNA	33
2.10.3.	Polymerase chain reaction (PCR) for genotyping	33

2.10.4.	Metabolic characterization	35
2.10.5.	Investigation of body composition	35
2.10.6.	Brain lysates	36
2.10.7.	SDS-PAGE	36
2.10.8.	Western Blot	37
2.10.9.	Urea Tricine gel	38
2.10.10.	Dot Blot	39
2.10.11.	ELISA β -Amyloid _{40/42}	39
2.10.12.	Statistical analysis	39
2.10.13.	Histology	40
2.10.14.	RNA Isolation	40
2.10.15.	cDNA synthesis	41
2.10.16.	realTime PCR	41
2.10.17.	Behavioral studies and calorimetry	42
2.10.18.	False-coloure imaging	43
2.10.19.	Cloning strategy	43
2.10.20.	Generation of stably expressing cells	45
2.10.21.	Cell lysates	46
2.10.22.	Stimulation of cells with Insulin or IGF-1	46
2.10.23.	Proliferation assay	47
2.10.24.	Apoptosis in cells	47
3.	Results	48
3.1.	Verification of FoxO1DN expression in mice	51
3.2.	Characterisation of FoxO1DN mice	52
3.2.1.	Glucose homeostasis of FoxO1DN mice	52
3.2.2.	Analysis of IR/IGF-1R signaling in 28 weeks old FoxO1DN mice	54
3.2.3.	Growth of FoxO1DN mice	55
3.2.4.	Indirect calorimetric analysis of FoxO1DN mice	59
3.2.5.	Behaviour of FoxO1DN mice	62
3.3.	Role of FoxO1 in Alzheimer´s disease	63
3.3.1.	Glucose homeostasis of Tg2576/FoxO1DN mice	63
3.3.2.	Body weight of Tg2576/FoxO1DN mice	66
3.3.3.	Kaplan-Meier analysis of FoxO1DN mice in Tg2576 background	67
3.3.4.	IR/IGF-1R signaling in Tg2576/FoxO1DN mice	68
3.3.5.	APP Processing in Tg2576/FoxO1DN mice	70
3.4.	Verification of FoxO1ADA expressing mice	72

3.5.	Characterisation of FoxO1ADA mice	73
3.5.1.	Glucose homeostasis of FoxO1ADA mice	73
3.5.2.	Analysis of IR/IGF-1R signaling in 28 weeks old FoxO1ADA mice	75
3.5.3.	Growth of FoxO1ADA mice	76
3.5.4.	Indirect calorimetric analysis of FoxO1ADA mice	81
3.5.	Behaviour of FoxO1ADA mice	84
3.6.	Role of FoxO1 in Alzheimer's disease	86
3.6.1.	Glucose homestasis of Tg2576/FoxO1ADA mice	86
3.7.	Growth of Tg2576/FoxO1ADA mice	88
3.8.	Survival of FoxO1ADA mice	90
3.9.	IR/IGF-1R signaling pathway in Tg2576/FoxO1ADA	90
3.10.	APP Processing in Tg2576/FoxO1ADA mice	92
3.11.	<i>In vitro</i> analysis of stably expressing FoxO1DN, FoxO1ADA and FoxO1 neuroblastoma cells	93
3.11.1.	Characterisation of stably expressing FoxO1DN, FoxO1ADA and FoxO1 neuroblastoma cells	94
3.11.2.	Proliferation of FoxO1DN, FoxO1ADA and FoxO1 expressing neuroblastoma cells	96
3.11.3.	FoxO1 and oxidative stress	98
4.	Discussion	101
4.1.	Neuron-specific expression of FoxO1DN and FoxO1ADA	102
4.1.2.	Metabolic characterization	103
4.1.3.	Insulin/IGF-1R signaling in 28 weeks old animals	104
4.1.4.	Growth of FoxO1DN and FoxO1ADA mice	104
4.1.5.	Indirect calorimetric and locomotion analysis	105
4.1.6.	Behaviour of FoxO1DN and FoxO1ADA mice	106
4.2.	Alzheimer's disease	107
4.2.1.	Metabolic characterization of Tg2576/FoxO1DN and Tg2576/FoxO1ADA mice	107
4.2.2.	Body weight of Tg2576/FoxO1DN and Tg2576/FoxO1ADA mice	107
4.2.3.	Kaplan-Meier analysis of Tg2576/FoxO1DN and Tg2576/FoxO1ADA Mice	108
4.2.4.	IR/IGF-1R signaling in 60 weeks old Tg2576/FoxO1DN and Tg2576/FoxO1ADA mice	110
4.2.5.	APP processing in Tg2576/FoxODN and Tg2576/FoxO1ADA	111
4.3.	<i>In vitro</i> studies of FoxO1 in human neuroblastoma cells	112

4.3.1.	Characterization of FoxO1DN, FoxO1ADA and FoxO1 stably expressing neuroblastoma cells	113
4.3.2.	FoxO1 and proliferation	113
4.3.3.	FoxO1 and oxidative stress	114
5.	Summary	116
6.	Zusammenfassung	118
7.	References	119
8.	Supplementary	134
8.1.	Acknowledgement	135
8.2.	Erklärung	136
8.3.	Curriculum vitae	137

Figure Index

Figure 1:	Receptor isoforms and hybrids.	4
Figure 2:	Insulin and insulin-like growth factor-1 signaling pathway.	6
Figure 3:	Structure of forkhead box O transcription factor DNA binding domain.	9
Figure 4:	Phosphorylation sites of the FoxO transcription factors.	11
Figure 5:	Processing of the amyloid precursor protein (APP).	15
Figure 6:	A β detoxification mechanism via HSF-1 and DAF-16.	19
Figure 7:	Cre/loxP strategy for the FoxO1ADA and FoxO1DN expression in neurons.	21
Figure 8:	Structure of FoxO1, FoxO1ADA and FoxO1DN.	50
Figure 9:	Breeding strategy of neuron-specific expressing FoxO1ADA and FoxO1DN mice in Tg2576 background.	50
Figure 10:	Detection of FoxO1DN.	51
Figure 11:	Immunohistological staining of eGFP.	51
Figure 12:	Blood glucose of FoxO1DN female and male mice until 60 weeks of age.	52
Figure 13:	Glucose tolerance tests of FoxO1DN and wild-type mice.	53
Figure 14:	Insulin tolerance test of FoxO1DN mice.	54
Figure 15:	IR/IGF1R protein expression of 28 weeks old FoxO1DN mice.	54
Figure 16:	IR/IGF1R signaling pathway of 28 weeks old FoxO1DN mice.	55
Figure 17:	Body weight of FoxO1DN mice over 60 weeks.	56
Figure 18:	Body composition of FoxO1DN male mice.	57
Figure 19:	Analysis of bone density.	58
Figure 20:	Body length of 60 weeks FoxO1DN male mice.	58
Figure 21:	Food and water intake of 60 weeks old FoxO1DN male mice.	59
Figure 22:	RotaRod for FoxO1DN male mice.	59
Figure 23:	Locomotion activity of 60 weeks old FoxO1DN male mice.	60
Figure 24:	Energy expenditure normalized to lean body mass of 60 weeks old FoxO1DN mice.	61
Figure 25:	Respiratory quotient of 60 weeks old FoxO1DN mice.	61
Figure 26:	Nissl staining of the hippocampus of 28 weeks old FoxO1DN mice.	62
Figure 27:	Open field and O-Maze test of FoxO1DN.	62
Figure 28:	Water Maze test of FoxO1DN mice.	63
Figure 29:	Blood glucose of FoxO1DN mice in Tg2576 background.	64
Figure 30:	Glucose tolerance tests of Tg2576/FoxO1DNmice.	65
Figure 31:	Insulin tolerance test of Tg2576/FoxO1DN mice.	65
Figure 32:	Body weight of Tg2576/FoxO1DN mice until 60 weeks of age.	66

Figure 33:	Brain body ratio of Tg2576/FoxO1DN mice at 60 weeks of age.	67
Figure 34:	Kaplan-Meier curves of FoxO1DN mice in Tg2576 background until 60 weeks of age.	68
Figure 35:	IR and IGF-1R protein expression of 60 weeks old Tg2576/FoxO1DN mice.	68
Figure 36:	IR/IGF1R signaling pathway of 60 weeks old Tg2576/FoxO1DN mice.	69
Figure 37:	Expression of FoxO1 and FoxO3a in Tg2576/FoxO1DN mice.	70
Figure 38:	APP Processing of FoxO1DN mice in Tg2576 background.	70
Figure 39:	Quantification of A β 40 and A β 42 in hippocampi of Tg2576 and Tg2576/FoxO1DN female mice.	71
Figure 40:	Dot Blot for analysis of A β oligomers of Tg2576/FoxO1DN hippocampus.	71
Figure 41:	Expression of α -, β - and γ -secretases 60 weeks old Tg2576/FoxO1DN mice.	72
Figure 42:	Proteins involved in A β clearance in 60 weeks old Tg2576/FoxO1DN mice.	72
Figure 43:	Detection of FoxO1ADA.	73
Figure 44:	Blood glucose of FoxO1ADA female and male until 60 weeks of age.	74
Figure 45:	Glucose tolerance tests of FoxO1ADA and wild-type mice.	74
Figure 46:	Insulin tolerance tests of FoxO1ADA and wild-type mice.	75
Figure 47:	Expression level of IR and IGF-1R from 28 weeks old FoxO1ADA mice.	75
Figure 48:	IR/IGF1R signaling pathway of 28 weeks old FoxO1ADA mice.	76
Figure 49:	Body weight of FoxO1ADA mice over 60 weeks.	77
Figure 50:	Body composition of FoxO1ADA male mice.	78
Figure 51:	Analysis of bone density.	79
Figure 52:	Body length of 60 weeks old FoxO1ADA male mice.	79
Figure 53:	Food and water intake of 60 weeks old FoxO1ADA male mice.	80
Figure 54:	realTime PCR analysis of growth axis in 4 weeks old FoxO1ADA male mice.	81
Figure 55:	RotaRod test of FoxO1ADA male mice.	82
Figure 56:	Locomotion activity of 60 weeks old FoxO1ADA male mice.	82
Figure 57:	Energy expenditure of 60 weeks old FoxO1ADA mice.	83
Figure 58:	Respiratory quotient of 60 weeks old FoxO1DN mice.	83
Figure 59:	Nissl staining of the hippocampus of 28 weeks old FoxO1ADA mice.	84
Figure 60:	Open field and O-Maze test of FoxO1ADA.	85
Figure 61:	Water Maze test of FoxO1ADA mice.	86
Figure 62:	Blood glucose levels of FoxO1ADA mice in Tg2576 background.	87

Figure 63:	Glucose tolerance tests of Tg2576/FoxO1ADA and wild-type mice.	87
Figure 64:	Insulin tolerance tests of Tg2576/FoxO1ADA and wild-type mice.	88
Figure 65:	Body weight of Tg2576/FoxO1ADA until 60 weeks of age.	89
Figure 66:	Body brain ratio of Tg2576/FoxO1ADA mice at 60 weeks of age.	89
Figure 67:	Survival of FoxO1ADA mice in Tg2576 background until 60 weeks of age.	90
Figure 68:	IR and IGF-1R protein expression of 60 weeks old Tg2576/FoxO1ADA mice.	91
Figure 69:	IR/IGF1R signaling pathway of 60 weeks old Tg2576/FoxO1ADA mice.	91
Figure 70:	Expression of FoxO1 and p27 in 60 weeks old animals.	92
Figure 71:	APP Processing of FoxO1ADA mice in Tg2576 background.	92
Figure 72:	Level of A β 40 and A β 42 in hippocampi of Tg2576 and FoxO1ADA/Tg2576 female mice.	93
Figure 73:	Dot Blot for analysis of A β oligomers of FoxO1ADA/Tg2576 hippocampus.	93
Figure 74:	Verification of stably overexpressing FoxO1DN, FoxO1ADA and wild-type FoxO1 (FoxO1 \uparrow).	94
Figure 75:	IR/IGF1R signaling pathway in stably expressing FoxO1DN, FoxO1ADA and FoxO1 SHSY5Y cells.	95
Figure 76:	Nuclear and cytosolic localisation of FoxO1 in overexpressing neuroblastoma cells.	95
Figure 77:	Analysis of IR/IGF1R signaling pathway in stably expressing FoxO1DN, FoxO1ADA and FoxO1 neuroblastoma cells.	96
Figure 78:	Proliferation of stably expressing FoxO1DN and FoxO1ADA.	97
Figure 79:	Proliferation of stably expressing and FoxO1 neuroblastoma cells.	97
Figure 80:	Expression level of MnSOD in stably expressing FoxO1DN and FoxO1ADA neuroblastoma cells.	98
Figure 81:	Oxidative stress in stably expressing FoxO1DN and FoxO1ADA neuroblastoma cells.	98
Figure 82:	TUNEL assay of stably expressing FoxO1DN and FoxO1ADA neuroblastoma cells.	99
Figure 83:	Analysis of TUNEL assay with stably expressing FoxO1DN and FoxO1ADA neuroblastoma cells.	100

Table Index

Table 1:	Primer sequences of SynCre, Tg2576 and FoxO1 in ROSa26 locus.	34
Table 2:	PCR Programms for SynCre, Tg2576 (APP) and FoxO1 in the ROSA26 locus.	34
Table 3:	Primer used for the PCR to distinguish FoxO1ADA and –DN.	35
Table 4:	PCR Program to distinguish FoxO1ADA and –DN.	35
Table 5:	SDS-PAGE Gels (2 mini gels).	37
Tabel 6:	Tricine Gel (2 mini gels). Addition of 7.2 g Urea to resolving gel was used for proteïn expression analysis with small molecular size of 4kDa.	39
Table 7:	Primer for cloning of FoxO1WT, FoxO1ADA and FoxO1DN.	43
Table 8:	PCR program to amplify FoxO1ADA, -DN and FoxO1 wild type (FoxO1WT).	44

List of Abbreviations

A β	β -Amyloid
AD	Alzheimer's disease
ADAM	A Disintegrin and Metalloprotease domain
AFX	acute leukaemia fusion gene located in chromosome X
AKT	PKB synonym
α 2M	alpha 2 macroglobulin
apoE	Apolipoprotein E
APP	Amyloid Precursor Protein
APPsw	Swedish mutation of APP
APS	Ammonium-persulfate
ATP	Adenosintriphosphate
BACE-1	Beta-site APP Cleaving Enzyme-1
BAD	Bcl-2/Bcl-X-associated death promoter
BBB	Blood brain barrier
BME	Basal medium eagle
BSA	Bovine serum albumin
C83	83-amino-acid C-terminal APP fragment
C99	99-amino-acid C-terminal APP fragment
CDK	Cyclin-depoment kinase
CNS	Central Nervous System
CRAK	c-raf leukemia viral oncogene
CSF	Cerebrospinal fluid
DAF-2	abnormal dauer formation protein 2
DAF-16	abnormal dauer formation protein 16
DAF-18	abnormal dauer formation protein 18
ddH ₂ O	Double-disalled water
DMSO	Dimethyl sulfoxide
DYRK	Dual-specificity tyrosine-phosphorylated and regulated kinase
4E-BP	4E binding protein
eEF2	eukaryotic elongation factor 2
eIF4E	eukaryotic initiation factor 4E
ELISA	Enzyme Linked Immunosorbent Assays
ER	Endoplasmic reaculum
ERK	Extracellular signal-regulated kinase
FAD	familial Alzheimer's disease
FasL	Fas ligand

FCS	Fetal calf serum
Fos	FBJ osteosarcoma oncogene
FKHR	Forkhead in rhabdomyosarcomas
FKHRL1	Forkhead in rhabdomyosarcomas-like protein 1
FoxO	Forkhead box-O transcription factor
FoxO1ADA	constitutive active FoxO1
FoxO1DN	dominant negative FoxO1
FRE	FoxO-recognized element
GDP	Guanosine-diphosphate
GH	Growth hormone
GHR	Growth hormone receptor
GHRH	Growth hormone releasing hormone
GHRHR	Growth hormone releasing hormone receptor
GRB2	Growth factor receptor binding protein 2
GSK-3 α/β	Glycogen synthase kinase 3 α/β
GTP	Guanosine-triphosphate
IDE	Insulin degrading enzyme
IGF	Insulin-like growth factor
IGFBP1	Insulin-like growth factor binding protein 1
IGF-1R	Insulin-like growth factor receptor type I
IIS	IR/IGF-1R signaling
IKK β	κ B kinase β
IR	Insulin Receptor
IRa	Insulin receptor isoform a
IRb	Insulin receptor isoform b
IRS-1	Insulin receptor substrate 1
IRS-2	Insulin receptor substrate 2
IRSs	Insulin receptor substrates
JNK	C-June-N-terminal kinase
kDA	kilo Dalton
LOAD	Late onset of Alzheimer's disease
mA	milli Ampere
MAP-kinase	Mitogen-activated protein kinase
MAPKAP-K1	MAPK-activated protein 1
MDM2	Murine double minute
MEK	Mitogen-activated protein kinase kinase
MnSOD	Manganese dependent superoxide dismutase

mTOR	target of rapamycin
NFTs	Neurofibrillary tangles
nIGF-1R ^{-/-}	neuronal specific IGF-1R knockout
nIR ^{-/-}	neuronal specific IR knockout
NIRKO	brain-specific knockout of IR
P/S	Penicillin-Streptomycin; Pen Strep
p3	Short peptide containing the C-terminal region of A β
p90RSK	RSK ribosomal protein S6 kinase
PAGE	Polyacrylamide gel electrophoresis
PBS	Phosphate buffered saline
PCAF	p300-associated factor
PDK1	Phosphoinositide-dependent protein kinase 1
PDVF	Polyvinylidene difluoride
PEPCK	Phosphoenolpyruvate carboxykinase
PH	Pleckstrin homology
PI3K	Phosphatidylinositol-tri-phosphat kinase
PI _{3,4} P	Phosphatidylinositol-di-phosphat
PI _{3,4,5} P	Phosphatidylinositol-tri-phosphat
PKB	Protein kinase B
PP2A	Protein phosphatase 2A
PRMT1	Protein arginine N-terminal methyltransferase
PTB	Phosphotyrosin-binding
PTEN	Phosphatase and tensin homolog
RHEB	Ras homolog enriched in the brain
ROS	Reactive oxygen species
rpm	Rotations per minute
sAPP α	soluble APP α
sAPP β	soluble APP β
SCF ^{Skp2}	substrate-binding component of the Skp1/culin 1/F-box protein
SCPx	sterol carrier protein x
SCP2	sterol carrier protein 2
SDS	Sodium dodecyl sulfate
SDS-PAGE	Sodium dodecyl sulfate-polyacrylamide gel electrophoresis
SGK	Glucocorticoid-inducible kinases
SH2	Src-homology 2
SHP2	SH2-Phosphatase 2
SIRT1	Silent information regulator-1

SOS	Son of sevenless
SynCre	Synapsin 1 promoter driven Cre recombinase
TACE	Tumor necrosis factor-alpha converting enzyme
TBS	Tris buffered saline
TBS-T	Tris buffered saline 2% TWEEN 20®
TEMED	N,N,N',N'-tetramethylethylenediamine
Tg2576	Transgenic mouse model for Alzheimer's disease
TSC-2	Tuberine 2
TWEEN 20®	Polyoxyethylene (20) sorbitan monolaurate (Polysorbate 20)

1. Introduction

The mammalian forkhead box O transcription factor (FoxO) family contains 4 members, FoxO1, FoxO3a, FoxO4 and FoxO6. (Clark et al., 1993). FoxOs present a conserved DNA binding domain, the forkhead domain (FKHR) (Clark et al., 1993; Furayama et al., 2000) FoxOs play a role in metabolism, cell cycle control and stress resistance. FoxO mediated transcription is amongst others regulated via phosphorylation. Phosphorylation which negatively regulates FoxO action, leads to association of FoxO with 14-3-3 and transport out of the nucleus.

Phosphorylation of FoxOs is induced by the C-Jun-N-terminal kinase (JNK) pathway upon oxidative stress to regulate transcription of target genes (Esser et al., 2004). This pathway antagonizes the Insulin and Insulin-like growth factor 1 (IGF-1) signaling pathways which negatively regulates FoxOs. *In vitro* activation of JNK leads to phosphorylation of 14-3-3 ξ . This mediates dissociation of FoxO3a from 14-3-3 and in turn results in nuclear retention of FoxO3a and therefore it is active and promotes transcription of its target genes (Sunayama et al., 2005).

Furthermore phosphorylation of FoxOs occurs via the glucocorticoid-inducible kinases (SGKs) and AKT which are serine threonine kinase (Lin et al., 1997; Ogg et al., 1997; Brunet et al., 2001). Both kinases are regulated via the Phosphatidylinositide(PI)3 kinase (PI3K) pathway. These kinases are activated, translocate into the nucleus and phosphorylate FoxO which leads to inactivation of FoxO mediated transcription (Brunet et al., 2001).

Thus, FoxO are regulated via different pathways and FoxO mediated transcription is involved in several cellular functions. One of the main pathways involved in the pathogenesis of neurodegenerative diseases, is the insulin/insulin-like growth factor-1 (IGF-1) signal transduction. The present thesis focuses on the role of FoxO1, a downstream target of the insulin/IGF-1 signaling cascade in neurodegeneration.

1. 1. The Insulin and Insulin-like growth factor-1 signaling pathway

The Insulin and Insulin-like growth factor 1 (IGF-1) signaling pathways has several functions including growth, metabolic homeostasis, development and stress resistance. In addition, the Insulin and IGF-1 signaling pathway is involved in determination of lifespan (review in Broughton and Patridge, 2009).

1.1.1. Insulin- and Insulin-like growth factor-1 receptors

The Insulin- and Insulin-like growth factor-1 receptors (IR and IGF-1R) belong to the family of receptor tyrosine kinases. These receptors consist of a domain with tyrosine kinase activity bound to the membrane which phosphorylates tyrosine-residues of downstream signaling

proteins of the IR and IGF-1R signaling pathway. The IR was discovered in 1974 and its tyrosine kinase activity was found in 1982 (Megyesi et al., 1974; Kasuga et al., 1982; Kasuga et al., 1982). Later the IGF-1 receptor was discovered and classified as a receptor tyrosine kinase receptor as well (Megyesi et al., 1974; Jacobs et al., 1983; Rubinet al., 1983). Both IR and IGF-1R show a heterotetrameric structure. The α -subunits with a size of 135kDa are localized extracellular (Van Obberghen et al., 1981; Ullrich et al., 1986). The β -subunits which are about 95kDa are composed of a short extracellular, a transmembrane and an intracellular domain. The intracellular part contains ATP-binding motifs, autophosphorylation sites and tyrosine-specific protein kinase activity. Autophosphorylation sites of the IR are tyrosine 1146, 1150 and 1151 as well as 1131, 1135 and 1136 of the IGF-1R. The subunits of the receptor are linked via disulfide bonds. (Kahn et al., 1978; Kasuga et al., 1982; Chou et al., 1987; White, 1998).

The gene which encodes the insulin receptor contains 22 exons and 21 introns (Seino et al., 1989). Two different isoforms of the insulin receptor occur due to alternative splicing of exon 11 that codes for 12 amino acids. Isoform A of the IR lacks these 12 while isoform B contains these amino acids. The IGF-1R gene possesses no equivalent to exon 11, hence no isoforms exists. Both isoforms A and B of the IR bind to insulin with similar affinity (McClain, 1991). Isoform A shows an increased affinity to IGF-2 compared to isoform B (Yamaguchi et al., 1991; Frasca et al., 1999). The expression of the A-isoform of the IR mainly occurs in fetal tissue, hematopoietic cells and adult nervous system. Isoform B is predominantly expressed in adipose tissue, muscle and liver (Seino and Bell, 1989; Moller et al., 1989; Goldstein and Kahn, 1989; Mosthaf et al., 1990). In addition, different binding affinities to insulin or IGF-1 is dependent on the assembly of IR or IGF-1R (Pandini et al. 2002). IGF-1, IGF-2 and insulin are bound to the hybrid of IGF-1R and isoform A of the IR with similar affinity. However, IGF-1 is bound to the hybrid of IGF-1R and isoform B of the IR (Louvi et al., 1997) (Fig. 1).

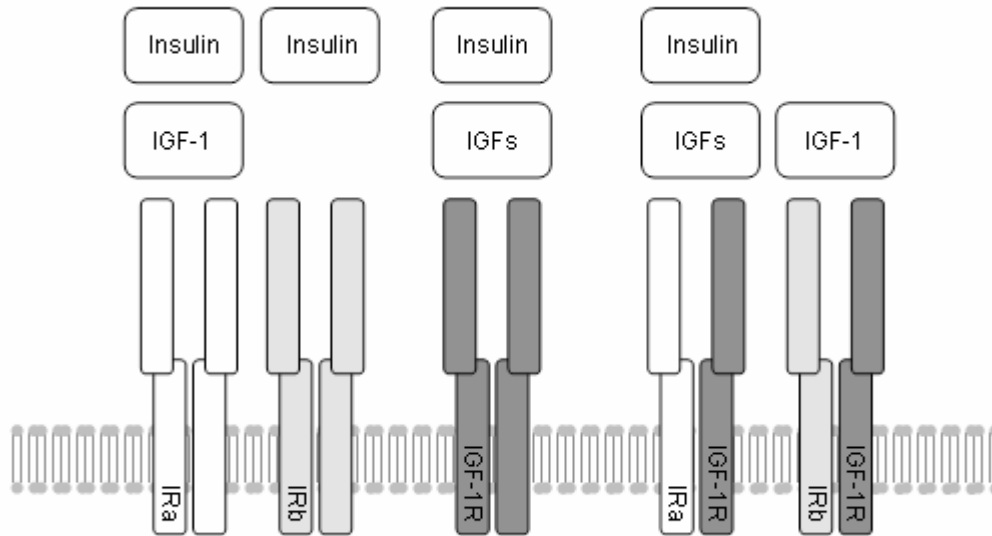


Figure 1: Receptor isoforms and hybrids.

Isoforms A and B of the IR bind to insulin with similar affinity. Isoform A shows an increased affinity to IGF-2 compared to isoform B. The IGF-1R and the receptor hybrid of IGF-1R and isoform A of the IR bind to insulin and both IGFs. The IGF-1R and isoform B of the IR receptor hybrid predominantly binds to IGF-1(modified, Freude and Schubert, 2010).

1.1.2. Insulin receptor substrates

Binding of insulin or IGF-1 to the IR or IGF-1R induces a conformational change of the receptor. This causes autophosphorylation of the β -subunits. The autophosphorylated receptors tyrosine kinase then recruit insulin receptor substrates (IRS) which become tyrosine phosphorylated (Fig. 2). The family of IRS proteins includes IRS-1 to IRS-4 (Sun et al. 1991; Lavan et al. 1997; Lavan, Lane, and Lienhard 1997). IRS was first described in 1985 and called pp185 because of its size of 185kDa and it was phosphorylated after exposure to insulin. Inactivated insulin was not able to induce phosphorylation of pp185. pp185 was first cloned in 1991 and the protein was named IRS-1 (White, Maron, and Kahn 1985; Sun et al. 1991). IRS-2 (160kDa) was discovered in 1995 and IRS-3 (60kDa) as well as IRS-4 (160kDa) were found in 1997 (Sun et. al 1995; Lavan et al. 1997; Lavan, Lane, and Lienhard, 1997).

IRS proteins show distinct expression patterns. IRS-1 and -2 are ubiquitously expressed while IRS-3 mainly occurs in murine adipose tissue and IRS-4 is expressed in kidney, heart, thymus as well as hypothalamus. All these IRS proteins present similar functions and structure (Giovannone et al., 2000; Schubert et al., 2003). Their structure is subdivided into an N-terminal pleckstrin homology (PH) domain, a phosphotyrosine-binding (PTB) domain and a C-terminal tail with multiple tyrosine phosphorylation sites. Lipids and especially phosphoinositides bind the the PH domain of IRS proteins (Fruman, Rameh, and Cantley 1999) facilitating binding of IRS proteins to the membrane. The PTB domain of the IRS

proteins associate with the tyrosine phosphorylated juxtamembrane domain of the IR or IGF-1R after binding of the receptor to insulin or IGF-1. Upon recruitment of IRS to this motif of the receptor, the IRS proteins get phosphorylated at the tyrosine residues (Cheatham and Kahn, 1995; White, 2002). Then Src homology(SH)2 domain containing proteins bind to the phosphotyrosine motifs of the IRS (Yenush and White, 1997).

Unique for IRS-2 is the KLRB domain which attaches to the phosphorylated kinase regulatory loop of the β -subunit of the IR (Sawka-Verhelle et al., 1997; Sawka-Verhelle et al., 1996).

Binding of insulin to the IR causes tyrosine and serine phosphorylation of IRS-1 (Gual, Le Marchand-Brustel, and Tanti 2005). The phosphorylation pattern of IRS-1 induces differential regulation of the downstream signaling proteins because the phosphorylation of the serine residues leads to activation or inactivation of IRS-1 (Weigert et al. 2005; Weigert et al. 2008). The regulation of IRS-1 action is dependent on phosphorylated serine sites (Herschkovitz et al. 2007) and specific timing of phosphorylation (Weigert et al. 2005; Weigert et al. 2008). The most favoured model of the role of phosphorylation timing is that serine residues positively regulating IRS-1 function are phosphorylated first. This supports IRS-1 action and protect it from negative regulation via phosphorylation of inhibitory serine residues (Weigert et al. 2005; Weigert et al. 2008; Gual, Le Marchand-Brustel, and Tanti 2005; Luo et al. 2007). Additionally, serine phosphorylation of IRS-1 might probably entrance or hamper the association with tyrosine phosphatases. Phosphorylation of Ser1223 might alter the recruitment of IRS-1 to the protein tyrosine phosphatase Src homology domain 2 (SH2)-containing phosphatase-2 (SHP-2). The mutation of Ser1223 to alanine caused prevention of phosphorylation and increased association with SHP-2. Furthermore tyrosine phosphorylation of IRS-1 upon stimulation with insulin was decreased as well as the association of IRS-1 with the p85 regulatory subunit of the phosphatidylinositol-3-kinase (Luo et al. 2005).

This model of IRS-1 phosphorylation is also supported by the localization of serine residues with positive and negative effect. Serine sites with inhibitory effect are located near to the PTB domain, therefore these sites are phosphorylated later than the residues with positive effect after induction of the insulin signaling pathway. In detail, the phosphorylation of the serine residues near the PTB domain causes disruption of the association of IRS-1 to IR leading to degradation of IRS-1. Phosphorylated inhibitory serine residues at the C-terminus of IRS-1 induces its disassociation and inactivation of the phosphatidylinositide (PI)3-kinase (Gual, Le Marchand-Brustel, and Tanti 2005; Boura-Halfon and Zick 2009). These serine sites are phosphorylated by different serine kinases such as p70S6 (S6K) kinase, target of rapamycin (mTor) and PKCzeta (Boura-Halfon and Zick 2009; Herschkovitz et al. 2007; Gual et al. 2003).

Inhibitory serine sites of IRS proteins are phosphorylated by c-Jun N-terminal kinase (JNK), SIK-2, mTor/S6K, extracellular signal regulated kinase (ERK) and κ B kinase β (IKK β) which might result in insulin and IGF-1 resistance (Boura-Halfon and Zick 2009; Herschkovitz et al. 2007). The serine phosphorylation residues of IRS-2 are not fully understood. JNK phosphorylates Thr348 located near the PTB domain of IRS-2 which might cause disassociation of IRS-2 from the IR or IGF-1R (Solinas et al. 2006). Additionally JNK phosphorylates Ser488 which supports the phosphorylation of Ser484 via glycogen synthase kinase (GSK)- β . This disturbs the insulin or IGF-1 signaling pathway (Sharfi and Eldar-Finkelmann, 2008).

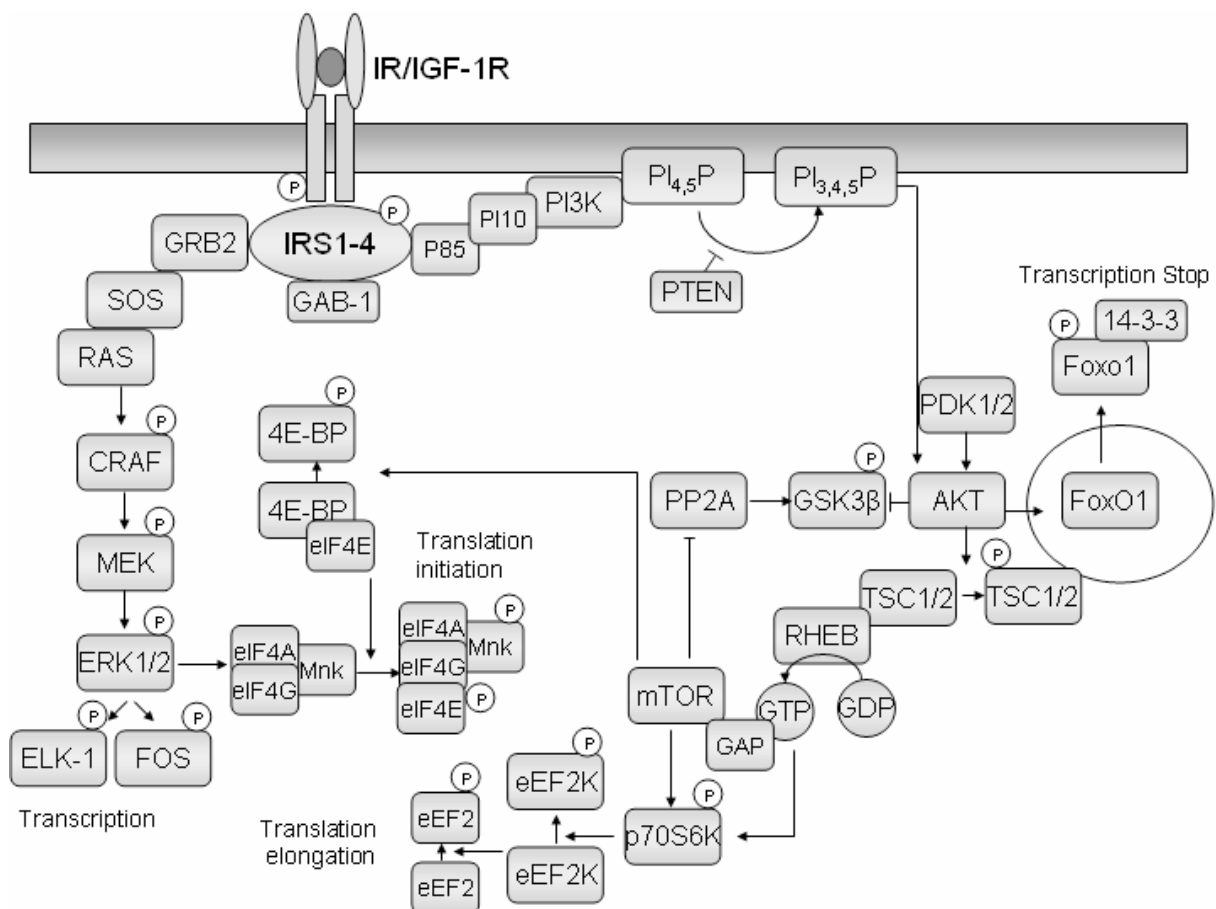


Figure 2: Insulin and insulin-like growth factor-1 signaling pathway.

Binding of insulin or insulin-like growth factor-1 (IGF-1) to the insulin-or IGF-1 receptor (IR or IGF-1R) induces a conformational change of the receptor leading to autophosphorylation. This is followed by recruitment and activation of insulin receptor substrates 1 to 4 (IRS-1 to -4). Then the MAP kinase (MAPK) and the Phosphatidylinositide(PI)3 kinase (PI3K) signaling are activated leading to inhibition of FoxO1 mediated transcription (modified, Moll et al., 2011).

1.1.3. Phosphatidylinositide(PI)3 kinase signaling

The mammalian PI3 kinase family is subclassified into classes I to III. Class I is additionally subdivided into Ia and Ib (Vanhaesbroeck et al., 2005). These kinases phosphorylate the 3'hydroxyl position of phosphatidyl-myo-inositol lipids. The PI3K activated after insulin or IGF-1 stimulus belongs to the class Ia kinases (Fruman et al., 1998). This kinase shows a

heterodimer structure with a catalytic subunit of 110 kDa which is noncovalently associated with a 50-, 55- or 85 kDa regulatory subunit. After binding of insulin or IGF-1 to the IR or IGF-1R and association of IRS to the receptor, the PI3K is recruited to the membrane by the p85 regulatory subunit. In addition, growth factor binding protein (GRB)-2 and the SH2-Phosphatase(SHP)2 are recruited. After activation of PI3 kinase phosphatidylinositide-diphosphate ($PI_{4,5}P$) is phosphorylated to generate phosphatidylinositide-triphosphate ($PI_{3,4,5}P$). This phosphorylation is reversible via phosphatase and tensin homolog deleted on chromosome ten (PTEN) (Fig. 1). The production of $PI_{3,4,5}P$ induces activation of the downstream signaling targets phosphoinositide-dependent protein kinase (PDK) and protein kinase B (PKB, AKT). PDK has two isoforms called PDK-1 and PDK-2. PDK-1 phosphorylates AKT at the residue Thr308 leading to a partial activation of AKT. To entirely activate AKT it has to be phosphorylated at Ser473 (Stokoe et al., 1997; Alessi et al., 1996; Lawlor and Alessi, 2001).

AKT is a serine/threonine kinase which is about 57 kDa. Three isoforms of AKT, AKT1 to AKT3 exist which show a conserved structure, a PH domain at the N-terminus, a kinase domain and a regulatory subunit at the C-terminus (Hreasko et al., 2003). After AKT is activated, it phosphorylates tuberlin 2 (TSC-2) which can form a heterodimer with TSC-2 and contains GTPase activity that inhibits the GTPase RAS homolog enriched in the brain (RHEB). The consequence of phosphorylation by AKT is the accumulation of the RHEB-GTP complex which activates mTOR (Astrinidis and Henske, 2005; Hay et al., 2004). mTor and PDK-1 phosphorylate and activate S6K.

IGF-1 controls protein synthesis via regulation of intrinsic activity and binding properties of the translation initiation and elongation factors eIFs and eEFs. Phosphorylation of 4E binding protein (4E-BP) via mTor results in the release of eukaryotic initiation factor 4E (eIF4E). These factors form a complex which activates S6K and facilitates translation initiation. S6K phosphorylates and activates the eukaryotic elongation factor 2 (eEF2) leading to release of eEF2 and initiation of elongation (Nojima et al., 2003; Oshiro et al., 2004).

The glycogen synthase kinase(GSK)-3 β and Bcl-2/Bcl-X-associated death promoter (BAD) are also regulated by the IR and IGF-1R signaling pathway. GSK-3 β is a major tau kinase and BAD, a proapoptotic factor, which both become inactivated upon insulin or IGF-1 stimulus (Song et al., 2005).

BAD mainly interacts with the apoptosis suppressor Bcl-X_L via its BH3 homology domain but also with Bcl-2 (Yang et al., 1995; Zha et al., 1997). The phosphorylation of BAD regulates this interaction. After phosphorylation BAD associates with 14-3-3 and releases its binding partner Bcl-X_L or Bcl2 to prevent apoptosis. The main phosphorylation sites of BAD to regulate apoptosis are Ser112 (Zha et al., 1996), Ser136 (Zha et al., 1996), Ser155 (Licano et al., 2000; Tan et al., 2000) and Ser170 (Drams et al., 2002). Several kinases are able to

phosphorylate BAD such as AKT (Datta et al., 1997), PI3K (Pastorino et al., 1999), PKA (Harada et al., 1999), PKC (Bertolotto et al., 2000) and Rsk also known as MAPK-activated protein 1 (MAPKAP-K1) (Bertolotto et al., 2000). The phosphorylation sites Ser112 and Ser136 of BAD regulate the binding to 14-3-3 (Zha et al., 1996) and phosphorylation of Ser155 leads to dissociation of BAD from Bcl-X_L (Licano et al., 2000). Thus IR/IGF-1R signaling pathway inhibits apoptosis via BAD phosphorylation and the release of antiapoptotic factors (Schubert et al., 2003).

1.1.4. Forkhead box O transcription factors

After insulin or IGF-1 stimulus AKT becomes activated and phosphorylates the forkhead box O transcription factor (FoxO). This event causes the binding of FoxO to 14-3-3 followed by export out of the nucleus and FoxO mediated transcription is inhibited. So far known FoxOs regulate transcription of genes involved in metabolism, growth, development, ageing and apoptosis (Patridge and Bruning, 2008). In *Caenorhabditis elegans* and *Drosophila melanogaster* a single FoxO transcription factor was identified, abnormal dauer formation protein 16 (DAF-16), and dFOXO in *D. melanogaster*. The mammalian FoxO protein family contains 4 members, FoxO1, FoxO3a, FoxO4 and FoxO6. (Clark et al., 1993).

The FoxO1 gene was discovered during studies of the t(2,13)(q35;q14) and t(1,13)(p36;q14) chromosomal translocations which occur in alveolar rhabdomyosarcoma. Meanwhile FoxO1 was called forkhead in rhabdomyosarcomas (FKHR) (Galili et al., 1993). FoxO3a, originally termed as forkhead in rhabdomyosarcomas-like protein 1 (FKHRL1) was found during the analysis of the chromosomal translocation t(6;11)(q21;q23) in leukaemia (Hillion et al., 1997) and cDNA library screening (Anderson et al., 1998). FoxO4 which was first called acute leukemia fusion gene located in chromosome X (AFX) was identified during the analysis of the chromosomal translocation t(X;11)(q12;q23) was analyzed (Borkhardt et al., 1997; Corral et al., 1993; Parry et al., 1994). FoxO6 was characterized by Jacobs and coworkers in 2003 (Jacobs et al., 2003).

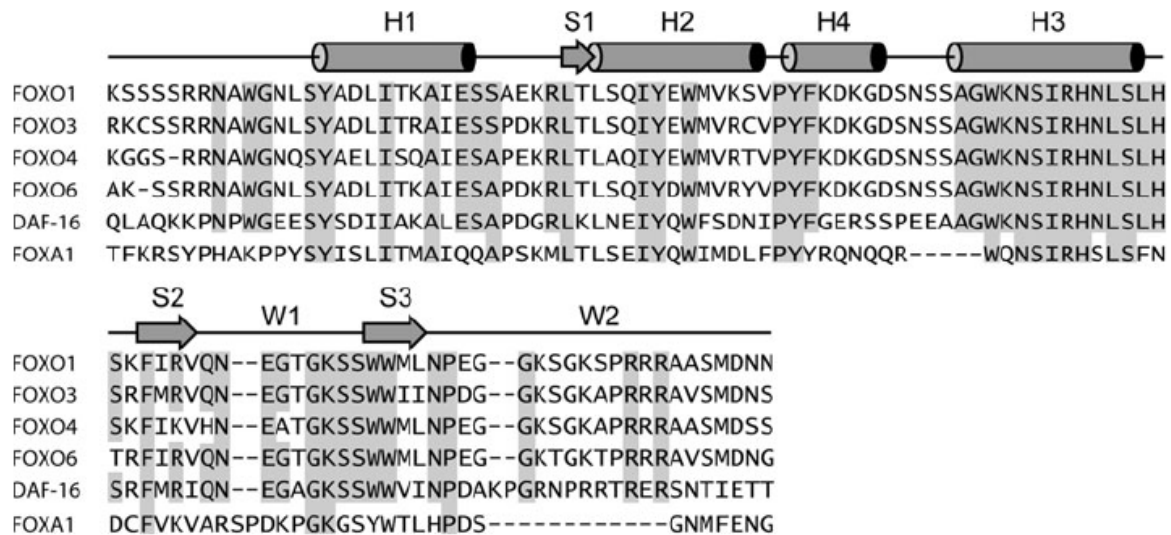


Figure 3: Structure of forkhead box O transcription factor DNA binding domain.

Amino acids of the conserved DNA binding domain of the FoxO family are shown. Displayed are FoxO1, FoxO3a, FoxO4, FoxO6, DAF-16, the orthologue of FoxO in *C.elegans*, and FoxA1 also known as hepatocyte nuclear factor 3- α which is liver-specific and a member of the forkhead family (Van der Vos and Coffey; 2011).

FoxOs contain a nuclear localization signal, a nuclear export signal and a transactivation domain. Additionally, FoxOs share the same conserved DNA binding domain, the forkhead domain (FKHR) and recognize the core binding motif sequence: TTGTTTAC (Clark et al., 1993; Furayama et al., 2000). The DNA binding domain is composed of three α -helices H1 to H3, three β -strands S1 to S3 as well as two wing-like loops W1 and W2 (Fig. 3) (Boura et al., 2007). The consensus FoxO-recognized element (FRE) was identified during high-affinity DNA-binding studies and contains the sequence (G/C)(T/A)AA(C/T)AA (Biggs et al., 1999; Furayama et al., 2000; Gilley et al., 2003). This FRE sequence exists in the promoter region of e.g. Fas ligand (FasL) (Brunet et al., 1999), insulin-like growth factor binding protein 1 (IGFBP1) (Barthel et al., 2005; Cichy et al., 1998), Bim (Dijkers, Medema, Lammers et al., 2000), p27^{KIP1} (Dijkers, Medema, Pals et al., 2000; Medema et al., 2000) and manganese dependent superoxide dismutase (MnSOD) (Kops et al., 2002).

FoxO1, FoxO3a and FoxO4 are ubiquitously expressed but FoxO6 is only present in the brain (Furayama et al., 2000; Jacob et al., 2003). The FoxO transcription factors show distinct expression patterns in the murine brain. FoxO1 is mainly expressed in the striatum, dentate gyrus and ventral hippocampus. FoxO3a compared to FoxO1 is more diffusely expressed e.g. in cortex, cerebellum and hippocampus. FoxO6 is highly expressed in nucleus accumbens, claustrum, amygdale-hippocampal area and hippocampus. (Hoekman et al., 2006).

1.1.4.1. Regulation of FoxO mediated transcription

Post-translational modifications of FoxO transcription factors regulate their activity. Phosphorylation of FoxOs mainly controls FoxO mediated transcription. AKT phosphorylates FoxO1 at Thr24, Ser256 and Ser319 (Biggs et al., 1999; Brunet et al., 1999; Kops et al., 1999; Rena et al., 1999; Tang et al., 1999) and FoxO3a becomes phosphorylated at Thr32, Ser253 and Ser315 (Brunet et al., 1997). After insulin or IGF-1 stimulation these sites get phosphorylated via AKT and FoxO interacts with 14-3-3 and translocates out of the nucleus which inactivates FoxO mediated transcription (Brunet et al., 1999). FoxOs are also phosphorylated by other kinases which are dependent on certain stimuli (review in Huang and Tindall, 2007). E.g. FoxO1 can additionally be phosphorylated by dual-specificity tyrosine-phosphorylated and regulated kinase (DYRK). DYRK phosphorylates FoxO1 at Ser329 (Woods et al., 2001). This phosphorylation inhibits FoxO1 activity (Rena et al., 2002). Furthermore FoxOs are phosphorylated via glucocorticoid-inducible kinases (SGKs) (Brunet et al., 2001). Similar to AKT these kinases are serine/threonine kinases which are regulated by the PI3K pathway the same way AKT is regulated. Upon activation SGKs translocate into the nucleus and phosphorylates FoxO3a which in turn inactivates FoxO3a. SGK1 predominantly phosphorylates Ser319 while AKT prefers Ser256 of FoxO3a (Brunet et al., 2001).

In addition activation of the C-Jun-N-Terminal kinase (JNK) upon oxidative stress leads to nuclear localization of FoxO3a (Lehtinen et al., 2006) (Fig. 4).

Another post-translational modification of FoxOs is ubiquitylation after phosphorylation by AKT, ERK-1/2 and I κ B kinase (IKK). FoxO1 is polyubiquitylated by Skp2, the substrate-binding component of the Skp1/culin 1/F-box protein (SCF^{Skp2}) E3 ligase complex upon phosphorylation of Ser256 via AKT or it is ubiquitylated by murine double minute (MDM2) after phosphorylation by ERK-1/2 (Huang et al., 2005, Yang, Zong et al., 2008; Yang, Dolloff et al., 2008; Fu et al., 2009).

FoxO1 and FoxO3a have to be polyubiquitylated for degradation in contrast to FoxO4 which gets monoubiquitylated for degradation (van der Horst et al., 2006).

Furthermore FoxO transcription factors are methylated. FoxO1 is methylated at Arg248 and Arg250 located in the AKT phosphorylation motif. This methylation is mediated by the protein arginine N-terminal methyltransferase 1 (PRMT1) and protects FoxO1 from being phosphorylated by AKT and nuclear exclusion (Yamaga et al., 2008).

Finally FoxO transcription factors are acetylated. CBP and p300 with their interacting proteins like CBP- and p300-associated factor (PCAF) have intrinsic histone acetyltransferase activity. Hence CBP and p300 can promote transcription through histone acetylation or immediately regulate transcription by acetylation of the transcription factor itself (Li et al., 2002). Acetylation of FoxO decreases DNA binding and promotes phosphorylation

of FoxO at Ser256 via AKT which inactivates FoxO. However the recruitment of CBP and p300 to the promoter by FoxO in addition mediates the acetylation of histones and might facilitate initiation of transcription (Daitoku et al., 2004; Matsuzaki et al., 2005). Deacetylation of FoxO is performed by silent information regulator 1 (SIRT1) which is a nicotinamide adenine dinucleotide(NAD)-dependent histone deacetylase. It has been shown that FoxOs are deacetylated by SIRT2 and -3. These deacetylases bind to acetylated FoxOs upon stress stimuli and induce deacetylation to control FoxO mediated transcription (Brunet et al., 2004; Kitamura et al., 2005).

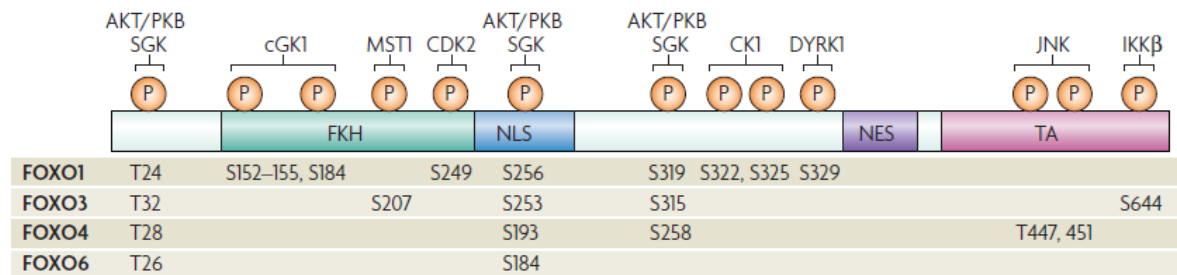


Figure 4: Phosphorylation sites of the FoxO transcription factors. The structure of FoxOs consists of a forkhead domain (FKH), a nuclear localization signal (NLS), a nuclear export signal (NES) and a transactivation domain (TA). Kinases which phosphorylate FoxOs are shown above. The exact phosphorylation sites are presented beneath the FoxO structure (modified, van der Horst and Burgering, 2007)

1.1.5. Function of FoxOs

FoxOs are involved in metabolism, cell cycle control and stress resistance. Besides triggering glucose uptake insulin controls FoxO mediated transcription of phosphoenolpyruvate carboxykinase (PEPCK) and glucose-6-phosphatase which are part of the gluconeogenesis machinery. In general FoxO1 suppresses transcription of the genes which are involved in glycolysis and gluconeogenesis (Barthel et al., 2001; Nakae et al., 2001; Zhang et al., 2006).

FoxOs additionally induce cell cycle arrest. These transcription factors regulate the G1-S and G2-M phase of the cell cycle. Cell cycle is adjusted by several cyclins and cyclin-dependent kinases (CDKs). CDKs phosphorylate and thereby regulate different targets which play a role in cell cycle progression. An important inhibitor of CDKs is p27, a member of the Cip/Kip protein family. p27, p21 and p57 bind to cyclins and CDKs complexes and inhibit their action. Targets of p27 are cyclin A-, cyclin D- and cyclin E-CDK complexes (review in Besson et al., 2008). The expression of p27 is regulated by FoxOs. Other cell cycle inhibitors regulated by FoxOs are p130Rb2, cyclin D1 and cyclin G2 (Medema et al., 2000; Kops et al., 2002; Martinez-Gac et al., 2004; Schmidt et al., 2002) as well as p15 and p19 which are also CDK inhibitors (Besson et al., 2008). Under fasting conditions the insulin signaling cascade is inactive but FoxOs are still active and can promote cell cycle arrest and quiescence (Kops et al., 2002). Therefore FoxOs promote survival under fasting conditions. This is comparable to

C.elegans dauer formation which is induced by DAF-16. Furthermore FoxOs regulate transcription of the insulin receptor and IRS2 to guarantee a fast adaptation to higher glucose levels (Puig and Tjian, 2005; review in van der Horst and Burgering, 2007).

Another function of FoxOs is the regulation of oxidative stress response. In response to oxidative stress which occurs under fasting conditions when ATP production has to be promoted via fatty-acid oxidation. FoxOs counteract the oxidative stress induced reactive oxygen species (ROS) via increasing expression of antioxidant enzymes. Such enzymes are catalases (Nemoto and Finkel, 2002) and manganese superoxide dismutase (MnSOD) (Kops et al., 2002). In addition FoxOs promote the upregulate the fatty acyl-CoA carriers, sterol carrier protein-x (SCPx) and sterol carrier protein-2 (SCP2) (Dansen et al., 2004).

1.1.5. MAPK signaling

In addition to the PI3 kinase signaling pathway insulin or IGF-1 can induce the activation of the mitogen activated protein kinase (MAPK) cascade. Insulin or IGF-1 bind to the IR or IGF-1R leading to autophosphorylation of the receptor, recruitment and phosphorylation of IRS followed by the binding of IRS to the SH2 domain of downstream signaling proteins like GRB-2 (White, 2000). Next GRB-2 binds to son of sevenless (SOS) which is a GDP/GTP exchange factor. Then the small G-protein rat sarcoma (RAS) is activated and recruits c-raf leukemia viral oncogene (CRAF) to the membrane which activates MAP-ERK kinases (MEK) and finally the extracellular signal-regulated kinase (ERK)-1/-2 (Kolch, 2000). Furthermore ERK-1/-2 controls phosphorylation of FBJ osteosarcoma oncogene (FOS) by p90RSK (RSK: ribosomal protein S6 kinase) as well as phosphorylation of ETS oncogene family (ELK-1). The activity of ERK-1/-2 is involved in long-term potentiation and memory consolidation within the CNS (review in Sweatt, 2001).

1.2. Alzheimer's disease

Alzheimer's disease (AD) is a chronic and progressive neurodegenerative disorder and the most common form of dementia and to loss of cognitive abilities and finally to death (Citron, 2002; Cole et al., 2007). AD was first discovered by Alois Alzheimer in 1906 (Alzheimer, 1907).

Characteristic for AD is the accumulation of intracellular neurofibrillar tangles (NFT) and extracellular amyloid plaques. The NFTs are composed of hyperphosphorylated tau proteins (Ross et al., 2005). Amyloid plaques mainly consist of aggregated amyloid- β (A β) peptides (Masters et al., 1985). The aggregation of A β might be the most important cause for neurodegeneration in the pathology of AD (Masters et al., 1985).

1.2.1. Pathology of Alzheimer's disease

Patients with AD show cognitive dysfunctions which are categorized into three subgroups: The first group of cognitive dysfunctions includes language disabilities, loss of memory and loss of executive functions like the ability to plan or to coordinate. The second group, the non-cognitive symptoms, include psychiatric symptoms and disturbances of behavior such as hallucinations and depression. The last group of cognitive dysfunctions are disturbed performing activities which are subdivided into instrumental and basic performing activities. Alzheimer's disease progresses from mild cognitive impairment to severe dementia (Burns et al., 1990).

AD is subdivided by the age of onset and the form of inheritance. Up to 6% of all AD patients develop the disease before the age of 65, so called early onset. Nearly 60% of these patients display the familial form of AD and from these cases about 13% inherited an autosomal dominant form of AD (Rocca et al., 1991; Campion et al., 1999). This form of AD is called familial Alzheimer's disease (FAD) and starting at the age of 30 to 40 years. The late onset AD is developed by patients of 65 years or older.

1.2.2. Hyperphosphorylation of tau

In the human brain six isoforms of tau have been investigated. These isoforms result from alternative splicing of exons 2, 3 and 10. Both exons 2 and 3 partially encode the N-terminus of tau. In contrast exon 10 encodes the additional MTB (microtubule binding) domain. Consequently tau can consist of three or four MTB repeats (reviewed in Ballatore et al., 2007; Goeders et al., 2006). The exact function of tau is not clearly understood yet. A possible function is the stabilization of microtubules and the regulation of transports along the axons (Götz et al., 2006). Tau is mainly found in axons of neurons (Hirokawa et al., 1996) but it might also be located in dendrites of neuron (Ittner et al., 2010).

Tau is phosphorylated at several sites by different kinases including cyclin-dependent kinase 5 (Cdk5), c-Jun N-terminal kinase (JNK), protein kinase A (PKA), ERK1/2 and glycogen synthase kinase 3 (GSK3 β). Abnormal high phosphorylation by these kinases is called "hyperphosphorylation" (Robertson et al., 1993; Hanger et al., 1992; Flaherty et al., 2000; Cho et al., 2004; Stoothoff et al., 2005). A major tau kinase is GSK3 β . GSK3 β is inactivated after phosphorylation of Akt at Ser9 and is dephosphorylated by PP2A the predominant tau phosphatase in the human brain. Tau is dephosphorylated by PP2A at Thr205, Thr212, Ser214, and Ser262 *in vitro* (Qian et al., 2010). This complex regulation might indicate the importance of the equilibrium of phosphorylation and dephosphorylation (Sontag et al., 1996; Liu et al., 2008; review in Milliward et al., 1999). The phosphorylation of tau particularly at Ser422 rescues tau from degradation (Guillozet-Bongaarts et al., 2006).

1.2.3. Generation of amyloid- β

Amyloid- β is produced by endoproteolytic cleavage of the amyloid precursor protein (APP). APP is a type-1 integral membrane protein and was discovered in 1987 (Kang et al., 1987; Tanzi et al., 1987; Goldgaber et al., 1987, Robakis et al., 1987). APP consists of an N-terminal extracellular domain and a smaller C-terminal domain located in the cytoplasm. Different APP splicing variants are distinguishable by length of the resulting protein, APP with a size of 751 or 770 amino acids (APP751 and APP770) are basically expressed in non-neuronal tissue. APP with a size of 695 amino acids (APP695) mainly occurs in neurons (Kang and Muller-Hill, 1990). The function of APP and APP-like protein (APLP) are not well understood. These proteins might be involved in apoptosis, axonal transport and cell adhesion. APP and APLP are expressed in nearly all vertebrates and invertebrates (Zheng and Koo, 2006; Anliker and Muller, 2006; Cao and Sudhof, 2001).

Maturation of APP includes N-glycosylation in the endoplasmic reticulum and early Golgi network. N-glycosylated APP cannot be cleaved via secretases (Tomita et al., 1998). Trafficking within the Golgi network causes a change from N-glycosylation to O-glycosylation. Thereafter APP enters the secretory pathway (Small and Gandy, 2006).

APP is cleaved via the α -secretase ADAM9, ADAM10 (a disintegrin and metalloproteinase-like 9 or 10) or TACE (tumour necrosis factor- α convertase) (also known as ADAM17) represents the “non-amyloidogenic pathway”. Additionally APP is processed by the β -secretase BACE1 (β -site APP-cleaving enzyme) resulting in the “amyloidogenic pathway”.

α -secretase cleavage of APP leads to a C-terminal fragment C83 and soluble sAPP α . The γ -secretase, a complex formed by presenilin, nicastrin, Aph-1 and Pen-2 cleaves C83 and thereby generates p3 (~3 kDa) and APP-intracellular domain (AICD, ~6kDa).

Cleavage of APP by the β -secretase BACE1, a type 1 membrane protease, is the rate limiting step in the production of A β . This secretase cleaves APP at Asp⁺¹ at the N-terminus which results in generation of soluble sAPP β and the C-terminal fragment C99. Following this event C99 is cleaved via the γ -secretase releasing A β (4 kDa) and AICD. A β occurs mainly in two variants; A β 40 ending at residue 40 and A β 42 which ends at residue 42. The decision whether the α - or β -secretase cleaves APP is dependent on the competition between these enzymes. It has been shown that an increase of β -secretase cleavage of APP leads to a decreased α -secretase cleavage and vice versa (Vassar et al., 1999; Skovronsky et al., 2007) (Fig. 5).

In a healthy brain A β 40 represents about ~90% of all A β peptides. The production of A β 42 is less with ~5-10% (Walsh et al., 2007). The accumulation and aggregation of these A β 42 peptides is a major step in the formation of amyloid plaques (Iwatsubo et al., 1994). The ratio of A β 42 to A β 40 is used for diagnosis of AD (Haass et al., 2007).

The aggregation of A β leads to the generation of several intermediates like A β monomers. These monomers are soluble and amphipathic with α -helical conformation mixture (Coles et al., 1998; Crescenzi et al., 2002). A β dimers have an hydrophobic core and are located intracellular *in vivo* (Roher et al., 1996). The small A β oligomers are thought to be cytotoxic compared to inert A β fibrils (Dahlgren et al., 2002; McLean et al., 1999; Cleary et al., 2005; Lesne et al., 2006). Furthermore A β -peptides form A β -derived diffusible ligands (ADDLs) without fibrillar structure. These ADDLs are neurotoxic at a size of about 17 to 42 kDa (Chromy et al., 2003; Klein, Stine, and Teplow, 2004; Lambert et al., 1998). Especially the levels of ADDLs are linked to cognitive impairments of patients suffering from AD (Georganopoulou et al., 2005). A β protofibrils which have a rod-like and flexible structure display the precursors of A β fibrils (Harper et al., 1999; Arimon et al., 2005; Harper et al., 1997; Kheterpal et al., 2003; Walsh et al., 1997; Williams et al., 2005). These A β fibrils are insoluble and thermodynamically stable aggregates with a high content of β -sheets sheets (Ross and Poirier, 2005). The characteristic amyloid plaques are formed by extracellular aggregated A β fibrils (Muller-Hill and Beyreuther, 1989). As a defence mechanism plaques are beset with astrocytes, microglia and dystrophic dendrites (Selkoe, 2004).

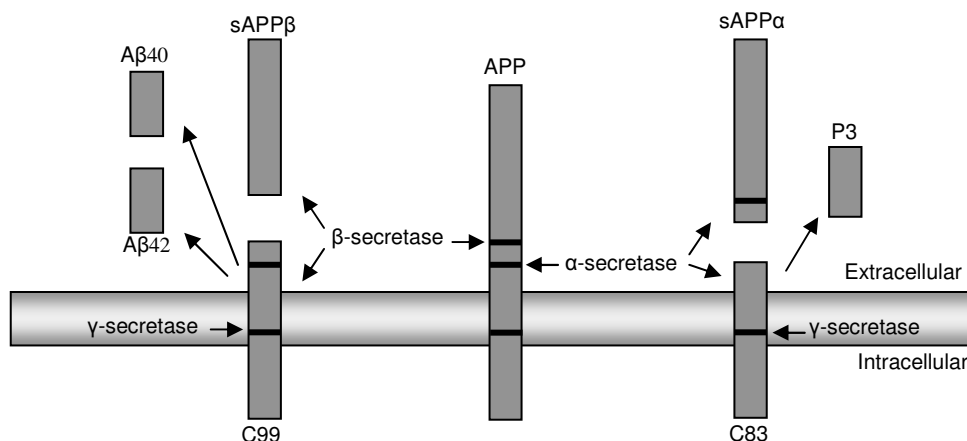


Figure 5: Processing of the amyloid precursor protein (APP).

APP is a type 1 membrane protein and is cleaved by α - or β -secretase. In case of cleavage by the α -secretase sAPP α and C-terminal fragment C83 are generated. The γ -secretase cleaves C83 and P3 is produced. β -secretase cleaves APP releasing the sAPP β and C99 is produced. γ -secretase degrades C99 leading to generation of A β 40 and A β 42 (modified Moll et al., 2011).

1.2.4. Degradation and clearance of amyloid- β

A β is transported and degraded out of the brain via a receptor-mediated process or by phagocytosis via macroglia. Insulin degrading enzyme (IDE), Neprilysin (NEP), endothelin converting enzyme (ECE) and angiotensin converting enzyme (ACE) are involved in degradation of A β . IDE is a mainly cytosolic, a 110kDa zinc metallo-endopeptidase which

plays a role in degradation of different peptides like insulin, transforming growth factor α (TGF α), glucagon, A β and AICD (Duckworth et al., 1998).

It has been shown that IDE knockout mice display increased levels of endogenous A β and AICD in the brain which suggests a role of IDE in A β clearance (Selkoe, 2001; Farris et al., 2003). Consistently the overexpression of IDE in APP^{sw} expressing mice showed a up to 50% reduction of A β plaques as well as reduction of A β 40 and A β 42 monomer levels. Furthermore it has been shown that a polymorphism of IDE might be involved in late onset AD (Leissring et al., 2003; Bertram and Tanzi, 2004). The second enzyme facilitating A β degradation is NEP, a type 2 membrane protein with extracellular catalytic domain. The function of NEP is similar to the function of IDE. It degrades peptides like neuropeptide Y and ekephalin (Turner et al., 2001). Further studies showed that the intracerebral injection of a lentiviral vector transducing the human NEP gene in a transgenic mouse model of cerebral amyloidosis leads to an up to 50% reduction of cortical amyloid deposits (Marr et al., 2003).

The other pathway of A β clearance is the receptor-mediated transport across the blood brain barrier (BBB). This transport is promoted by low-density lipoprotein receptor-related protein (LRP) (Zlokovic, 2004). This transport requires the association of LRP to the LRP ligands apoE and α 2Macroglobulin (α 2M). After crossing the BBB A β is transported to peripheral tissue e.g. liver for degradation (Tanzi, Moir and Wagner, 2004).

The exact toxic effect of A β is still under investigation but might be promoted by the generation of membrane disruption, ion channel, induction of apoptosis, inflammation and oxidative stress (Hardy and Selkoe, 2002; Nakagawa et al., 2000; Soto, 2003; Roberson and Mucke, 2006).

1.2.5. Genetic risk factors of Alzheimer's disease

The APP gene is located on chromosome 21 and patients suffering from trisomy 21 carrying an additional APP allele have an increased risk to develop Alzheimer's disease. The duplication of the APP gene can cause Alzheimer-like pathologies, cerebral amyloid and angiopathy (Rovelet-Lecrux et al., 2006; Sleegers et al., 2006). Furthermore certain mutations (e.g. APP^{sw}) in the APP gene are risk factors for developing Alzheimer's disease. Patients with these mutations suffer from so called early onset familial Alzheimer's disease (Vassar, 2004; Bertram and Tanzi, 2005). In addition to alterations in the APP gene, mutations in presenilin 1 and presenilin 2 may result in familial early-onset AD as well (Tabaton et al., 2007; Sherrington et al., 1996; Tanzi et al., 1992; Schnellenberg et al., 1992; Van Broeckhoven et al., 1992, St George-Hyslop et al., 1992; Rogaeve et al., 1995). Early-onset AD usually starts to be symptomatic at the age of 43 to 62 years (Tanzi et al., 1987; Campion et al., 1996; Goate, 1997). Mutations in the APP gene can cause changes in

processing of APP leading to higher A β generation. The presenilin 1 gene is located on chromosome 14 and it is part of the γ -secretase complex (1.2.3.). The detailed function of the transmembrane protein presenilin 1 is not completely understood. The homologue of presenilin 1 in *C. elegans* is SEL-12 (Van Broekhoven, 1995; Levitan and Greenwald, 1995). SEL-12 plays a role during the development of *C. elegans*. The knockout of presenilin 1 gene in mice leads to impaired neurogenesis, neuronal cell death and developmental defects in skeletal formation. These mice die soon after birth (Wong et al., 1997; Shen et al., 1997). Mutation of the presenilin 1 gene, a gain of function mutation causes up to 80% of familial AD. The presenilin 2 gene is located on chromosome 1 (Levy-Lahad et al., 1995). Mutations in this gene result in AD at the age of 40 to 88 years of age (Goate, 1997). Presenilin 1 and 2 present 67% homologous sequence and might have similar functions but they are not able to compensate for each other. The mutations of these three genes cause an increased generation of the toxic A β_{42} (Jarrett et al., 1993; Duff et al., 1996; Scheuner et al., 1996; Citron et al., 1997).

Furthermore certain variants of Apolipoprotein E (ApoE) increase the risk for AD. ApoE consists of three allelic forms $\epsilon 2$, $\epsilon 3$ and $\epsilon 4$. Allelic form $\epsilon 2$ is associated with the lowest risk for late onset Alzheimer's disease (LOAD). In contrast $\epsilon 4$ increases the risk to develop LOAD up to 15-fold (Farrer et al., 1997). ApoE is involved in regulation of A β peptide levels in the brain and the allelic form $\epsilon 4$ might promote aggregation of A β by increasing the amount of A β_{40} and reducing A β clearance (Holtzman, 2001; Cedazo-Minguez, 2007).

1.2.6. IR/IGF-1R signaling in Alzheimer's disease

Several clinical studies showed a link between AD and type 2 diabetes (Janson et al. 2004; Ott et al. 1999; Stewart and Liolitsa 1999; Lovestone 1999). The association of impaired insulin secretion, glucose intolerance and the risk to develop AD was analysed in several studies (Ott et al. 1996; Luchsinger et al. 2004; Ronnema et al. 2008). In addition patients with AD have a higher probability to develop impaired glucose tolerance and type 2 diabetes (Janson et al. 2004).

The IR/IGF-1R signaling pathway is disrupted in the central nervous system of patients suffering from AD (Frolich et al. 1998; Frolich et al. 1999; Moloney et al. 2010). The measurement of mRNA levels of insulin and IR in the CNS of AD patients shows a reduction of 80% compared to healthy patients (Moloney et al. 2010; Rivera et al. 2005). Furthermore the IGF-1R expression is reduced in brains of patients with AD compared to controls (Moloney et al. 2010; Rivera et al. 2005). In contrast levels of IGF-1 in the serum of AD patients are increased which might indicate IGF-1 resistance in AD (Rivera et al. 2005; Vardy et al. 2007). Additionally the expression of IRS-1 and IRS-2 is lower in brains of AD patients

compared to healthy brains. The phosphorylation level of IRS-1 at Ser312 and Ser616 is increased as well. This inhibits the action of IRS-1 leading to an inactive IR/IGF-1R signaling pathway (1.1.2.). Because of these observations AD is also called “brain type” diabetes (Pilcher 2006). Until now it is not known whether this brain specific insulin and IGF-1 resistance is a cause or consequence of AD.

The knockout of IGF-1 in mice shows an increase of tau phosphorylation at Ser202 and Ser396 in the presence of unaltered tau expression (Cheng et al. 2005). The brain-specific knockout of the IR, called NIRKO mice, presents hyperphosphorylation of tau at Thr231 (Schubert et al. 2004). In contrast knockout of IRS-2 displays hyperphosphorylation at Ser202 (Schubert et al. 2003). These differences in phosphorylation of tau might indicate the requirement of other factors than insulin actively influencing tau phosphorylation e.g. hyperglycemia or hyperinsulinemia (Freude et al., 2009).

Tg2576 mice are well established mice models of AD. These mice express the Swedish mutation of APP (APP^{sw}) (Vassaret et al. 1999; De Strooper 2003; Holsinger et al. 2002; Sinha et al. 1999; Harada et al. 2006). The knockout of IRS-2 (IRS-2^{-/-}) or the neuron specific IGF-1R knockout (nIGF-1R^{-/-}) in Tg2576 mice reduces or delays A β accumulation and rescues these animals from premature death (Freude et al. 2009).

The clearance of A β is affected by the IR/IGF-1R signaling pathway. It has been shown that the IR/IGF-1R signaling pathway induces the expression of IDE, one of the major enzymes involved in A β degradation (Zhao et al. 2004).

1.2.7. FoxO action in Alzheimer's disease

AD is linked to oxidative stress inducing activation of different signaling pathways and oxidative damage (Markesbery and Carney 1999; Beal 2002). Studies in a *D. melanogaster* AD model indicate that oxidative stress might be the main cause for neurodegeneration (Dias-Santagata et al. 2007). Oxidative stress is associated with increased JNK signaling which leads to insulin resistance (Ozcan et al. 2004). Activated JNK induces activation of the γ -secretase which in turn increases A β -peptide generation (Shen et al. 2008) and A β accumulation is linked to the formation of hydrogen peroxide (Tabner et al. 2005). The brains of patients with AD show an increased expression of nitric oxide synthase 1-3 and NADPH oxidase 1 and 3. These play a role in generation of reactive nitrogen and oxygen species (de la Monte and Wands 2006). Consistently, AD brains display an increased lipid peroxidation (Montine et al. 2002).

Oxidative stress induces FoxO-mediated transcription of target genes like manganese superoxide dismutase (MnSOD) and MnSOD is involved in protection of the brain against oxidative stress in several tissues and cell types.

In *C. elegans* it has been shown that the knockdown of DAF-2, the orthologue of the mammalian IR and IGF-1R, decreases toxicity of A β 42 (Cohen et al. 2006). DAF-16 and heat shock transcription factor 1 (HSF-1) both act downstream of the signaling pathway and are involved in the reduction of A β 42 induced damage (Hsu, Murphy, and Kenyon 2003; Birkenkamp and Coffey 2003; Cohen et al. 2006). A model of detoxification of A β 42 contains two mechanisms: The first mechanism describes the function HSF-1 in disaggregation of neurotoxic A β -oligomers and degradation. The second mechanism predicts DAF-16 to regulate A β hyperaggregation because aggregates with high molecular weight are less toxic compared to low molecular mass aggregates with high toxicity (Fig. 6) (Cohen et al. 2006). Further studies have shown A β hyperaggregation as a mechanism of A β detoxification in an IGF-1 resistant mouse model of AD (Cohen et al. 2009).

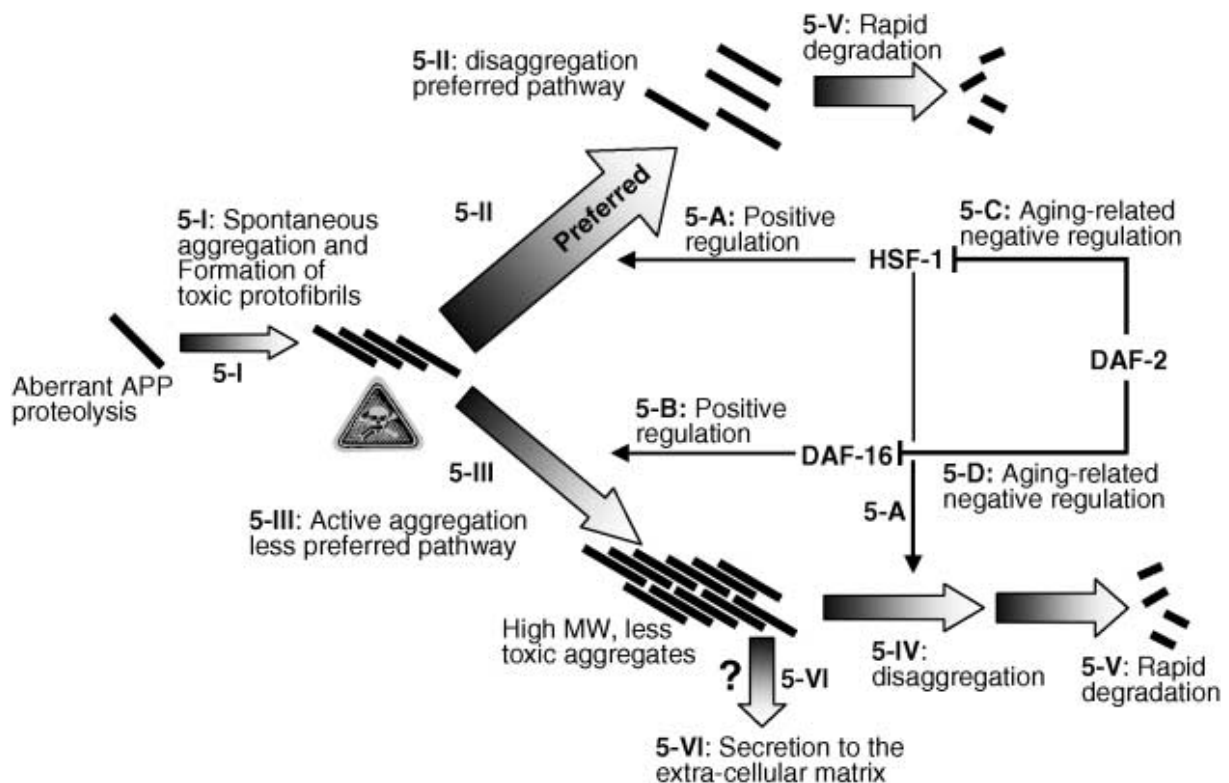


Figure 6: A β detoxification mechanism via HSF-1 and DAF-16

A β peptides form toxic aggregates with low molecular mass (5-I). Then aggregates are identified and disaggregated (5-II). The products become rapidly degraded (5-V). This mechanism is preferred and promoted by HSF-1 (5-A) and inhibited by DAF-2 (5-C). Whether this mechanism is overloaded a second mechanism promotes hyperaggregation to form high molecular mass aggregates with low toxicity (5-III). This mechanism is advanced by DAF-16 (5-B) and inhibited by DAF-2 (5-D). These high molecular mass aggregates can be disaggregated and degraded via the HSF-1 controlled mechanism (5-IV and 5-V) or are secreted to the extracellular matrix (5-VI) (Cohen et al., 2006).

1.3. Mouse models

The current study analyses the role of FoxO1 in the neurodegenerative Alzheimer's disease, because FoxO1 is strongly expressed in the hippocampus which is mainly affected by AD.

Therefore, influence of a constitutively active and the dominant negative form of FoxO1 in a mouse model of AD, Tg2576, was investigated. In order to achieve nerve specificity the Cre/loxP system under the neuron specific synapsin 1 promoter was used in the present study.

1.3.1. Constitutive active and dominant negative forms of FoxO1

The constitutive active form of FoxO1 displays mutations within the three AKT phosphorylation sites Thr24, Ser256 and Ser319 (Biggs et al., 1999; Brunet et al., 1999; Kops et al., 1999; Rena et al., 1999; Tang et al., 1999). Thr24 is substituted by Ala24, Ser256 is replaced by Asp256 and Ser319 by Ala319. This form of FoxO1 is called FoxO1ADA and cannot be phosphorylated by AKT resulting in constitutively nuclear expression. The other form is a dominant negative variant of FoxO1 harbouring a deletion of the nuclear export signal and the transactivation domain. This form still binds to the target promoter region, but cannot mediate transcription of its target genes and is called FoxO1 Δ 256 or FoxO1DN.

To induce site specific DNA recombination the Cre/loxP system was used. This system was first described in the bacteriophage P1. Necessary for this system is the 34 bp DNA sequence with two 13 bp inverted repeats and the asymmetric 8 bp spacer region called locus of X-over in P1 (loxP). This sequence targets the site of recombination. In addition the Cre recombinase, a 343 amino acid monomeric protein, is required for this system. For the *in vivo* study mouse lines carrying the loxP site flanked stop cassette followed by the FoxO1 gene (FoxO1ADA or FoxO1DN) in the Rosa26 locus were used (Fig. 7). The other mouse lines encode the tissue or celltype specific Cre recombinase. In this study the Synapsin 1 promoter driven Cre recombinase was used.

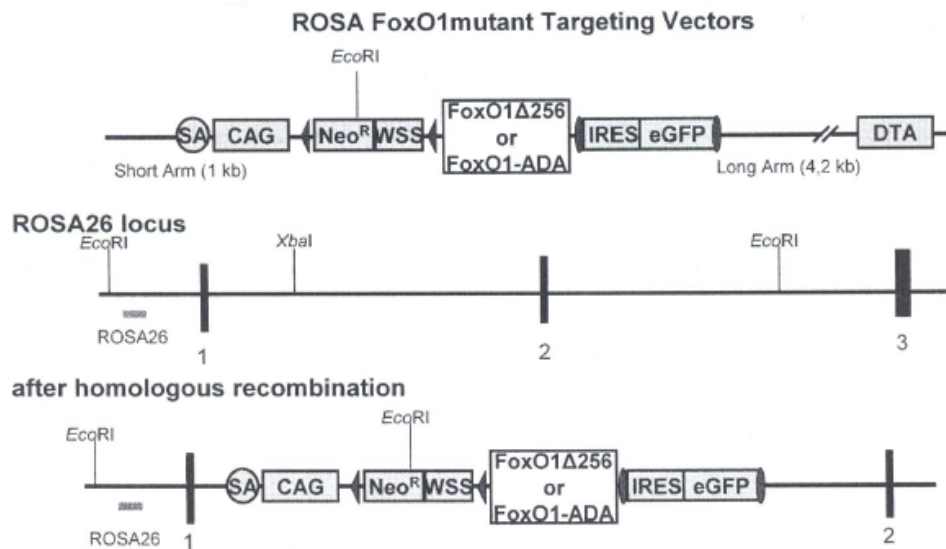


Figure 7: Cre/loxP targeting strategy for the FoxO1ADA and FoxO1DN expression in neurons. The upper panel presents the ROSA FoxO1mutant targeting vector which contains the splice acceptor (SA), the pCMV promoter region (CAG), the loxP sites (triangles) flanked neomycin resistance gene (Neo^R) and westphale stop cassette (WSS), the FoxO1 gene (FoxO1 Δ 256 or FoxO1-ADA) which are followed by the FRT site flanked internal ribosomal entry site (IRES) and enhanced green fluorescent protein (eGFP). After homologous recombination this region is inserted into the Rosa26 locus of the mouse model (lower panel).

1.3.2. Synapsin 1 promoter driven expression of the Cre recombinase

Synapsin is a neuronal phosphoprotein linked to the membrane of synaptic vesicles. It binds to the cytoskeleton and is involved in the release of neurotransmitters. The protein family of synapsin is subdivided into four proteins. These result from alternative splicing of two genes (Sudhof et al., 1989). In contrast to other vesicle bound proteins synapsins are first peripheral proteins rather than integral membrane proteins and in non-neuronal tissue no homologous proteins occur. This indicates that synapsin proteins are neuron specific. In a previous study it has been shown that the injection of synapsin 1 into *Xenopus* blastomeres promotes the development of neuromuscular synapses (Lu et al., 1992; Valtorta et al., 1995). Another study concerning the function of synapsin 1 showed that embryonic hippocampal neurons of synapsin 1-deficient mice present an outgrowth of predendritic neurites and retarded axons. In addition the formation of synapses was delayed. These results show evidence for the role of synapsin I in axogenesis and synaptogenesis (Chin et al., 1995). The previous use of synapsin 1 promoter driven Cre recombinase (SynCre) in mouse models revealed an expression pattern of the Cre recombinase in cortical and spinal cord neurons as well as high expression in the hippocampus (Zhu et al., 2001). Because of this predominant expression in the hippocampus the synapsin 1 promoter driven Cre recombinase is a useful model to generate neuronal specific expression of the gene of interest.

1.3.3. Tg2576, a model for Alzheimer's disease

Different mutations cause AD (1.2.5.). The mouse model Tg2576 overexpresses the human APP (695 amino acids) with the Swedish mutation which consists of a substitution of Lys670 to Asn and Met671 to Leu. This mutation was first discovered in a Swedish family suffering from FAD (sw). For this reason this mutation was named the Swedish mutation (APP^{sw}). This mouse model displays age-dependent memory impairments which start at the age of 40 weeks. Additionally, these mice present histopathological characteristics of AD like neurotic dystrophy, astrogliosis, reactive microgliosis, formation of amyloid plaques and to less extend abnormal tau phosphorylation formation of amyloid plaques (Hsiao et al., 1996; Irizarry et al., 1997; Frautschy et al., 1998).

The human APP^{sw} gene was cloned into the open reading frame of the hamster prion protein cosmid vector where the expression of APP^{sw} is driven by the hamster prion protein gene promoter. This vector was then used to generate the Tg2576 mice. The genetic background of these mice affects mortality. Tg2576 mice in a clear C57BL/6 background die within the first months of life which complicates the analysis of amyloid accumulation (Carlson et al., 1997). Hence, Tg2576 mice were bred into a B6/SJL hybrid background. Progenies were then used to analyse the APP processing, amyloid accumulation, APP^{sw} induced mortality and the effect of FoxO1 mediated transcription on Alzheimer's disease (Bothe Gerald, 2005).

1.4. Aims of the present thesis

In previous studies the neuronal knockout of the IGF-1R (nIGF-1R^{-/-}) in Tg2576 mice displayed a rescue of premature death and decreased A β accumulation. Furthermore haploinsufficiency of the IGF-1R increases A β hyperaggregation which indicates to be a rescue mechanism (1.2.7.) (Cohen et al., 2009; Freude et al., 2009). To elucidate whether the orthologue of the *C.elegans* transcription factor DAF-16 the mammalian FoxO induces these effects FoxO1 was chosen because this is the predominantly expressed FoxO in the hippocampus (Hoekman et al., 2006). Two mouse lines each expressing FoxO1ADA or FoxO1DN in Tg2576 mice were analysed.

The analysis contains Kaplan-Meier investigations up to 60 weeks of age, investigation of glucose metabolism and analysis of APP processing as well as amyloid accumulation. These studies were performed using WT, SynCre/FoxO1ADA, SynCre/FoxO1DN, Tg2576, Tg2576/FoxO1ADA and Tg2576/FoxO1DN mice.

2. Material and Methodes

2.1. Chemicals

Acetic acid	Merck, Darmstadt, Germany
Acrylamide / Bis-acrylamide 30%	Rotiphorese® Gel 30 (37.5/1) Carl Roth GmbH + Co. KG, Karlsruhe, German
Acrylamide Solution (40%) Mix 29:1	AppliChem GmbH, Darmstadt, Germany
Agarose	Invitrogen Corporation, Carlsbad CA, USA
Ammonium-persulfate (APS)	AppliChem GmbH, Darmstadt, Germany
Avertin	Sigma-Aldrich Chemie GmbH, Steinheim, Germany
Benzamidine Sigma-Aldrich	Chemie GmbH, Steinheim, Germany
β-mercaptoethanol	Sigma-Aldrich Chemie GmbH, Steinheim, Germany
Bradford reagent	Bio-Rad Laboratories GmbH; Germany
Bromophenol blue	AppliChem GmbH, Darmstadt, Germany
96 % Bovine serum albumin (BSA)	Sigma-Aldrich Chemie GmbH, Steinheim, Germany
Chloroform	Sigma-Aldrich Chemie GmbH, Steinheim, Germany
Cresyl violet acetate	Sigma-Aldrich Chemie GmbH, Steinheim, Germany
DMSO Dimethyl sulfoxide	Sigma-Aldrich Chemie GmbH, Steinheim, Germany
DTT	Dithiothreitol AppliChem GmbH, Darmstadt, Germany
EDTA	Ethylenediaminetetraacetic acid AppliChem GmbH, Darmstadt, Germany
Ethanol	AppliChem GmbH, Darmstadt, Germany
Ethidium bromide	Sigma-Aldrich Chemie GmbH, Steinheim, Germany
Genitacin (G418)	Sigma-Aldrich Chemie GmbH, Steinheim, Germany
Glycerol	Glycerin, AppliChem GmbH, Darmstadt, Germany
Glycine	AppliChem GmbH, Darmstadt, Germany
HEPES	Sigma-Aldrich Chemie GmbH, Steinheim, Germany
Hydrogen peroxide	Carl Roth GmbH + Co. KG, Karlsruhe, Germany
IGF-1	Sigma-Aldrich Chemie GmbH, Steinheim, Germany
Insulin	Sigma-Aldrich Chemie GmbH, Steinheim, Germany
Isopropanol	AppliChem GmbH, Darmstadt, Germany
Kanamycin	AppliChem GmbH, Darmstadt, Germany
LB-Agar	Sigma-Aldrich Chemie GmbH, Steinheim, Germany
LB-Medium	AppliChem GmbH, Darmstadt, Germany
Methanol 99%	Carl Roth GmbH + Co. KG, Karlsruhe, Germany
Magnesium chloride	Merck, Darmstadt, Germany
NP-40	Polyglycol ether (Nonidet® P40 Substitute) FLUKA

	Chemika/Biochemika Chemie AG, Buchs, Switzerland
PIPES	AppliChem GmbH, Darmstadt, Germany
PMSF	Phenylmethylsulphonylfluoride Sigma-Aldrich Chemie GmbH, Steinheim, Germany
Paraformaldehyde (PFA)	AppliChem GmbH, Darmstadt, Germany
Potassium chloride	Merck, Darmstadt, Germany
Sucrose	AppliChem GmbH, Darmstadt, Germany
SDS	Sodium dodecyl sulfate AppliChem GmbH, Darmstadt, Germany
Sodium fluoride	Merck, Darmstadt, Germany
Sodium bicarbonate	Carl Roth GmbH + Co. KG, Karlsruhe, Germany
Sodium chloride	Carl Roth GmbH + Co. KG, Karlsruhe, Germany
Sodium orthovanadate	Sigma-Aldrich Chemie GmbH, Steinheim, Germany
TAE	AppliChem GmbH, Darmstadt, Germany
TEMED	N,N,N',N'-Tetramethylethylenediamine Sigma-Aldrich Chemie GmbH, Steinheim, Germany
Tris	AppliChem GmbH, Darmstadt, Germany
TritonX-100	AppliChem GmbH, Darmstadt, Germany
Trizol	Invitrogen Corporation, Carlsbad CA, USA
Trypsin	Roche, Mannheim, Germany
TWEEN 20®	Polyoxyethylene (20) sorbitan monolaurate, Caesar and Lorentz GmbH, Bonn, Germany
Xylol	AppliChem GmbH, Darmstadt, Germany

2.2. Enzymes

DNase	Invitrogen Corporation, Carlsbad CA, USA
Proteinase K	Fermentas GmbH, St. Leon-Rot, Germany
RNase Out Ribonuclease Inhibitor	Invitrogen Corporation, Carlsbad CA, USA
Rnase A	Invitrogen Corporation, Carlsbad CA, USA
SuperScript II RT	Invitrogen Corporation, Carlsbad CA, USA
Rnase H	Invitrogen Corporation, Carlsbad CA, USA
Phusion	Finnzymes Oy, Vantaa, Finland
T4 DNA Ligase	Fermentas GmbH, St. Leon-Rot, Germany
XhoI	Fermentas GmbH, St. Leon-Rot, Germany
BamHI	Fermentas GmbH, St. Leon-Rot, Germany
SspI	Fermentas GmbH, St. Leon-Rot, Germany

GoTaq® Hot Start Polymerase	Promega Corporation, Madison, USA
Shrimp alkaline phosphates (SAP)	Fermentas GmbH, St. Leon-Rot, Germany

2.3. Vectors, Primer and supplies

Desoxy-Ribonucleotid-Triphosphate

dNTPs	Fermentas GmbH, St. Leon-Rot, Germany
Random Primer	Invitrogen Corporation, Carlsbad CA, USA
pCMV-Tag 2C	Agilent Technologies, Santa Clara CA, USA

2.4. Buffer and solution

SDS-PAGE running buffer	194mM Glycine 25mM Tris 0.1% SDS
4 x SDS sample buffer	250mM Tris-HCl (pH 6.8) 200mM DTT 40% Glycerol 8% SDS 0.01% Bromophenol blue
Stripping solution	62.5mM Tris-HCL pH 6.8 100mM β -mercaptoethanol 2%SDS
TBS buffer (pH 7.6)	137mM NaCl 20mM Tris
TBS-T buffer (pH 7.6)	137mM NaCl 20mM Tris 0.1% Tween 20®
Western Blot antibody solution	137mM NaCl 20mM Tris 5% Western Blocking Reagent (Roche)
Western Blot blocking solution	137mM NaCl 20mM Tris 10% Western Blocking Reagent (Roche)
Western Blot transfer buffer	194mM Glycin 25mM Tris 20% Methanol (99%) 0.05% SDS
DNA loading dye	50% Glycerin 5XTAE

2. Material and Methodes

CaCl ₂ buffer	60mM CaCl ₂ 15% Glycerin 10mM PIPES pH 7
Tail biopsies lysis buffer	100 mM Tris HCl (pH 8.5), 5 mM EDTA, 0.2% (w/v) SDS, 0.2M NaCl, 500 mg/ml proteinase K)
Cell lysis buffer	50 mM NaCl 50 mM Tris-HCl (pH 7.4) 5 mM EDTA 1 % Nonidet® P40 Substitute
Organ lysis buffer	50 mM HEPES (pH 7.4) 50 mM NaCl 1 % Triton X-100 10 mM EDTA 0.1 M NaF 17 µg/ml Aprotinine 2 mM Benzanidine 0.1 % SDS 1 mM Phenylmethylsulfonyl fluoride (PMSF) 10 mM Na ₃ VO ₄
Nuclear cell lysis buffer	420mM KCl 20mM HEPES 1mM EDTA 0,1mM Na ₃ VO ₄ 20% Glycerin
Cytosolic cell lysis buffer	10mM KCl 20mM HEPES 1mM EDTA 0,1mM Na ₃ VO ₄ 10% Glycerin 0,2% NP 40
Tricine gel buffer	3M TrisHCl pH8.45 0.3% SDS
10x Cathode buffer	1M Tris 1M Tricine 1% SDS pH 8.25
10x Anode buffer	2.1M Tris pH8.9
ECL, Amersham ECLTM Western Blotting Detection Reagents	GE Healthcare UK Ltd; England
Fetal bovine serum (FBS)	Invitrogen GmbH; Germany

Phosphate buffered saline 10 fold (pH 7.2)	Invitrogen GmbH; Germany
PageRuler™ Prestained Protein Ladder	Fermentas GmbH, St. Leon-Rot, Germany
Trypsin, 0.25% (1x) with EDTA	Roche, Mannheim, Germany
Western Blocking Reagent	Roche Diagnostics GmbH; Germany
DMEM High Glucose with Glutamax™, 4500mg/L Glucose, Sodium Pyruvate	PAA Laboratories GmbH, Cölbe; Germany

2.5. Cells and bacteria

OmniMax	Invitrogen Corporation, Carlsbad CA, USA
SHSY5Y	Sigma-Aldrich Chemie GmbH, Steinheim, Germany

2.6. Kits

RNeasy MiniKit	Qiagen GmbH, Hilden, Germany
RNeasy Lipid Tissue Mini Kit	Qiagen GmbH, Hilden, Germany
Qiaprep Spin Maxiprep Kit	Qiagen GmbH, Hilden, Germany
QiAquick Gel Extraction Kit	Qiagen GmbH, Hilden, Germany
Qiaprep Spin Miniprep Kit	Qiagen GmbH, Hilden, Germany
DeadEnd™ Fluorometric TUNEL System	Promega Corporation, Madison, USA
ELISA A β ₁₋₄₀	Invitrogen Corporation, Carlsbad CA, USA
ELISA A β ₁₋₄₂	Invitrogen Corporation, Carlsbad CA, USA
Effectene Transfection Reagent	Qiagen GmbH, Hilden, Germany
BrdU assay	Millipore, Billerica, MA, USA

2.7. Primary Antibodies

-Actin Antibody; Monoclonal mouse antibody detects an epitope conserved in human actin; MP Biomedicals, USA; Item # 69100; Western Blotting Dilution 1:5000

-ADAM 10 Antibody; Polyclonal rabbit antibody detects human ADAM10 (H-300); Santa Cruz Biotechnology, Inc., USA; Item # sc-25578; Western Blotting Dilution 1:1000

-ADAM 17/TACE Antibody; Polyclonal rabbit antibody detects human ADAM17/TACE; Assay Designs, Inc., USA; Item # 905249; Western Blotting Dilution 1:1000

-AKT Antibody; Polyclonal rabbit antibody detects endogenous levels of total AKT1, AKT2 and AKT3 proteins; Cell Signaling Technology, Inc., USA; Item # 9272; Western Blotting Dilution 1:1000.

-ApoE Antibody; Polyclonal goat antibody detects a peptide mapping the C-terminus of apoE of mouse origin; Santa Cruz Biotechnology, Inc., USA; Item # sc-6384; Western Blotting Dilution 1:1000

-APP C-Term (Amyloid Precursor Protein, C-Term) Antibody; Synthetic peptide developed in rabbit detects the C-terminal of human APP 695 (amino acids 676-695); Sigma-Aldrich, USA; Item # A8717; Western Blotting Dilution 1:1000

- α 2M Antibody Polyclonal goat antibody detects epitope mapping near the N-terminus of α -2M of human origin Santa Cruz Biotechnology, Inc., USA; Item # sc-8513; Western Blotting Dilution 1:1000

-BACE-1 (Beta Site APP Cleaving Enzyme 1) Antibody; Polyclonal rabbit antibody raised against amino acids 458 to 501 of human BACE; Chemicon (Millipore), USA; Item # AB 5832; Western Blotting Dilution 1:1000

-Beta Amyloid Antibody; Polyclonal rabbit antibody detects several isoforms of β -amyloid peptide ($A\beta$), such as $A\beta$ 1-40, $A\beta$ 1-42 etc, regardless of phosphorylation state; Cell Signaling Technology, Inc., USA; Item # 2454; Western Blotting Dilution 1:1000

-Caspase-3 Antibody; Polyclonal rabbit antibody detects endogenous levels of full length caspase-3 (35 kDa) and the large fragment of caspase-3 resulting from cleavage (17 kDa); ; Cell Signaling Technology, Inc., USA; Item # 9662; Western Blotting Dilution 1:1000

-Erk Antibody; Polyclonal rabbit antibody detects endogenous levels of total p44/42 MAP kinase (Erk1/Erk2) protein; Cell Signaling Technology, Inc., USA; Item # 9102; Western Blotting Dilution 1:1000

-Anti-Flag Affinity Gel; Anti-FLAG M2 binds FLAG at the N-terminal, Met-N-terminal, C-terminal and internal locations of fusion proteins; Sigma-Aldrich Chemie GmbH, Steinheim, Germany Item # A2220

-FoxO1 (C29H4) Antibody, Monoclonal rabbit antibody detects the C-terminus of endogenous FoxO1; Cell Signaling Technology, Inc., USA; Item # 2880; Western Blotting Dilution 1:1000

-FoxO1 (L27) Antibody; Polyclonal rabbit antibody detects the N-terminus of endogenous FoxO1; Cell Signaling Technology, Inc., USA; Item # 9454; Western Blotting Dilution 1:1000

-FoxO3a (75D8) Antibody; Monoclonal rabbit antibody detects exogenous and endogenous levels of FoxO3a; Cell Signaling Technology, Inc., USA; Item # 2497; Western Blotting Dilution 1:1000

-GFP (D5.1) Antibody; Monoclonal rabbit antibody detects exogenous GFP; Cell Signaling Technology, Inc., USA; Item # 2959; Western Blotting Dilution 1:1000

-GSK-3- β Antibody; Monoclonal rabbit antibody detects endogenous levels of total GSK-3 β protein; Cell Signaling Technology, Inc., USA; Item # 9315; Western Blotting Dilution 1:1000

-Holo APP Antibody; Polyclonal rabbit antibody detects endogenous levels of several isoforms of both mature and immature amyloid β (A4) precursor protein, including APP695, APP770 and APP751; Cell Signaling Technology, Inc., USA; Item # 2452; Western Blotting Dilution 1:1000

-HSF1 Antibody; Polyclonal rabbit antibody detects endogenous levels of total HSF1 protein; Cell Signaling Technology, Inc., USA; Item # 4356; Western Blotting Dilution 1:1000

-IDE Antibody; Polyclonal rabbit; Millipore Corporation 290 Concord Road, Billerica, MA 01821, USA; Item # AB9210; Western Blotting Dilution 1:1000

-IGF-1 Receptor β Antibody; Polyclonal rabbit antibody detects endogenous levels of IGF-IR β . Does not cross-react with insulin receptor; Cell Signaling Technology, Inc., USA; Item # 3027; Western Blotting Dilution 1:1000

-IR- β Antibody; Polyclonal rabbit antibody detects a peptide mapping at the C-terminus of insulin R β (C19) of human origin; Santa Cruz Biotechnology, Inc., USA; Item # sc-711; Western Blotting Dilution 1:1000

-IRS-1 Antibody; Monoclonal rabbit antibody detects C-terminal 14 amino acid peptide ([C]YASINFQKQPEDRQ) of rat liver IRS-1. Rat, mouse and human crossreactivity; Upstate Cell Signaling Solutions, USA; Catalog # 06-248; Western Blotting Dilution 1:1000

-IRS-2 Antibody; Polyclonal rabbit antibody detects endogenous levels of total IRS-2 protein; Cell Signaling Technology, Inc., USA; Item # 4502; Western Blotting Dilution 1:1000

-MnSOD Antibody; Polyclonal rabbit antibody detects MnSOD; Upstate Cell Signaling Solutions, USA; Catalog # 06-984; Western Blotting Dilution 1:1000

-Neprilysin Antibody; Polyclonal rabbit antibody; Millipore Corporation 290 Concord Road, Billerica, MA 01821, USA; Item # AB5458; Western Blotting Dilution 1:1000

-Anti-Oligomer (A11); Polyclonal rabbit antibody recognizes amino acid sequence-independent oligomers of proteins or peptides; Invitrogen Corporation, Carlsbad CA, USA, Catalog #AHB0052; Western Blotting Dilution 1:1000

-p27 (C-19) Antibody; Polyclonal rabbit antibody detects the C-terminus of p27; Santa Cruz Biotechnology, Inc., USA; Item #sc-528; Western Blotting Dilution 1:1000

-Phospho-AKT Antibody; Polyclonal rabbit antibody detects endogenous levels of AKT1 only when phosphorylated at Ser473. Also recognizes AKT2 and AKT3 when phosphorylated at the corresponding residues; Cell Signaling Technology, Inc., USA; Item # 9271; Western Blotting Dilution 1:1000

-Phospho-p44/42 MAP Kinase (Thr202/Tyr204) Antibody; Polyclonal rabbit antibody raised against endogenous levels of p44 and p42 MAP Kinase (Erk1 and Erk2) when phosphorylated either individually or dually at Thr202 and Tyr204 of Erk1 (Thr185 and Tyr187 of Erk2); Cell Signaling Technology, Inc., USA; Item # 9101; Western Blotting Dilution 1:1000

-Phospho-GSK-3 β (Ser9) Antibody; Polyclonal rabbit antibody detects endogenous levels of GSK-3 β only when phosphorylated at serine 9; Cell Signaling Technology, Inc., USA; Item # 9336; Western Blotting Dilution 1:1000

-Phospho-GSK-3 α / β (Ser21)/(Ser9) Antibody; Polyclonal rabbit antibody detects endogenous levels of GSK-3 α / β only when phosphorylated at serine 21 or 9; Cell Signaling Technology, Inc., USA; Item # 9327; Western Blotting Dilution 1:1000

-Phospho-FKHR (Ser319) Antibody; Polyclonal rabbit antibody detects a short amino acid sequence containing phosphorylated Ser319 of FKHR of human origin; Santa Cruz Biotechnology, Inc., USA; Item #sc-19807; Western Blotting Dilution 1:1000

-Phospho-FoxO3a (Ser253) Antibody; Polyclonal rabbit antibody detects endogenous levels of FoxO3a only when phosphorylated at serine 253; Cell Signaling Technology, Inc., USA; Item # 9466; Western Blotting Dilution 1:1000

-Presenilin 1 (C20) Antibody; Polyclonal goat antibody detects a peptide mapping at the C-terminus of Presenilin 1 of human origin; Santa Cruz Biotechnology, Inc., USA; Item # sc-1244; Western Blotting Dilution 1:1000

-PTEN Polyclonal Rabbit mAb detects endogenous levels of total PTEN protein; Cell Signaling Technology, Inc., USA; Item # 138G6; Western Blotting Dilution 1:1000

2.8. Secondary Antibodies

-Anti Goat IgG (whole molecule), peroxidase conjugated; Affinity isolated antigen specific antibody obtained from rabbit anti-goat antiserum by immunospecific purification; Sigma-Aldrich, USA; Item # A5420; Western Blotting Dilution 1:1000

-Anti Mouse IgG (Fab specific), peroxidase conjugated; Developed in goat using purified mouse IgG Fab fragment as immunogen, the antibody is isolated from goat anti-mouse IgG antiserum by immunospecific purification; Sigma-Aldrich, USA; Item # A9917; Western Blotting Dilution 1:15000

-Anti Rabbit IgG, peroxidase conjugated; Developed in goat using purified rabbit IgG as immunogen, the antibody is isolated from goat anti-rabbit IgG antiserum by immunospecific purification; Sigma-Aldrich, USA; Item # A6154; Western Blotting Dilution 1:1000

2.9. Material

-Blotting chamber Trans-Blot® Semi-Dry Transfer Cell
Bio-Rad Laboratories, USA

-Blotting membrane Immun-Blot™ PVDF Membrane for Protein Blotting
Bio-Rad Laboratories, USA

-Blotting paper Whatman® Gel Blotting Paper
Schleicher & Schuell, Germany

-Cover-slips Cover glasses 24 x 50 mm
VWR International GmbH, Germany

Cover-slips Cover glasses 12 mm
Medishop, Möglingen, Germany

-Culture culture dishes 145cm

Greiner Bio-One GmbH, Frickenhausen, Germany

-Culture culture dishes 10cm
Greiner Bio-One GmbH, Frickenhausen, Germany

-iCycler Thermocycler
Bio-Rad Laboratories, USA

-Gewebe-Homogenisator
VWR International GmbH, Germany

-Microplate reader Mithras LB 940 multimode microplate reader
Berthold Technologies GmbH & Co. KG, Germany

-Fluorescence Microscope Olympus IX81
Olympus Deutschland GmbH, Hamburg, Germany

-Micro-Radiography Faxitron x-Ray System
Faxitron BiopticsLincolnshire, USA

-Micro-Radiography films Agfa Structurix,D4 DW ETE, NDT Systems (18 x 24 cm)
Agfa-Gevaert, Sepestraat, Belgium

-Microscope slides Microscope slides 76x26 mm
Menzel GmbH &Co KG, Braunschweig, Germany

-Minigel-Twin Gel Electrophoresis Apparatus, Minigel-Twin
Biometra GmbH, Germany

-NanoDrop NanoDrop™ Spectrophotometer ND 1000
ThermoFisher Scientific, USA

-NMR Analyzer minispec mq7.5
Burker Optik, Ettlingen, Germany

-Photo-paper Amersham Hyperfilm™ ECL
GE Healthcare UK Ltd, England;

-Powerpac Biometra Standard Power Pack P25
Biometra GmbH, Germany

-Research Miroscope Olympus BX51
Olympus Deutschland GmbH, Hamburg, Germany

-Thermomixer
Eppendorf, Hamburg, Germany

Tube Rotator, STUART®
Bibby Scientific Limited, Staffordshire, UK

2.10. Methods

2.10.1. Mice breeding

FoxO1ADA and FoxO1DN expressing mice were crossed with Synapsin 1 promoter driven Cre recombinase expressing mice (SynCre) to ensure neuron-specific protein synthesis. Mice without APPsw or SynCre were used as controls. These mice were kept in a 12 hour light and dark cycle from 7a.m. to 7p.m. They were fed with standard rodent diet. Tg2576 mice which express APPsw were purchased from Taconic Corporate, Hudson, NY, USA and present a B6/SJL background. Experiments with the mice were performed in agreement with the German Laws for Animal Protection and were approved by the local animal care committee and the Bezirksregierung Köln.

2.10.2. Isolation of genomic DNA

Mouse tail biopsies were incubated over night in lysis buffer (tail biopsie lysis buffer and 500mg/ml proteinase K) in a thermomixer at 55°C. The DNA was then precipitated via addition of the equivalent volume of isopropanole. After mixing the lysates were centrifuged at 13.000rpm at room temperature for 15 minutes. Supernant was discarded and 150µl 70% Ethanol was added. The samples were mixed and centrifuged at 13.000rpm at room temperature for 15 minutes. Supernant was discarded, the pellet was dried and resuspended in 100mM TrisHCl pH8.

2.10.3. Polymerase chain reaction (PCR) for genotyping

DNA concentrations of tail biopsies lysis were measured with NanoDrop® ND-100 UV Spectrophotometer at 260nm. After that the DNA was used to genotype mice for expression of synapsin driven Cre recombinase, APPsw, and FoxO1ADA or -DN expression in the ROSA 26 locus. Reactions were performed in a Thermocycler PCR machine. All reactions contained not less than 100ng DNA, 25pmol of each primer (Table 1), 25µM dNTP Mix, 4mM MgCl₂, 10% DMSO, 1xgoTaq reaction buffer and 1 unit of goTaq DNA polymerase.

Primer	Sequence	Orientation
SynCre 5´	ACCTGAAGATGTTTCGCGATTATCT	sense
SynCre 3´	ACCGTCAGTACGTGAGATATCTT	antisense
Tg2576 5´	CTGACCACTCGACCAGGTTCTGGG	sense
Tg2576 3´	GTGGATAACCCCTCCCCCAGCCTAGACCA	antisense
FoxO1 5´	AAAGTCGCTCTGAGTTGTTATC	sense
FoxO1 3´	TGTCGCAAATTAAGTGTGAATC	antisense
FoxO1 3´	GATATGAAGTACTGGGCTCTT	antisense

Table 1: Primer sequences of SynCre, Tg2576 and FoxO1 in ROSa26 locus.

PCR programmes are presented in table 2. Resulting DNA fragments were used for Gelelectrophoresis on 2% (w/v) agarose gels (1 x TAE, 0.5 µg/ml ethidium bromide) and separated at 120V.

Programm	Cycles	Degree	Time
SynCre	single	95 °C	5min
	45 repeats	95 °C	30sec
		55 °C	45sec
		72 °C	45sec
	single	72 °C	10min
		4 °C	∞
Tg2576	single	94 °C	5min
	35 repeats	94 °C	30sec
		66 °C	45sec
		72 °C	45sec
	single	72 °C	7min
		4 °C	∞
FoxO1	single	94 °C	3min
	45 repeats	94 °C	30sec
		56 °C	45sec
		72 °C	1.5min
	single	72 °C	10min
		4 °C	∞

Table 2: PCR Programms for SynCre, Tg2576 (APP) and FoxO1 in the ROSA26 locus.

To distinguish mice with FoxO1ADA or FoxO1DN located in the ROSA26 locus another PCR was established. Contents of the PCR reaction are presented above. The primers used for this PCR are presented in table 3.

Primer	Sequence	Orientation
FoxO1ADA and DN	GACATGGTAAGTAAGCTTATA AC	sense
FoxO1ADA and DN	AGAGAATAGGAACTTCGGAAT AG	antisense

Table 3: Primer used for the PCR to distinguish FoxO1ADA and –DN.

PCR Programm to distinguish FoxO1ADA and –DN mice is shown in table 4:

Programm	Cycle	Degree	Time
FoxO1ADA and -DN	single	98 °C	2min
	32 repeats	98 °C	30sec
		50 °C	45sec
		72 °C	6min
	single	72 °C	10min
single	4 °C	∞	

Table 4: PCR Program to distinguish FoxO1ADA and –DN.

2.10.4. Metabolic characterization

Mice were weaned at the age of 4 weeks. After that body weight and blood glucose via blood glucose meter (GlucoMen, A. Menarini diagnostics, Berlin-Chemie, Neuss, Germany) were measured every week until the age of 12 weeks. Then body weight and blood glucose were checked every 4 weeks. Blood was collected from the tail tip. At the age of 10 and 11 weeks insulin and glucose tolerance tests were performed. For insulin tolerance tests mice were starved overnight for 16 hours. Afterwards 0.75U per kg body weight of human insulin (Novo Nordisk, Copenhagen, Denmark) was injected into the peritoneal cavity. During this test blood glucose was measured before and 15, 30 and 60 minutes after the injection of insulin. Results are presented in % of initial blood glucose level. For glucose tolerance tests mice were also starved overnight. Then the mice were injected with 2g per kg body weight of glucose solution into the peritoneal cavity. Blood glucose was measured before and 15, 30, 60 as well as 120 minutes after the injection of glucose solution via glucose meter. Results are shown in mg/dl.

2.10.5. Investigation of body composition

To measure body composition of mice nuclear magnetic resonance (NMR) was used. (NMR Analyzer minispec mq7.5). Radiofrequency (RF) pulse sequences are transmitted into the tissue via minispec. After that hydrogen produces RF signals were measured by the

minispec. The character of the analysed tissue is identified by the amplitude and duration of the responding signal.

2.10.6. Brain lysates

The different brain regions were lysed in organ lysis buffer via a hand homogenizer. Lysates were then rotated on a tube rotator at 4°C for 45 minutes. Afterwards lysates were centrifuged at 13.000rpm at 4°C. The supernant was added into a new tube and the pellet was discarded.

Protein levels were measured using the Bradford method. Bradford reagent was diluted 1:5 and 99µl were added to 1µl of each sample in a 96well plate. Standard curve was generated with 0, 1, 2.5, 5 and 10µg of BSA. Detection of protein levels were performed at 600nm via a microplate reader. Protein expression levels were analysed with 100µg protein of lysates in Laemmli buffer. The samples were denatured at 95°C for 5 minutes and then resolved on SDS-PAGE.

2.10.7. SDS-PAGE

Sodium dodecyl sulfate (SDS) polyacrylamide gel electrophoresis (PAGE) also called SDS-PAGE is used to separate proteins with regard to their molecular mass. Proteins are denatured and linearized by heat and anionic detergent SDS. Such samples are negatively charged in proportion to its molecular mass. Samples are supplied to the polyacrylamide gel in a gel apparatus (Minigel-Twin) filled with 1xSDS-PAGE running buffer. An electric current is applied and the negatively charged proteins migrate through the gel with different speed depending on the molecular size of the proteins. Small proteins migrate more easily through the gel while larger proteins migrate more slowly. The stacking gel collects the proteins and the resolving gel seperates the proteins according to their molecular size. The resolving gel shows a contcentration from 8, 10 or 15% acrylamide (Table 5). The different concentrations are dependent on the molecular size of the proteins of interest. 8% resolving gels are used for proteins with high molecular weight and 15% resolving gels are used for small molecular weight proteins.

Chemicals	Stacking Gel	Resolving Gel [8%]	Resolving Gel [10%]	Resolving Gel [15%]
ddH ₂ O	2.74ml	7.14ml	6.34ml	3.5ml
1M TrisHCl	0.5ml			
3M TrisHCl		1.5ml	1.5ml	1.3ml
10% SDS	40µl	120µl	120µl	105µl
30% Acrylamid	680µl	3.2ml	4ml	5.25ml
10% APS	80µl	160µl	160µl	140µl
TEMED	4µl	12µl	12µl	10.5µl

Table 5: SDS-PAGE Gels (2 mini gels).

Polyacrylamide gels contain the catalyst of polymerization Ammonium-persulfate (APS). N,N,N',N'-tetramethylethylenediamine (TEMED) is added at last to initiate polymerization. Samples and 10µl PageRuler™ Prestained Protein Ladder is added on the gel. Electrophoresis of samples in the stacking gel is promoted at 120V and in the resolving gel at 150V.

2.10.8. Western Blot

Western blot were performed to transfer the seperated proteins on the polyacrylamidegel to a polyvinylidene difluoride (PVDF) membrane via electrophoresis using semidry-blotting. An electric current transfers the negative charged proteins from the polyacrylamid gel onto the PVDF membrane (7x9cm). First three transferbuffer soaked whatman papers (7x9cm) were placed on a horizontally localized cathode plate. Then the PVDF membrane was incubated in 99% methanol for 30sec and put onto the whatman papers. After cutting off the stacking gel, the resolving gel is placed on the membrane and covered by three additional transferbuffer soaked whatman papers. Air bubbles were removed by carefully rolling over the stack with a pipette. Then the anode plate is placed on top of the stack. These two electric plates are close to each other because only seperated by the stack to provide a high field strength (V/cm) for the protein transfer.

The transfer was performed with an electric current of about 200 milli-ampere (mA). The time of transfer was dependent on the molecular mass of the proteins of interest. Proteins with a size up to 100kDa were transferred for 1 hour, proteins with a higher molecular mass for 1.5 hours. Afterwards the gel and whatman papers were discarded and the membrane was incubated in blocking solution (10% western blocking solution in 1xTBS) for 1 hour at room temperature to saturate vacant membrane protein binding sites. Then the membrane was incubated with the primary antibody to detect the protein of interest (antibody in 5% western blocking solution in 1xTBS) over night at 4°C. Subsequently the membrane was washed four times every 15 minutes with 1xTBS consisting of 0.1 % TWEEN 20® (TBS-T). These

processes were performed on a rocker at room temperature and removed unbound antibodies. After that the membrane was added to the secondary antibody solution (antibody in 5% western blocking solution in 1xTBS) for 1 hour. The secondary antibody was conjugated to horseradish peroxidase (HRP) via protein cross-linking. Afterwards the membrane was washed four times for each 15 minutes with TBS-T. Enhanced chemiluminescence (ECL) assay was used to detect proteins of interest with photographic film. β -actin served as loading control. For phosphorylated proteins the unphosphorylated form of the protein served as loading control.

ECL displays a light-emitting system. The HRP conjugated to the secondary antibody catalyzes the oxidation of luminol which causes light emitting. This light can be detected on a photograph film and further analysed by densitometry. For this detection membrane is incubated in two detecting reagents (Amersham ECL™ Western Blotting Detection Reagent), which are mixed together with the same volume of each substance for 1 minute. Afterwards the membrane was covered with plastic foil and placed into a metal cassette. In a darkroom the membrane was exposed to a photosensitive film (Amersham™ Hyperfilm ECL). The time of exposure depended on the intensity of emitted light and lasted from 10 seconds to 30 minutes. Then the film was developed (CURIX60, Agfa-Gevaert, Sepestraat, Belgium).

The PVDF membrane was cleared from antibodies, called stripping to be incubated with an antibody detecting another protein. This was performed once for each blot to obtain proper protein detection. The membrane was incubated in stripping solution at 60°C for 20 minutes in a shaking water-bath. Then the membrane was washed for four times in TBS-T followed by blocking (10% western blocking reagent in 1xTBS) for 1 hour at room temperature. Afterwards another primary antibody could be added to the membrane.

2.10.9. Urea Tricine gel

Proteins with small molecular mass like A β with a size of 4kDa were separated with a Urea Tricine gel (table 6) following the same principle like in 2.9.8. 200 μ g of proteins denatured in Laemmli-buffer were added to gel located in a gel apparatus with 1x cathode and 1x anode buffer. The transfer of the proteins was also done with the cathode and anode buffer. The transfer was performed with 100mA for 30 minutes. After that the procedure was the same as for western blot.

Chemicals	Stacking Gel	Resolving Gel
40% Acrylamid	1.05ml	5ml
Tricine Gel buffer	2.5ml	5ml
70% Glycerol		2ml
H ₂ O	6.7ml	3.1ml
10% APS	80µl	66µl
TEMED	8µl	6.6µl

Tabel 6: Tricine Gel (2 mini gels). Addition of 7.2 g Urea to resolving gel was used for protein expression analysis with small molecular size of 4 kDa.

2.10.10. Dot Blot

Dot Blots detect the level of oligomeric A β in lysates of hippocampi from Tg2576, FoxO1ADA/Tg2576 and FoxO1DN/Tg2567 mice. 5, 10 and 25 µg of proteins from lysates produced as described in 2.9.6. were spotted on a PVDF membrane at 4°C. After the membrane dried it was incubated for 30sec in 9% methanol and then blocked in 10 western blocking reagent in 1xTBS overnight at 4°C on a rocker. Afterwards the membrane was incubated in Oligomer A11 antibody (antibody dilution 1:1000 in 5% western blocking reagent in 1xTBS) for 1 hour at room temperature. After that the membrane was washed three times every 5 minutes. Then the secondary antibody was added which was also used for western blots. This incubation step needed 1 hour at room temperature. Another washing step for three times every 5 minutes was performed before ECL was added and results were detected with a photograph film.

2.10.11. ELISA β -Amyloid_{40/42}

β -amyloid from hippocampi of Tg2576, FoxO1ADA/Tg2576 and FoxO1DN/Tg2567 mice was extracted with 5M guanidine HCl in 50mM Tris HCl pH8.0. Afterwards ELISAs were performed to detect the level of A β 40 and A β 42 according to the protocol of the manufacturer (Cat# KHB3482/ 3442; Invitrogen Corporation, Carlsbad, CA, USA).

2.10.12. Statistical analysis

The software AIDA (Version 4.00.027, Raytest, Straubenhardt, Germany) was used to quantify changes in optical density of western blot signals. Statistical analysis of different study groups was performed by Student's t-test. Statistical significance was reached when the p-value was p<0.05.

For Kaplan-Meier analysis XLSTAT-Life software was used (Microsoft Excel add-in; www.xlstat.com). To compare the different mouse study groups Wilcoxon rank tests were used. In addition statistical significance was reached at a p-value of $p \leq 0.05$.

2.10.13. Histology

SynCre mice were crossed with FoxO1ADA or FoxO1DN mice in Tg2576 background. Mice were anesthetized and transcardially perfused with physiological saline solution and then with 4% paraformaldehyde (PFA) in 0.1M phosphate-buffered saline (PBS pH7.4). Brains were incubated in 4% PFA over night and then for three days in 20% sucrose in PBS pH7.4 at 4°C. Then brains were frozen in tissue-freezing medium (Jung Tissue Freezing Medium; Leica Microsystems, Wetzlar, Germany). These samples were axially sectioned via Research Cryostat Leica CM3050 S (Leica, Wetzlar, Germany) harvest on slides and stored at -80 °C.

Nissl staining

Frozen sections were dried at room temperature and then washed with distilled water for 30 seconds. Afterwards sections were stained in Nissl staining solution (0.1% Cresyl violet in distilled water) for 20 minutes followed by an additional washing step in distilled water for 30 seconds. The length of the next steps was dependent on the speed of destaining of sections. Sections were incubated in 40%, then 70%, 95% and at last in 100% ethanol for up to 10 minutes for each step. Afterwards slides were incubated in Xylol for 5 minutes and additional in fresh Xylol for 2 minutes. Slides were dried and mounted in Entellan (Merck, Catalog # 1079610100, Darmstadt, Germany). Pictures were taken with a Research Microscope Olympus BX51.

2.10.14. RNA Isolation

RNA isolation of hippocampi for microarray studies was performed with RNeasy Lipid Tissue Mini Kit according to the protocol of the manufacturer (Qiagen GmbH, Catalog # 74804, Hilden, Germany)

RNA of liver, hypothalamus and pituitary for cDNA synthesis and realTime analysis was first precipitated with Trizol and then use of the RNeasy Mini kit (Qiagen GmbH, Hilden, Germany) to cleanup the isolated RNA.

The tissue was first homogenized at 4°C and then incubated in 1ml Trizol at room temperature. Afterwards the tissue was “needeled” using a needle and the syringe to draw out the lysates. After that 200µl chloroform were added to the tissue lysates and incubated

for three minutes at room temperature. Then the samples were centrifuged at 13.000rpm and 4°C for 15 minutes. RNA was localized in the aqueous phase and supplied to a new tube. 500µl Isopropanol were added to the RNA and incubated at room temperature for 10 minutes. Then the samples were centrifuged at 13.000rpm and 4°C for 10 minutes. After this the supernant was discarded and the pellet washed with 70% ethanol. The samples were additionally centrifuged at 10.000rpm 4°C for 5 minutes. Then the supernant was discarded and the pellets were dried at room temperature. After the pellets were dry they were resuspended in 30µl DEPC water. Then RNA concentration was measured via NanoDrop at 260nm.

2.10.15. cDNA synthesis

cDNA synthesis was performed to analyse mRNA level of the target gene via realTime PCR or Microarrays.

For all steps of cDNA synthesis an iCycler was used. First 3µg RNA in a total volume of 8µl was used as well as 1xDnase buffer and 1Unit Dnase. This reaction was incubated at 37°C for 15 minutes. Then 2.5mM EDTA was added to the reaction and incubated at 68°C for 15 minutes to inactivate the Dnase. For the next step the cDNA synthesis started with the addition of 200ng random primer and 770µM dNTPs and incubation at 65°C for 5 minutes followed by 4°C for 5 minutes. Next 1xFirst-strand buffer, 5µM DTT and 40Units Rnase Out Ribonuclease inhibitor were added, gently mixed and incubated at 42°C for 5 minutes. Afterwards 200Units of SuperScript II reverse transcriptase were added and following incubation steps were performed: 25°C for 10 minutes, 42°C for 50 minutes, 70°C for 15 minutes to inactivate the enzymes and 4°C for 2 minutes. Then 2Units of Rnase H were added and incubated at 37°C for 20 minutes. The cDNA concentration was measured at 260nm with NanoDrop.

2.10.16.realTime PCR

cDNA amplification was performed using TaqMan Gene Expression Master Mix and TaqMan Gene Expressing Assays (Mm01303638_m1 for GHR, Mm01250745_m1 for GHRH, Mm01326479_m1 for GHRHR and Mm00439560_m1 for IGF-1; Applied Biosystems). HPRT1, GUSB and β-Actin (Mm00446968_m1 for HPRT1, Mm00446953_m1 for GUSB and Mm00607939_s1 for β-Actin; Applied biosystems) served as endogenous control. Quantitative PCR was performed via the Applied Biosystems 7900 HT (Darmstadt, Germany). Analysis was performed via comparative method ($\Delta\Delta CT$).

2.10.17. Behavioral studies and calorimetry

Behavioural studies and calorimetry were performed to test whether neuronal specific expression of FoxO1ADA and –DN cause any changes in behaviour, memory or calorimetry. For the following tests only SynCre/FoxO1ADA and –DN male mice were used. Morris Water Maze, Elevated O-Maze, Open Field and calorimetry were performed by Dr. Hella Brönneke, Mouse Facility, University of Cologne.

RotaRod

The RotaRod is an analysis of motion. Mice were placed on a rotating wheel with different speeds and the time was measured until the mice fell off the wheels. First the mice had to learn to run on the wheels. After this period the measurements were performed at 4, 8, 16rpm and accelerated speed.

Morris Water Maze Test

The Morris Water Maze test is to check regional learning and memory. Each mouse was tested for 5 days. During this period the mice have to learn the position of the platform which is located 1cm under the surface of the water which is coloured so that the mouse could not see the platform. For orientation outside of the water basin different signs were located on each wall like a square or a circle. The last day of the analysis the platform was removed and the time each mouse swam in the quadrant the platform was before was measured. Documentation was performed via video system.

Elevated O-Maze Test

The Elevated O-Maze test is an established method to analyse fear and explorative behaviour. Each mouse was placed on a ring-shaped runway which contains two open and two closed sections. The closed sections are bordered by walls with a height of 10cm. Analysis was performed via video system.

Open Field Test

The Open Field Test analyses fear and explorative behaviour. Each mouse was placed into a 50 x 50cm box with 40cm high walls. Light was adjusted to the middle of the box and the surrounding was shadowy. Documentation was performed via video system.

Indirect Calorimetry

Mice were kept in specific cages for 3 days. During that time activity of the animals, food and water intake, energy expenditure and the respiratory quotient were measured. Computertomography (CT) was used to measure lean body mass and fat content.

2.10.18. False-coloure imaging

X-ray images of mice were performed via the Faxitron x-Ray System. Images were taken with Agfa Structurix film and parameters were 55 kv for 30 sec. False-coloure images were done with the computer program Morphomet v1.1.3 (Dipl.-Ing. Zenon Wrzosek) by Jutta Knifka (Anatomie, University of Cologne).

2.10.19. Cloning strategy

Template for amplification of FoxO1ADA and -DN were pCAGS-FoxO1ADA and DN. Wild type FoxO1 was amplified from cDNA from wild type mouse brains. PCR reactions contained 20µM dNTPs, 1 Unit of Phusion Polymerase with proof reading, 25pmol of each primer (table 7), 10% DMSO, 1xHF buffer and 100ng of template DNA. The primers inserted specific digestion enzyme sites into the sequence in front of the start codon and after the stop codon of the target gene. The inserted site in front of the start codon of the gene is digested by BamHI and the site after the stop codon is digested by XhoI.

Primer	Sequence	Orientation
FoxO1BamHI 5´	AAACGGATCCGTATGGCCGAAGCGCCCCAG	sense
FoxO1XhoI 3´	AAACTCGAGTTAGCCTGACACCCAGCTGTGTG	antisense
FoxO1DNXhoI	AAACTCGAGGTCCATGGACGCAGCTCTTCTCCG	antisense

Table 7: Primer for cloning of FoxO1WT, FoxO1ADA and FoxO1DN.

To amplify the FoxO1ADA, -DN and the wild type form of FoxO1 (FoxO1WT) a gradient PCR (iCycler) was used. PCR program is shown in table 8. The temperature gradient was between 50 and 75°C. The elongation time was dependent on the amplified gene. FoxO1ADA and FoxO1WT were amplified for 3 minutes; FoxO1DN was amplified for one minute.

Programm	Cycle	Deegree	Time
Amplification of FoxO1, FoxO1ADA and -DN	single	98°C	2min
	32 repeats	98°C	30sec
		50-65°C	45sec
		72°C	1-3min
	single	72°C	10min
single	4°C	∞	

Table 8: PCR program to amplify FoxO1ADA, -DN and FoxO1 wild-type (FoxO1WT).

Amplified fragments were separated on a 1% Agarose gel (in TAE). Fragments were cut out of the gel and were extracted via the QiAquick Gel Extraction Kit (Qiagen GmbH, Hilden, Germany) according to the protocol of the manufacturer.

Digestion and Ligation

Fragments and the vector pCMV-Tag2C were then double digested by BamHI and XhoI (10Units enzyme per 1kb DNA). The restriction reaction was incubated for 2 hours at 37°C. In case of the vector during the last 45 minutes of incubation 4Units of shrimp alkaline phosphatase were added. This phosphatase was then inactivated at 60°C for 10 minutes. The digested vector was separated via a 1% Agarose gel and cut out. Then the vector and digested fragments were cleaned up with the QiAquick Gel Extraction Kit (Qiagen GmbH, Hilden, Germany) according to the protocol of the manufacturer.

For Ligation 5Units of T4 DNA Ligase (Fermentas GmbH, St. Leon-Rot, Germany), 20ng vector, 40ng of the fragment and 1xT4 DNA Ligase buffer were used. The ligation was incubated at room temperature overnight.

Transformation and Plasmid isolation

Transformation of CaCl₂-competent *Escherichia coli* (Omnimax) is performed to amplify a specific vector in shaking culture of 100ml LB-medium followed by isolation of the Plasmid (Qiaprep Spin Maxiprep Kit, Qiagen GmbH, Hilden, Germany) or to separate single bacteria colonies on a agar plate. Both medium and agar plate contain the specific antibiotic to guarantee bacteria growth which include the vector with the specific antibiotic resistance gene.

For transformation of CaCl₂-competent *E. coli* bacteria were incubated at 4°C with 7µl of the ligation reaction added for 25 minutes. After that a heat shock is performed at 42°C for 1.5 minutes. Then bacteria were harvested at 4°C for 5 minutes followed by addition of 400µl of LB-medium and shaking at 37°C for one hour. Afterwards the bacteria were plated on an

agar plate (kanamycin 25µg/ml) which had to dry and th was then incubated at 37°C overnight in a bacteria incubator (BINDER GmbH, Tuttlingen, Germany).

The next day single bacteria colonies were grown. These colonies were picked and each added to single tubes with LB-medium (kanamycin 25µg/ml) and shaken in a bacteria shaker (INFORS AG, Bottmingen, Switzerland) at 37°C overnight.

Plasmids were isolated using the Qiaprep Spin Miniprep Kit (Qiagen GmbH, Hilden, Germany) according to the protocol of the manufacturer. The plasmids of the single bacteria clones were digested with BamHI and XhoI as described above to identify plasmids which contain the target gene. These plasmids were sequenced via T3 and T7 sequencing primers (Eurofins MWG Operon, Ebersberg, Germany). Plasmids which showed disruptions of the target gene like frame shifts were again transformed into CaCl₂-competent *E. coli*, grown in 100ml shaking LB-medium culture followed by isolation of the plasmid (Qiaprep Spin Maxiprep Kit, Qiagen GmbH, Hilden, Germany) to obtain an increased amount of it for further transfection.

Generation of CaCl₂-competent *E. coli*

CaCl₂-competent *E. coli* were grown in 100ml LB-medium at 37°C overnight in a bacteria shaker (INFORS AG, Bottmingen, Switzerland). Then 2ml of this culture was added to new 200ml LB-medium and shaken at 37°C until the culture reached an OD₆₀₀ of 0.4. Measurements were performed with NanoDrop. The bacteria culture was incubated at 4°C for 10 minutes to stop growth. Then the culture was centrifuged at 3000rpm at 4°C for 5 minutes. The supernant was discarded and bacteria were resuspended in 100ml CaCl₂-buffer. Afterwards this suspension was incubated at 4°C for 25 minutes and then centrifuged at 3000rpm and 4°C for 4 minutes. The supernant was discarded and the pellet was resuspended in 5ml CaCl₂-buffer. Bacteria were separated in 100µl aliquots and harvested at -80°C.

2.10.20. Generation of stably expressing cells

The pCMV-Tag 2C vector containing FoxO1ADA, -DN or WT (2µg), were linearized with 4Units Sspl for 2 hours at 37°C. Transfection of SHSY5Y cells was performed via Effectene (Quiagen GmbH, Hilden, Germany) according to the protocol of the manufacturer. SHSY5Y cell transfected with the empty vector were used as controles (EV). Cells were treated with selection medium containing 1mg/ml G418 (Sigma-Aldrich Chemie GmbH, Steinheim, Germany) two days after transfection. Single cells were separated on 96-well plates after 3 weeks of selection with G418. Cell clones were tested for expression of FoxO1ADA, -DN or –

WT and positive clones were used for further experiments. After that cells were grown without G418.

2.10.21. Cell lysates

For whole cell lysates, cells were twice washed with PBS and then incubated at -80°C for 30 minutes. After that cell lysis buffer was added to the cells (100µl for 10cm plates and 150µl for 15cm plates). Then cells were scraped up from the culture dishes via cell scraper (Greiner Bio-One GmbH, Frickenhausen, Germany), incubated at 4°C for 30 minutes and needed. Afterwards cell lysates were centrifuged at 13.000rpm and 4°C for 30minutes. Supernant was added into a new tube and the pellet was discarded.

Cytosolic and nuclear lysates

For cytosolic and nuclear lysates the cells were washed twice with PBS and then cytosolic lysis buffer was added (100µl for 10cm plates and 150µl for 15cm plates). Then cells were scraped off the culture dishes and incubated at 4°C for 30 minutes. Afterwards the lysates were centrifuged at 1.600rpm and 4°C for 20 seconds. Supernant was again centrifuged at 1.600rpm and 4°C for 5 minutes. Then the supernant was needed and centrifuged at 13.00rpm and 4°C for 30 minutes. The supernant was added to a new tube and used as a cytosolic fraction. The pellet of the first centrifugation step was used to generate the nuclear fraction. To the pellet nuclear lysis buffer was added (100µl for 10cm plates and 150µl for 15cm plates), incubated at 4°C for 30 minutes and needed. After that lysates were centrifuged at 13.000rpm and 4°C for 30 minutes. The supernant was added to a new tube and used gain as a nuclear fraction. The protein concentration was measured using the Bradford method.

2.10.22. Stimulation of cells with IGF-1

Cells were starved overnight (14h) in medium without FBS. Then they were stimulated with medium containing 0, 1, 10 and 100nM IGF-1 for 5 minutes. After that the cells were immediately washed twice with PBS and harvested at -80°C. Subsequently cell lysates are produced (2.9.21).

2.10.23. Proliferation assay

Proliferation assay was performed with 1000 cells per well of each cell line. For FoxO1ADA, -DN and -WT stably expressing cells 3 clones were analyzed. First cells were counted using the Neubauer Zählkammer and 1000 cells were put into a well of a 96-well plate. The next day cells were starved in a medium without FBS overnight (14h) to stop cell proliferation. After that a medium with 10% FBS was added for 8 hours. Subsequently the proliferation assay (BrdU assay, Millipore, Billerica, MA, USA, item #HCS201) was performed according to the protocol of the manufacturer.

2.10.24. Apoptosis in cells

Analysis of apoptosis was performed with the induction of oxidative stress via hydrogen peroxide. First circled single cover slips were added into each well of a 24 well plate. These cover slips were coated with 30µg/ml of collagen (Biochrom AG, Berlin, Germany) in PBS at 4°C overnight. Subsequently 1.5×10^5 cells per well were added. The next day these cells were starved for 4 hours followed by addition of 500µM hydrogen peroxide overnight (14h). The next steps were performed according to the protocol of the manufacturer (DeadEnd™ Fluorometric TUNEL System; Catalog #G7130; Corporation, Madison, USA). After that the cells were mounted with Vectashield mounting medium (Vector Laboratories INC. Catalog # H-1200, Burlingame, USA).

3. Results

Clinical studies have shown that Alzheimer's disease and type 2 diabetes are linked to each other (Janson et al. 2004; Ott et al. 1999; Stewart and Liolitsa 1999; Lovestone 1999). Results from these studies demonstrated that the IR/IGF-1R signaling pathway is disturbed in patients suffering from AD (Frolich et al. 1998; Frolich et al. 1999; Moloney et al. 2010). Therefore AD is described as a "brain type diabetes" (Pilcher, 2006). The knockout of IRS-2 (IRS-2^{-/-}) or the neuron-specific IGF-1R knockout (nIGF-1R^{-/-}) in Tg2576 mice, a well established mouse model of AD expressing the Swedish mutation of APP (APP^{sw}) (Vassaret et al. 1999; De Strooper 2003; Holsinger et al. 2002; Sinha et al. 1999; Harada et al. 2006) causes decreased accumulation of A β and rescues Tg2576 mice from their premature death (Freude et al., 2009).

The clearance of A β is affected by the IR/IGF-1R signaling pathway. In earlier studies it has been shown that the IR/IGF-1R signaling pathway might induce the expression of IDE (Zhao et al. 2004) indicating a potential role of the IR/IGF-1R signaling pathway in the pathogenesis of AD.

Furthermore *C. elegans* it has been demonstrated that DAF-16, the orthologue of mammalian FoxO transcription factors regulated via the IR/IGF-1R signaling cascade, is involved in detoxification of A β (Cohen et al., 2006). FoxO1 is mainly expressed in the striatum, dentate gyrus and ventral hippocampus (Hoekman et al., 2006) regions which are highly affected in AD. Therefore the present study analyses the role of FoxO1 for amyloid pathology. Two different mouse lines were used FoxO1ADA as well as FoxO1DN were inserted into the Rosa26 locus and neuron-specifically expressed. An activated IR/IGF-1R signaling pathway stimulates AKT which in turn inactivates FoxO1 mediated transcription. AKT phosphorylates FoxO1 at Thr24, Ser256 and Ser319 (Biggs et al., 1999; Brunet et al., 1999; Kops et al., 1999; Rena et al., 1999; Tang et al., 1999) and promotes binding to 14-3-3 and nuclear export followed by degradation. In case of inactivated IR/IGF-1R signaling FoxO1 stays in the nucleus and promotes transcription of its target genes (Brunet et al., 1999). FoxO1DN is the dominant negative form of FoxO1 and displays a deletion of the nuclear export signal and the transactivation domain. This form remains in the nucleus and binds to the target promoter region but cannot mediate transcription. FoxO1ADA harbours amino acid replacements of the phosphorylation sites recognized by AKT. Therefore FoxO1ADA is not phosphorylated by AKT and constitutive active (Fig. 8).

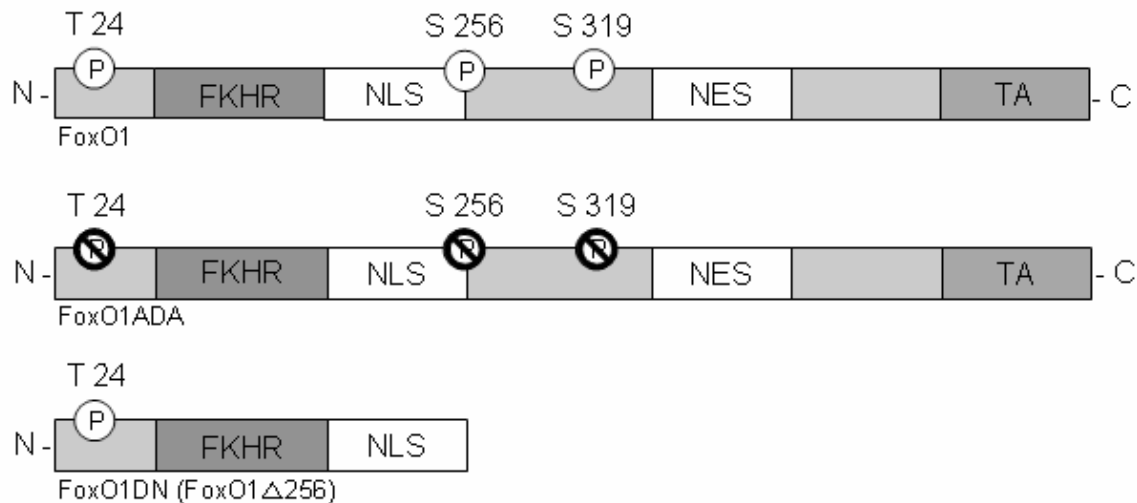


Figure 8: Structure of FoxO1, FoxO1ADA and FoxO1DN. FoxO1 contains a conserved forkhead domain (FKHR), the DNA binding domain. Furthermore it contains a nuclear localisation signal (NLS), a nuclear export signal (NES), a transactivation domain (TA) and the three phosphorylation sites of AKT (T24, S256 and S319). FoxO1ADA harbours amino acid substitutions leading to a constitutive active FoxO1 form. FoxO1DN is dominant negative and displays a transactivation domain and NES deletion.

Male mice with FoxO1ADA or FoxO1DN inserted into the Rosa26 locus were crossed with female mice expressing the synapsin 1 promoter driven Cre recombinase (SynCre) to guarantee a neuron-specific expression of the two FoxO1 forms. The female SynCre/FoxO1ADA or SynCre/FoxO1DN mice were then crossed with Tg2576 mice to generate those with neuron-specific expression of FoxO1ADA or FoxO1DN in Tg2576 background (Fig. 9).

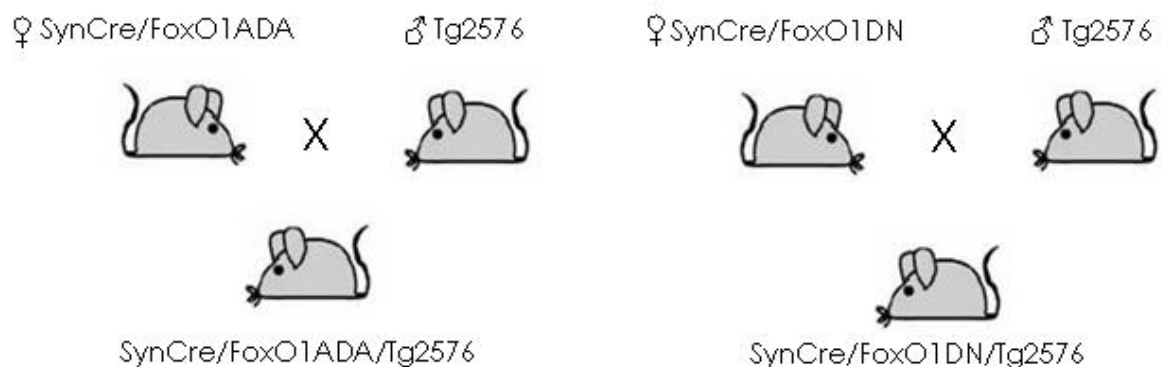


Figure 9: Breeding strategy of neuron-specific expressing FoxO1ADA and FoxO1DN mice in Tg2576 background. Mice with FoxO1ADA or FoxO1DN inserted in the Rosa26 locus were crossed with synapsin 1 promoter driven Cre recombinase expressing mice. Female mice were then crossed with Tg2576 mice to generate neuronal expressing FoxO1ADA or FoxO1DN mice in Tg2576 background.

For the following results “FoxO1DN” and “FoxO1ADA” represent mice expressing the synapsin 1 promoter driven Cre recombinase and FoxO1DN or FoxO1ADA inserted into the Rosa26 locus. Thus FoxO1ADA and FoxO1DN mice express the particular FoxO1 form in a neuron-specific manner.

3.1. Verification of FoxO1DN expression in mice

The FoxO1DN insert in the Rosa26 locus was detected via the FoxO1DN and –ADA specific PCR (2.9.3.). The primers bind to the sequence which flanks the inserted gene. The size of the amplified DNA fragment shows whether each animal is FoxO1ADA or FoxO1DN positive. The amplified fragment of FoxO1DN shows a size of about 750bp (Fig. 10A).

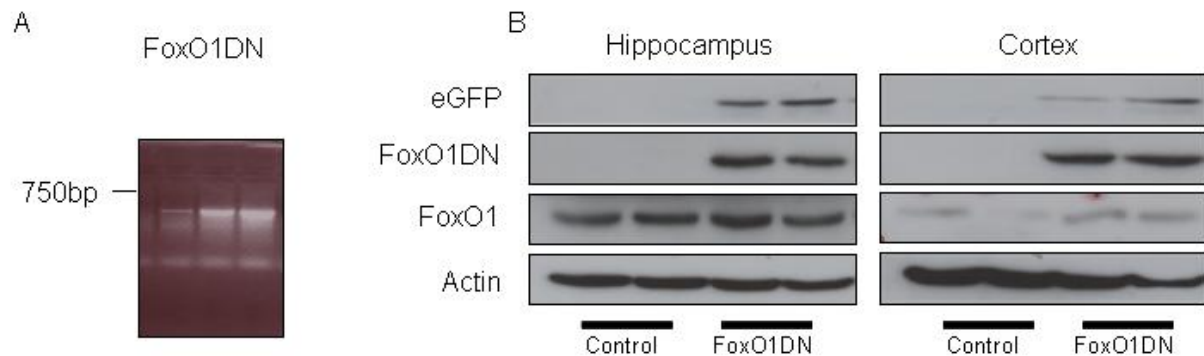


Figure 10: Detection of FoxO1DN.

(A) FoxO1ADA and FoxO1DN specific PCR (2.9.3.). The FoxO1DN fragment shows a size of about 750bp. (B) FoxO1DN and eGFP expression in the hippocampus and frontal cortex of FoxO1DN female and male mice. 100 μ g total proteins were separated via 10% SDS-PAGE.

The expression of FoxO1DN in the hippocampus and frontal cortex is shown in Fig. 7B. No expression of FoxO1DN and GFP is detected in hippocampus and cortex of wild-type female and male mice. Hence, FoxO1DN and GFP are expressed in hippocampus and cortex of female and male FoxO1DN mice. Additionally FoxO1 expression is shown in figure 10B. There are no changes in FoxO1 expression in the wild-type animals compared to the FoxO1DN mice.

The immunohistochemical staining of GFP shows an expression of GFP mainly in the hippocampus of FoxO1DN mice not in the wild-type mice (Fig. 11).

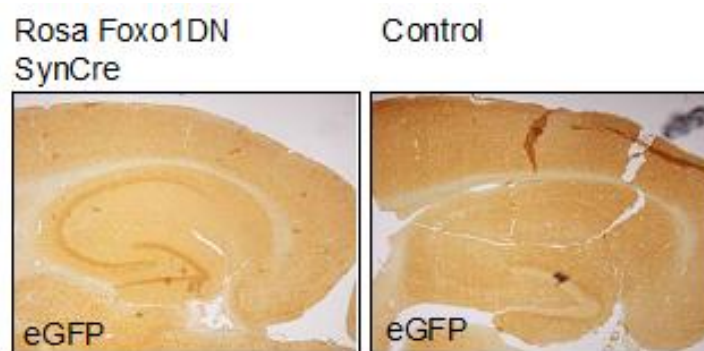


Figure 11: Immunohistological staining of eGFP.

The FoxO1DN mice crossed with the synapsin 1 promoter driven Cre recombinase expressing mice additionally express eGFP (enhanced green fluorescent protein). The GFP staining of FoxO1DN mice displays the expression of GFP mainly in the hippocampus. The brown coloured staining of GFP is not observed in the control mice (Stöhr et al., 2011).

3.2. Characterisation of FoxO1DN mice

Changes in glucose homeostasis and growth might affect survival and the pathology of Alzheimer's disease. Previous studies showed that the deletion of the IGF-1R in neurons and glia cells of the CNS result in growth retardation and abnormal behaviour (Kappeler et al., 2008). The neuron-specific knockout of the IR displays an increased body weight in females compared to wild-type animals on a normal chow diet and both genders show an increase in adipose tissue (Brüning et al., 2000). IRS-1 knockout mice display normal glucose tolerance beside insulin resistance and hyperinsulinemia (Terauchi et al., 1997). The deletion of brain derived IRS-2 leads to increased food intake and body weight (Masaki et al., 2004, Lin et al., 2004). Therefore the metabolism of FoxO1DN and FoxO1ADA mice was analysed in detail.

3.2.1. Glucose homeostasis of FoxO1DN mice

Glucose homeostasis of FoxO1DN mice was analysed via measurement of blood glucose every week after weaning until 12 weeks of age and then every 4 weeks up to the age of 60 weeks. In addition at the age of 10 and 11 weeks glucose and insulin tolerance tests were performed.

The measurement of blood glucose over a time period of 60 weeks showed a slightly increased glucose concentration of FoxO1DN in females between 16 to 24 weeks of age compared to wild-type ($p \leq 0.04$) (Fig. 12A). FoxO1DN male mice displayed no changes in blood glucose. At 60 weeks of age there was a slight increased blood glucose concentration in FoxO1DN males (Fig. 12B).

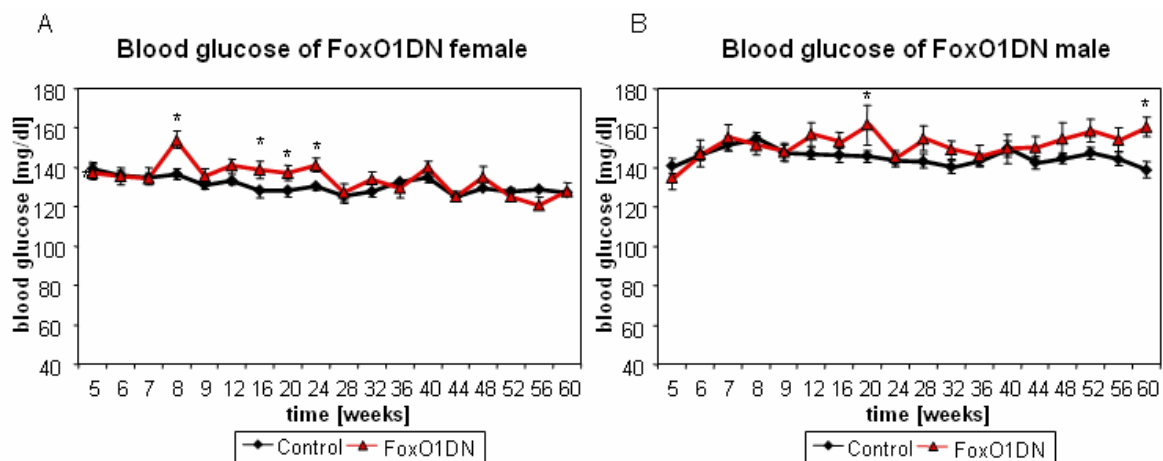


Figure 12: Blood glucose of FoxO1DN female and male mice until 60 weeks of age.

(A) Blood glucose of FoxO1DN ($n=35$, red) and wild-type ($n=71$, black) mice up to 60 weeks (B) Blood glucose of FoxO1DN ($n=29$, red) and wild-type ($n=67$, black) mice until 60 weeks of age ($*p \leq 0.04$, Student's t-test)

For glucose tolerance tests 2g glucose per kg body weight was injected into the peritoneal cavity. Blood glucose measurements were performed 15, 30, 60 and 120 minutes after

3. Results

injection. Glucose tolerance tests of FoxO1DN female mice compared to wild-type animals revealed no changes. 32 FoxO1DN female and 38 female wild-type mice as well as 21 FoxO1DN male and 38 control male mice were used (Fig. 13). FoxO1DN male mice showed slight decreased glucose concentrations which reached significance 60 minutes ($p \leq 0.03$) after the injection of glucose (Fig. 13B).

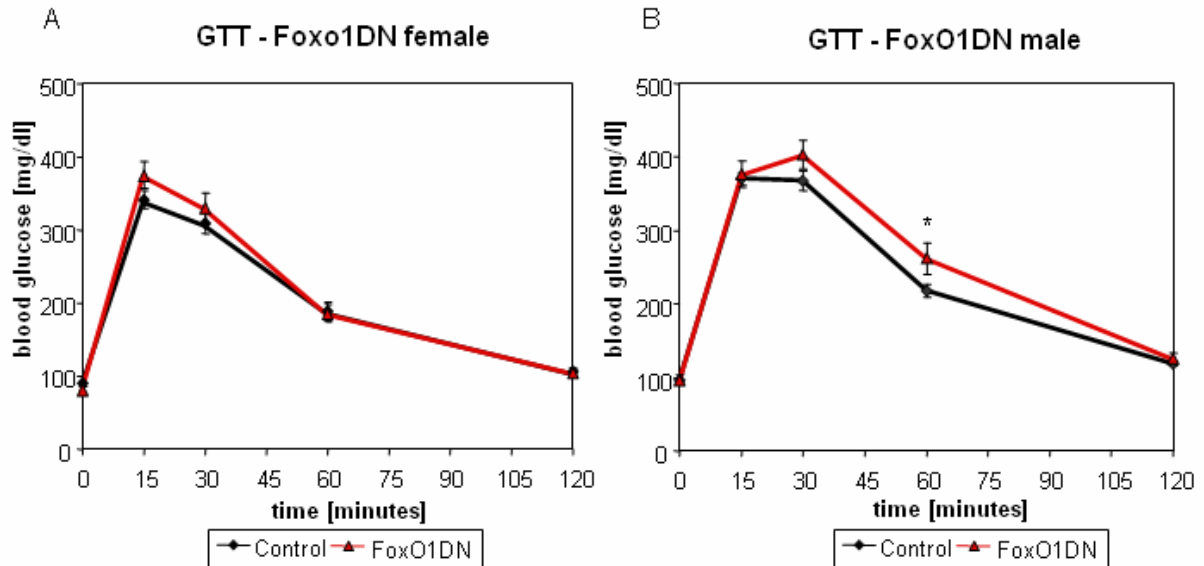


Figure 13: Glucose tolerance tests of FoxO1DN and wild-type mice.

(A) Glucose tolerance tests of FoxO1DN female (n=32; red) compared to control animals (n=38; black). (B) Glucose tolerance test of FoxO1DN male (n=21; red) and wild-type mice (n=38; black) (* $p \leq 0.03$, Student's t-test)

For insulin tolerance tests 0.75 U of insulin per kg body weight was injected into the peritoneal cavity of animals starved for 16 hours. Insulin tolerance tests of the same set of animals used for the glucose tolerance test revealed no changes of blood glucose of FoxO1DN and wild-type animals. Additionally similar results were observed for female and male mice (Fig. 14A and B).

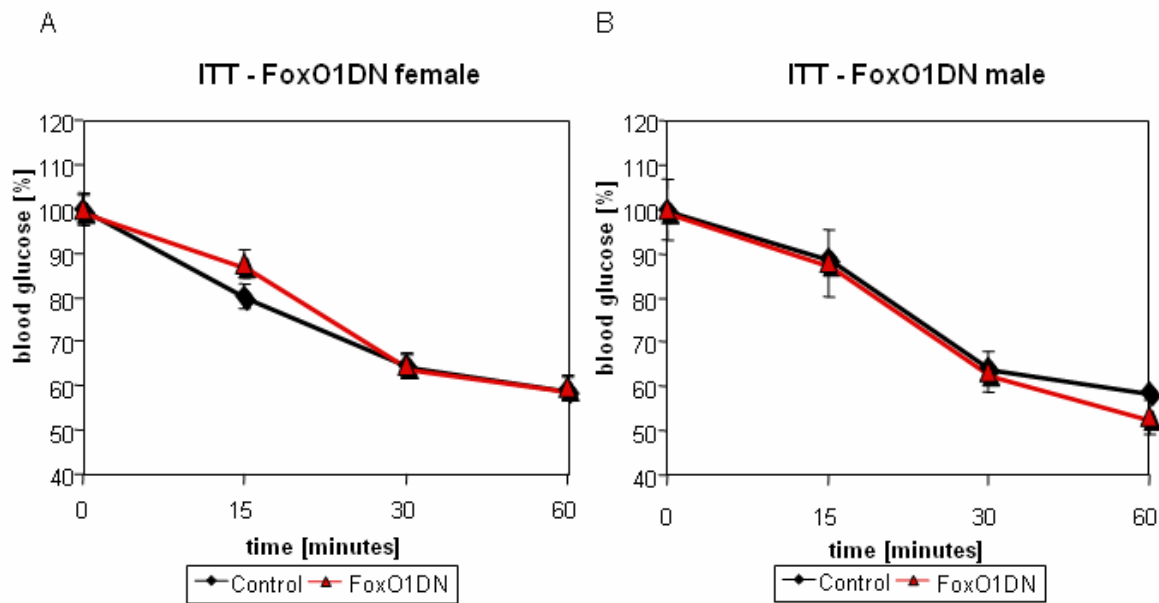


Figure 14: Insulin tolerance test of FoxO1DN mice.

(A) Insulin tolerance tests of FoxO1DN female (n=32) (red) mice compared to wild-type mice (n=38) (black). (B) Insulin tolerance test of FoxO1DN male (22) (red) mice compared to controls (n=38) (black).

3.2.2. Analysis of IR/IGF-1R signaling in 28 weeks old FoxO1DN mice

To analyse whether neuronal-specific expression of FoxO1DN affects the IR or IGF-1R signaling pathway, protein expression of the IR and IGF-1R was performed via western blots of hippocampus and frontal cortex from wild-type and FoxO1DN female and male mice at 28 weeks of age. Figure 15 shows no changes in respect to the different genotypes of IR and IGF-1R protein levels.

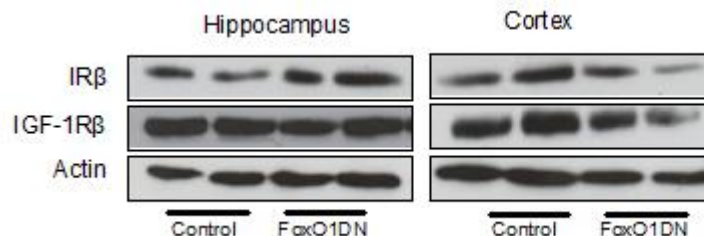


Figure 15: IR/IGF1R protein expression of 28 weeks old FoxO1DN mice.

Expression level of the IR and IGF-1R with actin as control is shown. Protein levels of hippocampus and frontal cortex from female and male wild-type (control) and FoxO1DN mice. Actin was served as loading control. 100 μ g of total proteins were used and separated via 10% SDS-PAGE.

Furthermore the activation of the kinases AKT, ERK1/2 and GSK3 β which are regulated via the IR and IGF-1R signaling pathway were analysed. Phosphorylated AKT, ERK1/2 and GSK3 β show no alterations in female and male wild-type compared to FoxO1DN female and male mice (Fig. 16).

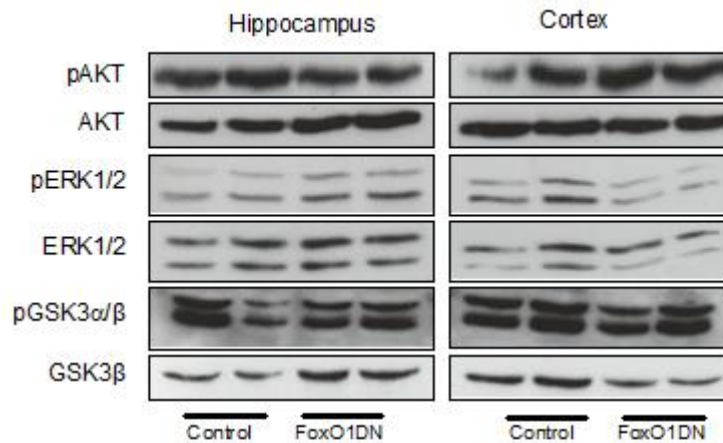


Figure 16: IR/IGF1R signaling pathway of 28 weeks old FoxO1DN mice. Phosphorylation level of AKT (pAKT, Ser473), ERK1/2 (pERK1/2, Thr202/Tyr204) and GSK3β (pGSK3β, Ser9) are shown. As control served unphosphorylate protein level of AKT, ERK1/2 and GSK3β. Female and male wild-type mice (control) are compared to FoxO1DN female and male mice at the age of 28 weeks. Protein phosphorylation in hippocampus and frontal cortex are shown. 100 µg of total proteins were used and separated via 10% SDS-PAGE.

3.2.3. Growth of FoxO1DN mice

FoxO1 mediated transcription might be involved in somatic growth (Patridge and Bruning, 2008). Therefore body weight of FoxO1DN female and male mice was measured over 60 weeks and compared to female and male wild-type mice. No changes of body weight from FoxO1DN female and male mice compared to wild-type female and male mice were observed from weaning until 60 weeks of age (Fig. 17A and B). For illustration body weight of FoxO1DN mice at 28 weeks of age are shown in Fig. 17C and D. 26 female FoxO1DN mice were compared to 65 wild-type mice and 17 FoxO1DN male mice were compared to 59 wild-type mice. No alterations of body weight have been observed.

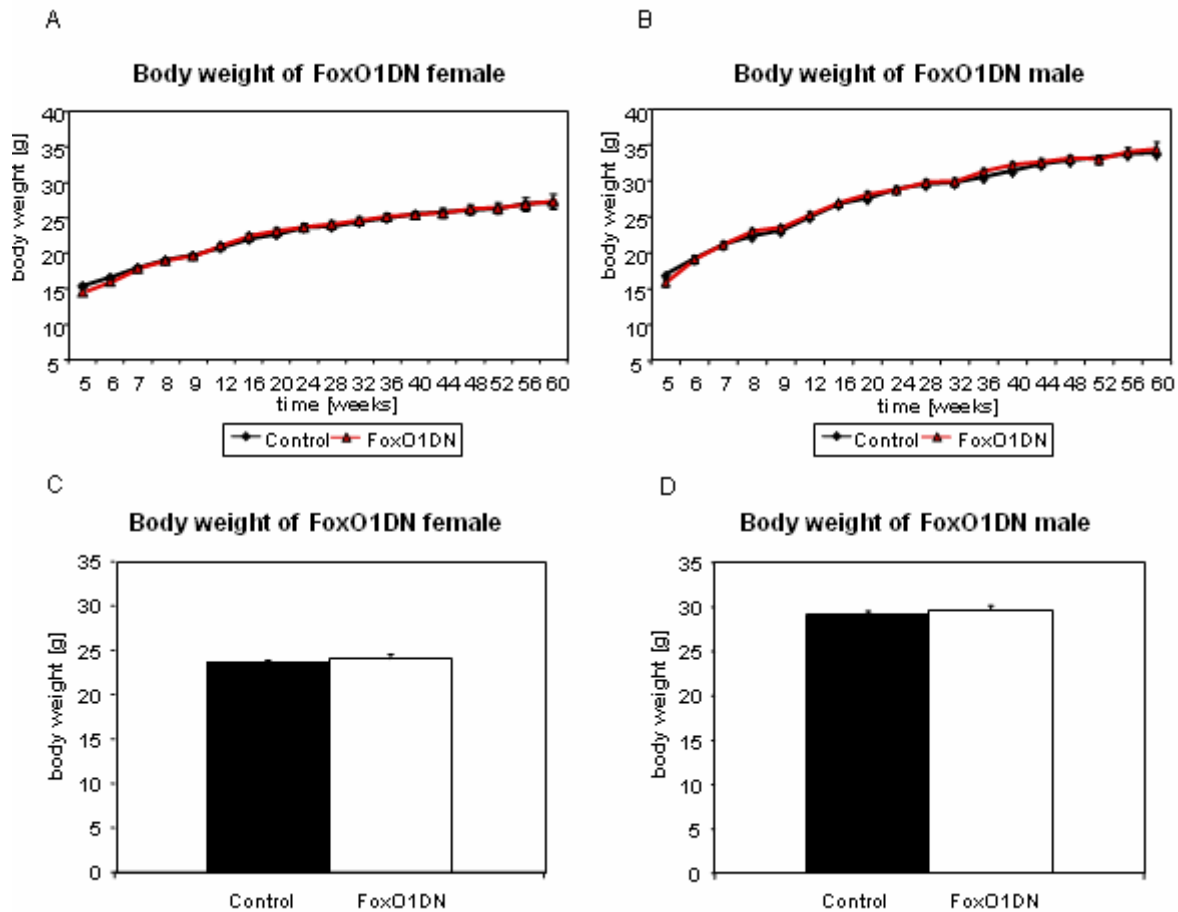


Figure 17: Body weight of FoxO1DN mice over 60 weeks.

(A) Body weight of FoxO1DN female mice (n=35, red) compared to wild-type female mice (n=71, black). (B) Body weight of FoxO1DN male mice (n=29, red) compared to wild-type male mice (n=67, black). (C) Body weight of FoxO1DN female (n=26) and wild-type mice (n=65) at the age of 28 weeks. (D) Body weight of FoxO1DN male (n=17) compared to wild-type animals (n=59).

Furthermore the body composition of FoxO1DN male mice was investigated via CT and NMR (2. Material and Methods). Results are presented for both methods as confirmation. For NMR 6 FoxO1DN and 5 wild-type male mice were analysed (Fig. 18 B and D). In addition 6 FoxO1DN and 6 male wild-type mice were used for CT (Fig. 18A and C). No changes of body fat ratio and lean body mass were detected. The same mice analysed via CT were used for further investigation of food and water intake, locomotion, activity and energy expenditure. These mice were 60 weeks old.

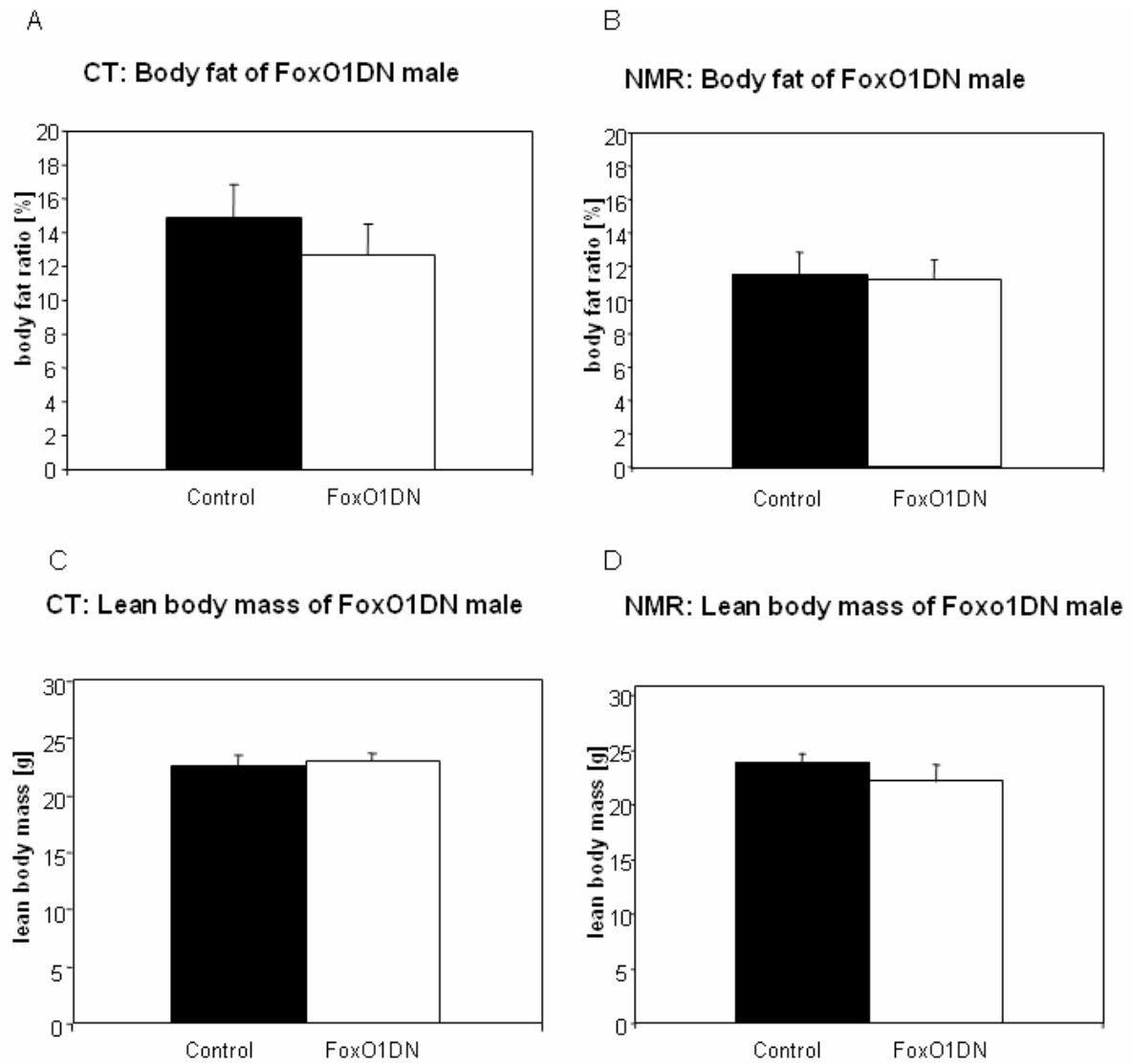


Figure 18: Body composition of FoxO1DN male mice.

(A and C) Body fat and lean body mass of FoxO1DN male mice (n=6) compared to wild-type mice (n=6) via CT. (B and D) Body fat and lean body mass of FoxO1DN male mice (n=6) and wild-type mice (n=5) via NMR. The mice used for analysis of body composition were 60 weeks old.

X-ray and false-colour imaging of FoxO1DN male revealed no alterations of bone density or skeletal structures compared to wild-type mice at 60 weeks of age (Fig. 18).

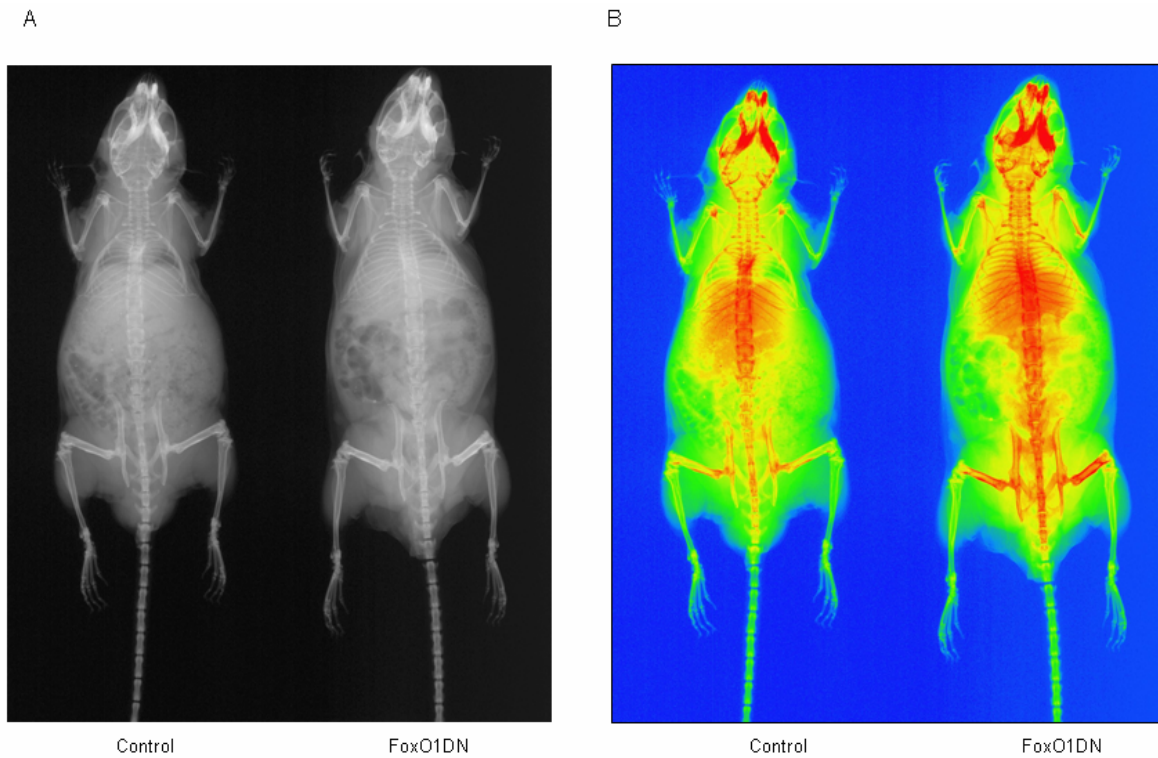


Figure 19: Analysis of bone density.

(A) X-ray of FoxO1DN male compared to wild-type mice at 60 weeks of age. (B) False-coloured imaging of FoxO1DN male compared to wild-type mice at 60 weeks of age.

Furthermore body length of 60 weeks old animals was measured and no differences were observed (Fig. 19).

Body length of Foxo1DN male

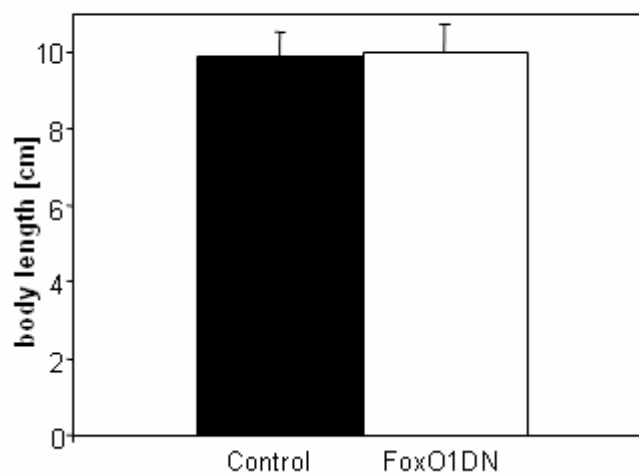


Figure 20: Body length of 60 weeks FoxO1DN male mice.

Body length of FoxO1DN (n=4) compared to wild-type (n=4) male mice at 60 weeks of age.

To complete the analysis, food and water intake were measured. FoxO1DN male mice showed no difference in food or water intake compared to wild-type male mice at 60 weeks of age (Fig. 21A and B).

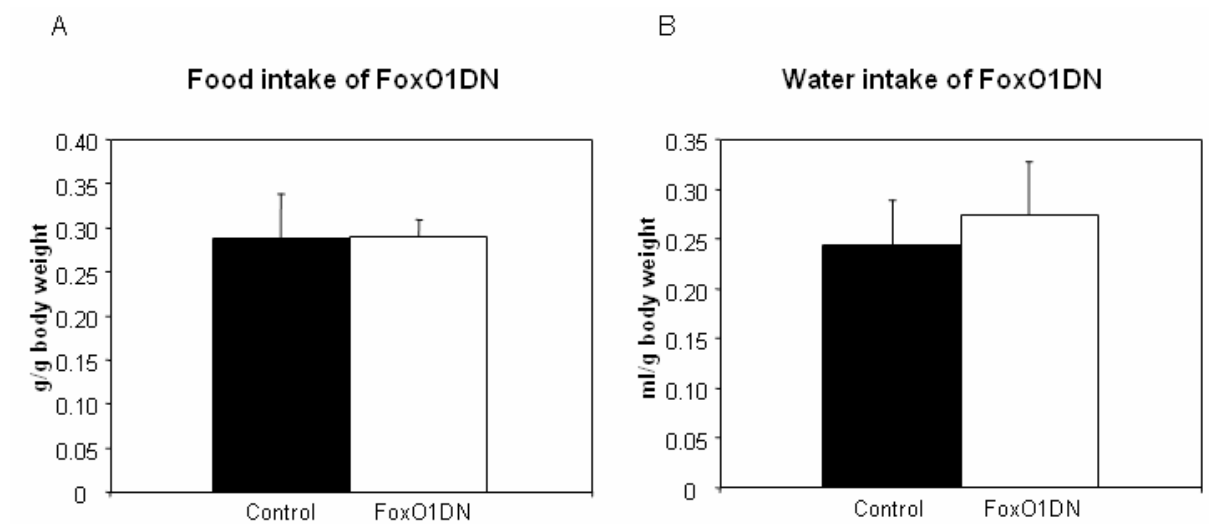


Figure 21: Food and water intake of 60 weeks old FoxO1DN male mice. (A and B) Food and water intake of FoxO1DN male mice (n=6) compared to wild-type male mice (n=6).

3.2.4. Indirect calorimetric analysis of FoxO1DN mice

Before analysis of locomotion, activity and energy expenditure motion coordination was investigated via RotaRod. Mice were put on a rotating wheel with different speed and time was measured until the mouse falls down. For this test adult mice from 14 to 20 weeks of age were used. No difference has been observed for FoxO1DN mice compared to wild-type mice (Fig. 22).

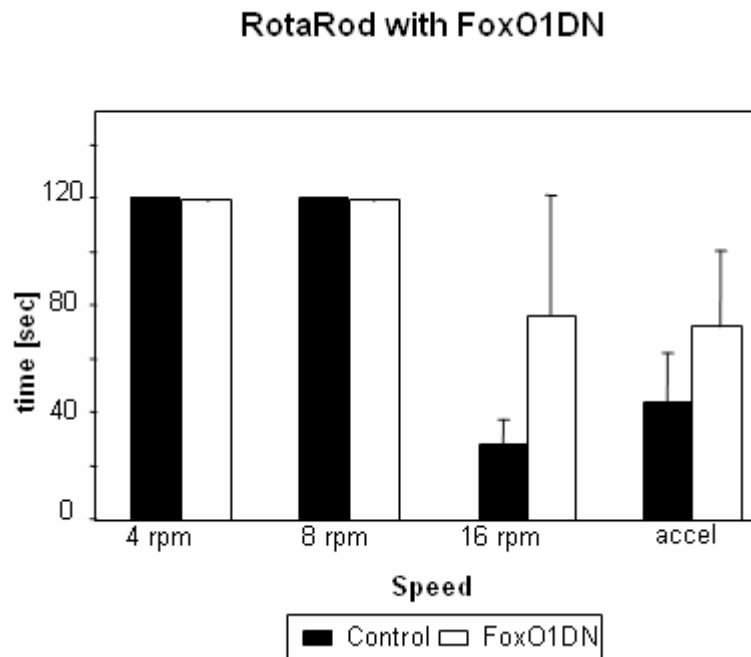


Figure 22: RotaRod for FoxO1DN male mice. The RotaRod test analyses the motion coordination of male FoxO1DN (n=6) compared to wild-type animals (n=6). Animals were between 14 and 20 weeks old.

3. Results

For analysis of locomotion activity 6 FoxO1DN and 6 wild-type male mice were used. Mice are more active during the night and rest during the day. Measurements for FoxO1DN mice were performed for 2 days and activity was measured via times crossing a light barrier (counts) (Fig. 23A) using the TSE system.

The activity of FoxO1DN male mice was less compared wild-type mice during the light phase ($p \leq 0.03$). Furthermore the FoxO1DN mice display a slight but statistically significant increase of activity compared to wild-type mice ($p \leq 0.002$) during the dark phase as expected. The activity of FoxO1DN and wild-type mice was less during the light and increased during the dark phase ($p \leq 0.001$) (Fig. 23B).

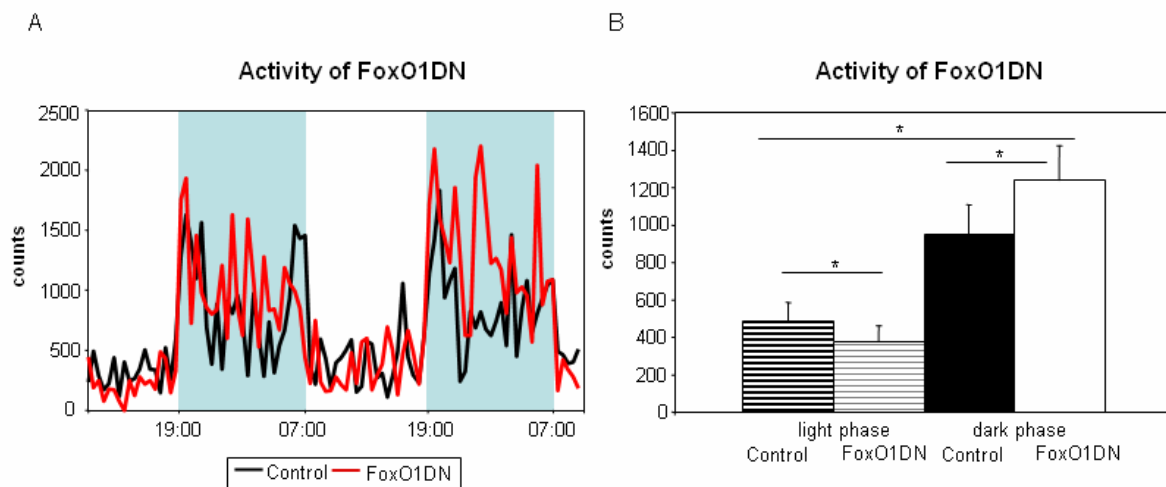


Figure 23: Locomotion activity of 60 weeks old FoxO1DN male mice.

(A) Activity of FoxO1DN male mice ($n=6$, red) compared to wild-type mice ($n=6$, black). Measurements were performed for 2 days. Light and dark phase were separated from 7 to 19 o'clock. (B) Mean value of activity from FoxO1DN male mice ($n=6$) and wild-type mice ($n=6$) ($*p \leq 0.03$, Student's t-test).

In addition to activity, the energy expenditure was measured. Figure 24 displays energy expenditure normalized to lean body mass investigated via CT (see Fig. 18). FoxO1DN mice show no difference in the level of energy expenditure compared to wild-type mice during the light phase. At dark phase the energy expenditure of FoxO1DN mice was statistically significant increased ($p \leq 0.001$) compared to wild-type mice (Fig. 24).

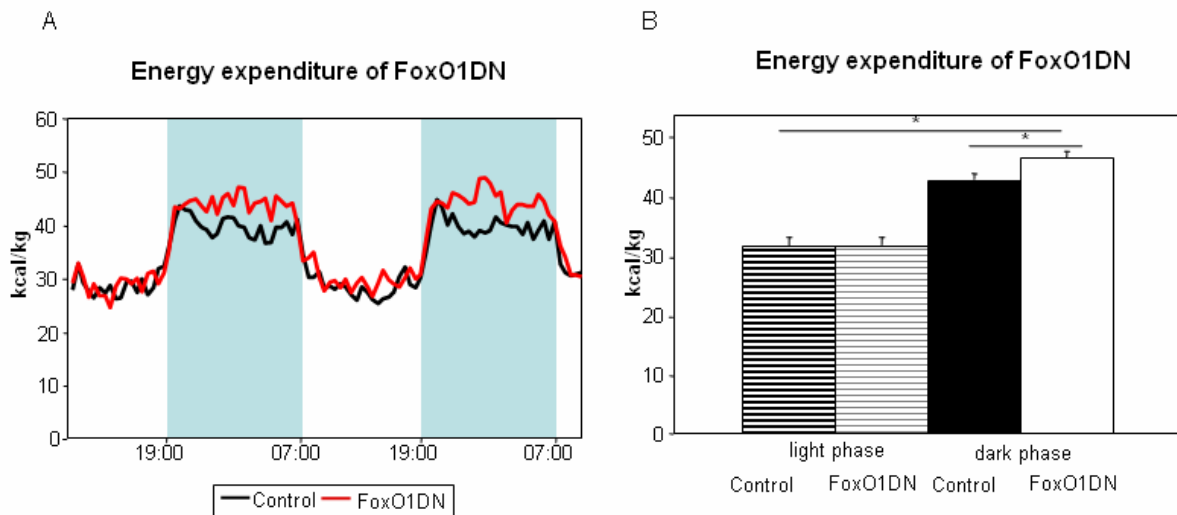


Figure 24: Energy expenditure normalized to lean body mass of 60 weeks old FoxO1DN mice. (A) Energy expenditure of FoxO1DN male mice (n=6, red) compared to wild-type mice (n=6, black). Analysis was performed for 2 days. Day and night were separated from 7 to 19 o'clock. (B) Mean value of energy expenditure from FoxO1DN male mice (n=6) and wild-type mice (n=6). Statistically significance was reached during the dark phase (*p≤0.001, Student's t-test).

The respiratory quotient (RQ) is calculated from eliminated CO₂ and consumed O₂. It indicates the substrate metabolized by the particular organism. The respiratory quotient of FoxO1DN mice is not different compared to wild-type mice. But, as expected it is reduced during the light phase compared to the dark phase for FoxO1DN and wild-type animals (p≤0.001). The RQ of both FoxO1DN and wild-type is 0.9 during the light phase. This shows proteins to be the major metabolized source during the day which is the resting phase of mice. At night the RQ is nearly 1. This identifies carbohydrates to be predominantly metabolized (Fig. 25).

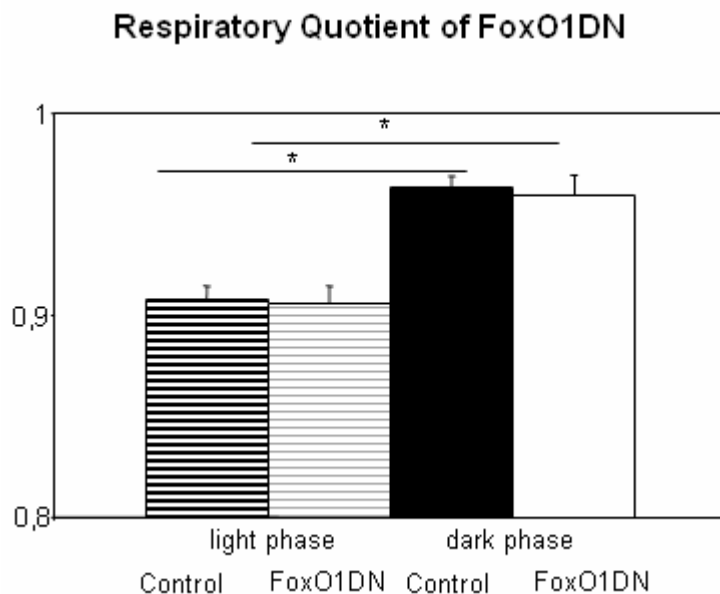


Figure 25: Respiratory quotient of 60 weeks old FoxO1DN mice. Respiratory quotient of FoxO1DN male mice (n=6) compared to wild-type mice (n=6). Analysis was performed for 2 days. Dark and light phase were separated from 7 to 19 o'clock. Comparison of light and dark phase was significant (*p≤0.001, Student's t-test).

3.2.5. Behaviour of FoxO1DN mice

FoxO1DN is expressed in neurons. To investigate whether this neuron-specific expression of FoxO1DN alters brain structures or behaviour of the mice Nissl stainings and behavioural testings were performed. The tests used particularly analysed explorative and fear behaviour of mice. Furthermore the spatial learning potential was investigated. Only male mice were analysed because less hormonal fluctuations affect their behaviour.

Nissl staining of serial sections of brains from wild-type and FoxO1DN mice at 28 weeks of age displayed no structural differences e.g. of hippocampal formation (Fig. 26).

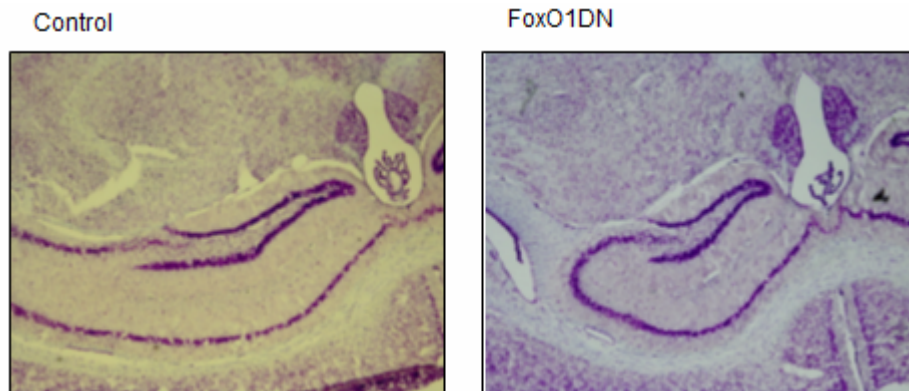


Figure 26: Nissl staining of the hippocampus of 28 weeks old FoxO1DN mice. Nissl staining of the hippocampal formation of 28 weeks old FoxO1DN male mice compared to wild-type mice.

During the Open field test the time how long the mice stood in the center or border of the box was measured. For FoxO1DN mice no difference was detected compared to wild-type mice was detected (Fig. 27A). The O-Maze additionally analyses fear behaviour of mice. This test showed that FoxO1DN mice stayed slightly longer in the open than in the closed sections compared to wild-type mice. However, this difference was not significant (Fig. 27B).

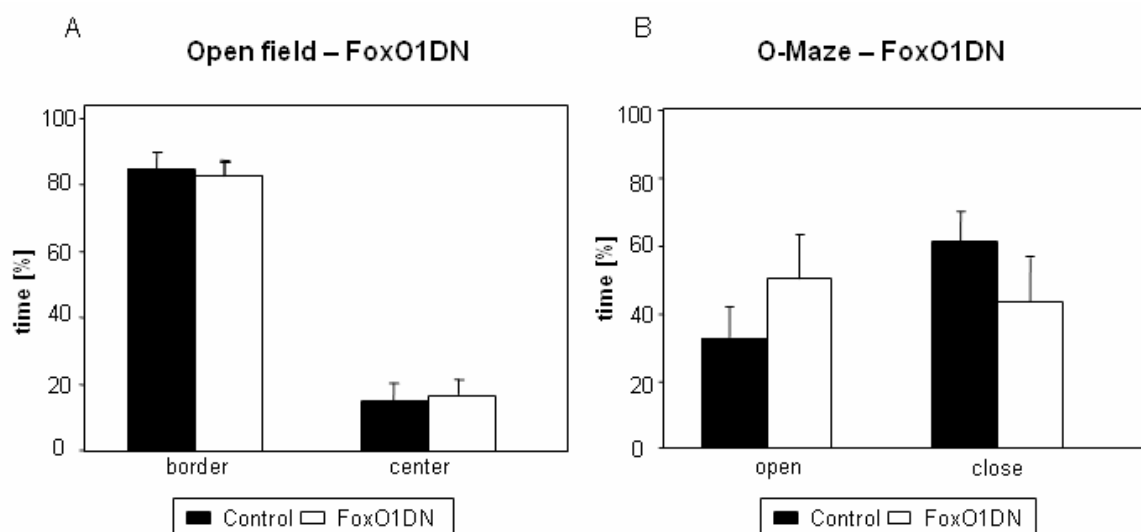


Figure 27: Open field and O-Maze test of FoxO1DN. (A) Open field test of FoxO1DN male mice (n=6) compared to wild-type mice (n=6). (B) O-Maze test of FoxO1DN male mice (n=6) compared to wild-type mice (n=6). Animals were 60 weeks old.

Furthermore spatial learning abilities of FoxO1DN mice were analysed. Therefore the Morris Water Maze test was used. The test was performed for 5 days. The time was measured till the mouse reached the platform which was hidden under the water surface. Each test was performed for 1 minute. At day 5 the platform was removed and the time the mouse spends in the quadrant where the platform originally stood was measured. The Water Maze test revealed no difference between FoxO1DN and wild-type mice (Fig. 28A and B).

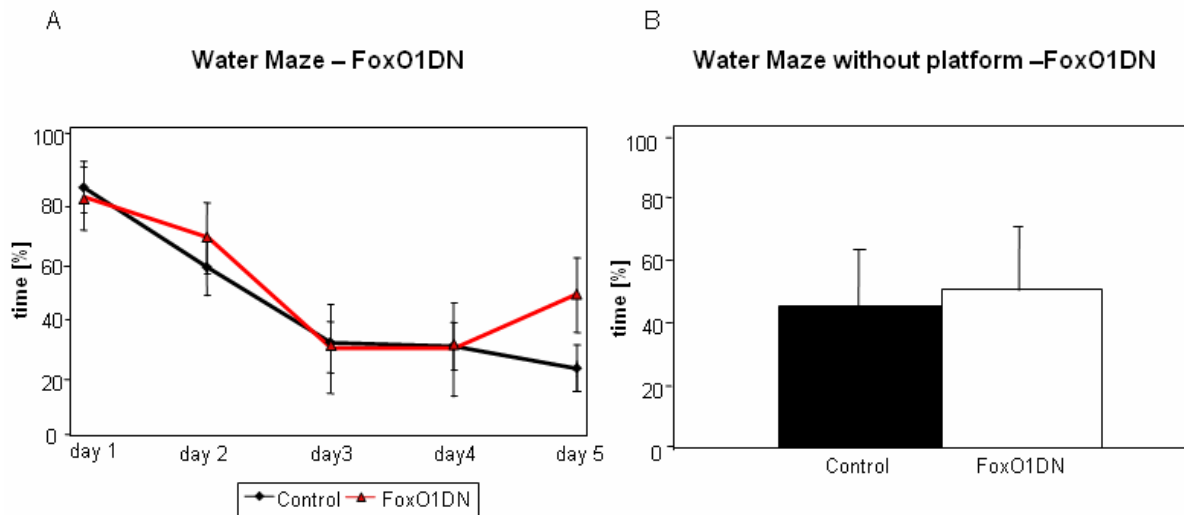


Figure 28: Water Maze test of FoxO1DN mice.

(A) Morris Water Maze test was performed over 5 days to compare FoxO1DN (n=4, red) and wild-type (n=6, black) spatial learning abilities. Time was measured to find the platform, maximum time was 1 minute. (B) After 5 days the platform was removed and the time was measured while the mouse was swimming in the quadrant where the platform originally was.

3.3. Role of FoxO1 in Alzheimer's disease

Previous studies showed that the IR/IGF-1R signaling pathway is disturbed in the central nervous system of patients suffering from AD (Frolich et al. 1998; Frolich et al. 1999; Moloney et al. 2010). Neuron-specific deletion of the IGF-1R rescues premature mortality and a decreased processing of APP compared to Tg2576 mice (Freude et al., 2009). To analyse whether this effect is mediated through FoxO1 the dominant negative (FoxO1DN) and constitutive active form of FoxO1 (FoxO1ADA) were analysed in Tg2576 background.

3.3.1. Glucose homeostasis of Tg2576/FoxO1DN mice

Glucose homeostasis of FoxO1DN mice in Tg2576 background was investigated. Blood glucose was measured until 60 weeks of age, and glucose and insulin tolerance tests were performed as well. Blood glucose of Tg2576/FoxO1DN female mice was similar to that of Tg2576 mice. Tg2576/FoxO1DN females show much the same blood glucose concentration compared to FoxO1DN mice (Fig. 29A). Tg2576/FoxO1DN male mice exhibit no differences

3. Results

in blood glucose compared to Tg2576 mice, except of the 6 weeks time point ($p \leq 0.02$). Furthermore Tg2576/FoxO1DN male mice presented a decrease of blood glucose compared to Tg2576 which reached significance at 6, 12, 20, 24, 28, 52 and 56 weeks of age ($p \leq 0.05$) (Fig. 29B).

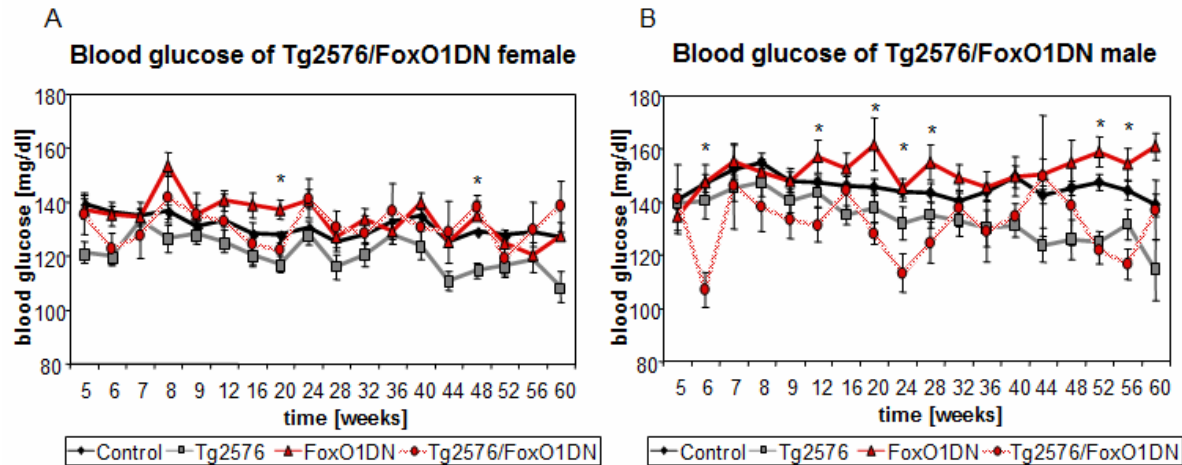


Figure 29: Blood glucose of FoxO1DN mice in Tg2576 background.

(A) Blood glucose of female Tg2576/FoxO1DN ($n=14$, light red), FoxO1DN ($n=35$, red), Tg2576 ($n=48$, grey) and wild-type mice ($n=71$, black) until 60 weeks of age. (B) Blood glucose of male Tg2576/FoxO1DN ($n=12$, light red), FoxO1DN ($n=29$, red), Tg2576 ($n=35$, grey) and wild-type mice ($n=67$, black) until 60 weeks of age (comparison of Tg2576/FoxO1DN and Tg2576, $*p \leq 0.05$, Student's t-test).

Glucose tolerance tests were performed using 11 Tg2576/FoxO1DN, 32 FoxO1DN, 37, Tg2576 and 38 wild-type female and 9 Tg2576/FoxO1DN, 21 FoxO1DN, 29 Tg2576 and 38 wild-type male mice.

Glucose tolerance tests of Tg2576/FoxO1DN female mice showed no changes in blood glucose concentrations during GTT (Fig 30A). Tg2576/FoxO1DN male mice presented a slight decrease of glucose levels reaching significance at 15 minutes ($p \leq 0.03$) compared to Tg2576 animals. In addition Tg2576/FoxO1DN male mice showed increased glucose levels compared to FoxO1DN mice at 60 minutes after injection of glucose ($p \leq 0.05$) (Fig. 30B).

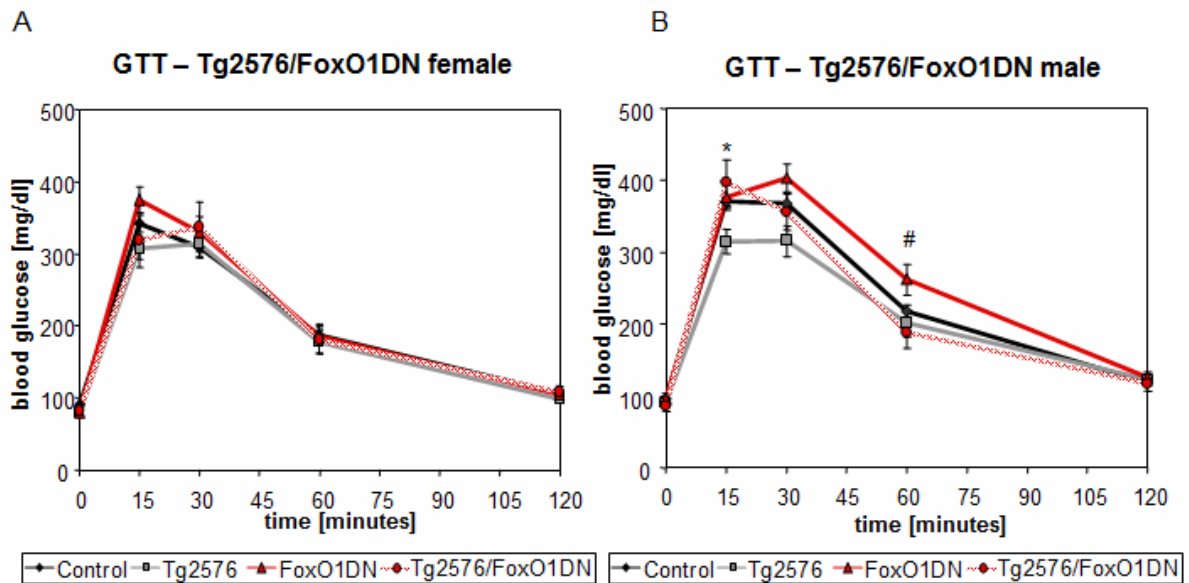


Figure 30: Glucose tolerance tests of Tg2576/FoxO1DN mice.

(A) Glucose tolerance tests of female FoxO1DN/Tg2576 (n= 11, light red), FoxO1DN (n=32, red), Tg2576 (n=37, grey) and wild-type mice (n=38, black). (B) Glucose tolerance tests of male FoxO1DN/Tg2576 (n=9, light red), FoxO1DN (n=21, red), Tg2576 (n=29, grey) and wild-type mice (n=38, black) (*comparison of Tg2576/FoxO1DN and Tg2576; # comparison of Tg2576/FoxO1DN and FoxO1DN, p≤0.05, Student’s t-test)

Insulin tolerance tests exhibit an increased, but statistically not significant, insulin sensitivity of Tg2576/FoxO1DN female mice compared to Tg2576 mice. No changes could be observed in Tg2576/FoxO1DN female mice compared to FoxO1DN mice (Fig. 31A). Tg2576/FoxO1DN male mice show no alterations in insulin sensitivity (Fig. 31B).

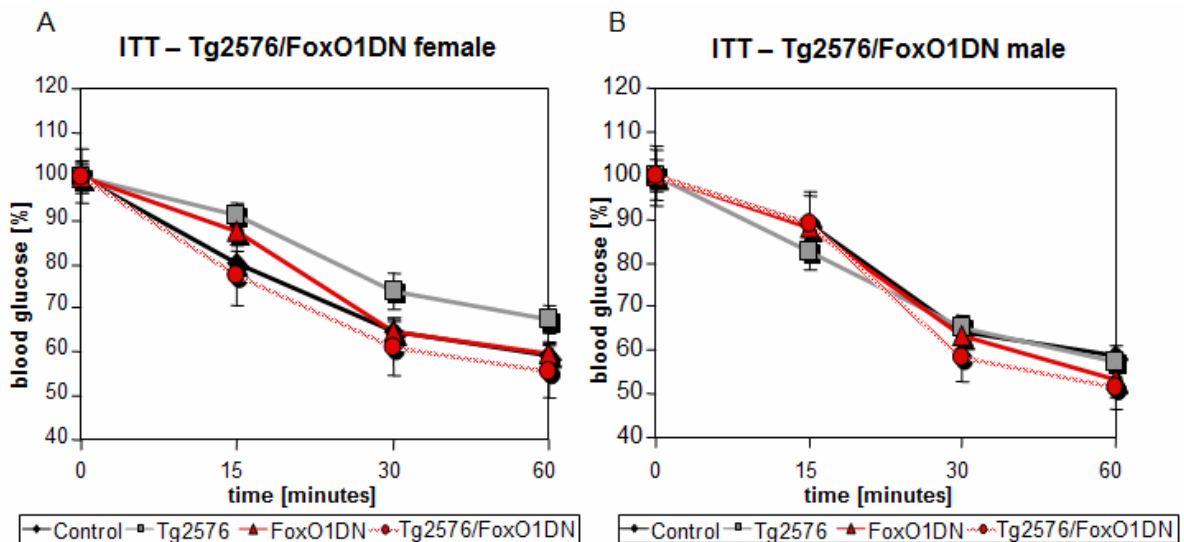


Figure 31: Insulin tolerance test of Tg2576/FoxO1DN mice.

(A) Insulin tolerance tests of female FoxO1DN/Tg2576 (n= 11, light red), FoxO1DN (n=32, red), Tg2576 (n=37, grey) and wild-type mice (n=38, black). (B) Insulin tolerance tests of male FoxO1DN/Tg2576 (n=9, light red), FoxO1DN (n=21, red), Tg2576 (n=29, grey) and wild-type mice (n=38, black).

3.3.2. Body weight of Tg2576/FoxO1DN mice

Body weight of Tg2576/FoxO1DN mice was measured until 60 weeks of age. No changes of body weight have been observed for Tg2576/FoxO1DN female mice compared to Tg2576 mice. However, Tg2576/FoxO1DN female mice displayed a decreased body weight compared to FoxO1DN mice reaching significance from 5 till 40 weeks of age ($p \leq 0.05$) (Fig. 32A). Tg2576/FoxO1DN male mice showed a slight decrease in body weight compared to Tg2576 reaching statistical significance at 6, 7, 16, 56 and 60 weeks of age ($p \leq 0.02$). Additionally Tg2576/FoxO1DN male mice weighed less compared to FoxO1DN male mice between 5 and 60 weeks of age (Fig. 32B).

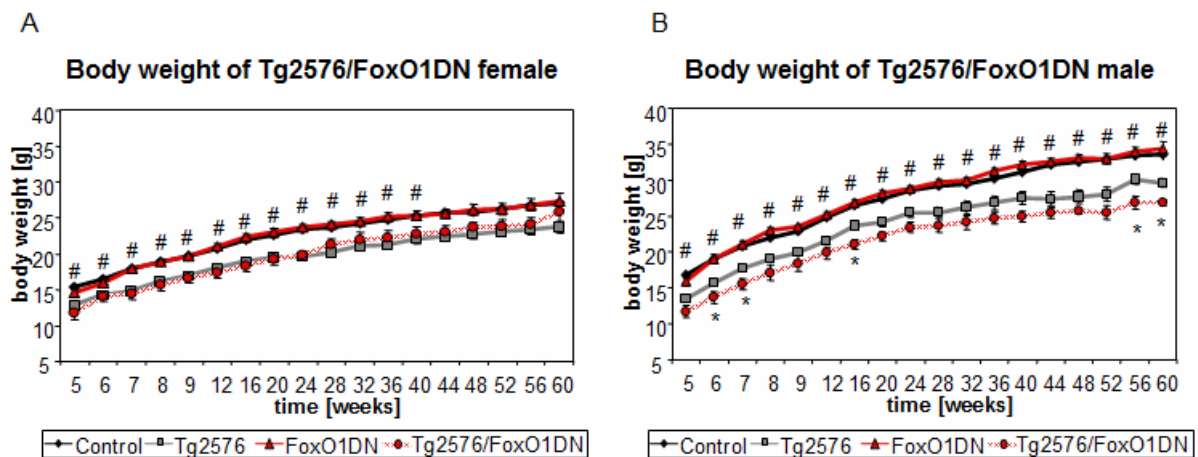


Figure 32: Body weight of Tg2576/FoxO1DN mice until 60 weeks of age.

(A) Body weight of female FoxO1DN/Tg2576 ($n=14$, light red), FoxO1DN ($n=35$, red), Tg2576 ($n=48$, grey) and wild-type mice ($n=71$, black) until 60 weeks of age. (B) Body weight of male FoxO1DN/Tg2576 ($n=12$, light red), FoxO1DN ($n=29$, red), Tg2576 ($n=35$, grey) and wild-type mice ($n=67$, black) until 60 weeks of age (* comparison of Tg2576/FoxO1DN and Tg2576; # comparison of Tg2576/FoxO1DN and FoxO1DN, $p \leq 0.05$, Student's t-test).

Brain body ratio was similar in FoxO1DN female mice compared to wild-type mice as well as Tg2576 (Fig. 33A). Statistically significant differences in brain body ratio were found in wild-type compared to Tg2576/FoxO1DN mice, FoxO1DN compared to Tg2576/FoxO1DN and wild-type compared to Tg2576 ($p \leq 0.04$) (Fig. 33B).

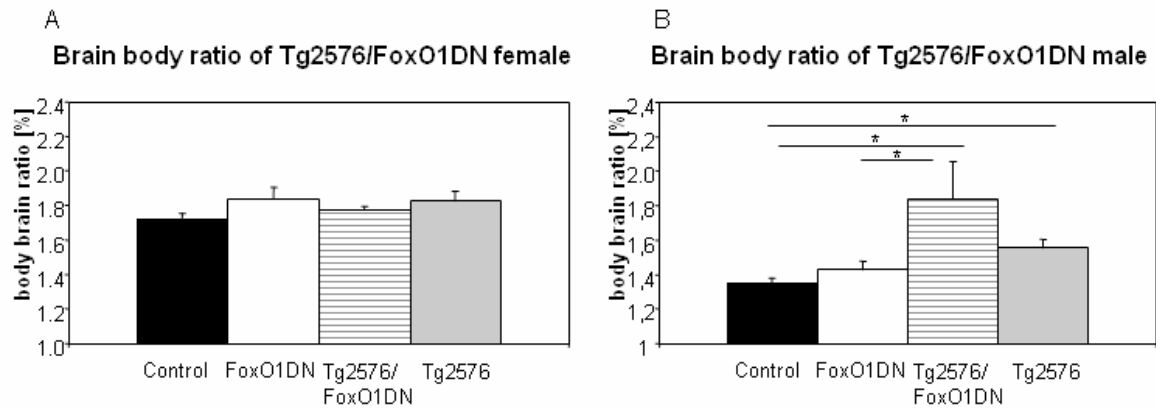


Figure 33: Brain body ratio of Tg2576/FoxO1DN mice at 60 weeks of age.

(A) Body brain ratio of wild-type (n=26), FoxO1DN (n=7), Tg2576/FoxO1DN (n=3) and Tg2576 (n=19) female mice at 60 weeks of age. (B) Body brain ratio of 60 weeks old wild-type (n=28, black), FoxO1DN (n=6), Tg2576/FoxO1DN (n=3) and Tg2576 (n=20) male mice at 60 weeks of age (* $p \leq 0.04$, Student's t-test).

3.3.3. Kaplan-Meier analysis of FoxO1DN mice in Tg2576 background

Survival of Tg2576/FoxO1DN mice was analysed via Kaplan-Meier analysis. Figure 34A shows survival of female and male Tg2576/FoxO1DN mice. No significant differences were recognized between the survival of FoxO1DN mice compared to wild-type mice and Tg2576/FoxO1DN to Tg2576 mice. At 60 weeks of age nearly 70% of Tg2576/FoxO1DN and Tg2576 as well as 90% of FoxO1DN and wild-type mice were still alive. FoxO1DN mice showed increased survival compared to Tg2576/FoxO1DN mice ($p \leq 0.05$, Wilcox-rank). For female mice 80% of Tg2576/FoxO1DN and Tg2576 were alive at 60 weeks of age. Furthermore 90% of FoxO1DN and wild-type mice still lived at 60 weeks of age (Fig. 34B). Tg2576/FoxO1DN male survived no longer than Tg2576 mice. 40% of Tg2576/FoxO1DN and Tg2576 mice were dead at 60 weeks of age and 10% of FoxO1DN and wild-type male mice died until 60 weeks of age (Fig. 34C).

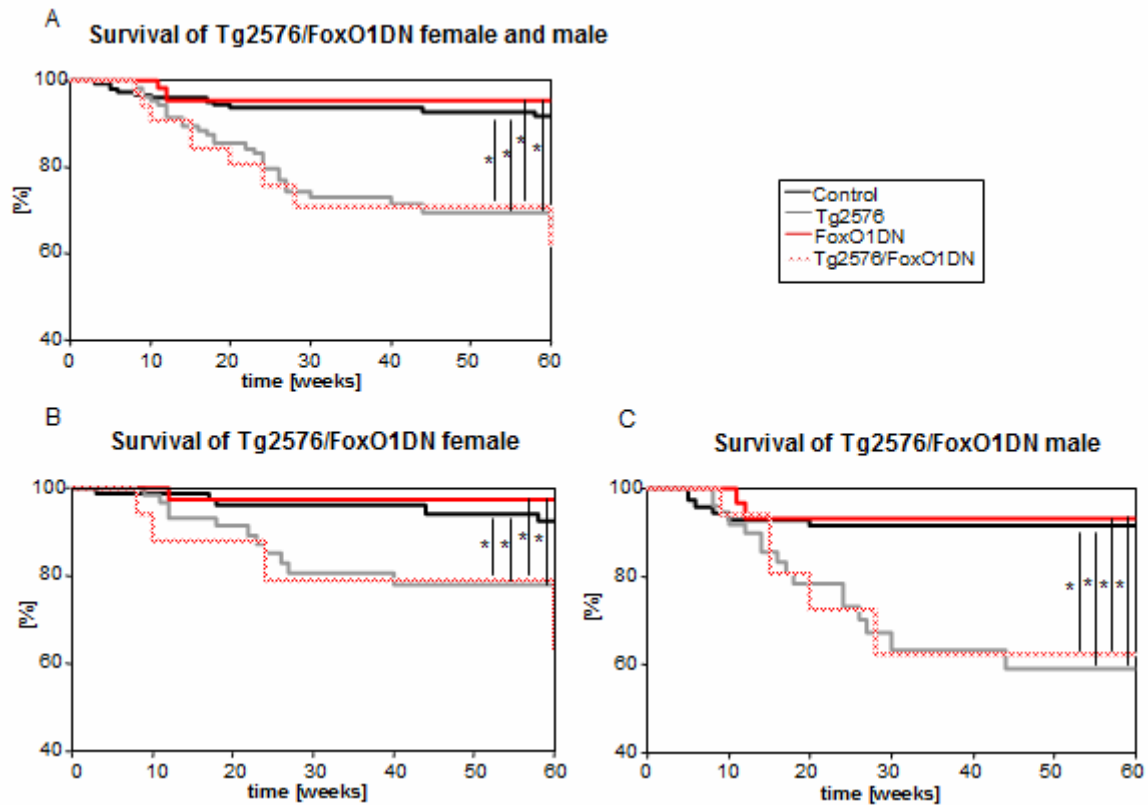


Figure 34: Kaplan-Meier curves of FoxO1DN mice in Tg2576 background until 60 weeks of age. (A) Survival of Tg2576/FoxO1DN (n=26, light red), Tg2576 (n=83, grey), FoxO1DN (n=64, red) and wild-type (n=138, black) female and male mice. (B) Survival of female Tg2576/FoxO1DN (n=14, light red), Tg2576 (n=48, grey), FoxO1DN (n=35, red) and wild-type (n=71, black). (C) Survival of male Tg2576/FoxO1DN (n=12, light red), Tg2576 (n=35, grey), FoxO1DN (n=29, red) and wild-type (n=67, black) (* $p \leq 0.05$, Wilcoxon rank).

3.3.4. IR/IGF-1R signaling in Tg2576/FoxO1DN mice

The IR/IGF-1R signaling of Tg2576/FoxO1DN was analysed via SDS-PAGE and western blot. Protein levels were analysed in the hippocampus and frontal cortex. Comparison of Tg2576/FoxO1DN, Tg2576, FoxO1 and wild-type female and male mice presents no changes in IR and IGF-1R expression (Fig. 35).

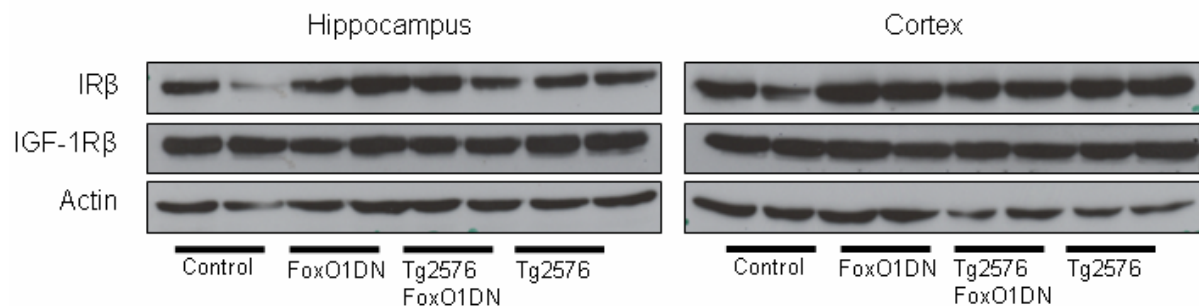


Figure 35: IR and IGF-1R protein expression of 60 weeks old Tg2576/FoxO1DN mice. Expression level of the IR, IGF-1R and actin as loading control is shown. Protein levels of hippocampus and frontal cortex from female and male wild-type (control), FoxO1DN, Tg2576/FoxO1DN and Tg2576 micel. 100 μ g of total proteins were used and separated via 10% SDS-PAGE.

3. Results

The activation of the PI3 kinase and the MAP kinase pathway was analysed via antibodies against the specific phosphorylation sites (Ser473 for pAKT; Thr202/Tyr204 for pERK1/2 and Ser9 for pGSK3 β). No changes of AKT phosphorylation has been observed in Tg2576/FoxO1DN, Tg2576, FoxO1DN and wild-type female and male mice. Additionally phosphorylation of ERK1/2 showed a slight increase in the hippocampus and frontal cortex of the FoxO1DN male mice and was increased in mice with AD background. Phosphorylation of GSK3 β was not changed (Fig. 36).

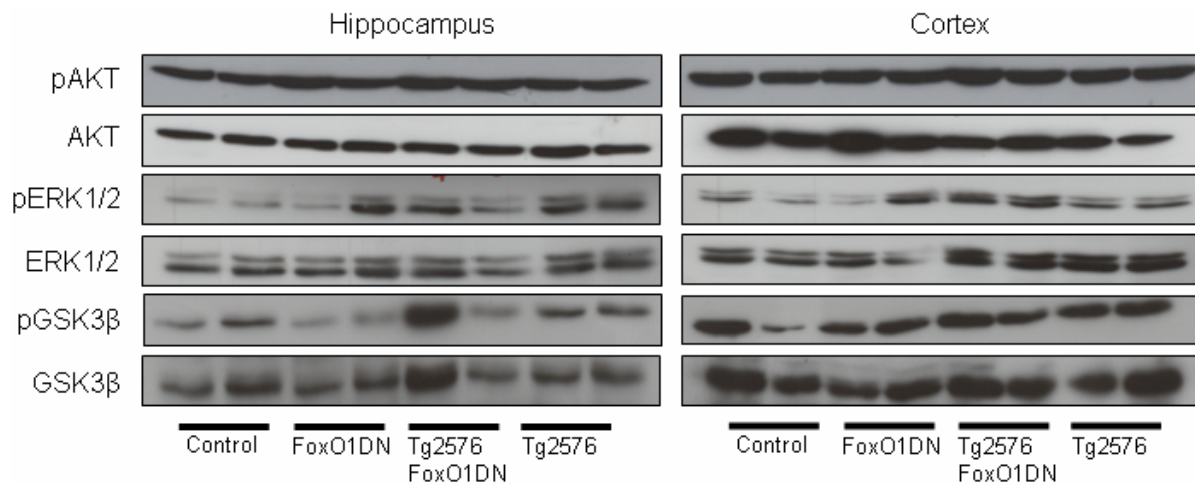


Figure 36: IR/IGF1R signaling pathway of 60 weeks old Tg2576/FoxO1DN mice. Phosphorylation level of AKT (pAKT, Ser473), ERK1/2 (pERK1/2, Thr202/Tyr204) and GSK3 β (pGSK3 β , Ser9) are shown. As control served unphosphorylated protein level of AKT, ERK1/2 and GSK3 β . Female and male wild-type mice (control) are compared to FoxO1DN female and male mice at the age of 60 weeks. 100 μ g of total proteins were used and separated via 10% SDS-PAGE.

Furthermore expression of FoxO1 and FoxO3a was analysed via western blots. No changes in FoxO1 and FoxO3a expressed have been detected in Tg2576/FoxO1DN, Tg2576, FoxO1DN and wild-type female and male mice. As expected, FoxO1DN is shown in FoxO1DN and Tg2576/FoxO1DN mice. Possible target genes of FoxO1 were p27 and MnSOD. Both were not altered in FoxO1DN mice compared to wild-type mice (Fig. 37).

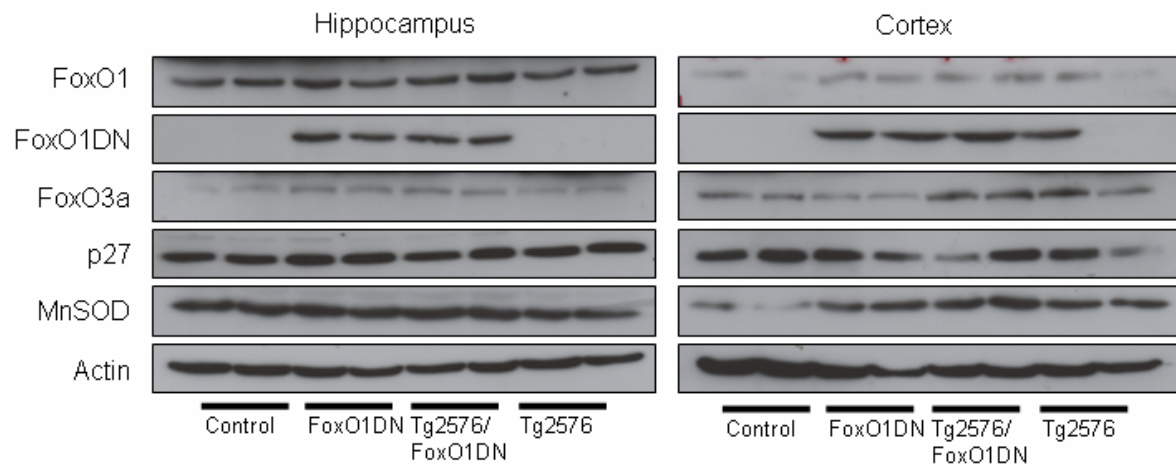


Figure 37: Expression of FoxO1 and FoxO3a in Tg2576/FoxO1DN mice.

FoxO1 and FoxO3a expression as well as p27 and MnSOD of 60 weeks old Tg2576/FoxO1DN female and male mice. Hippocampus and frontal cortex were analysed and actin served as control. 100 μ g of total proteins were used and separated via 10% SDS-PAGE.

3.3.5. APP Processing in Tg2576/FoxO1DN mice

To analyse whether FoxO1 affects processing of APP and generation of A β SDS-PAGE and western blots, A β -ELISA and Dot blots were used. Expression of APP in Tg2576/FoxO1DN mice is not changed compared to Tg2576 and there are no differences in female and male mice. The generation of α/β CTFs is not altered. Furthermore the production of A β shows no differences in Tg2576/FoxO1DN compared to Tg2576 female and male mice (Fig. 38).

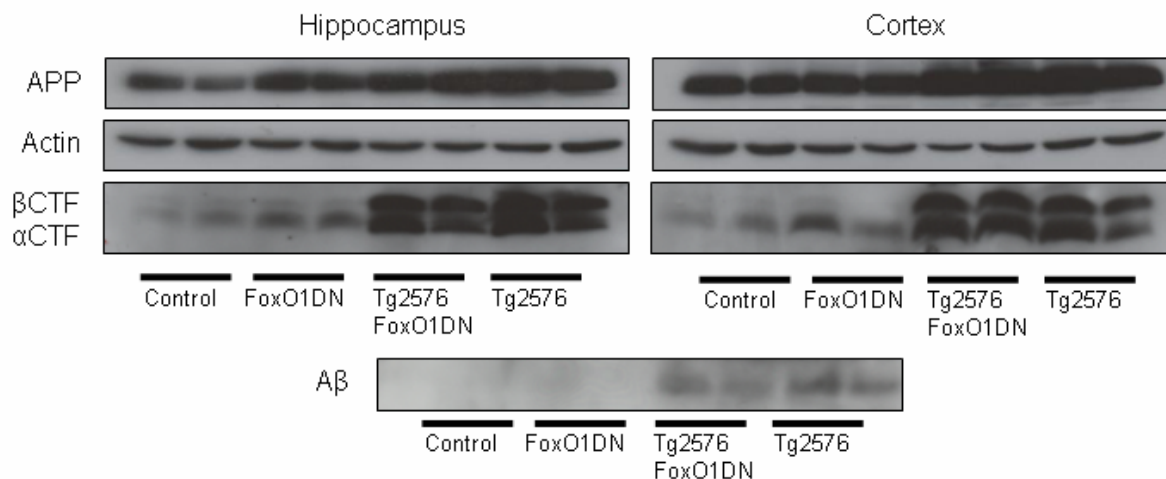


Figure 38: APP-Processing of FoxO1DN mice in Tg2576 background.

APP expression and generation of α/β CTFs are shown for FoxO1DN mice compared to wild-type female and male mice as well as female and male FoxO1DN in the Tg2576 background and Tg2576 mice. 100 μ g of total proteins were used and separated via 10% or 15% SDS-PAGE. For A β quantification 200 μ g of total proteins were separated via a urea tricine SDS-PAGE.

The generation of A β in female mice was further analysed via ELISA. The production of A β 40 was slightly increased in Tg2576/FoxO1DN mice but not statistically significant. The A β 42 level was not changed in Tg2576/FoxO1DN mice compared Tg2576 mice (Fig. 39).

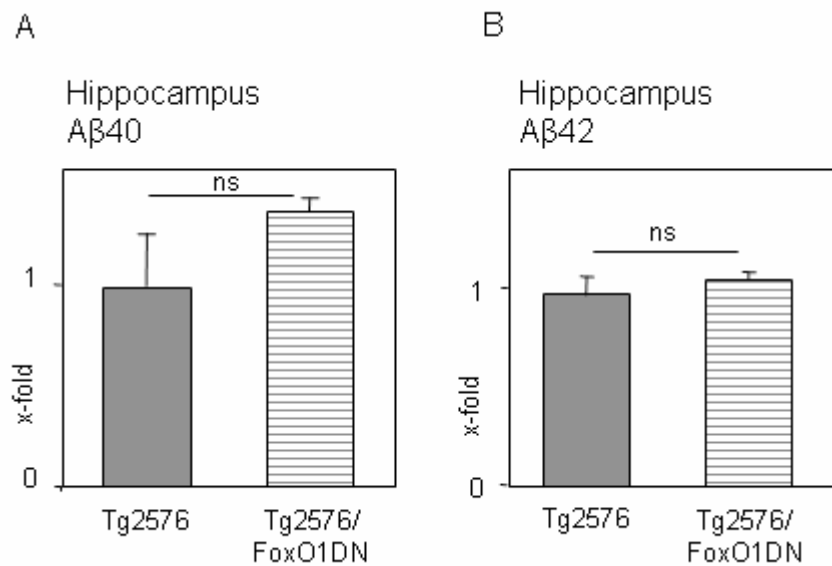


Figure 39: Quantification of A β 40 and A β 42 in hippocampi of Tg2576 and Tg2576/FoxO1DN female mice. A β 40 and A β 42 generation in hippocampi of Tg2576/FoxO1DN (n=3) mice compared to Tg2576 mice (n=3).

Dot blot analysis was performed to detect oligomeric structures of A β which are thought to be the major neurotoxic A β species in AD. Figure 40 shows the dot blot of Tg2576/FoxO1DN compared to Tg2576. No changes of A β oligomers could be observed in Tg2576/FoxO1DN compared to Tg2576 mice. Additionally no differences between female and male were detected (Fig. 40).

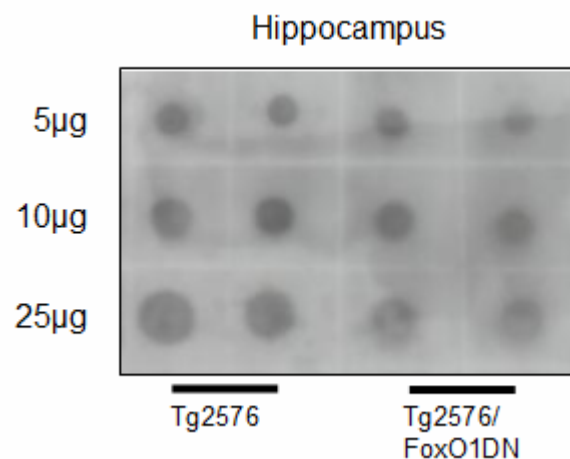


Figure 40: Dot Blot for analysis of A β oligomers of Tg2576/FoxO1DN hippocampus. Dot Blot analysis of A β oligomers in FoxO1ADA/Tg2576 female and male mice compared to Tg2576. Different protein concentrations were used for Dot Blots (5, 10 and 25 μ g).

Cleavage of APP by α - or β -secretases promotes the generation of α - or β -CTFs. As indicated in figure 38 the expression of the β -secretase BACE-1 and the α -secretase ADAM10 or ADAM17 (TACE) were not changed in 60 weeks old Tg2576/FoxO1DN female and male mice compared to Tg2576 mice. Furthermore no altered protein expression of Presenilin-1, the catalytic active part of the γ -secretase complex, was detected (Fig. 41).

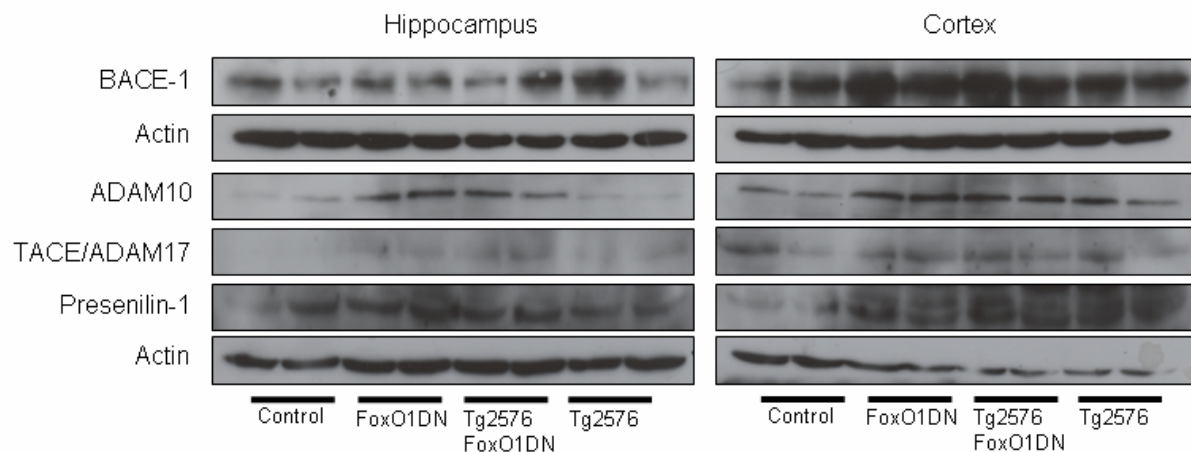


Figure 41: Expression of α -, β - and γ -secretases 60 weeks old Tg2576/FoxO1DN mice.

BACE-1, ADAM10, TACE/ADAM17 and Presenilin-1 expression in hippocampus and frontal cortex of 60 weeks old Tg2576/FoxO1DN female and male mice compared to Tg2576 mice. Actin serves as control. 100 μ g of total proteins were used and separated via 10% SDS-PAGE.

Expression of proteins involved in A β clearance is shown in figure 42. HSF1 is thought to play a role in the degradation of A β . The expression of HSF1 is not changed in Tg2576/FoxO1DN female and male mice compared to Tg2576 mice. Furthermore the expression level of α -2Macroglobulin and ApoE are not altered in Tg2576/FoxO1DN female and male mice compared to Tg2576 mice (Fig. 42).

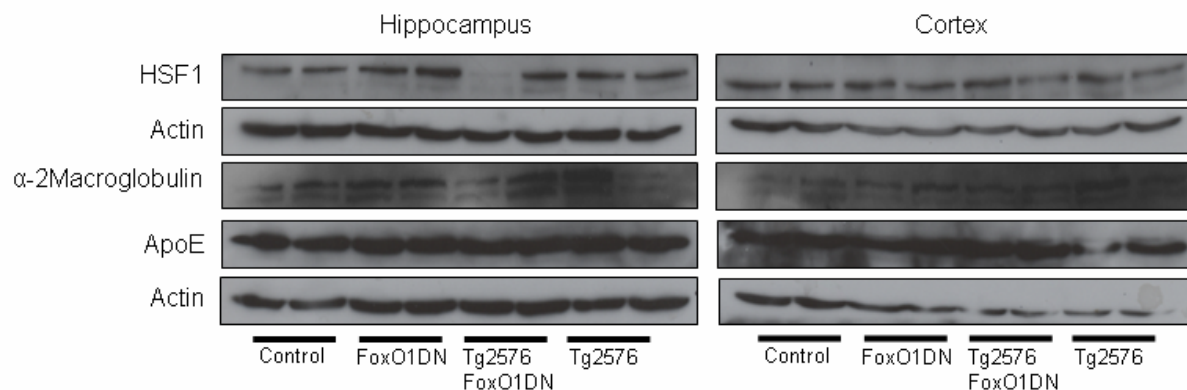


Figure 42: Proteins involved in A β clearance in 60 weeks old Tg2576/FoxO1DN mice.

Expression of HSF1, α -2Macroglobulin and ApoE in hippocampus and frontal cortex of 60 weeks Tg2576/FoxO1DN female and male mice compared to Tg2576 mice. Actin serves as control. 100 μ g of total proteins were used and separated via 10% SDS-PAGE.

3.4. Verification of FoxO1ADA expressing mice

Homologous recombination of the FoxO1ADA gene was controlled via FoxO1ADA and -DN specific PCR. The primers bind in the sequence of the Rosa26 locus which flanks the inserted gene (2.9.3.). To distinguish FoxO1ADA and -DN the size of the amplified DNA fragment is important. The fragment size of about 2000bp displays the FoxO1ADA gene (Fig. 43A). The expression of FoxO1 in the hippocampus and frontal cortex is shown in figure 40B.

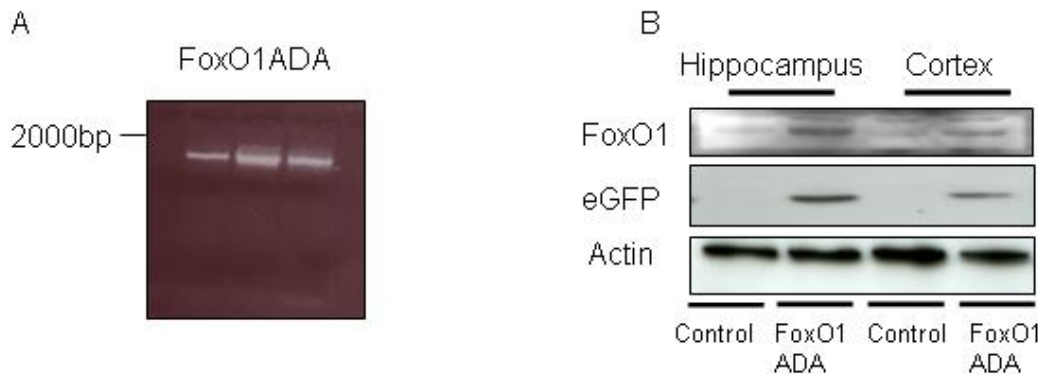


Figure 43: Detection of FoxO1ADA.

(A) FoxO1ADA and specific PCR (2.9.3.). (B) FoxO1ADA and eGFP expression in the hippocampus and frontal cortex of SynCre/FoxO1ADA mice and wild-type mice as controls. 100 μ g total proteins were separated via 10% SDS-PAGE.

3.5. Characterisation of FoxO1ADA mice

Changes in glucose homeostasis and growth might affect survival and the pathology of Alzheimer's disease. Previous studies showed that the deletion of the IGF-1R in neurons and glia cells of the CNS result in growth retardation and abnormal behaviour (Kappeler et al., 2008). The deletion of brain derived IRS-2 or IR leads to increased food intake and body weight (Brüning et al., 2000; Masaki et al., 2004, Lin et al., 2004). Therefore the metabolism of FoxO1DN and FoxO1ADA mice was analysed.

3.5.1. Glucose homeostasis of FoxO1ADA mice

Analysis of glucose homeostasis of FoxO1ADA was performed. Blood glucose was measured beginning at 5 weeks until 60 weeks of age. No alterations of blood glucose concentration in the FoxO1ADA female mice have been detected (Fig. 4A). FoxO1ADA male mice showed a slight decreased blood glucose concentration from 5 to 7 weeks of age compared to wild-type mice ($p \leq 0.002$). An increase of blood glucose from FoxO1ADA male mice occurred at 36 until 52 weeks. However, this did not reach significant (Fig. 44B).

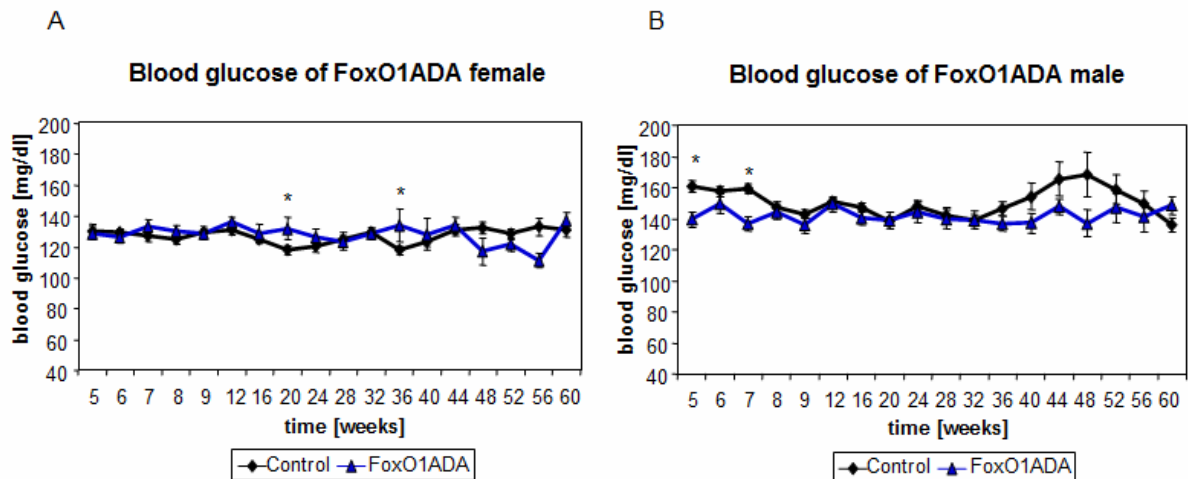


Figure 44: Blood glucose of FoxO1ADA female and male until 60 weeks of age. (A) Blood glucose of FoxO1ADA (n=22, blue) and wild-type (n=51, black) female mice up to 60 weeks. (B) Blood glucose of FoxO1ADA (n=33, blue) and wild-type (n=61, black) male mice until 60 weeks of age (*p<0.002, Student's t-test).

Glucose tolerance tests and insulin tolerance tests were performed at 10 and 11 weeks of age. In total 21 female FoxO1ADA, 20 female wild-type, 23 male FoxO1ADA and 23 male wild-type mice were analysed. Glucose tolerance tests of FoxO1ADA female revealed no changes compared to wild-type mice (Fig. 45A). In contrast FoxO1ADA male mice show decreased but not statistically significant glucose tolerance in comparison to wild-type mice (Fig. 45B).

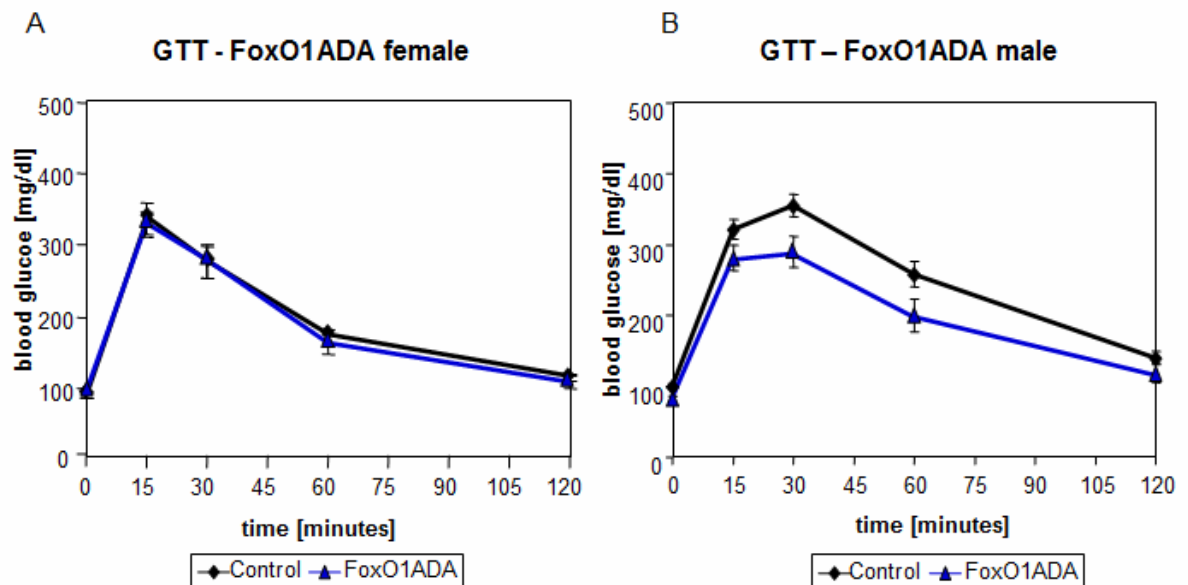


Figure 45: Glucose tolerance tests of FoxO1ADA and wild-type mice. (A) Glucose tolerance tests of FoxO1ADA female (n=21; blue) compared to control animals (n=20; black). (B) Glucose tolerance test of FoxO1ADA male (n=23; blue) and wild-type mice (n=23; black).

Insulin tolerance tests of FoxO1ADA female revealed no alteration in insulin sensitivity compared to wild-type animals (Fig. 46A). In contrast FoxO1ADA male mice display a statistical significant (p<0.01) increased insulin sensitivity compared to wild-type mice (Fig. 46B).

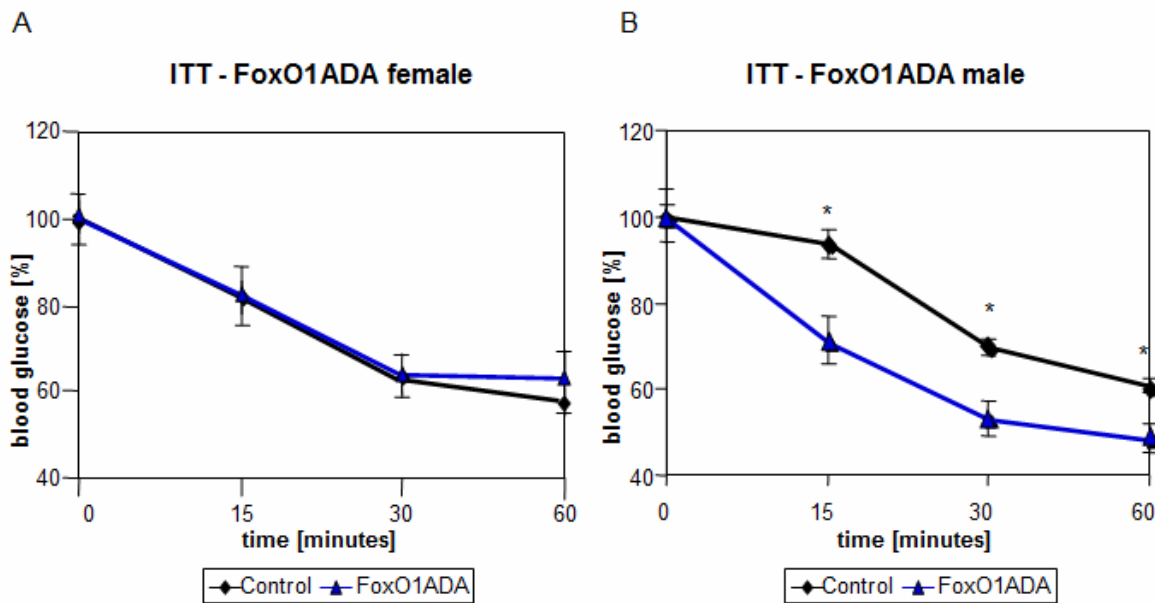


Figure 46: Insulin tolerance tests of FoxO1ADA and wild-type mice. (A) Insulin tolerance tests of FoxO1ADA female (n=21; blue) compared to control animals (n=20; black). (B) Insulin tolerance test of FoxO1ADA male (n=23; blue) and wild-type mice (n=23; black) (*p<0.01, Student's t-test).

3.5.2. Analysis of IR/IGF-1R signaling in 28 weeks old FoxO1ADA mice

Alterations of protein expression and phosphorylation level were analysed via western blots. 28 weeks old FoxO1ADA female and male mice present no changes in IR and IGF-1R expression compared to female and male wild-type animals. The analysed brain regions were hippocampus and the frontal cortex (Fig. 47).

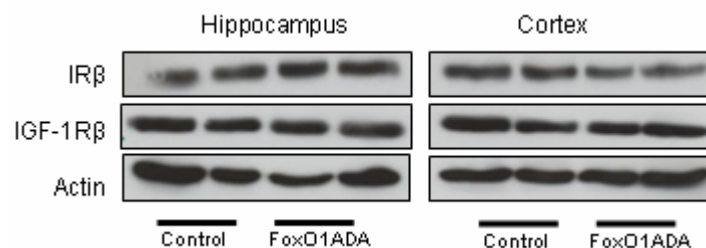


Figure 47: Expression level of IR and IGF-1R from 28 weeks old FoxO1ADA mice. Expression level of the IR, IGF-1R and actin as loading control are shown. Protein levels of hippocampus and frontal cortex from female and male wild-type (control) and FoxO1ADA mice. 100 µg of total proteins were separated via 10% SDS-PAGE.

Phosphorylation status of AKT, ERK1/2 and GSK3β were analysed to estimate activation of the PI3 kinase and MAP kinase signaling pathways which are both regulated via the IR and IGF-1R. Phosphorylation of AKT and ERK1/2 are not changed in both female and male mice. Phosphorylation of GSK3β was increased in hippocampus lysates of female wild-type and female FoxO1ADA mice. However this was due different levels of GSK3β (Fig. 48).

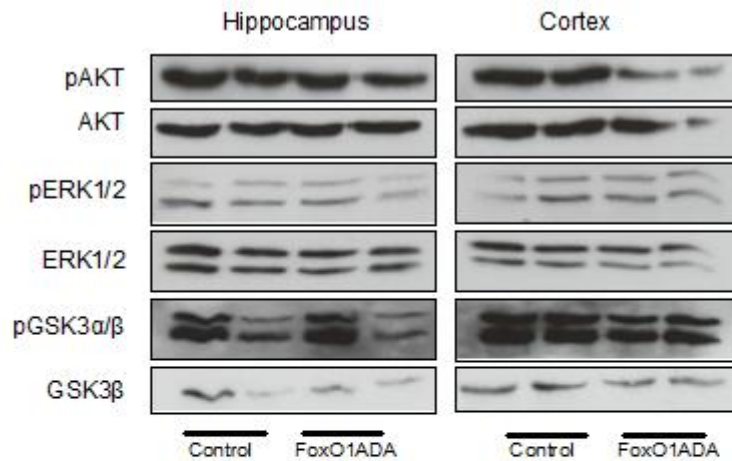


Figure 48: IR/IGF1R signaling pathway of 28 weeks old FoxO1ADA mice. Phosphorylation level of AKT (pAKT, Ser473), ERK1/2 (pERK1/2, Thr202/Tyr204) and GSK3 β (pGSK3 β , Ser9) are shown. As control served unphosphorylated protein level of AKT, ERK1/2 and GSK3 β . Female and male wild-type mice (control) are compared to FoxO1ADA female and male mice at the age of 28 weeks. 100 μ g of total proteins were separated via 10% SDS-PAGE.

3.5.3. Growth of FoxO1ADA mice

Body growth of FoxO1ADA mice was analysed because FoxO1 mediated transcription is amongst others involved in regulating somatic growth. Therefore body weight was measured from 5 till 60 weeks of age. Furthermore CT and NMR analysis were performed to detect body fat and lean body mass. Additionally X-rays as well as measurements of body length, food and water intake were performed.

FoxO1ADA female mice weight significantly less than wild-type mice up to 60 weeks of age (Fig. 49A). The difference of body weight at 28 weeks was about 1.7 g (Fig. 49C). At this time point 14 female FoxO1ADA and 46 wild-type mice were measured ($p \leq 0.03$). In addition FoxO1ADA male mice showed lower body from 5 to 56 weeks of age (Fig. 49B) with a more pronounced difference than in female mice. The difference at 28 weeks was about 2.5 g ($p \leq 0.01$) for FoxO1ADA males compared to wild-type male mice (Fig. 49D).

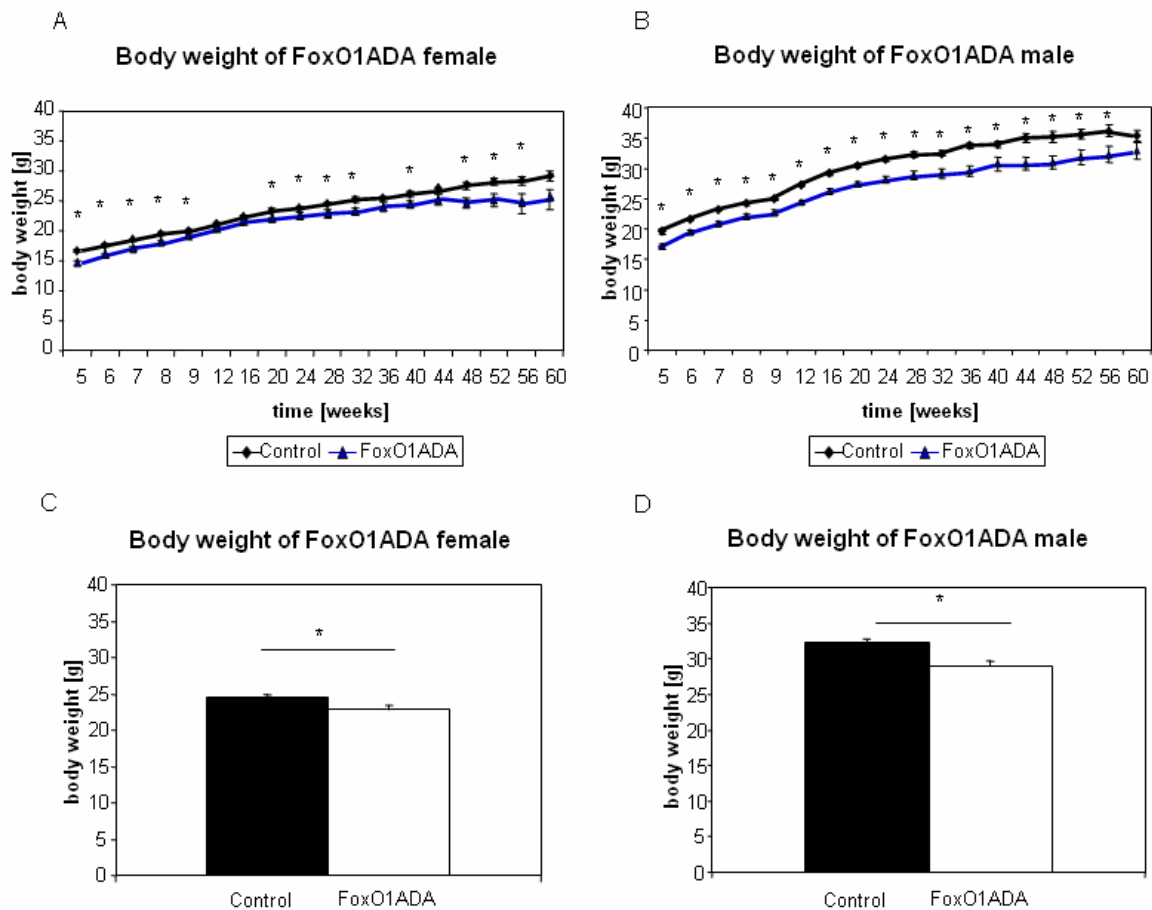


Figure 49: Body weight of FoxO1ADA mice over 60 weeks.

(A) Body weight of FoxO1ADA female mice (n=22, blue) compared to wild-type female mice (n=51, black). (B) Body weight of FoxO1ADA male mice (n=33, blue) in comparison to wild-type male mice (n=61, black). (C) Body weight of female FoxO1ADA (n=14, Blue) and wild-type mice (n=46, black) at the age of 28 weeks ($p \leq 0.03$, Student's t-test). (D) Body weight of male FoxO1ADA (n=23, blue) and wild-type mice (n=46, black) at 28 weeks ($p \leq 0.01$, Student's t-test).

To analyse body composition CT and NMR of 60 weeks old FoxO1ADA and wild-type male mice were performed. 6 animals of each genotype were studied. Body fat was not changed in FoxO1ADA male mice compared to wild-type mice using both methods, CT and NMR (Fig. 50A and B). However lean body mass of FoxO1ADA male mice was statistically significant reduced compared to wild-type mice (CT $p \leq 0.02$, NMR $p \leq 0.002$). The difference in lean body mass was nearly about 5 gram (Fig. 50C and D).

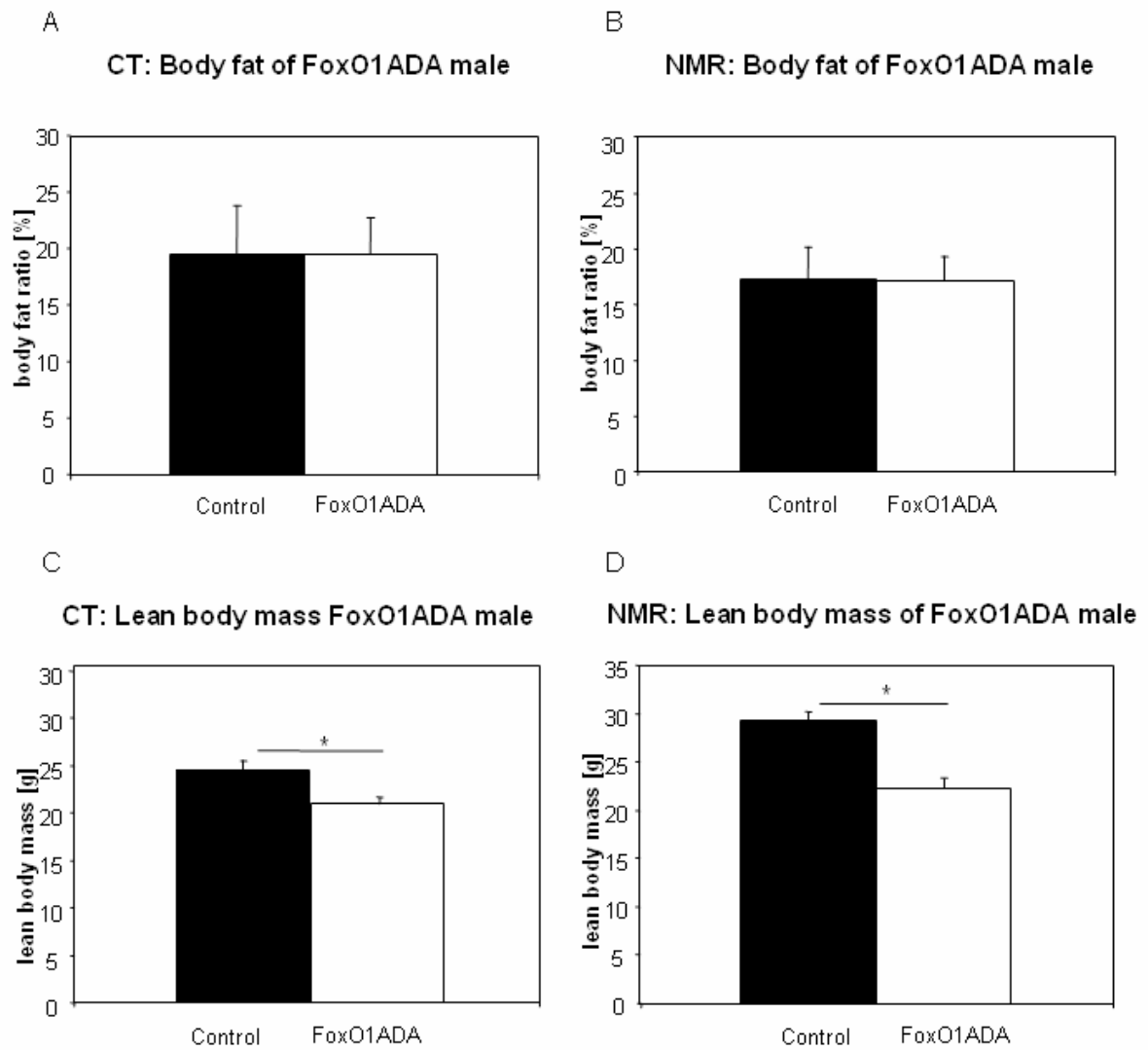


Figure 50: Body composition of FoxO1ADA male mice.

(A and C) Body fat ratio and lean body mass of FoxO1ADA male mice (n=6) compared to wild-type mice (n=6) via CT. (B and D) Body fat ratio and lean body mass of FoxO1ADA male mice (n=6) and wild-type mice (n=5) via NMR. The mice used for analysis of body composition were 60 weeks old (CT* $p \leq 0.02$, NMR* $p \leq 0.002$, Student's t-test).

X-ray and false-coloured imaging of FoxO1ADA 60 weeks old male mice showed similar bone densities and no skeletal deformation. What becomes obvious is that FoxO1ADA presented a thinner body (Fig. 51 A and B).

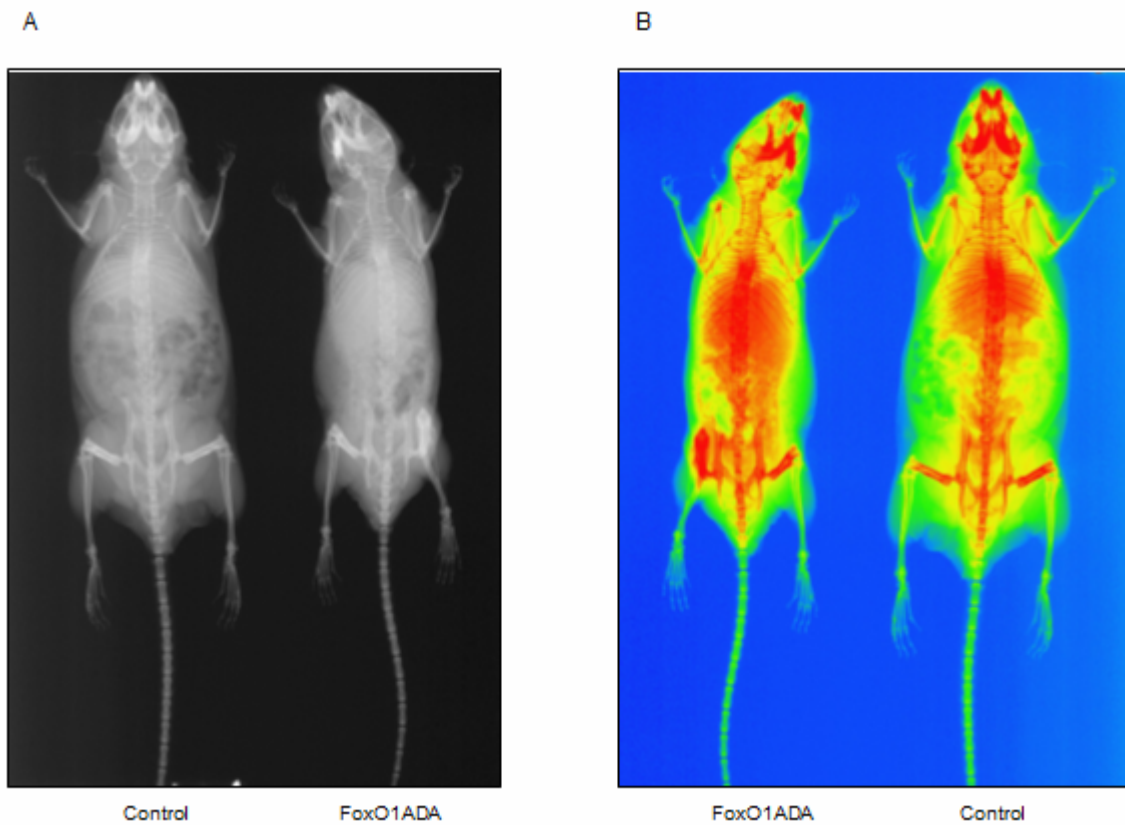


Figure 51: Analysis of bone density.

(A) X-ray of FoxO1ADA male compared to wild-type mice at 60 weeks of age. (B) False-coloured imaging of FoxO1ADA male compared to wild-type mice at 60 weeks of age.

Body length of 60 weeks old FoxO1ADA mice and wild-type showed no significant changes. For this analysis 3 FoxO1ADA and 6 wild-type animals at the age of 60 weeks were used (Fig. 52).

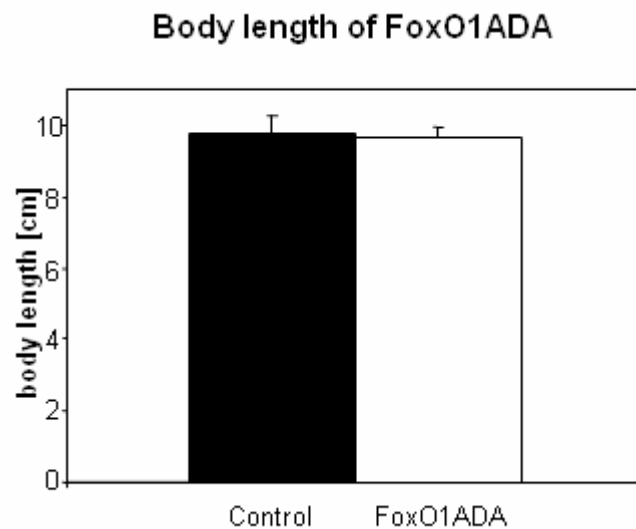


Figure 52: Body length of 60 weeks old FoxO1ADA male mice.

Body length of FoxO1ADA male mice (n=3) compared to wild-type mice (n=6).

3. Results

For estimated food and water intake 6 FoxO1ADA and 6 wild-type male mice were used. Food intake of FoxO1ADA male mice was slightly but not significantly increased compared to wild-type mice (Fig. 53A). Water intake was not altered in FoxO1ADA mice (Fig. 53B).

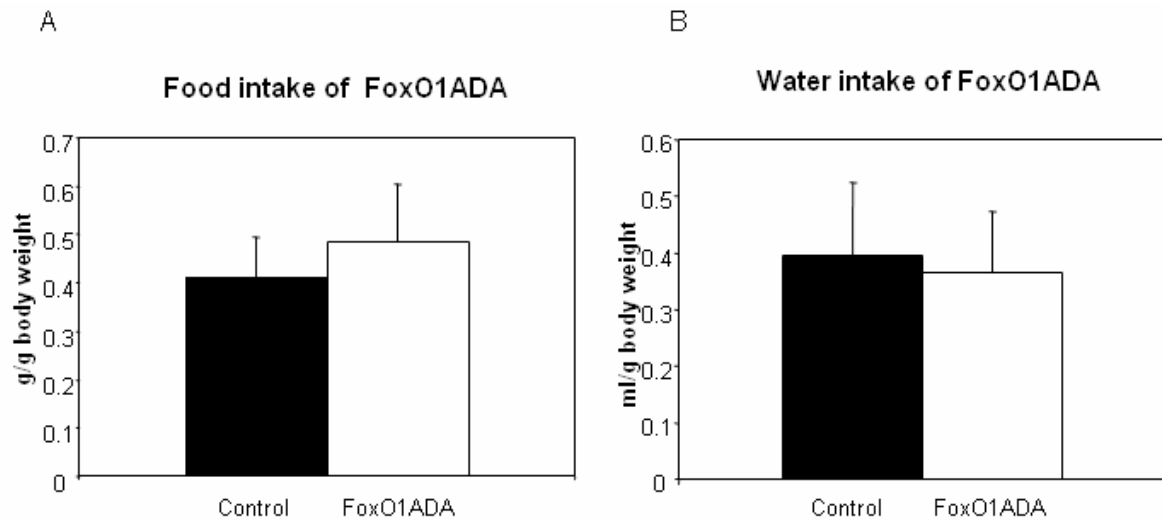


Figure 53: Food and water intake of 60 weeks old FoxO1ADA male mice. (A and B) Food and water intake of FoxO1ADA male mice (n=6) compared to wild-type male mice (n=6).

To exclude changes of key mediators of growth FoxO1ADA mice were studied via realTime PCR analysis of the growth hormone axis. The RNA levels of growth hormone releasing hormone (GHRH) in hypothalamus, growth hormone releasing hormone receptor (GHRHR) and growth hormone (GH) in pituitary as well as growth hormone receptor (GHR) and IGF-1 in liver were detected in 4 weeks old FoxO1ADA male mice. Only male FoxO1ADA mice were analysed because these mice presented a more prominent difference in body weight than female FoxO1ADA mice (Fig. 46). The animals were dissected at the same time of day to exclude hormonal changes during the day. A slight but not significant reduction of GHRH in the hypothalamus could be observed. Furthermore no changes of GHRHR and GH in pituitary as well as of GHR in liver were detected (Fig. 54).

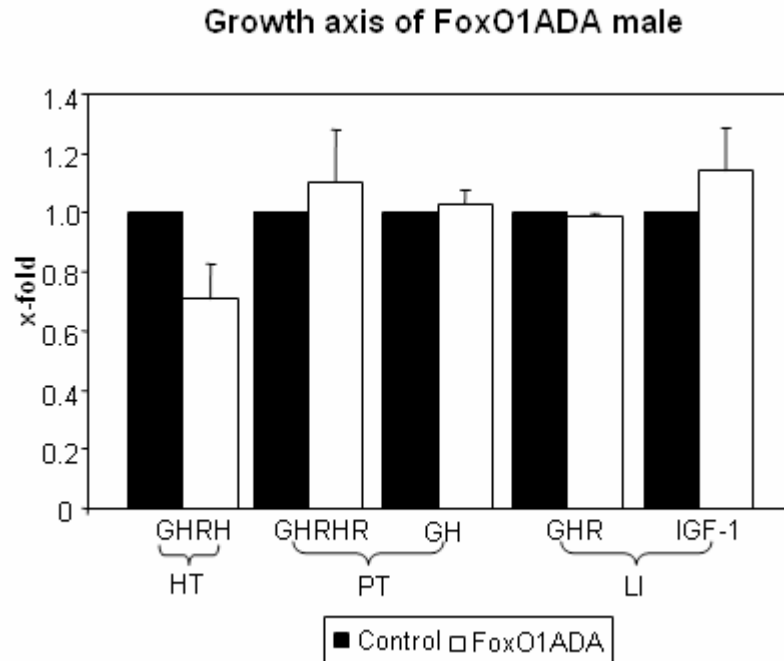


Figure 54: realTime PCR analysis of growth axis in 4 weeks old FoxO1ADA male mice. Analysis of mRNA levels of growth hormone releasing hormone (GHRH) in hypothalamus (HT), growth hormone releasing hormone receptor (GHRHR) and growth hormone (GH) in pituitary (PT) as well as growth hormone receptor (GHR) and IGF-1 in liver (LI) of 4 weeks old FoxO1ADA mice (n=4) compared to wild-type (n=6). mRNA levels of wild-type mice were set as 1.0.

3.5.4. Indirect calorimetric analysis of FoxO1ADA mice

FoxO1ADA mice showed a lower body weight compared to wild-type mice. These differences were observed in female and to a larger extent in male mice. To further analyse metabolism of these mice indirect calorimetry was performed. First the motor abilities of FoxO1ADA mice was tested via RotaRod which presented no affected motor coordination of FoxO1ADA male mice compared to wild-type mice (Fig. 55).

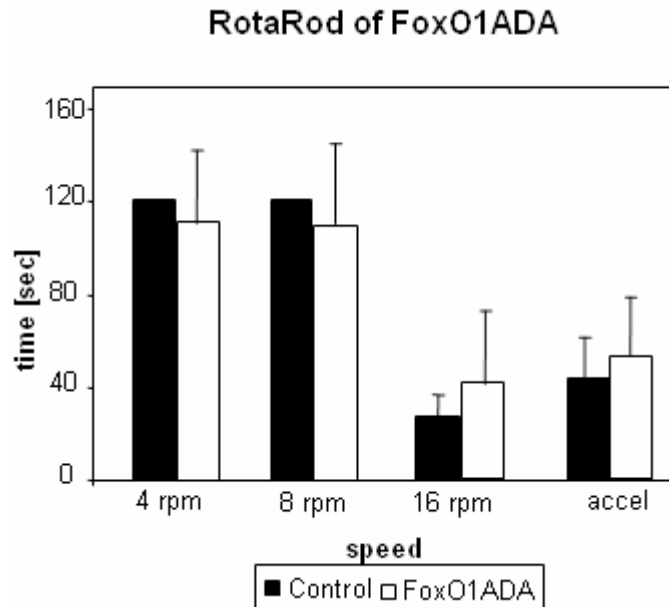


Figure 55: RotaRod test of FoxO1ADA male mice. RotaRod test in FoxO1ADA (n=6) compared to wild-type animals (n=6). Animals were between 14 and 20 weeks old.

Furthermore locomotive activity of FoxO1ADA mice was analysed. FoxO1ADA male mice show an increased activity compared to wild-type mice at 60 weeks of age. This difference in activity was statistically significant ($p \leq 0.001$) and was about 500 counts during the dark phase (Fig. 56).

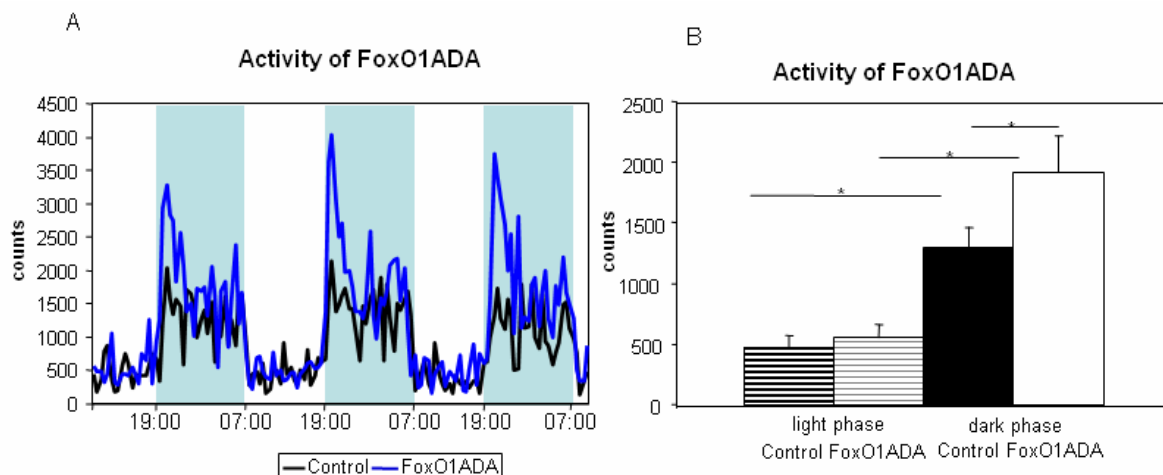


Figure 56: Locomotion activity of 60 weeks old FoxO1ADA male mice. (A) Activity of FoxO1ADA male mice (n=6, blue) compared to wild-type mice (n=6, black). Measurements were performed for 3 days. (B) Mean value of activity from FoxO1ADA male mice (n=6) and wild-type mice (n=6) (* $p \leq 0.001$, Student's t-test).

Interestingly energy expenditure normalized to lean body mass of these animals displayed no changes during the dark phase while activity is increased in FoxO1ADA male mice (Fig. 56). In addition energy expenditure of FoxO1ADA mice is slightly increased during the light phase ($p \leq 0.001$) (Fig. 57).

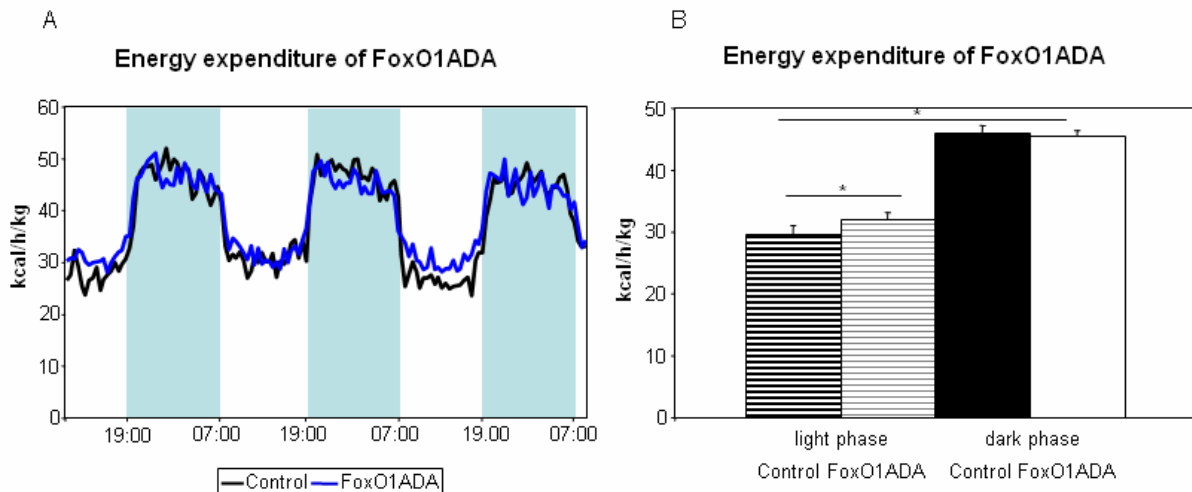


Figure 57: Energy expenditure of 60 weeks old FoxO1ADA mice. (A) Energy expenditure normalized to lean body mass of FoxO1ADA male mice (n=6, blue) compared to wild-type mice (n=6, black). Analysis was performed for 3 days. (B) Mean value of energy expenditure from FoxO1ADA male mice (n=6) and wild-type mice (n=6) (* $p \leq 0.001$, Student's t-test).

The respiratory quotient (RQ) is calculated from eliminated CO_2 and consumed O_2 . The RQ is significantly decreased in wild-type mice compared to FoxO1ADA male mice at the dark phase ($p \leq 0.001$). The RQ of FoxO1ADA during the dark phase was about 0.9 which indicates carbohydrates to be predominantly metabolized. During the light phase FoxO1ADA displayed a significant decrease of the RQ ($p \leq 0.002$). Hence, for wild-type and FoxO1ADA mice proteins are the major metabolized sources at day (Fig. 58).

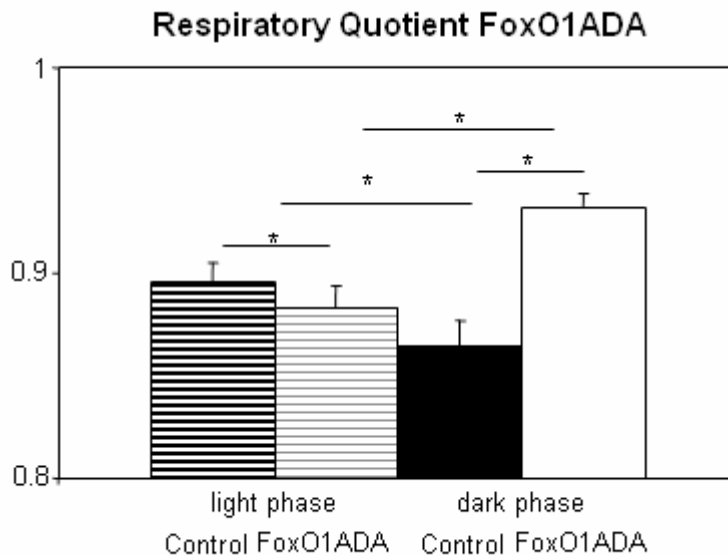


Figure 58: Respiratory quotient of 60 weeks old FoxO1DN mice. Respiratory quotient of FoxO1ADA male mice (n=6) compared to wild-type mice (n=6). Analysis was performed for 2 days (* $p \leq 0.002$, Student's t-test).

3.5. Behaviour of FoxO1ADA mice

To analyse whether the neuron-specific FoxO1ADA expression affects brain structure or behaviour of the FoxO1ADA mice Nissl stainings of serial sections of the brain and behavioural tests (exploration, fear behaviour) were performed. Furthermore the spatial learning potential of the mice was investigated. Only male mice were analysed because less hormonal fluctuations affect the behaviour.

Nissl staining of brains from wild-type and FoxO1ADA male mice which were 28 weeks old displayed unaltered brain structures e.g. hippocampal formation (Fig. 59).

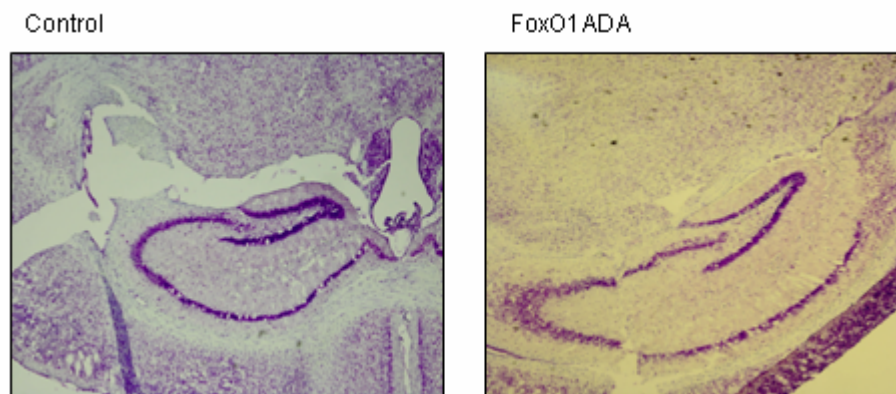


Figure 59: Nissl staining of the hippocampus of 28 weeks old FoxO1ADA mice. Nissl staining of the hippocampal formation of 28 weeks old FoxO1ADA male mice compared to wild-type mice.

The Open field test analyses explorative and fear behaviour of mice. Time how long the mice stood in the center or border of the box was measured. FoxO1ADA mice showed no difference in time spend in the center or at the border of the test box compared to wild-type mice (Fig. 60A). Furthermore fear behaviour of these mice was investigated via O-Maze. This test showed that FoxO1ADA male mice present similar fear behaviour as wild-type mice at 60 weeks of age (Fig. 60).

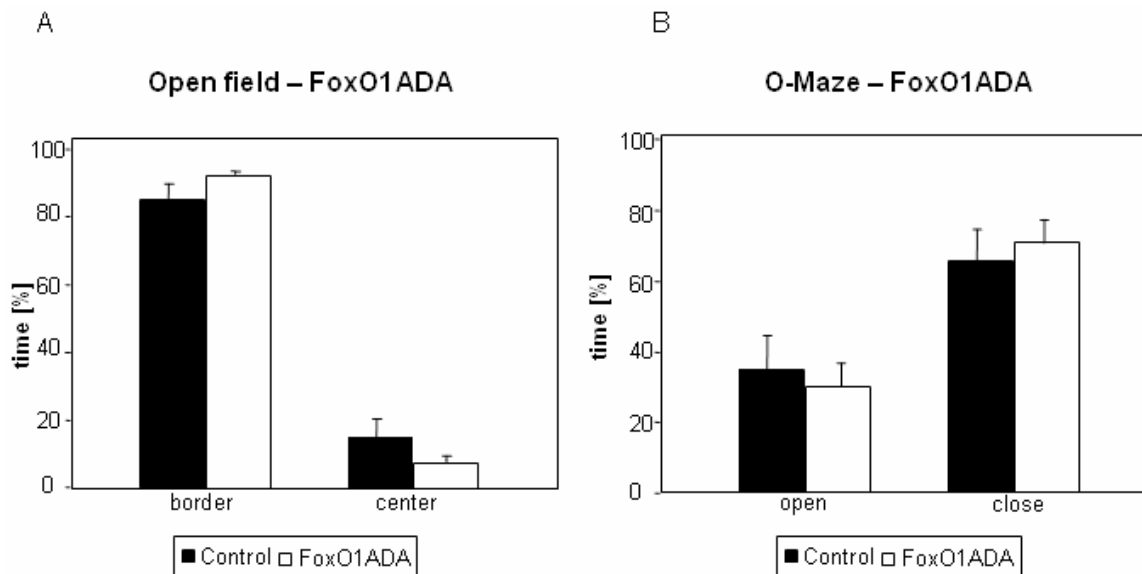


Figure 60: Open field and O-Maze test of FoxO1ADA.

(A) Open field test of FoxO1ADA male mice (n=6) compared to wild-type mice (n=6). (B) O-Maze test of FoxO1ADA male mice (n=6) compared to wild-type mice (n=6). Animals were 60 weeks old.

Moreover, spatial learning behaviour of FoxO1ADA male mice was analysed. For that reason the Morris Water Maze test was used. The test took 5 days and the time was measured till the mouse reaches the platform which was hidden under the water surface (escape latency). Each test was performed for 1 minute. At day 5 the platform was removed and the time the mouse swam in the quadrant where the platform originally was located was analysed. Interestingly FoxO1ADA mice found the platform faster than wild-type in this task. At day 1 the difference in time was statistically significant ($p \leq 0.02$). During the 5th day wild-type mice showed a learning ability and from day 3 to day 5 there were no differences in time needed to reach the platform between (Fig. 61A). On the last day of the tests the platform was removed and the time was measured while each mouse swims in the target quadrant. FoxO1ADA spend longer time in the quadrant the platform originally was located compared to wild-type mice but this difference was not significant (Fig.61B).

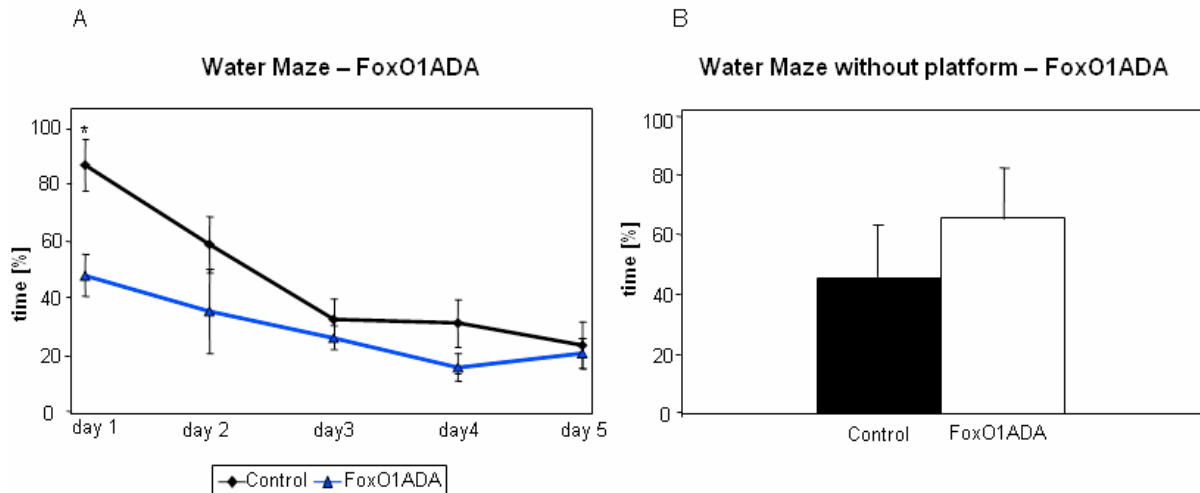


Figure 61: Water Maze test of FoxO1ADA mice.

(A) Water Maze test was performed over 5 days to compare FoxO1ADA (n=4, red) and wild-type (n=6, black) spatial learning behaviour. The time was measured until they found the platform, maximum time was 1 minute. (B) After 5 days the platform was removed and the time was measured while the mouse was swimming in the quadrant where the platform originally was (* $p \leq 0.02$, Student's t-test).

3.6. Role of FoxO1 in Alzheimer's disease

Previous studies might suggest that the IR/IGF-1R signaling pathway is disturbed in the central nervous system of patients suffering from AD (Frolich et al. 1998; Frolich et al. 1999; Moloney et al. 2010). Neuron-specific deletion of the IGF-1R rescues premature mortality and a decreased processing of APP in Tg2576 mice (Freude et al., 2009). To analyse whether this effect is mediated through FoxO1 the dominant negative (FoxO1DN) and constitutive active form of FoxO1 (FoxO1ADA) were analysed in a Tg2576 background.

3.6.1. Glucose homeostasis of Tg2576/FoxO1ADA mice

Blood glucose was measured from 5 till 60 weeks of age. Blood glucose concentrations of FoxO1ADA, wild-type, Tg2576/FoxO1ADA and Tg2576 female mice were similar during the whole study period. Significant changes have been observed at 5 ($p \leq 0.04$) and 44 weeks ($p \leq 0.05$). At 5 weeks blood glucose levels were decreased in Tg2576/FoxO1ADA mice and at 44 weeks higher than in Tg2576. From 36 to 52 weeks blood glucose concentration of Tg2576 female mice was decreased compared to Tg2576/FoxO1ADA mice (Fig. 62A). Tg2576/FoxO1ADA male mice had a lower blood glucose concentration compared to the other genotypes (Fig. 62B). The measurement ended at 12 weeks of age because all Tg2576/FoxO1ADA male died (see Fig. 67).

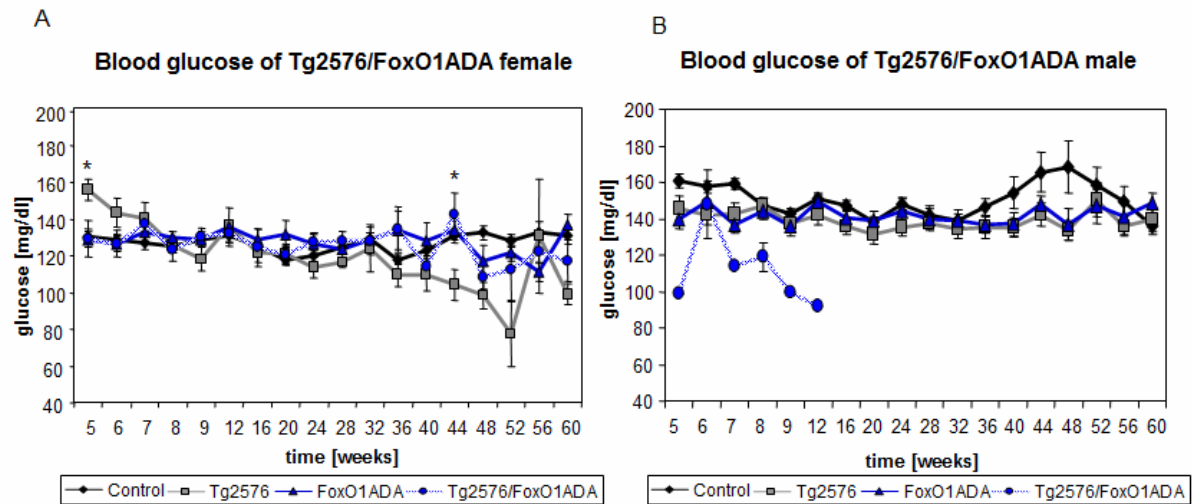


Figure 62: Blood glucose levels of FoxO1ADA mice in Tg2576 background.

(A) Blood glucose concentration of female Tg2576/FoxO1ADA (n=14, light blue), FoxO1ADA (n=22, blue), Tg2576 (n=29, grey) and wild-type mice (n=51, black) until 60 weeks of age. (B) Blood glucose of male Tg2576/FoxO1ADA (n=3, light blue), FoxO1ADA (n=33, blue), Tg2576 (n=31, grey) and wild-type mice (n=61, black) until 60 weeks of age (*Tg2576/FoxO1ADA compared to Tg2576, $p \leq 0.05$, Student's t-test).

Glucose tolerance tests of Tg2576/FoxO1ADA female mice revealed an initially higher blood glucose level in Tg2576/FoxO1ADA compared to Tg2576 female mice ($p < 0.05$). Glucose tolerance of Tg2576/FoxO1ADA was similar compared to Tg2576 female mice (Fig. 63A). Additionally Tg2576/FoxO1ADA male mice displayed a slightly decreased glucose concentration during GTT compared to FoxO1ADA mice which reaches significance at 15 minutes after glucose injection ($p \leq 0.05$). Tg2576/FoxO1ADA male mice also showed slight increased glucose levels during GTT compared to Tg2576 mice at 30 and 60 minutes after injection which did not reach significance (Fig. 63).

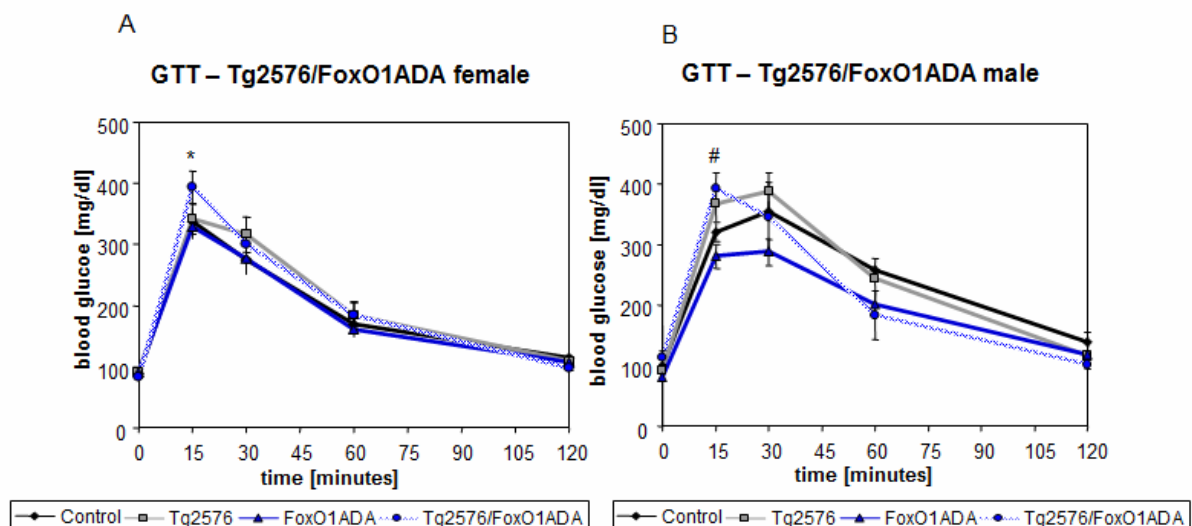


Figure 63: Glucose tolerance tests of Tg2576/FoxO1ADA and wild-type mice.

(A) Glucose tolerance tests of Tg2576/FoxO1ADA (n=13, light blue), Tg2576 (n=24, grey), FoxO1ADA female (n=21; blue) and control animals (n=20; black). (B) Glucose tolerance test of Tg2576/FoxO1ADA (n=3; light blue), Tg2576 (n=13, grey) FoxO1ADA male (n=23; blue) and wild-type mice (n=23; black) (*comparison of Tg2576/FoxO1ADA and Tg2576, $p \leq 0.05$; # comparison of Tg2576/FoxO1ADA and FoxO1ADA, $p \leq 0.05$, Student's t-test)

Insulin tolerance tests revealed nearly unaltered insulin sensitivity from Tg2576/FoxO1ADA female mice compared to Tg2576 mice. However, glucose concentrations at 15 minutes were significantly higher in Tg2576/FoxO1ADA compared to Tg2576 mice ($p \leq 0.04$) (Fig. 64A). Insulin sensitivity of Tg2576/FoxO1ADA male mice compared to Tg2576 mice shows no changes. (Fig. 64B).

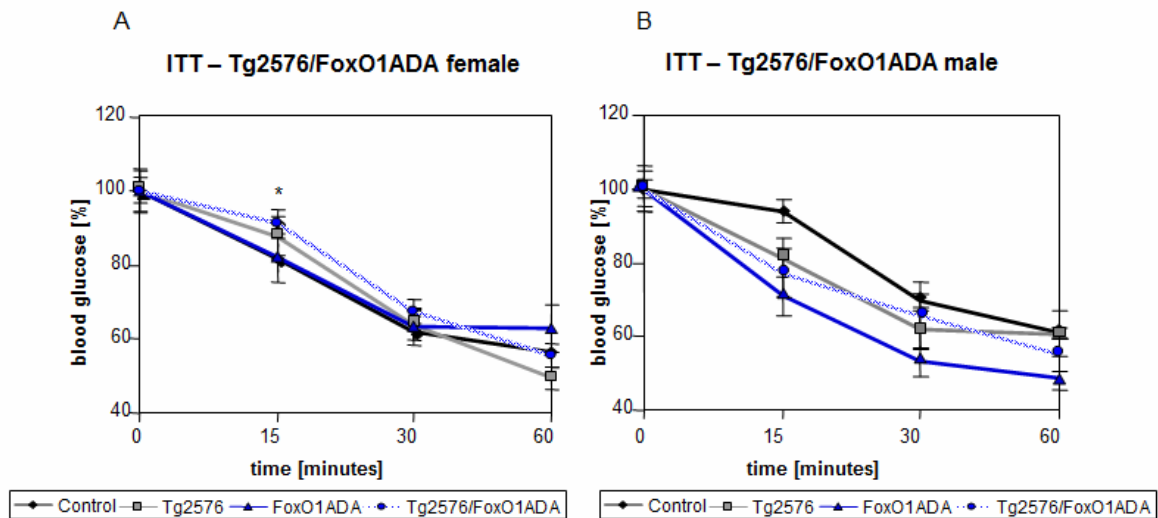


Figure 64: Insulin tolerance tests of Tg2576/FoxO1ADA and wild-type mice. (A) Insulin tolerance tests of Tg2576/FoxO1ADA ($n=13$, light blue), Tg2576 ($n=24$, grey), FoxO1ADA female ($n=21$; blue) and control animals ($n=20$; black). (B) Insulin tolerance test of Tg2576/FoxO1ADA ($n=2$; light blue), Tg2576 ($n=13$, grey) FoxO1ADA male ($n=23$; blue) and wild-type mice ($n=23$; black) (*comparison of Tg2576/FoxO1ADA and Tg2576 $p \leq 0.04$).

3.7. Growth of Tg2576/FoxO1ADA mice

Body weight of Tg2576/FoxO1ADA mice was measured from 5 till 60 weeks of age. Comparison of Tg2576/FoxO1ADA to Tg2576 female mice revealed that Tg2576/FoxO1ADA mice weight less from 5 till 20 weeks of age. This difference reached significance at 5 and 6 weeks ($p \leq 0.05$). Furthermore Tg2576/FoxO1ADA female mice had a lower body weight compared to FoxO1ADA mice from 5 till 20 weeks of age. Statistically significant differences were found at 5 to 9 weeks and at 16 weeks ($p \leq 0.03$) (Fig. 65A). Tg2576/FoxO1ADA male mice had a lower body weight compared to Tg2576 animals. This difference was significant at week 5 and 7 ($p \leq 0.03$). In addition Tg2576/FoxO1ADA male mice present a decreased body weight in comparison to FoxO1ADA mice reaching significance at week 5 till 7 ($p \leq 0.02$). Measurements of Tg2576/FoxO1ADA male ended at 9 weeks of age because animals died (Fig. 65B). Interestingly FoxO1ADA female and male mice had nearly the same body weight compared to Tg2576 mice.

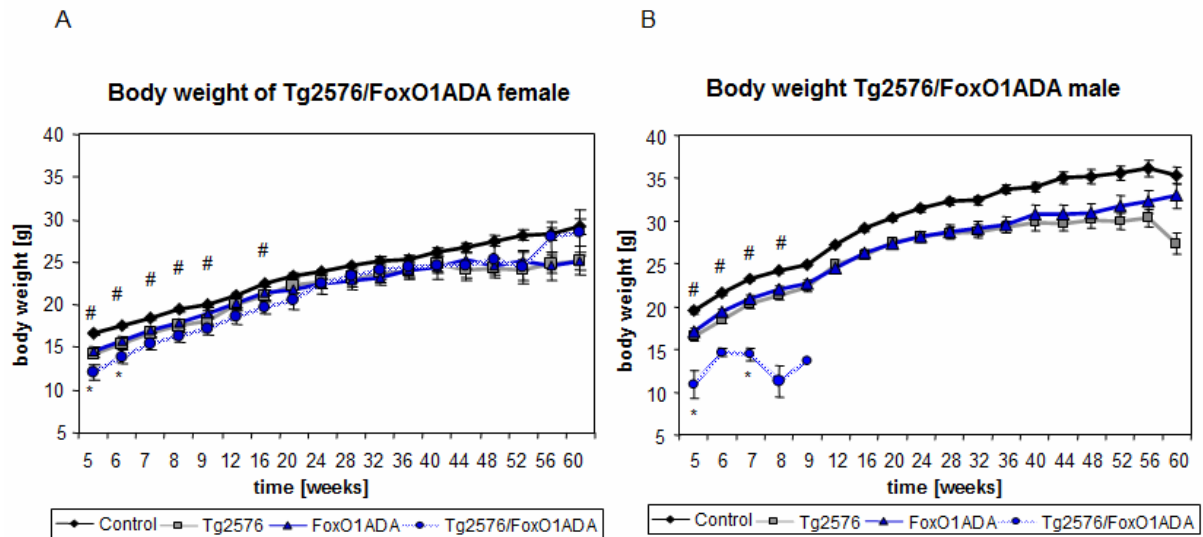


Figure 65: Body weight of Tg2576/FoxO1ADA until 60 weeks of age. (A) Body weight of female Tg2576/FoxO1ADA (n=14, light blue), FoxO1ADA (n=22, blue), Tg2576 (n=29, grey) and wild-type mice (n=51, black) until 60 weeks of age (* comparison of Tg2576/FoxO1ADA and Tg2576 $p \leq 0.05$, # comparison of Tg2576/FoxO1ADA and FoxO1ADA $p \leq 0.03$, Student's t-test). (B) Body weight of male Tg2576/FoxO1ADA (n=3, light blue), FoxO1ADA (n=33, blue), Tg2576 (n=31, grey) and wild-type mice (n=61, black) until 60 weeks of age. Significances are shown for comparisons of FoxO1DN and Tg2576/FoxO1ADA as well as Tg2576/FoxO1ADA and Tg2576 mice (* comparison of Tg2576/FoxO1ADA and Tg2576 $p \leq 0.03$, # comparison of Tg2576/FoxO1ADA and FoxO1ADA $p \leq 0.02$, Student's t-test).

Brain body ratio of 60 weeks old Tg2576/FoxO1ADA female mice showed no differences between wild-type and FoxO1ADA as well as Tg2576/FoxO1ADA and Tg2576 mice (Fig. 66A). In contrast body brain ratio of 60 weeks old wild-type and FoxO1ADA male mice presented a significant increase in FoxO1ADA mice ($p \leq 0.02$). Tg2576/FoxO1ADA male could not be analysed because this genotype died between 12 and 16 weeks of age (Fig. 66B and see Fig. 67).

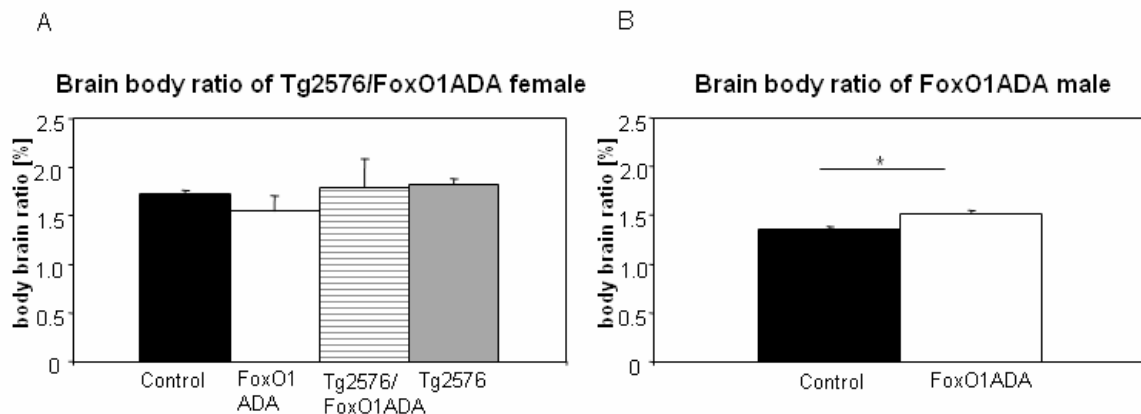


Figure 66: Brain body ratio of Tg2576/FoxO1ADA mice at 60 weeks of age. (A) Body brain ratio of wild-type (n=26), FoxO1ADA (n=4), Tg2576/FoxO1ADA (n=3) and Tg2576 (n=19) female mice at 60 weeks of age. (B) Body brain ratio of 60 weeks old wild-type (n=28) and FoxO1ADA (n=6) male mice at 60 weeks of age (* $p \leq 0.02$, Student's t-test).

3.8. Survival of FoxO1ADA mice

Survival of the different genotypes was analysed via Kaplan-Meier curves. Significances were shown for the comparisons of wild-type and Tg2576, wild-type and Tg2576/FoxO1ADA, FoxO1ADA and Tg2576 as well as FoxO1ADA and Tg2576/FoxO1ADA mice ($p \leq 0.05$, Wilcoxon-rank) (Fig. 67A). Kaplan-Meier analysis of female mice shows that none of the FoxO1ADA mice were dead 60 weeks of age but nearly 10% of wild-type female mice are dead. 50% of the Tg2576/FoxO1ADA and 30% of Tg2576 female mice were dead at the age of 60 weeks (Fig. 67B) and about 95% of FoxO1ADA and 85% of wild-type mice were alive at the end of the study. Furthermore nearly 70% of Tg2576 male mice still lived at 60 weeks of age. Tg2576/FoxO1ADA male mice all died between 12 and 16 weeks ($p \leq 0.05$, Wilcoxon-rank). As in females Tg2576 male mice showed significant decreased survival compared to wild-type and FoxO1ADA mice ($p \leq 0.05$, Wilcoxon-rank) (Fig. 67C).

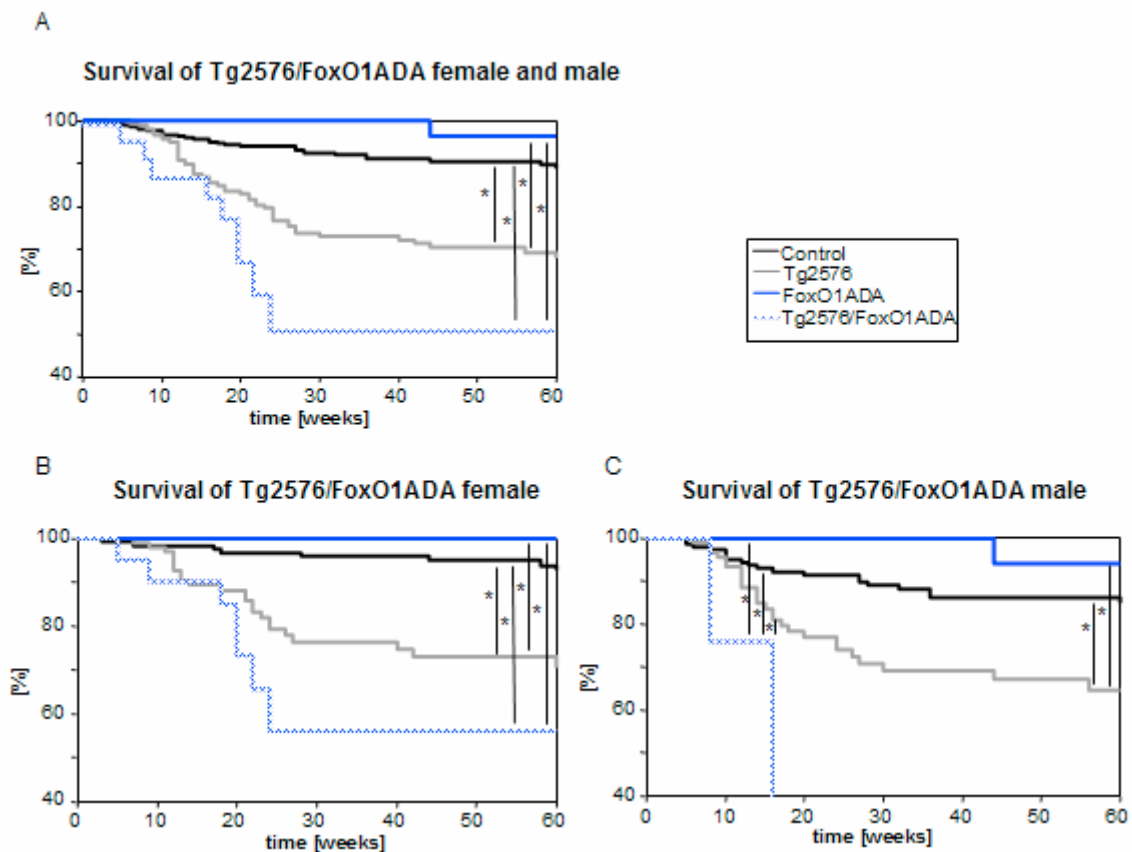


Figure 67: Survival of FoxO1ADA mice in Tg2576 background until 60 weeks of age.

(A) Survival of Tg2576/FoxO1ADA (n=14, light blue), Tg2576 (n=29, grey), FoxO1ADA (n=22, blue) and wild-type (n=51, black) female and male mice. (B) Survival of female Tg2576/FoxO1ADA (n=3, light blue), Tg2576 (n=31, grey), FoxO1ADA (n=33, blue) and wild-type (n=61, black). (C) Survival of male Tg2576/FoxO1ADA (light blue), Tg2576 (grey), FoxO1ADA (blue) and wild-type (black) (* $p \leq 0.05$, Wilcoxon-rank).

3.9. IR/IGF-1R signaling pathway in Tg2576/FoxO1ADA

The IR/IGF-1R signaling pathway was analysed via western blots. The expression levels of the IR and IGF-1R were the same in 60 weeks old wild-type, FoxO1ADA as well as

Tg2576/FoxO1 and Tg2576 mice. In addition expression levels were similar in female and male mice (Fig. 68).

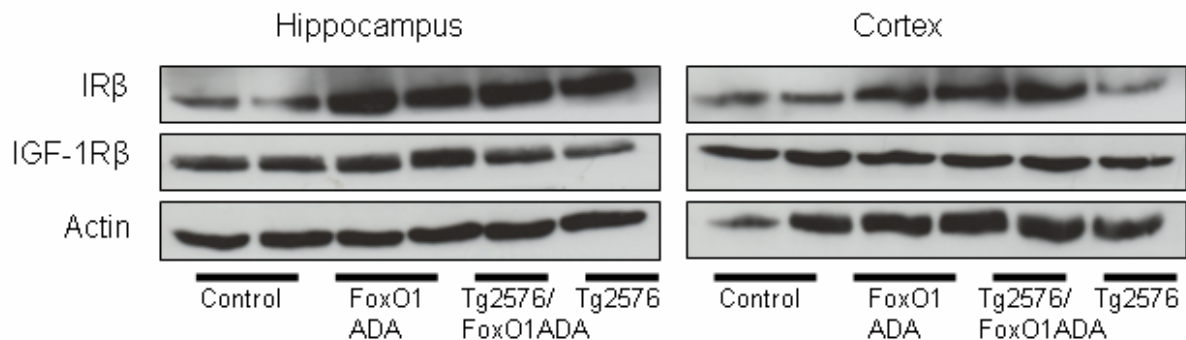


Figure 68: IR and IGF-1R protein expression of 60 weeks old Tg2576/FoxO1ADA mice. Expression level of the IR and IGF-1R with actin as control is shown. Protein levels of hippocampus and frontal cortex from female and male wild-type (control), FoxO1ADA, Tg2576/FoxO1ADA and Tg2576 mice. Actin was served as loading control. 100 µg of total proteins were used and separated via 10% SDS-PAGE.

Activation of the PI3 kinase and MAP kinase pathway was analysed via phosphorylation of AKT and ERK1/2. Phosphorylation levels were similar in all genotypes and gender at 60 weeks of age. Only female Tg2576/FoxO1ADA mice were analysed because Tg2576/FoxO1ADA male mice died before 60 weeks of age (Fig. 69).

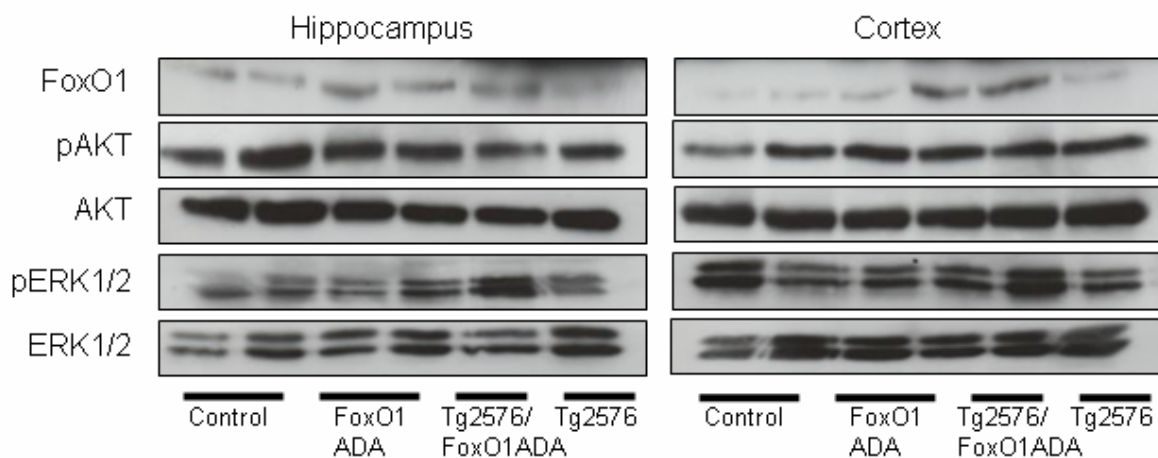


Figure 69: IR/IGF1R signaling pathway of 60 weeks old Tg2576/FoxO1ADA mice. Phosphorylation level of AKT (pAKT, Ser473) and ERK1/2 (pERK1/2, Thr202/Tyr204) are shown. As control served unphosphorylate protein level of AKT and ERK1/2. Female and male wild-type mice (control) are compared to FoxO1ADA female and male mice at the age of 60 weeks. Protein phosphorylation in hippocampus and frontal cortex are shown. 100 µg of total proteins were used and separated via 10% SDS-PAGE gels.

Furthermore the expression level of the FoxO1 target gene p27 was analysed via wetsern blots. Expression level of p27 which is a regulator of cell cycle shows no differences in 60 weeks old FoxO1ADA and wild-type mice (Fig. 70).

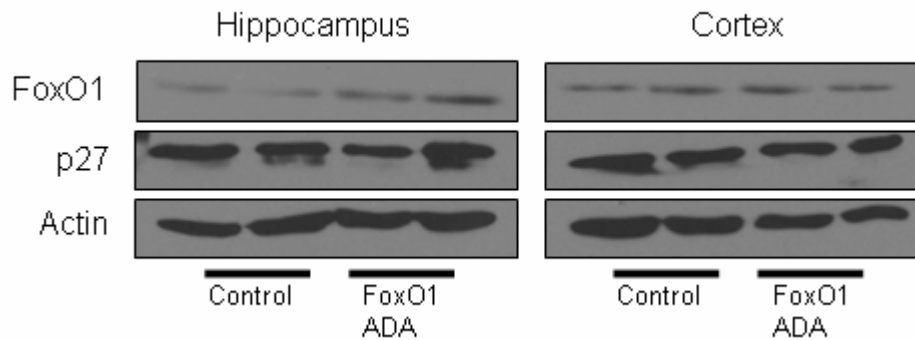


Figure 70: Expression of FoxO1 and p27 in 60 weeks old animals
FoxO1 expression as well as target gene expression from p27 of 60 weeks old FoxO1ADA female and male mice. Hippocampus and frontal cortex were analysed and actin served as control. 100 μ g of total proteins were used and separated via 10% SDS-PAGE.

3.10. APP Processing in Tg2576/FoxO1ADA mice

To analyse APP processing in Tg2576/FoxO1ADA mice western blots, ELISA and dot blots were performed. Figure 71 shows a similar expression of APP in the different genotypes. Unaltered levels of α/β CTFs suggested no changes in APP processing in Tg2576/FoxO1ADA mice. Furthermore the amount of A β is similar in Tg2576/FoxO1ADA compared to Tg2576 female mice (Fig. 71).

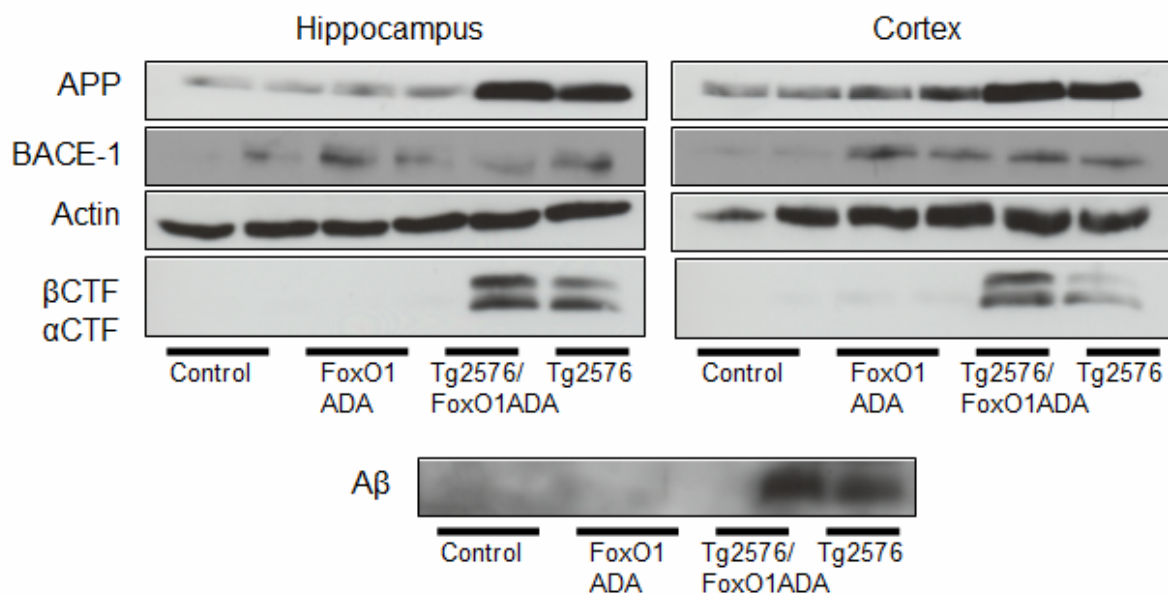


Figure 71: APP Processing of FoxO1ADA mice in Tg2576 background.
APP expression and generation of α/β CTFs are shown. As control wild-type, FoxO1ADA mice female and male mice are shown. Only female FoxO1ADA in Tg2576 background were generated. Therefore female Tg2576 mice are presented in this figure. 100 μ g of total proteins were used and separated via 10% or 15% SDS-PAGE. For A β amount 200 μ g of total proteins were separated via a urea tricine gel.

To further analyse the concentration of A β 40 and A β 42 ELISAs were performed. A β 40 is increased in Tg2576/FoxO1ADA female mice compared to Tg2576 mice. However, this

difference did not reach significance. A β 42 levels were not changed in both genotypes (Fig. 72).

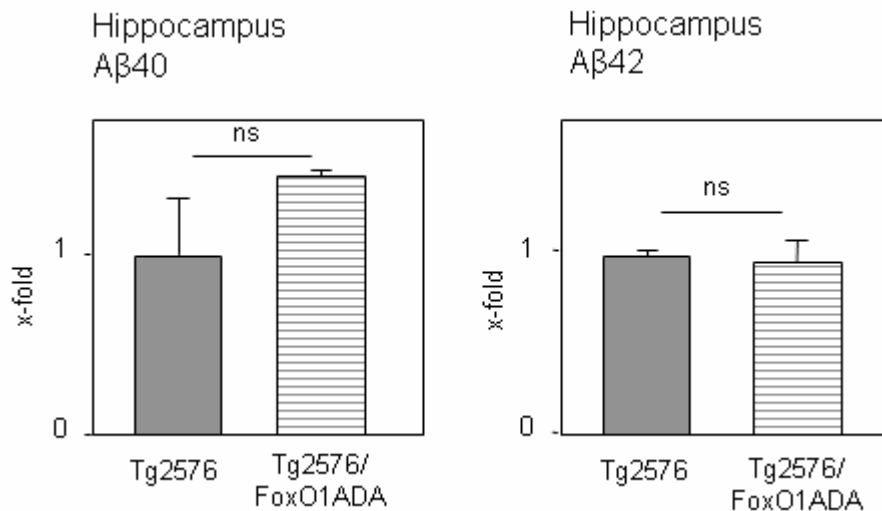


Figure 72: Level of A β 40 and A β 42 in hippocampi of Tg2576 and FoxO1ADA/Tg2576 female mice. A β 40 and A β 42 generation is not altered in Hippocampi of FoxO1ADA/Tg2576 mice (n=3) compared to Tg2576 mice (n=3).

To investigate the level of neurotoxic oligomers formed by A β dot blots were used. The amount of oligomers was similar in Tg2576/FoxO1ADA compared to Tg2576 female mice (Fig. 73).

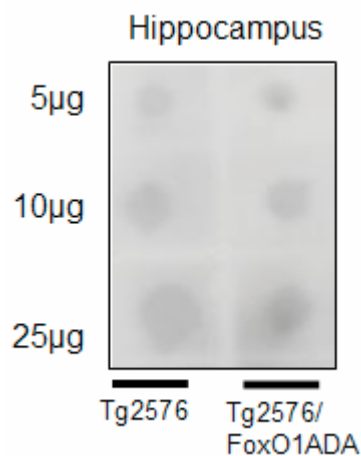


Figure 73: Dot Blot for analysis of A β oligomers of FoxO1ADA/Tg2576 hippocampus. Dot Blot analysis of A β oligomer formation in FoxO1ADA/Tg2576 female mice compared to Tg2576 mice. Different amounts of total proteins were used for Dot Blots (5, 10 and 25 μ g).

3.11. *In vitro* analysis of stably expressing FoxO1DN, FoxO1ADA and FoxO1 neuroblastoma cells

For *in vitro* studies SH-SY5Y human neuroblastoma cells were stably transfected with pCMV-Tag-2C which includes mouse derived FoxO1DN, FoxO1ADA or wild-type FoxO1. Vectors were linearized and then transfected into the neuroblastoma cells. 2 days after transfection cells were selected with Geneticin. Single cell clones were grown and tested for

target expression. For all experiments 3 clones of each FoxO1 cell line were used. Wild-type cells and cells transfected with the empty vector served as controls. Cell lines were analysed in respect to proliferation, cell cycle and apoptosis after oxidative stress.

3.11.1. Characterisation of stably expressing FoxO1DN, FoxO1ADA and FoxO1 neuroblastoma cells

The proof of FoxO1DN, FoxO1ADA and FoxO1 expression was performed via western blot. FoxO1DN present a size of about 30kDa and its expression was quite strong in stably transfected neuroblastoma cells (Fig. 74, left, lowest panel). Interestingly FoxO1DN cells indicate a downregulation of wild-type FoxO1 expression (Fig. 74, left, upper panel). Expression of FoxO1ADA is shown within the same western blot as FoxO1DN expression is shown. In addition neuroblastoma cells which overexpress wild-type mouse derived FoxO1 were generated. The verification of expression in these cell lines is presented in figure 74.

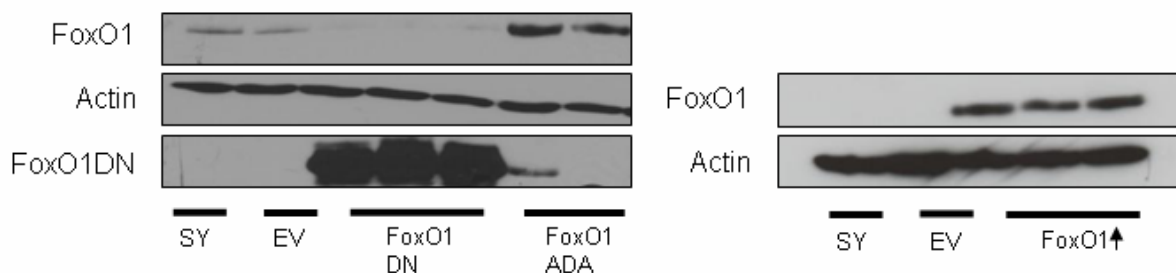


Figure 74: Verification of overexpression of FoxO1DN, FoxO1ADA and wild-type FoxO1 (FoxO1 \uparrow). Human SH-SY55 neuroblastoma cells stably overexpressing mouse derived FoxO1DN, FoxO1ADA and wild-type FoxO1 (FoxO1 \uparrow). 100 μ g total proteins were separated via 10% SDS-PAGE.

The IR/IGF-1R signaling pathway of the different FoxO1 cell lines was analysed. Activation of the PI3 kinase signaling was estimated via phosphorylation of AKT (Ser473) and activation of the MAP kinase pathway was shown via the phosphorylation of ERK1/2 (Thr202/Tyr204). Expression level of AKT and ERK1/2 serve as control. FoxO1DN expressing cells showed no differences in phosphorylation of AKT and ERK1/2. FoxO1ADA cell presented no changes in phosphorylation of ERK1/2. Interestingly phosphorylation of AKT in FoxO1ADA and FoxO1 overexpressing neuroblastoma cells was decreased compared to wild-type and empty vector control cells (Fig. 75 upper panels). Furthermore phosphorylation of GSK3 β (Ser9) was analysed via western blot. Again GSK3 β levels were used as controls. All FoxO1 cell lines presented similar amount of phosphorylation from GSK3 β as wild-type and empty vector control cells. Additionally expression of the FoxO1 target p27 was detected. FoxO1DN and FoxO1 overexpressing neuroblastoma cells show no differences compared to control cell lines. However, FoxO1ADA cells which express the constitutive active form of FoxO1, displayed an increased expression of p27 compared to wild-type and empty vector control cells (Fig. 75).

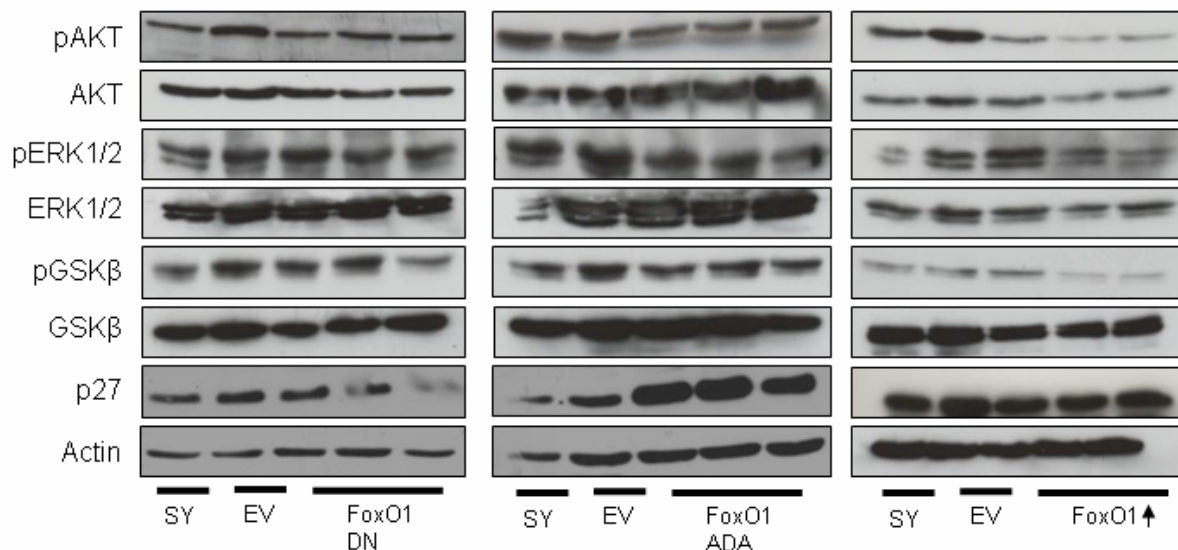


Figure 75: IR/IGF1R signaling pathway in stably FoxO1DN, FoxO1ADA and FoxO1 (\uparrow) expressing SHSY5Y cells. Phosphorylation level of AKT (pAKT, Ser473), ERK1/2 (pERK1/2, Thr202/Tyr204) and GSK3 β (pGSK3 β , Ser9) are shown. As control served unphosphorylated protein level of AKT, ERK1/2 and GSK3 β . Wild-type cells (SY), empty vector control (EV) are used as control cell lines. Expression of FoxO1 target gene p27 is displayed. Actin served as control. 100 μ g of total proteins were used and separated via 10% and 15% SDS-PAGE.

To investigate whether the localization of FoxO1 in FoxO1 overexpressing cells is predominantly in the nucleus which suggests an increased activation of FoxO1 western blot of nuclear and cytosolic fractions of these cells were performed. As shown in figure 76 the empty vector control cell line presented an increased level of FoxO1 in the nucleus compared to the cytosolic fraction. Furthermore one of the 3 FoxO1 overexpressing clones present a similar amount of FoxO1 in the nucleus and in the cytosol. The other two clones present a higher amount of FoxO1 in the cytosol (Fig. 76).

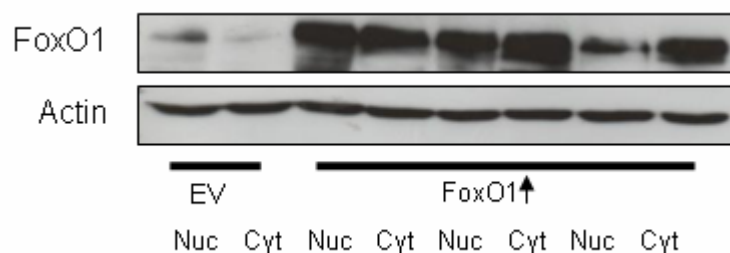


Figure 76: Nuclear and cytosolic localisation of FoxO1 in overexpressing neuroblastoma cells. FoxO1 levels in nuclear and cytosolic fractions of empty vector control cells (EV) and FoxO1 overexpressing neuroblastoma cells. Actin served as control. 100 μ g of total proteins were used and separated via 10% SDS-PAGE.

To further analyse whether FoxO1 changes expression level of upstream signaling proteins of the IR/IGF-1R signaling pathway expression level of IRS-2 was analysed. In FoxO1DN and FoxO1 overexpressing cells no differences of IRS-2 expression were observed. In contrast IRS-2 level in FoxO1ADA cells was slightly decreased compared to wild-type cell and empty vector control cells (Fig. 77, upper panel). In addition expression of p85, the regulatory subunit of the PI3K, was analysed. The expression levels of p85 in all FoxO1 neuroblastoma cell lines were not different. Furthermore the levels of phosphatase and

tensin homolog deleted on chromosome ten (PTEN) was analysed. PTEN reverses the phosphorylation of PI_{4,5}P to generate PI_{3,4,5}P via the PI3K. The expression levels of PTEN were similar to those in wild-type and empty vector control cell lines (Fig. 77).

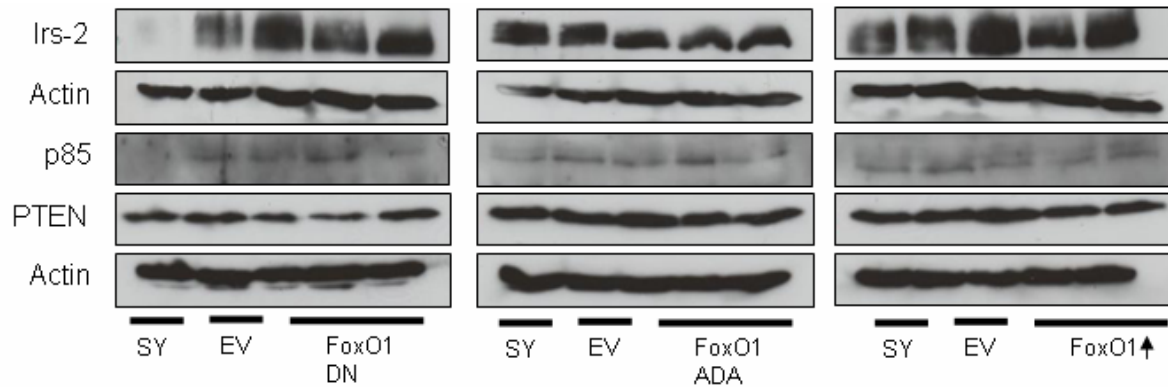


Figure 77: Analysis of IR/IGF1R signaling pathway in stably expressing FoxO1DN, FoxO1ADA and FoxO1 neuroblastoma cells.

Expression level of IRS-2, p85 and PTEN in stably expressing FoxO1DN, FoxO1ADA and FoxO1 neuroblastoma cells analysed via western blot. Wild-type cells (SY), empty vector control (EV) are used as control cell lines. Actin served as loading control. 100 µg of total proteins were used and separated via 8% and 10% SDS-PAGE.

3.11.2. Proliferation of FoxO1DN, FoxO1ADA and FoxO1 expressing neuroblastoma cells

FoxO1 control proliferation and cell cycle (review in Besson et al., 2008). The increased expression level of p27 in FoxO1ADA neuroblastoma cells indicated the regulation via FoxO1 (Fig. 78). For analysis of proliferation cells were starved over night (16h) to stop proliferation. Then proliferation was initiated with 10% FCS. This synchronized proliferation of the different cell lines. For further analysis empty vector control cells were used. Proliferation was measured via BrdU incorporation. No significant difference in proliferation of FoxO1DN and FoxO1ADA cells compared to control cells were detected (Fig. 78).

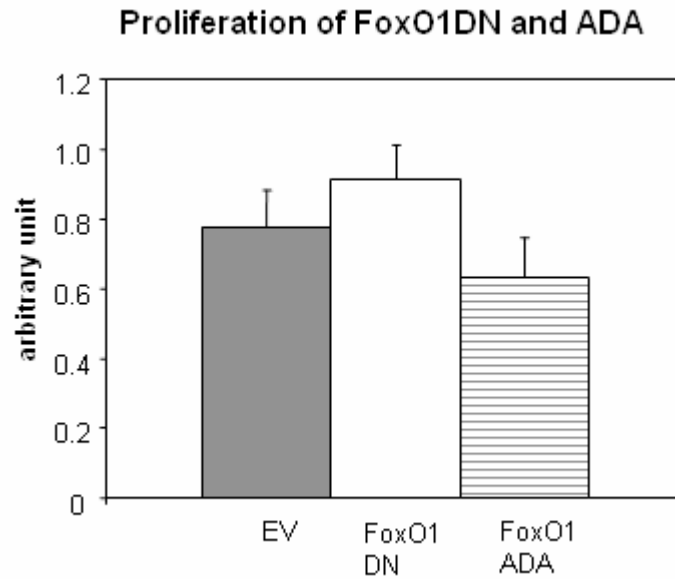


Figure 78: Proliferation of stably expressing FoxO1DN and FoxO1ADA. Proliferation analysis of stably expressing FoxO1DN (red) and FoxO1ADA (blue) neuroblastoma cells performed via BrdU incorporation assay. Empty vector controls (EV) (grey) were used as control cell lines. Cells were starved overnight (16h) and proliferation was induced by adding 10%FCS.

Additional proliferation analysis was performed using IGF-1 to induce proliferation. Proliferation initiation via 100 nM IGF-1 for 5 hours presents no differences of FoxO1 overexpressing neuroblastoma cells proliferation compared to control neuroblastoma cells (Fig. 79).

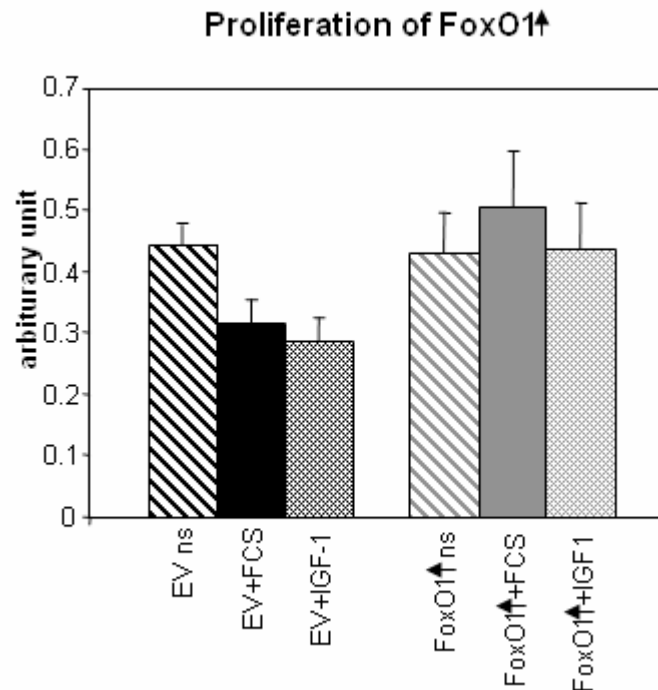


Figure 79: Proliferation of stably expressing FoxO1 neuroblastoma cells. Proliferation analysis of stably expressing FoxO1↑ compared to empty vector (EV) neuroblastoma cells via BrdU assay. Cells were starved overnight (16h) and proliferation was induced with 10%FCS or 100nM IGF-1. As control cells were not starved and stimulated (ns).

3.11.3. FoxO1 and oxidative stress

FoxO1 counteracts oxidative stress via detoxification of reactive oxygen species (ROS) increasing expression of antioxidant enzymes. Such enzymes are catalases (Nemoto and Finkel, 2002) and manganese superoxide dismutase (MnSOD) (Kops et al., 2002). For analysis of apoptosis upon oxidative stress FoxO1DN and FoxO1ADA cell were used. The expression of MnSOD was detected via western blots. The expression level of MnSOD in FoxO1DN and FoxO1ADA cell lines were not altered in comparison to empty vector control cells (Fig. 80).

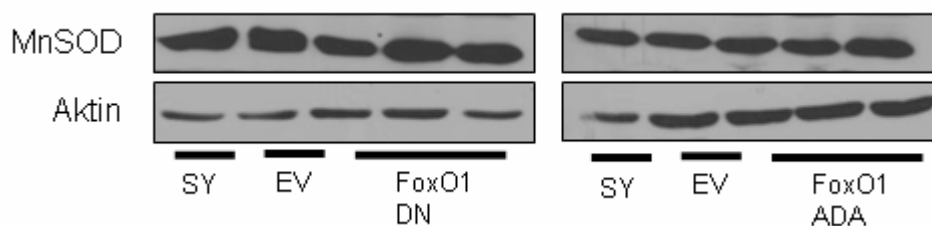


Figure 88: Expression level of MnSOD in stably expressing FoxO1DN and FoxO1ADA neuroblastoma cells. Expression level of MnSOD in FoxO1DN and FoxO1ADA expressing neuroblastoma cells was analysed via western blot. Wild-type cells (SY), empty vector control (EV) are used as control cell lines. Actin served as control. 100 μ g of total proteins were used and separated via 10% SDS-PAGE.

To induce oxidative stress cells were starved for 4 hours and then 500 μ M H₂O₂ were added for 16h. To investigate whether apoptosis was induced cleavage of Caspase 3 was detected with western blots. As shown in figure 82 treatment of the cells with 500 μ M H₂O₂ induces cleavage and therefore activation of Caspase 3. FoxO1DN and FoxO1ADA expressing neuroblastoma cells showed a slight decrease of activated Caspase 3 compared to empty vector control cells (Fig. 81, left panel). Control cells were starved but not treated with H₂O₂ and no cleavage of Caspase 3 was detected (Fig. 81, right panel).

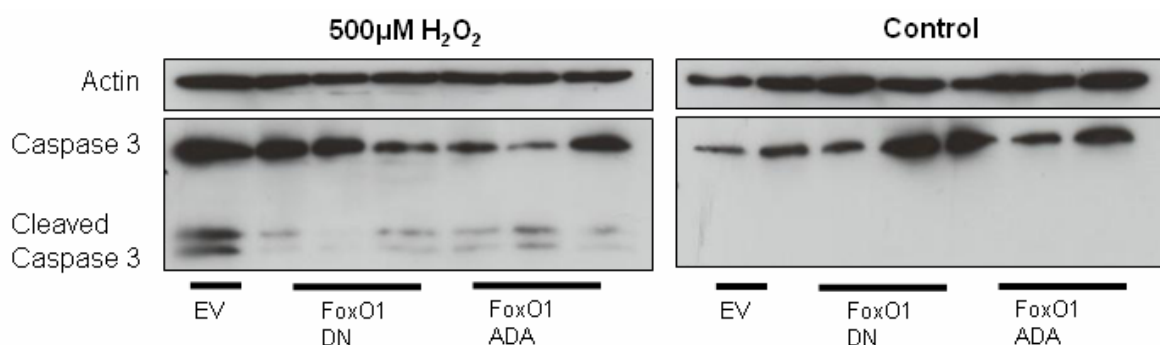


Figure 81: Oxidative stress in stably expressing FoxO1DN and FoxO1ADA neuroblastoma cells. Expression level of Caspase 3 in stably expressing FoxO1DN and FoxO1ADA neuroblastoma cells was analysed via western blots. Wild-type cells (SY), empty vector control (EV) are used as control cell lines. Actin served as loading control. 100 μ g of total proteins were used and separated via 15% SDS-PAGE.

During apoptosis double-strand breaks are induced. These breaks were labeled with Fluorescin-12-UTP in the TUNEL assay (Fig. 83 lowest panel). To stain the nuclei of the cells DAPI was used which shows a blue fluorescence (Fig. 82 middle panel). Representative

pictures of the TUNEL assay of stably expressing FoxO1DN and FoxO1ADA neuroblastoma cells compared to empty vector controls are shown in figure 82. Additional to fluorescent pictures also bright field pictures of the same localization were performed (Fig. 82 upper panel).

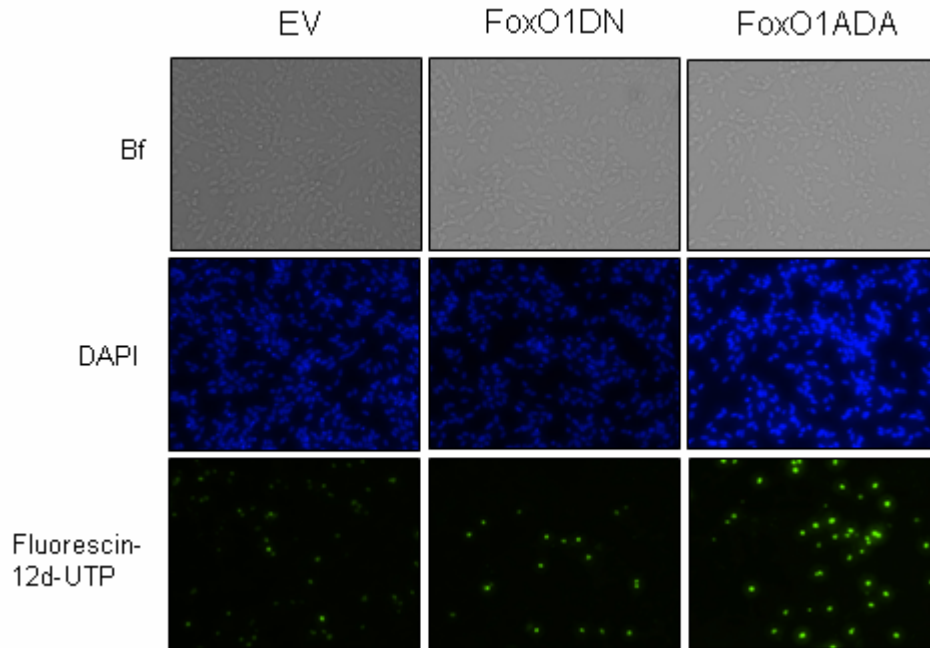


Figure 82: TUNEL assay of stably expressing FoxO1DN and FoxO1ADA neuroblastoma cells. Apoptosis was analysed via TUNEL assay of stably expressing FoxO1DN and FoxO1ADA neuroblastoma cells. Empty vector controls (EV) are used as control cell lines. Apoptosis was induced with 500 μ M H₂O₂. Upper lane: Bright field (Bf) pictures of the different cell lines. Middle panel: Staining of cell nuclei with DAPI (blue). Lower panel: Fluorescin-12d-UTP (green) staining of apoptotic cells.

After performing the TUNEL assay total amount of cells and apoptotic cells were counted. The proportion of apoptotic FoxO1DN, FoxO1ADA and empty vector control cells was calculated. FoxO1DN cells presented slightly less apoptotic cells and FoxO1ADA cells display a slight decrease in apoptotic cells in comparison to empty vector control cells as well (Fig. 83). However, this tendency did not reach statistical significance.

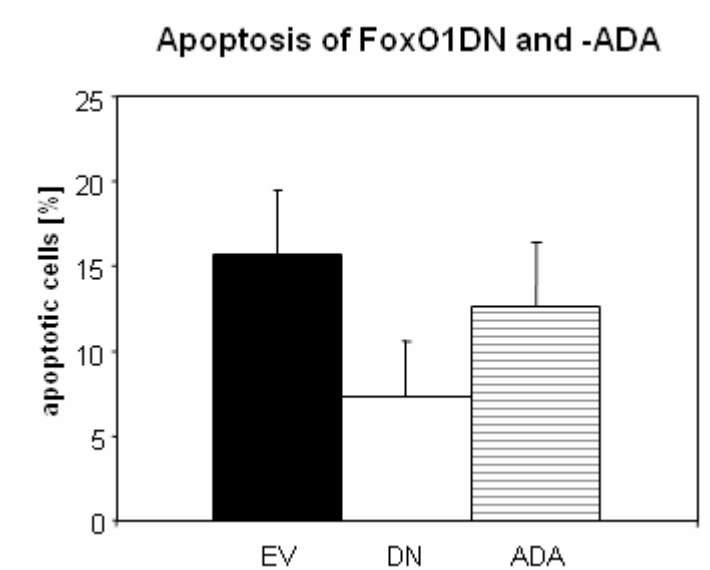


Figure 83: Analysis of TUNEL assay with stably expressing FoxO1DN and FoxO1ADA neuroblastoma cells. Level of apoptotic empty vector control, FoxO1DN and FoxO1ADA neuroblastoma cell lines was measured via TUNEL assay after treatment with H₂O₂.

4. Discussion

Alzheimer's disease (AD) is a chronic and progressive neurodegenerative disease characterized by accumulation of intracellular neurofibrillar tangles (NFT) and extracellular amyloid plaques. Amyloid plaques mainly consist of aggregated amyloid- β (A β) peptides (Masters et al., 1985). The aggregation of A β is thought to be the putative cause for neurodegeneration in AD (Masters et al., 1985). Previous studies have shown that AD is linked to type 2 diabetes (Janson et al. 2004; Ott et al. 1999; Stewart and Liolitsa 1999; Lovestone 1999). Interestingly the IR/IGF-1R signaling pathway is disrupted in the central nervous system of patients suffering from AD (Frolich et al. 1998; Frolich et al. 1999; Moloney et al. 2010). Therefore AD is described as "brain type" diabetes (Pilcher 2006). In *C. elegans* it has been shown that DAF-16, the orthologue of mammalian FoxOs both act downstream of the signaling pathway and are involved in the reduction of A β 42 toxicity (Hsu, Murphy, and Kenyon 2003; Birkenkamp and Coffey 2003; Cohen et al. 2006). FoxO1 is predominantly expressed in the hippocampus formation which is mainly affected by AD (Hoekman et al., 2006). For the present study mice with neuron-specific expression of the dominant negative (FoxO1DN) and the constitutive active form (FoxO1ADA) of FoxO1 were used. These animals were crossed with Tg2576 mice, a well established mouse model of AD and express the Swedish mutation of APP (APP^{sw}) (Vassaret et al. 1999; De Strooper 2003; Holsinger et al., 2002; Sinha et al., 1999; Harada et al., 2006).

4.1. Neuron-specific expression of FoxO1DN and FoxO1ADA

For neuron-specific expression of FoxO1DN and FoxO1ADA the Synapsin 1 promoter driven Cre recombinase (SynCre) expressing mice was used. Only female mice expressing Cre recombinase under the control of the Synapsin 1 promoter were used for breedings because its expression has been detected within the testes after being bred into a floxed transgenic mouse line. These mice then displayed a germline recombined floxed allele. This was not observed in progeny from female mice carrying the SynCre allele (Rampe et al., 2006). Crossing of lacZ reporter and SynCre mice followed by β -galactosidase staining revealed SynCre activity in hippocampus and to a lesser extent in the frontal cortex (Freude et al., 2009). In the present experiments mice expressing the dominant negative (FoxO1DN) and the constitutive active form (FoxO1ADA) of FoxO1 in a neuron-specific manner. As expected expression of FoxO1DN and FoxO1ADA was detected in the hippocampus and to less extent in the cortex.

4.1.2. Metabolic characterization

Previous studies showed that the whole body knockout of IRS-2 leads to hyperglycemia in male mice (Whiters et al., 1998). In addition up to 80% of pure C57BL/6 mice present a spontaneous hyperglycemia during the first 6 month of life. This hyperglycemia might influence lifespan in Tg2576 mice (Freude et al., 2009; Selman et al., 2008; Doria et al., 2008). Therefore investigations glucose homeostasis was analysed in all genotypes. Furthermore blood glucose and insulin sensitivity as well as glucose tolerance tests of FoxO1DN and FoxO1ADA mice were performed.

Expression of FoxO1 in insulin responsive tissue plays an important role in glucose metabolism and the pathogenesis diabetes. Previous studies showed that heterozygous deletion of FoxO1 restored insulin sensitivity and rescued diabetes in insulin receptor mutant mice (Nakae et al., 2002). In the liver active FoxO1 increases gluconeogenesis and in the pancreas FoxO1 regulates proliferation and function of beta cells (Kitamura et al., 2002).

Neuron-specific expression of FoxO1DN revealed no changes of blood glucose from 5 till 60 weeks of age as well as a similar glucose tolerance and insulin sensitivity. Furthermore FoxO1ADA mice displayed no differences in blood glucose and a slight increased glucose tolerance, but significant increased insulin sensitivity revealed by ITTs, via a so far unknown mechanism.

Glucose production is regulated via gluconeogenesis and glycolysis in the liver and insulin strongly inhibits glucose generation. Important enzymes involved in these processes are the phosphoenol-pyruvate carboxykinase (PEPCK) and glucose-6-phosphatase (G6P). FoxO1 confers insulin sensitivity and promotes glucose generation by the liver (Kanazawa et al., 2009). FoxO1 binds to PPAR γ which promotes the expression of PEPCK and G6P (Saleem et al., 2010). Insulin inhibits glucose production via activation of the PI3k pathway and inactivation of FoxO1 in the liver (Nakae et al., 2002).

The brain-specific knockout of IRS-2 in male mice developed hyperglycemia and impaired glucose tolerance (Leissring et al., 2003; Freude et al., 2009).

Furthermore the IGF-1-deficient (LID) mice crossed with GH (growth hormone) antagonistic (GHa) mice displayed increased insulin sensitivity (Yakar et al., 2004). GH deficiency has been shown to increase the expression of IR without directly regulating its transcription (Dominici et al., 2000). GH and insulin share some of the downstream signaling targets like IRS. GH promotes tyrosine phosphorylation of IRS-1 and IRS-2 via activation of JAK2 (Janus kinase 2) (Argetsinger et al., 1995; Argetsinger et al., 1996). Additionally GH promotes phosphorylation of Shc, the adaptor protein that activates MAPK signaling pathway (Thirone et al., 1999; Vanderkuur et al., 1995; Vanderkuur et al., 1997). Through induction of MAPK signaling cascade GH activates the S6K (Kilgour et al., 1996). GH increases expression of suppressors of cytokine signaling (SOCS). Previous studies have been shown that SOCS-1,

-3 and -6 affect the insulin promoted interaction of p85 and IRS-1 and IRS-2 which leads to degradation of IRS (Adams et al., 1998; Peraldi et al., 2001; Dey et al., 2000; Rui et al., 2002). Furthermore SOCS-1 deficient mice display increased insulin sensitivity (Kawazoe et al., 2001).

The mechanism of neuronal FoxO1 regulating glucose metabolism is yet unknown, but an association of insulin sensitivity and neuron-specific expression of the constitutive active FoxO1 has been observed in the present study. Several questions concerning this phenotype remain open, most likely the effect is mediated via a neuroendocrine mechanism or the autonomous nervous system.

4.1.3. Insulin/IGF-1R signaling in 28 weeks old animals

Both FoxO1DN and FoxO1ADA mice presented no changes in the insulin and IGF-1R signaling pathway in the CNS. Expressions of the IR and IGF-1R as well as activation of the PI3K and MAPK pathway were analysed. In hepatocytes adenoviral-mediated expression of FoxO1ADA activated PI3K and MAPK pathway but FoxO1DN was not able to induce any changes of the PI3K and MAPK pathways (Naimi et al., 2007). This effect was not mediated via FoxO1 promoted transcription of IRS-1 or -2 but FoxO1 increased p38 expression. p38 might play a role in activation of the AKT and inhibition of FoxO1 (Naimi et al., 2007). In neuron-specific expressing FoxO1DN and FoxO1ADA mice no differences in expression of components of the IR/IGF-1R signaling pathway compared to wild-type animals were observed. In addition no alterations between both genders were detectable. This indicates that FoxO1 does not influence the upstream IR/IGF-1R signaling pathway in neurons *in vivo*.

4.1.4. Growth of FoxO1DN and FoxO1ADA mice

FoxO1DN mice displayed no differences in growth compared to wild-type mice. Interestingly FoxO1ADA mice showed a significantly decreased body weight in both female and male mice in comparison to wild-type from 5 till 60 weeks old animals. The difference was about 1.7 g for female mice and 2.5 g for male mice at 28 weeks of age. Food and water intake of FoxO1ADA male mice showed a similar consumed amount compared to wild-type mice. Analysis of body composition revealed no difference of body fat ratio but a decrease of lean body mass. This result was in contrast to previous findings in IR and IGF-1R knockout mice, even though these mice could have overactive FoxO1 like the FoxO1ADA mice. The brain-specific knockout of the IR (NIRKO) displayed no differences in body weight of male mice until 6 months of age. Female NIRKO presented an up to 15% increased body weight on a normal chow diet. But both presented an increase of body fat mass. Female NIRKO mice

displayed a 2-fold increase of perigonadal white adipose tissue (WAT) and male mice showed a 1.5-fold increase (Brüning et al., 2000). It needs to be mentioned that the brain-specific knockout of the IR was generated using the Nestin-promoter driven Cre recombinase. Nestin is an intermediate filament protein which is predominantly expressed in neuroepithelial stem cells (Lendahl et al., 1990; Tronche et al., 1999). This Nestin-promoter driven Cre recombinase leads to deletion of the IR during early development and naturally in neurons as well as in astrocytes and oligodendrocytes (Brüning et al., 2000).

IRS-2 knockout mice display similar changes in body weight and body composition like the NIRKO mice. IRS-2 mice showed an increased body weight with an increase in body fat (Withers et al., 1999; Burks et al., 2000).

Interestingly liver IGF-1-deficient (LID) mice crossed with GH antagonistic (GHa) mice to counteract increased GH secretion in LID mice, had a decreased body weight in comparison to wild-type mice and additionally showed an increased insulin sensitivity but an increased fat content as well (Yakar et al., 2004).

To further analyse this difference in growth of FoxO1ADA, realTime analyses of important regulators of the growth hormone axis (GH) were performed. The GH is produced in the pituitary and regulated via the hypothalamus. This regulation is controlled by the growth hormone releasing hormone (GHRH) and the growth hormone inhibiting hormone (GHIH, somatostatin) (Jansson et al., 1985; Sato et al., 1989; Carlsson et al., 1990). In the pituitary binding of GHRH to the growth hormone releasing hormone receptor (GHRHR) results in the release of GH. GH binds to the growth hormone receptor of the liver where it induces the production of IGF-1. No significant changes have been observed in the growth hormone axis of 4 weeks FoxO1ADA male compared to wild-type mice. This result indicates a growth hormone independent mechanism in balancing growth in FoxO1ADA mice. Possibly these mice display a reduced body weight during early postnatal development indicating a role of neuronal FoxO1 in early development of mice.

4.1.5. Indirect calorimetry and locomotor coordination

Analyses of FoxO1DN and FoxO1ADA male mice displayed no changes in motor coordination during the RotaRod. Both genotypes presented an elevated locomotor activity compared to wild-type mice. FoxO1DN mice showed an increase of about 250 and FoxO1ADA about 500 counts during dark phase. Furthermore FoxO1DN male mice demonstrated a higher energy expenditure of 5kcal/kg lean body mass. In contrast FoxO1ADA mice showed no increased energy expenditure during dark phase despite an increased activity.

Energy homeostasis is tightly regulated via adipose tissue. Adipocytes store energy in form of triglycerides. These triglycerides get oxidized during time periods of energy deprivation (Large et al., 2004). Adipocytes secrete adipokines which regulate energy homeostasis of adipocytes themselves, the brain and other target tissues. FoxO1 is able to suppress adipogenesis, the differentiation of preadipocytes to adipocytes. Previous studies have been shown that FoxO1ADA inhibits the differentiation of preadipocytes. Conversely FoxO1DN promotes adipogenesis in embryonic fibroblasts of IR knockout mice *in vitro* (Nakae et al., 2003).

The respiratory quotient (RQ) is calculated from eliminated CO₂ and consumed O₂. It indicates which substances are metabolized by a specific organism. Respiratory quotient (RQ) of FoxO1DN mice was similar to the RQ of wild-type animals. The RQ of both FoxO1DN and wild-type was 0.9 during the light phase, indicating proteins to be the major metabolized substrate and during dark phase it is close to 1. This identifies carbohydrates to be predominantly metabolized. FoxO1ADA displayed the similar RQs during light and dark phase compared FoxO1DN and wild-type, but the wild-type animals used for comparisons to FoxO1ADA mice showed a decreased RQ during dark phase which might be a methodical problem because wild-type animals of the FoxO1DN comparison did not show such a decrease in RQ.

The neuronal alteration of FoxO1 mediated transcription affects activity of mice without causing larger changes in energy expenditure. However, the exact mechanisms are unknown yet.

4.1.6. Behaviour of FoxO1DN and FoxO1ADA mice

To investigate whether the neuron-specific expression of FoxO1DN or FoxO1ADA changes fear and explorative behaviour or memory formation Open field, O-Maze and Morris Water Maze tests were performed. FoxO1DN and FoxO1ADA male mice display similar fear behaviour compared to wild-type animals. Analysis of spatial memory using the Morris Water Maze testing revealed no changes in memory formation of FoxO1DN mice but a slight increased performance of FoxO1ADA mice. This might be due to a higher increase in activity, because FoxO1ADA displayed no better learning performance at the 5th day of testing when the platform was removed. Nissl staining of each genotype did not show any differences in brain structure of the different genotypes.

Thus FoxO1 mediated transcription in mature neurons does not affect brain structure as well as behaviour and spatial memory.

4.2. Alzheimer's disease

Alzheimer's disease (AD) is characterized by accumulation of intracellular neurofibrillar tangles (NFT) and extracellular amyloid plaques. NFTs contain hyperphosphorylated tau proteins (Ross et al., 2005) and amyloid plaques mainly consist of aggregated amyloid- β (A β) peptides (Masters et al., 1985). This aggregation of A β is hypothesized to be the cause of neurodegeneration in AD (Masters et al., 1985). Tg2576 mice are a well established mouse model for the analysis of AD pathology. Tg2576 mice overexpress the human derived APP form consisting of 695 amino acids. The APP gene harbours an amino acid substitution of Lys670 to Asn and Met671 to Leu, the swedish mutation (APP^{sw}). This causes an increased cleavage via the β -secretase which in turn leads to a 5-fold increase of A β 40 and an up to 14-fold increase of A β 42. Additionally these mice present an age dependent deficit in learning behaviour (Lewis et al., 2001). Tg2576 mice nearly do not form intracellular neurofibrillar tangles and therefore are not suitable to analyse tau pathology. The present thesis concentrates on the processing of APP as well as generation of A β and therefore Tg2576 is a useful mouse model for this investigation. However, the role of FoxO1 mediated transcription in Tau pathology needs to be achieved in a different model.

4.2.1. Metabolic characterization of Tg2576/FoxO1DN and Tg2576/FoxO1ADA mice

Previous studies of APP overexpressing mice have been shown that lethality of these mouse models is affected by the genetic background (Meilandt et al., 2009). Nearly all Tg2576 mice in a pure C57BL/6 background died during the first months of age. Therefore Alzheimer's pathology cannot be analysed in this particular genetic background. One contributing factor might be the hyperglycaemia developing in C57BL/6 mice during aging (Freude et al., 2009). Therefore blood glucose, glucose and insulin tolerance tests as well as survival and APP processing were analysed in hybrid background.

Blood glucose concentrations as well as insulin sensitivity and glucose tolerance were not changed of the different genotypes in Tg2576 background. Tg2576/FoxO1ADA mice in the hybrid background had similar basal blood glucose concentration and glucose tolerance as neuron-specific knockout of the IR (nIR^{-/-}) or the IGF-1R (nIGF-1R^{-/-}) (Freude et al., 2009, Stöhr et al., 2011). Thus, altered glucose metabolism is excluded as influencing factor in the present study.

4.2.2. Body weight of Tg2576/FoxO1DN and Tg2576/FoxO1ADA mice

Body weight was measured from 5 till 60 weeks of age to analyse whether changes in body weight might be an influencing factor in these mice. A reduction in body weight of Tg2576

and APP23 mice compared to wild-type mice was analysed in previous studies (Toyama et al., 2005; Vloeberghs et al., 2008). Food intake was unaltered in these mice (Lalonde et al., 2009). But food intake of APP23 mice was actually slightly increased (Vloeberghs et al., 2008). This APP23 transgenic mouse model expresses the neuron-specific murine Thy1 promoter driven human APP751 protein which includes the swedish mutation (Sturchler-Pierrat et al., 1997).

Tg2576/FoxO1DN and Tg2576/FoxO1ADA female mice displayed no differences in body weight compared to Tg2576 mice. In contrast Tg2576/FoxO1DN showed a slight decrease and Tg2576/FoxO1ADA male mice displayed a decrease in body weight in comparison to Tg2576 male mice. This reduction of body weight from Tg2576/FoxO1ADA male mice could not be observed in nIGF-1R^{-/-} male mice which might demonstrate a similar activation of FoxO1 (Hettich, PhD thesis). In, IRS-2 knockout mice crossed with Tg2576 mice displayed no changes of body weight until 48 weeks of age (Freude et al., 2009).

Brain body ratio revealed no severe alterations in the different genotypes which indicate that FoxO1 does not influence the development and size of the brain. The analysis of body weight largely excludes body weight in as major factor possibly influencing the data on metabolic APP processing of the different FoxO mutants.

4.2.3. Kaplan-Meier analysis of Tg2576/FoxO1DN and Tg2576/FoxO1ADA mice

Kaplan-Meier analysis of Tg2576/FoxO1DN female and male mice demonstrated no changes in survival. In addition FoxO1DN female and male mice presented a similar survival as wild-type animals. Furthermore 50% of Tg2576/FoxO1ADA female mice were alive at 60 weeks of age whereas 70% of Tg2576 mice still lived. 100% of FoxO1ADA female mice survived and 90% of wild-type mice over 60 weeks. In contrast Tg2576/FoxO1ADA male mice died between 12 and 16 weeks and no one reached 60 weeks of age. FoxO1ADA and wild-type male mice displayed a similar survival with about 90% survivals at 60 weeks of age. In *C. elegans* lifespan investigations were performed using the knockdown technique to manipulate the IR/IGF-1R signaling pathway (IIS). These studies identified neuronal DAF-2, the orthologue of the mammalian IR/IGF-1R, to regulate in longevity (Wolkow et al., 2000). The IIS in *C. elegans* is highly conserved to the mammalian IR/IGF-1R signaling pathway. An insulin-like ligand binds to DAF-2 followed by recruitment of the insulin receptor substrate 1 orthologue (IST-1) and AGE-1, the PI3K of *C. elegans* (Kenyon et al., 1993; Morris et al., 1996; Kimura et al., 1997). This leads to the generation of PI_{3,4,5}P followed by activation of AKT (Kops et al., 1999; Paradis and Ruvkun, 1998). DAF-18, the orthologue of PTEN, is the negative regulator of this signaling cascade (Oggs and Ruvkun, 1998). Activated AKT phosphorylates and negatively regulates DAF-16, the orthologue of the mammalian FoxO

familiy (Henderson and Johnson, 2001; Lee et al., 2001). Targets of DAF-16 are such as small heat-shock protein (HSP) chaperones (Murphy et al., 2003). Previous studies in *C. elegans* have been shown that activated DAF-16 extends lifespan and elevates stress resistance (Kenyon, 2005). Accordingly to heterozygous deletion of the IGF-1R in mice leads to extended lifespan and increased stress resistance (Holzenberger et al., 2003).

Drosophila melanogaster expresses a single FoxO transcription factor called dFOXO. Different studies have been shown that overexpression of dFOXO prolongs lifespan via affecting general mortality without decreasing age associated mortality of flies specifically (Pletcher et al., 2002). In addition dFOXO deficient flies were shown to be short lived (Giannakou et al., 2007; Min et al., 2008).

In addition the homozygous deletion of neuronal IGF-1R (nIGF-1R^{-/-}) in Tg2576 background rescues premature mortality of Tg2576 mice nearly completely. This effect was observed in female and male mice (Freude et al., 2009). In contrast mice with the neuronal deletion of the IR (nIR^{-/-}) crossed Tg2576 mice presented no survival rescue in both gender as demonstrated for Tg2576/nIGF-1R^{-/-} mice (Stöhr et al., 2011). Both mouse models mimic the situation of activated FoxO1. Furthermore brain-specific IRS-2 deficiency and heterozygous whole body IRS-2 knockout were shown to prolong lifespan in a hybrid and pure C57BL/6 background (Tagouchi et al., 2007; Selman et al., 2008). In contrast whole body knockout of the IR causes death of newborns within the first few hours because of severe hyperglycemia and ketoacidosis (Accili et al., 1996) without causing growth retardation.

IRS-2 deficiency reduces premature mortality of female mice in Tg2576 background (El Khoury et al., 2007, Leissring et al., 2007; Freude et al., 2009). This rescue could not be observed for Tg2576/IRS-2^{-/-} male mice. A possible reason is that male IRS-2^{-/-} mice develop hyperglycemia (Burks et al., 2000, Freude et al., 2009). Furthermore the whole body knockout of FoxO1 leads to embryonal lethality on embryo day 10.5 because of incomplete vascular development (Hosaka et al., 2004; Furuyama et al., 2004).

Tg2576/FoxO1ADA female mice mimic the situation of Tg2576/nIR^{-/-} mice but FoxO1ADA male mice in Tg2576 background male died from 12 till 16 weeks of age. However, only 2 Tg2576/FoxO1ADA male mice could be generated in a period of 4 years. The results for these FoxO1ADA crossed with Tg2576 mice are surprisingly since previous investigations in Tg2576/nIGF-1R^{-/-} and Tg2576/nIR^{-/-} mice did not show increased mortality compared to Tg2576 mice. Thus IR and IGF-1R mediate different genes involved in survival and stress resistance independent of FoxO1 mediated transcription. However FoxO1 is not the only FoxO protein in mammalian. FoxO3a is regulated via the IR/IGF-1R signaling cascade as well and might at least partially compensate in case of FoxO1DN and FoxO1ADA expression. Previous studies have been shown that FoxO3a promotes the expression of pro-apoptotic genes like Fas ligand and Bim, a member of the Bcl-2 protein family (Brunet et al.,

1999; Reif et al., 1997; stahl et al., 2002). Possibly the constitutive active form of FoxO1 also results in overexpression of such pro-apoptotic factors and in turn leads to neuronal apoptosis which might be the case in Tg2576/FoxO1ADA mice.

Tg2576/FoxO1DN mice showed no changes in survival compared to Tg2576 mice which might be explained by compensation via neuronal FoxO3a.

4.2.4. IR/IGF-1R signaling in 60 weeks old Tg2576/FoxO1DN and Tg2576/FoxO1ADA mice

Insulin resistance was described in patients suffering from AD by Watson and Craft in 2003 (Watson and Craft, 2003). This resistance was associated with high insulin levels in cerebrospinal fluid (Craft et al., 1998). In addition mRNA levels of IGF-1 in brains of patients with late stages of AD are reduced. But IGF-1 concentrations in serum of patients with AD exhibit an increased level. These findings indicate a role of IGF-1 resistance in the pathogenesis of AD (Rivera et al., 2005; Vardy et al., 2007).

Therefore possible changes in the signaling cascade were investigated. This analysis of the IR/IGF-1R signaling pathway revealed no differences in 60 weeks old Tg2576/FoxO1DN and Tg2576/FoxO1ADA mice compared to Tg2576.

IRS-2 deficient mice in Tg2576 background showed unaltered phosphorylation patterns compared to Tg2576 mice as well as no changes in IR and IGF-1R expression in the brain. Similar results were obtained in nIGF-1R^{-/-} mice crossed with Tg2576 (Freude et al., 2009). Furthermore Tg2576/nIR^{-/-} showed no changes of basal PI3K and MAPK cascade activation (Stöhr et al., 2011).

Furthermore target genes of FoxO1 like MnSOD or p27 were not changed indicating a different target gene pattern of FoxO1 in neurons than in other tissues. Furthermore FoxO-mediated transcription is not exclusively regulated via phosphorylation but also via acetylation which inhibits FoxOs because it might decrease DNA binding and promotes phosphorylation of FoxO at Ser256 via AKT which inactivates FoxO. In contrast the recruitment of CBP and p300 to the promoter by FoxO mediated the acetylation of histones and induces initiation of transcription (Daitoku et al., 2004; Matsuzaki et al., 2005). These regulatory mechanisms were not investigated in the present study and might provide an explanation for unchanged expression levels of the FoxO targets MnSOD and p27.

However, the IR/IGF-1R signaling pathway and target genes like p27 and MnSOD were not changed in FoxO1DN and FoxO1ADA mice in Tg2576 background indicating a minor neuronal regulatory function of FoxO1 or compensation via other factors.

4.2.5. APP processing in Tg2576/FoxO1DN and Tg2576/FoxO1ADA mice

Analysis of APP processing revealed no differences in generation of α - and β -CTFs in Tg2576/FoxO1DN compared to Tg2576 female and male mice as well as Tg2576/FoxO1ADA in comparison with Tg2576 female mice. Only Tg2576/FoxO1ADA mice were analysed because male mice died too early (4.2.3.). These investigations indicate no changes in activity of α - or β -secretase cleavage of APP. Furthermore no changes of expression level from ADAM10, BACE and TACE have been observed in the different genotypes. Additionally no significant differences in A β 40 and A β 42 burden has been demonstrated in Tg2576/FoxO1DN and Tg2576/FoxO1ADA compared to Tg2576 mice.

These results suggest that the reduced A β -accumulation in Tg2576/nIGF-1R^{-/-} and Tg2576/nIR^{-/-} is not mediated via FoxO1. In contrast to Tg2576/nIGF-1R^{+/-}, Tg2576/nIR^{-/-} mice displayed a reduction in α - and β -CTFs as well as a strongly decrease of A β 40 and A β 42 without influencing mortality induced by APPsw expression (Stöhr et al., 2011). Consistent with these observations Tg2576/nIRS-2^{-/-} mice showed a reduction of α - and β -CTF generation as well and decreased A β accumulation (Freude et al., 2009). These results might indicate different functions of the IR or IGF-1R signaling pathway in the regulation of A β toxicity.

A previous study using heterozygous knockout of the IGF-1R (IGF-1R^{+/-}) crossed with an AD mouse model overexpressing APPsw and human presenilin-1 Δ E9 (the deletion of exon 9 which causes familial AD) both under the regulation of the prion promoter (Jankowsky et al., 2001,) show beneficial effects of IGF-1 resistance in AD pathology. This mouse model is characterized by the generation of A β , formation of plaques and a slow progressive onset of AD like pathology (Jankowsky et al., 2004). Furthermore this model exhibits age dependent behaviour impairments like Tg2576 mice (Reiserer et al., 2007). The APPsw and human presenilin-1 Δ E9 mouse model is a less aggressive model of AD than other mouse models because the formation of A β plaques occurs at 6 to 7 months of age (Jankowsky et al., 2004). These APPsw and presenilin-1 Δ E9/Igf1r^{+/-} mice presented an identical expression level of BACE-1 and ADAM17 compared to APPsw and presenilin-1 Δ E9 mice (Cohen et al., 2009).

In *C. elegans* it has been shown that the knockdown of DAF-2, the orthologue of the mammalian IR and IGF-1R, decreases toxicity of A β 42 (Cohen et al. 2006). This effect was mediated through DAF-16 and the heat shock transcription factor 1 (HSF-1) both regulated via the IIS signaling pathway (Hsu, Murphy, and Kenyon 2003; Birkenkamp and Coffey 2003; Cohen et al. 2006). The detoxification mechanism mediated by HSF-1 induces disaggregation and degradation of A β aggregates. The second mechanism is facilitated through DAF-16 which promotes hyperaggregation of A β to form less toxic high molecular

mass aggregates (Cohen et al., 2006). The APP^{sw} and presenilin-1 $\Delta E9/Igf1r^{+/-}$ mouse model was protected from A β induced toxicity. A possible reason for that is the observation of an increased assembly of A β into densely packed, fibrillar structures during disease progression (Cohen et al., 2009). This hyperaggregation of A β was hypothesized to be induced via an active mechanism that converts highly neurotoxic A β oligomers into densely packed aggregates with lower toxicity. Thus, IGF-1 resistance protects APP^{sw} and presenilin-1 $\Delta E9/Igf1r^{+/-}$ mouse model from A β toxicity (Cohen et al., 2009).

Investigation of the formation of neurotoxic A β oligomers via dot blot revealed no differences in Tg2576/FoxO1DN compared to Tg2576 female and male mice as well as Tg2576/FoxO1ADA in comparison with Tg2576 female mice.

Thus the current results might indicate that neuronal FoxO1 does not mediate the decreased APP processing and hyperaggregation of A β observed in IGF-1 resistance in APP^{sw} expressing mice. In contrast, Tg2576/FoxO1ADA male mice died at 12 till 16 weeks of age via a yet unknown mechanism.

In contrast to *C. elegans* the mammalian FoxO protein family consists of 4 members, FoxO1, FoxO3a, FoxO4 and FoxO6 (Clark et al., 1993). Another FoxO candidate possibly mediating the protective effect observed in IGF-1 resistant mice against Alzheimer's disease is FoxO3a. A previous study has been shown that inactivation of FoxO3a is associated with attenuation of AD pathology (Qin et al., 2008). Caloric restriction activates the IR signaling pathway which leads to phosphorylation of FoxO3a and transport out of the nucleus. The inactivation of FoxO3a mediates attenuation of AD pathology and preservation of spatial memory in Tg2576 mice. *In vitro* studies of primary cortico-hippocampal Tg2567 neuron cultures expressing constitutive active FoxO3a, showed an increase of A β 40 and A β 42 and reduced sAPP α levels. This indicates an inhibition of the non-amyloidogenic APP cleavage pathway which might be due to decreased α -secretase activity. This event promoted the generation of A β (Qin et al., 2008). Furthermore FoxO3a becomes deacetylated via SIRT1 which might inactivates FoxO3a in response to caloric restriction. This causes the repression of Rho-associated protein kinase-1 (ROCK1) gene expression followed by activation of the nonamyloidogenic processing of APP via the α -secretase. This activation of nonamyloidogenic processing of APP leads to a reduction of A β levels (Qin et al., 2008).

4.3. *In vitro* studies of FoxO1 in human neuroblastoma cells

FoxOs regulate transcription of genes involved in cell metabolism, proliferation and apoptosis (Patridge and Bruning, 2008). To investigate the role of FoxO1 in neuronal proliferation and apoptosis upon oxidative stress was induced in stably overexpressing FoxO1DN, FoxO1ADA and wild-type FoxO1 neuroblastoma cells.

4.3.1. Characterization of FoxO1DN, FoxO1ADA and FoxO1 stably expressing neuroblastoma cells

The characterization of stably expressing FoxO1DN and FoxO1ADA neuroblastoma cells revealed slight changes of IR/IGF-1R signaling pathway for FoxO1ADA cells. Interestingly stably expressing FoxO1 and FoxO1ADA cells presented a decreased basal phosphorylation of AKT in 3 different cell clones. No changes of the upstream signaling cascade and PTEN, a negative regulator of the PI3K signaling pathway has been observed. These results might indicate a regulatory feedback loop to the IR/IGF-1R signaling pathway at least in these cell types.

4.3.2. FoxO1 and proliferation

FoxOs were shown to regulate the G1-S and G2-M phase transition mediated by transcription of cell cycle regulators e.g. p27 (review in Ho et al., 2008). Regulation of cell cycle occurs via several cyclin/CDKs which in turn phosphorylate and therefore regulate different downstream proteins involved in cell cycle control. The cell cycle inhibitor p27 is a member of the Cip/Kip family of CDK inhibitors. This inhibitor associates with p57 and p21 to cyclin D as well as A- and E-CDK (review in Besson et al., 2008).

Analysis of p27 which causes a cell cycle arrest showed an increase expression in FoxO1ADA neuroblastoma cells. Further analysis revealed no changes of proliferation via measurement of BrdU incorporation.

In hematopoietic cells it was shown that deprivation of cytokines which regulate proliferation and survival resulted in arrest in the G1 phase of the cell cycle (Dijkers et al., 2000; Hideshima et al., 2001; Stahl et al., 2002). Transcription of p21 was shown to be regulated via Smad transcription factors. Inhibition of proliferation of immune, epithelial and neuronal cells was demonstrated to be promoted via transforming growth factor β which activates Smad. In epithelial cells it was shown that p21 expression is enhanced by association of FoxO1, FoxO3a and FoxO4 and Smad. Furthermore activation of the PI3K pathway leads to inactivation of FoxOs and therefore inhibition of p21 (Seoane et al., 2004). In addition FoxOs regulate transcription of p15 and p19 which are CDK inhibitors of the INK4 family. Their action inhibits the cyclin D/CDK complex which blocks the binding of cyclin D (Besson et al., 2008). Increased expression of p15 and p19 is mediated by FoxO1 and FoxO3a. Mouse embryo fibroblasts of p15 or p19 deficient mice were shown to fail to arrest in G1 phase after incubation with the PI3K inhibitor LY294002 indicating an essential role of p15 and p19 for cell cycle arrest (Katayama et al., 2008). In contrast previous studies have been shown that FoxO mediated expression of p27 is involved in cell cycle arrest (Dijkers et al., 2000). This might indicate that p27 action requires p15 and p19 expression to inhibit the cyclin D (CDK

complex (van der Vos and Coffey, 2011). This might explain why no differences in proliferation were observed in case of FoxO1ADA, FoxO1DN and FoxO1 neuroblastoma cells. The expression of p15 and p19 might not be high enough or is even decreased in the neuroblastoma cell used in this study. In addition, FoxO3a might be involved and compensate the dominant negative or constitutive active form of FoxO1.

4.3.3. FoxO1 and oxidative stress

Oxidative stress and damage in the brain has been shown to be associated with AD (Markesbery and Caine, 1999; Beal, 2002). Oxidative stress activates c-Jun N-terminal kinases (JNK) which might link oxidative stress to neurodegeneration (Ozcan et al., 2004). Activation of JNK through hydrogen peroxide results in activation of the γ -secretase which is an important step in the formation of A β plaques and AD pathology (Shen et al., 2008). Furthermore, generation of hydrogen peroxide is correlated to A β production indicating a vicious circle (Tabner et al., 2005). Furthermore increased lipid oxidation as possible indication of oxidative stress was found in patients of AD (Montine et al., 2002).

Investigation of oxidative stress induced apoptosis in FoxO1DN and FoxO1ADA neuroblastoma cells revealed a slight decrease in FoxO1DN cells but no differences in FoxO1ADA cells compared to empty vector control cells. Additionally a similar expression level of the antioxidant enzyme MnSOD was detected in FoxO1DN, FoxO1ADA and control cells. Previous studies have been shown that FoxOs play a role in increased MnSOD and catalase expression upon oxidative stress (Kops et al., 2002; Nemoto and Finkel et al., 2002). Upregulation of FoxO regulated gene expression upon oxidative stress is controlled via wingless (Wnt) proteins and β -catenin. Wnt proteins inactivate GSK3 β after association to lipoprotein receptor-related protein 5/6 and frizzled. This binding occurs in the cytoplasm (Bejsovec, 2005). The inactivation of GSK3 β causes the interruption of β -catenin. This event is followed by accumulation and transport of β -catenin into the nucleus and regulates expression of e.g. the T-cell factor family transcription factors. This pathway is called canonical Wnt pathway which counteracts FoxO mediated transcription (Manolagas SC, Almeida, 2007). Reactive oxygen species (ROS) inhibits the canonical Wnt pathway promoting FoxO action (Almeida et al., 2009). This in turn leads to an increase of FoxO mediated transcription in the nucleus (Essers et al., Hoogeboom et al., 2008). Furthermore in pancreatic β -cells it has been shown that FoxO1 protects from oxidative stress (Martinez et al., 2008; Bellinger et al., 2008).

FoxO1ADA cells did not show any alterations in apoptotic cell upon oxidative stress indicating that other FoxOs might be involved in the induction of apoptosis. FoxO1DN displayed a decrease of apoptotic cells which might be due to inhibited expression of targets

like Fas ligand and Bim (Brunet et al., 1999; Reif et al., 1997; Stahl et al., 2002). However, the current results might indicate a minor effect of FoxO1 in regulation of oxidative stress response in neurons.

5. Summary

Clinical studies have shown that insulin receptor (IR) and the insulin-like growth factor(IGF)-1-receptor (IGF-1R) signaling are largely reduced in the brains of patients suffering from Alzheimer's disease (AD) and other neurodegenerative diseases. Whether the impaired IR/IGF-1R signaling is cause, consequence or even counterregulation to neurodegeneration and whether the accompanying changes in IR/IGF-1R mediated transcription are involved in the pathogenesis of AD is currently a matter of debate. Recent studies have shown that IGF-1 resistance induces A β hyperaggregation leading to A β -detoxification and rescues the increased mortality of APP (amyloid precursor protein) overexpressing mice. Since FoxO transcription factors are highly likely candidates to mediate these effects, two mouse strains have been established, one expressing a constitutively active FoxO1 mutant (FoxO1ADA), the other a dominant negative mutant FoxO1 (FoxO1DN). To analyse the role of FoxO1 mediated transcription for AD pathology Tg2576 mice overexpressing the human derived mutant APP form (APP^{sw}) with a size of 695 amino acids were used. This APP variant harbours an amino acid substitution of Lys670 to Asn and Met671 to Leu, so called "swedish mutation" (APP^{sw}) leading to an increased generation of A β . Mice expressing neuron-specifically the dominant negative (FoxO1DN) or the constitutive active form of FoxO1 (FoxO1ADA) were crossed with Tg2576 mice. The different genotypes (wild-type, FoxO1DN, Tg2576/FoxO1DN, FoxO1ADA, Tg2576/FoxO1ADA and Tg2576 mice) were used to analyse glucose metabolism, insulin and IGF-1 signaling, survival (Kaplan-Meier) and APP processing up to 60 weeks of age. Mice in Tg2576 background displayed unaltered glucose homeostasis. Furthermore, Kaplan-Meier analysis revealed no differences in survival of Tg2576/FoxO1DN female and male mice compared to Tg2576 mice. Surprisingly, Tg2576/FoxO1ADA female mice showed an increase of premature death in comparison with Tg2576 female mice without reaching statistical significance. Interestingly Tg2576/FoxO1ADA male mice did not live longer than 16 weeks. Additionally, western blot analysis from brain lysates of the different genotypes did not reveal alteration of the IR/IGF-1R signaling pathway. Processing of APP in Tg2576/FoxO1DN and Tg2576/FoxO1ADA mice was unchanged compared to Tg2576 mice. The level of α/β CTFs as well as A β 40 and A β 42 burden revealed no differences in the genotypes with AD background. Furthermore, accumulation of A β oligomers was not influenced by FoxO1 mediated transcription. The results of the current study exclude FoxO1 mediated transcription as the underlying mechanism of the beneficial effects of IGF-1 resistance on AD pathology in Tg2576 mice.

6. Zusammenfassung

Klinische Studien zeigen, dass der Insulin Rezeptor (IR) und Insulin-like growth factor(IGF)-1-Rezeptor Signalweg in Gehirnen von Patienten, die an Alzheimer oder anderen neurodegenerativen Erkrankungen leiden, stark verringert ist. Ob diese Veränderung im Signalweg Ursache, Konsequenz oder eine Gegenregulation zur Neurodegeneration ist und ob die begleitenden Unterschiede von IR/IGF-1R vermittelter Transkription in der Pathogenese von Alzheimer involviert sind, wird zurzeit diskutiert. Neueste Studien zeigen, dass IGF-1 Resistenz eine Hyperaggregation von A β induziert, die zur Entgiftung von A β führt und den vorzeitigen Tod von APP (amyloid precursor protein) überexprimierenden Mäusen verhindert. Da FoxO Transkriptionsfaktoren favorisierte Kandidaten darstellen, die diesen Effekt vermitteln könnten, wurden 2 verschiedene Mauslinien generiert, eine exprimiert die konstitutiv aktive FoxO1 Mutation (FoxO1ADA) und die andere die dominant negative Mutation von FoxO1 (FoxO1DN). Um die Rolle von FoxO1 vermittelter Transkription für die Pathogenese von Alzheimer zu analysieren, wurden Tg2576 Mäuse, welche eine humane APP Mutante (APP^{sw}) mit der Größe von 695 Aminosäuren exprimieren, verwendet. Diese APP Variante trägt einen Aminosäureaustausch von Lys670 zu Asn und Met671 zu Leu, welcher die schwedische Mutation (APP^{sw}) genannt wird und zu einer erhöhten A β Akkumulation führt. Mäuse, welche Neuronen-spezifisch die dominant negative (FoxO1DN) oder die konstitutiv aktive Form (FoxO1ADA) exprimieren, wurden mit Tg2576 Mäusen verpaart. Die entstehenden Genotypen (Wildtyp, FoxO1DN, Tg2576/FoxO1DN, FoxO1ADA, Tg2576/FoxO1ADA und Tg2576) wurden bezüglich des Glukose Metabolismus, des Insulin und IGF-1 Signalwegs, des Überlebens (Kaplan-Meier) und der APP Prozessierung bis zu einem Alter von 60 Wochen analysiert. Mäuse im Tg2576 Hintergrund zeigten eine unveränderte Glukose-Homeostase. Des Weiteren zeigten Kaplan-Meier Analysen keinen Unterschied im Überleben von weiblichen und männlichen Tg2576/FoxO1DN Mäusen im Vergleich zu Tg2576 Mäusen. Überraschend zeigten Tg2576/FoxO1ADA Weibchen eine erhöhte Mortalität im Vergleich zu Tg2576 Weibchen ohne statistisch signifikant zu sein. Interessanterweise lebten Tg2576/FoxO1ADA Männchen nicht länger als 16 Wochen. Western blot Analysen von Gehirnlisaten der verschiedenen Genotypen zeigten keine Änderungen des IR/IGF-1R Signalwegs. Die Prozessierung von APP in Tg2576/FoxO1DN und Tg2576/FoxO1ADA Mäusen zeigte keine Änderungen im Vergleich zu Tg2576 Mäusen. Das Auftreten von α/β CTF sowie A β 40 und A β 42 zeigte keine Unterschiede in den verschiedenen Genotypen mit Alzheimer-Pathologie. Des Weiteren wurde die Akkumulierung zu A β Oligomeren nicht durch FoxO1 vermittelte Transkription beeinflusst. Die Ergebnisse der vorliegenden Studie schließen FoxO1 vermittelte Transkription als zugrundeliegenden Mechanismus der günstigen Effekte einer IGF-1 Resistenz auf die Alzheimer Pathologie in Tg2576 Mäusen weitestgehend aus.

7. References

- Accili D, Drago J, Lee EJ, Johnson MD, Cool MH, Salvatore P, Asico LD, Jose PA, Taylor SI and Westphal H (1996). Early neonatal death in mice homozygous for a null allele of the insulin receptor gene. *Nat. Genet.* 12:106-109.
- Adams TE, et al. (1998). Growth hormone preferentially induces the rapid, transient expression of SOCS-3, a novel inhibitor of cytokine receptor signaling. *J. Biol. Chem.* 273:1285–1287.
- Anliker B and Muller U (2006). Functions of mammalian amyloid precursor protein and related amyloid precursor-like proteins. *Neurodegener. Dis.* 3: 239-246.
- Almeida M, Ambrogini E, Han L, Manolagas SC and Jilka RL (2009). Increased lipid oxidation causes oxidative stress, increased peroxisome proliferator-activated receptor-gamma expression, and diminished pro-osteogenic Wnt signaling in the skeleton. *J. Biol. Chem.* 284:27438–27448.
- Alessi DR, Andjelkovic M, Caudwell B, Cron P, Morrice N and Cohen P. Hemmings BA. Mechanism of action of protein kinase B by insulin and IGF-1. *EMBO J.* 15:6541-6551.
- Alzheimer A (1907). Über eine eigenartige Erkrankung der Hirnrinde. *Allg. Z. Psychiatr. Psychisch.-Gerichtl. Med.* 64: 146-148.
- Anderson MJ, Viars CS, Czekay S, Caeneo WK and Arden KC (1998). Cloning and characterization of three human forkhead genes that comprise an FKHR-like gene subfamily. *Genomics* 47:187-199.
- Argetsinger LS, et al. (1995). Growth hormone, interferon-gamma, and leukemia inhibitory factor promoted tyrosyl phosphorylation of insulin receptor substrate-1. *J. Biol. Chem.* 270:14685–14692.
- Argetsinger LS, Norstedt G, Billestrup N, White MF and Carter-Su C. (1996). Growth hormone, interferon-gamma, and leukemia inhibitory factor utilize insulin receptor substrate-2 in intracellular signaling. *J. Biol. Chem.* 271:29415–29421.
- Arimon M, Diez-Perez I, Kogan MJ, Durany N, Giralt E, Sanz F and Fernandez-Busquets X (2005). Fine structure study of Abeta1-42 fibrillogenesis with atomic force microscopy. *FASEB J* 19:1344-1346.
- Astrinidis A and Henske EP (2005). Tuberous sclerosis complex: linking growth and energy signaling pathways with human diseases. *Oncogene* 24:7475-7481.
- Ballatore C., Lee V.M. and Trojanowski J.Q. (2007). Tau-mediated neurodegeneration in Alzheimer's disease and related disorders. *Nature. Rev. Neurosci.* 8: 663-672.
- Barthel et al (2001). Differential regulation of endogenous glucose-6-phosphatase and phosphoenolpyruvate carboxykinase gene expression by the forkhead transcription factor FKHR in H4IIE-hepatoma cells. *Biochem. Biophys. Res. Commun.* 285:897-902
- Barthel A, Scmol D and Unterman TG (2005). FoxO proteins in insulin action and metabolism. *Trends. Endocrinol. Metab.* 16:183-189.
- Beal MF (2002). Oxidatively modified proteins in aging and disease. *Free Radic. Biol. Med.* 32: 97–803.
- Bejsovec A (2005). Wnt pathway activation: new relations and locations. *Cell* 120:11–14.
- Bertolotto C, Maulon L, Filippa N, Baier G and Auburger P (2000). Protein kinase C θ and ϵ promote T-cell survival by Rsk-dependent phosphorylation and inactivation of Bad. *J. Biol. Chem.* 275:37246-37250.
- Bertram L and Tanzi RE (2004). Alzheimer's disease: one disorder, too many genes? *Hum. Mol. Genet.* 13:R135–141.
- Bertram L and Tanzi RE (2005). The genetic epidemiology of neurodegenerative disease. *J. Clin. Invest.* 115:1449-1457.
- Bellinger FP, He QP, Bellinger MT, Lin Y, Raman AV, White LR et al (2008). Association of selenoprotein p with Alzheimer's pathology in human cortex. *J. Alzheimers Dis.* 15:465–472.
- Besson A, Dowdy SF and Roberts JM (2008). CDK inhibitors: cell cycle regulators and beyond. *Dev. Cell.* 14:159-169.
- Biggs WH 3rd, Meisenhelder J, Hunter T, Caveneo WK and Arden KC (1999). Protein kinase B/Akt-mediated phosphorylation promotes nuclear exclusion of the winged helix transcription factor FKHR1. *Proc. Natl. Acad. Sci. USA* 96:7421-7426.
- Birkenkamp KU and Coffey PJ (2003). Regulation of cell survival and proliferation by the FOXO (forkhead box, class O) subfamily of Forkhead transcription factors. *Biochem Soc Trans* 31: 292-297.
- Borkhardt A, Repp R, Haas OA, Leis T, et al. (1997). Cloning and characterization of AFX, the gene that fuses MLL in acute leukemias with a t(X;11)(q12;q23). *Oncogene* 14:195-202.
- Bothe Gerald WM (2005). Phenotyping of APP-SWE Transgenic Mice: Mortality, Neuroanatomy, Behavior. Neuroscience Conference, Washington, DC, Program # 83.6.
- Boura E, Silhan J, Herman P, Vecer J, Sulc M, Teisinger J, Obsilova V, and Obsil T (2007). Both the N-terminal loop and wing W2 of the forkhead domain of transcription factor Foxo4 are important for DNA binding. *J. Biol. Chem.* 282:8265-8275.

- Boura-Halfon S and Zick Y (2009). Phosphorylation of the IRS proteins, insulin action, and insulin resistance. *Am. J. Physiol. Endocrinol. Metab.* 296:E581-E591.
- Brunet A, Bonni A, Zigmond MJ, Lin MZ, Juo P, Hu LS, Anderson MJ, Arden KC, Blenis J and Greenberg ME (1999). Akt promotes cell survival by phosphorylation and inhibiting Forkhead transcription factor. *Cell* 19: 857-868.
- Brunet A, Park J, Tran H, Hu LS, Hemmings BA and Greenberg M E (2001). Protein kinase SGK mediates survival signals by phosphorylating the forkhead transcription factor FKHL1 (FOXO3a). *Mol. Cell. Biol.* 21, 952-965.
- Brunet A, Sweeney LB, Sturgill JF, Chun KF, Greer PL, Lin Y, Tran H, Ross SE, Mostoslavsky R, Cohen HJ et al (2004). Stress-dependent regulation of FOXO transcription factors by the SIRT1 deacetylase. *Science* 303:2011-2015.
- Brüning JC, Gautam D, Burks DJ, Gillette J, Schubert M, Orban PC, Klein R, Krone W, Müller-Wieland D and Kahn CR (2000). Role of brain insulin receptor in control of body weight and reproduction. *Science* 289(5481):2122-2125.
- Burks, DJ, de Mora JF, Schubert M, et al (2000). IRS-2 pathways integrate female reproduction and energy homeostasis. *Nature* 407; 377-382.
- Burns A, Jacoby R and Levy R (1990). Psychiatric phenomena in Alzheimer's disease. *Br J Psychiatry* 157:72-94.
- Campion D, Brice A, Dumanchin C, et al (1996). A novel presenilin-1 mutation resulting in familial Alzheimer's disease with an onset age of 29 years. *Neuroreport* 7:1582-4.
- Campion D, Dumanchin C, Hannequin D, Dubois B, et al (1999). Early-onset autosomal dominant Alzheimer disease: prevalence, genetic heterogeneity, and mutation spectrum. *Am J Hum Genet* 65:664-670.
- Cao X and Sudhof TC (2001). A transcriptionally active complex of APP with Fe65 and histone acetyltransferase Tip60. *Science* 293: 115-120.
- Carlson GA, Borchelt DR, Dake A, Turner S, Danielson V, Coffin JD, Eckman C, Meiners J, Nilsen SP, Younkin SG, Hsiao KK. (1997). Genetic modification of the phenotypes produced by amyloid precursor protein overexpression in transgenic mice. *Hum Mol Genet.* 11:1951-9.
- Carlsson L and JO Jansson (1990). Endogenous growth hormone (GH) secretion in male rats is synchronized to pulsatile GH infusions given at 3-hour intervals. *Endocrinology* 126 (1):6-10.
- Cedazo-Minguez A (2007). Apolipoprotein E and Alzheimer's disease: molecular mechanisms and therapeutic opportunities. *J. Cell Mol. Med.* 11:1227-1238.
- Cheatham B and Kahn CR (1995). Insulin action and the insulin signaling network. *Endocr. Rev.* 16:117-142.
- Cheng CM, Tseng V, Wang J, Wang D, Matyakjina L, Bondy CA (2005). Tau is hyperphosphorylated in the insulin-like growth factor-1 null brain. *Endocrinology* 146: 5086-5091.
- Chin LS, Li L, Ferreira A, Kosik KS and Greengard P (1995). Impairment of axonal development and of synaptogenesis in hippocampal neurons of synapsin I-deficient mice. *Proc. Nat. Acad. Sci.* 92: 9230-9234.
- Cho JH and Johnson GV (2004). Primed phosphorylation of tau at Thr231 by glycogen synthase kinase 3beta (GSK3beta) plays a critical role in regulating tau's ability to bind and stabilize microtubule. *J. Neurochem.* 88: 349-358.
- Chou CK, Dull TJ, Russell DS, Gherzig R, Lebowitz D, Ullrich A, et al (1987). Human insulin receptors mutated at the ATP-binding site lack protein tyrosine kinase activity and fail to mediate postreceptor effects of insulin. *J. Biol. Chem.* 262:1842-1847.
- Chromy BA, Nowak RJ, Lambert MP, Viola KL, Chang L, Velasco PT, Jones BW, Fernandez SJ, et al (2003). Self-assembly of Aβ(1-42) into globular neurotoxins. *Biochemistry* 42: 12749-12760.
- Cichy SB, Uddin s, Danilkovich A, Guo S, Klippel A and Unterman TG (1998). Protein kinase B/Akt mediates effects of insulin on hepatic insulin-like growth factor-binding protein-1 gene expression through a conserved insulin response sequence. *J. Biol. Chem.* 273:6482-6487.
- Citron M, Westaway D, Xia WM, et al (1997). Mutant presenilins of Alzheimer's disease increase production of 42-residue amyloid beta-protein in both transfected cells and transgenic mice. *Nat. Med.* 3:67-72.
- Citron M (2002). Alzheimer's disease: treatments in discovery and development. *Nat. Neurosci.* 5 (Suppl): 1055-1057.
- Clark KL, Halay ED, Lai E and Burley SK (1993). Co-crystal structure of the HNF-3/fork head DNA-recognition motif resembles histone H5. *Nature* 364:412-420.
- Cleary JP, Walsh DM, Hofmeister JJ, Shankar GM, Kuskowski MA, et al. (2005). Natural oligomers of the amyloid-beta protein specifically disrupt cognitive function. *Nat. Neurosci.* 8:79-84.
- Cohen RM, Innis RB (2005). PET imaging of brain with the beta-amyloid probe, [¹¹C]6-OHBT-1, in a transgenic mouse model of Alzheimer's disease. *Eur. J. Nucl. Med. Mol. Imaging.* 32(5):593-600.

- Cohen E, Bieschke J, Perciavalle RM, Kelly JW and Dillin A (2006). Opposing activities protect against age-onset proteotoxicity. *Science* 313: 1604-1610.
- Cohen E, Paulsson JF, Bliner P, Burstyn-Cohen T, et al. (2009). Reduced IGF-1 signaling delays age-associated proteotoxicity in mice. *Cell* 139(6):1157-69
- Cole AR, Astell A, Green C, Sutherland C (2007). Molecular connexions between dementia and diabetes. *Neurosci. Biobehav. Rev.* 31: 1046-1063.
- Coles M, Bicknell W, Watson AA, Fairlie DP and Craik DJ (1998). Solution structure of amyloid beta peptide(1-40) in a water-micelle environment: is the membrane-spanning domain where we think it is. *Biochemistry* 37:11064-11077.
- Corral J, Forster A, Thompson S, Lampert F, Kaneko Y, Slater R, Kroes WG, et al (1993). Acute leucemias of different lineages have similar MLL gene fusions encoding related chimeric proteins resulting from chromosomal translocation. *Proc. Natl. Acad. Sci. USA* 90: 8538-8542.
- Craft S, Peskind E, Schwartz MW, Schellenberg GD, Raskind M and Porte D (1998). Cerebrospinal fluid and plasma insulin levels in Alzheimer's disease: relationship to severity of dementia and apolipoprotein E genotype. *Neurology* 50:164-168.
- Crescenzi O, Tomaselli S, Guerrini R, Salvadori S, D'Ursi AM, Temussi PA and Picone D (2002). Solution structure of the Alzheimer amyloid beta-peptide (1-42) in an apolar microenvironment: similarity with a virus fusion domain. *Eur J Biochem* 269: 5642-5648.
- Dahlgren KN, Manelli AM, Stine WB Jr, Baker LK, Krafft GA and LaDu MJ (2002). Oligomeric and fibrillar species of amyloid-beta peptides differentially affect neuronal viability. *J. Biol. chem.* 277:32046-32053.
- Daitoku H, Hatta M, Matsuzaki H, Aratani S, Ohshima T, Miyagishi M, Nakajima T and Fukamizu A (2004). Silent information regulator 2 potentiates Foxo1-mediated transcription through its deacetylase activity. *Proc. Natl. Acad. Sci. USA* 101:10042-10047.
- Dansen TB, Kops GJ, Denis S, Jelluma N, Wanders RJ, Bos JL, Burgering BM, Wirtz KW (2004). Regulation of sterol carrier protein expression by the forkhead transcription factor FOXO3a. *J. Lipid Res.* 45: 81-88.
- Datta SR, Dudek H, Tao X, Masters S, Fu H, Gotoh Y and Greendberg MA (1997). Akt phosphorylation of BAD couples survival signals to the cell-intrinsic death-machinery. *Cell* 91:231-241.
- de la Monte SM and Wands JR (2006). Molecular indices of oxidative stress and mitochondrial dysfunction occur early and often progress with severity of Alzheimer's disease. *J Alzheimers Dis* 9:167-181.
- De Strooper B (2003). Aph-1, Pen-2 and Nicastrin with Presenilin generate an active gamma-Secretase complex. *Neuron* 38: 9-12.
- Dey BR, Furlanetto RW and Nissley P (2000). Suppressor of cytokine signaling (SOCS)-3 protein interacts with the insulin-like growth factor-I receptor. *Biochem. Biophys. Res. Commun.* 278:38-43.
- Dias-Santagata D, Fulga TA, Duttaroy A and Feany MB (2007). Oxidative stress mediates tau induced neurodegeneration in Drosophila. *J Clin Invest* 117:236-245.
- Dijkers PF, Medema RH, Lammers JW, Koenderman L and Coffey PJ (2000). Expression of the pro-apoptotic Bcl-2 family member Bim is regulated by the forkhead transcription factor FKHR-L1. *Curr. Biol.* 10:1201-1204.
- Dijkers PF, Medema RH, Pals C, Banerji L, Thomas NS, Lam EW, Burgering BM, Raaijmakers JA, Lammers JW, Koenderman L, and Coffey PJ (2000). Forkhead transcription factor FKHR-L1 modulates cytokine-dependent transcriptional regulation of p27(KIP1). *Mol. Cell Biol.* 20:9138-9148.
- Dijkers PF, Medema RH, Pals C, Banerji L, Thomas NS, Lam EW, Burgering BM, Raaijmakers JA, Lammers JW, Koenderman L et al (2000). Forkhead transcription factor FKHR-L1 modulates cytokine-dependent transcriptional regulation of p27(KIP1). *Mol. Cell Biol.* 20:9138-9148.
- Dominici FP, Arostegui Diaz G, Bartke A, Kopchick JJ and Turyn D (2000). Compensatory alterations of insulin signal transduction in liver of growth hormone receptor knockout mice. *J. Endocrinol.* 166:579-590.
- Doria A, Patti ME and Kahn CR,(2008). The emerging genetic architecture of type 2 diabetes. *Cell Metab.* 8(3):186-200.
- Drams S, Scheid MP, Maiti A, Hojabrpour P, Chen X, Schubert K, Goodlett DR, Aebersold R and Duronio V (2002). Identification of a novel phosphorylation site, ser-170, as a regulator of Bad pro-apoptotic activity. *J. Biol. Chem.* 277:6399-6405.
- Duckworth WC, Bennett RG and Hamel FG (1998). Insulin degradation: progress and potential. *Endocr. Rev.* 19:608-624.
- Duff K, Eckman C, Zehr C, et al (1996). Increased amyloid-beta- 42(43) in brains of mice expressing mutant presenilin-1. *Nature* 383:710-713.

- El Khoury J, Tof M, Hickman SE, Means TK, Terada K, Geula C and Luster AD (2007). Ccr2 deficiency impairs microglial accumulation and accelerates progression of Alzheimer-like disease. *Nat. Med.* 13:432–438.
- Emanuelli B, et al. (2000). SOCS-3 is an insulin-induced negative regulator of insulin signaling. *J. Biol. Chem.* 275:15985–15991.
- Essers MA, Weijzen S, de Vries-Smits AM, Saarloos I, de Ruiter ND, Bos JL and Burgering BM. (2004). FOXO transcription factor activation by oxidative stress mediated by the small GTPase Ral and JNK. *EMBO J.* 23, 4802-4812.
- Essers MA, de Vries-Smits LM, Barker N, Polderman PE, Burgering BM, Korswagen HC (2005). Functional interaction between beta-catenin and FOXO in oxidative stress signaling. *Science* 308:1181–1184.
- Fantin VR, Wang Q, Lienhard GE and Keller SR (2000). Mice lacking insulin receptor substrate 4 exhibit mild defects in growth, reproduction, and glucose homeostasis. *Am. J. Physiol. Endocrinol. Metab.* 278:E127-E133.
- Farrer LA, Cupples LA, Haines JL, Hyman B, Kukull WA, Mayeux R, et al (1997). Effects of age, sex, and ethnicity on the association between apolipoprotein E genotype and Alzheimer disease. A meta-analysis. APOE and Alzheimer Disease Meta Analysis Consortium. *JAMA* 278:1349-1356.
- Farris W, Mansourian S, Chang Y, Lindsley L, Eckman EA, Frosch MP, Eckman CB, Tanzi RE, Selkoe DJ and Guenette S (2003). Insulin-degrading enzyme regulates the levels of insulin, amyloid beta-protein, and the beta-amyloid precursor protein intracellular domain in vivo. *Proc. Natl. Acad. Sci. USA* 100:4162–4167.
- Flaherty DB, Soria JP, Tomasiewicz HG and Wood JG (2000). Phosphorylation of human tau protein by microtubule-associated kinases: GSK3beta and cdk5 are key participants. *J. Neurosci. Res.* 62: 463-472.
- Frasca F, Pandini G, Scalia P, Sciacca L, Mineo R, Costantino A, Goldfine ID, Belfiore A, Vigneri R (1999). Insulin receptor isoform A, a newly recognized, high affinity insulin-like growth factor II receptor in fetal and cancer cells. *Mol. Cell Biol.* 19:3278-3288.
- Frautschy SA, Yang F, Irrizarry M, Hyman B, Saido TC, Hsiao K, Cole GM (1998). Microglial response to amyloid plaques in APPSW transgenic mice. *Am. J. Pathol.* 152, 307–317.
- Freude S, Hettich MM, Schumann C, Stöhr O, Koch L, Udelhoven M, et al (2009). Neuronal IGF-1 reduces Aβ accumulation and protects against premature death in a model of Alzheimer's disease. *FASEB J.* 23: 3315-3324.
- Freude S and Schubert M (2010). Insulin receptor substrate signaling in the central nervous system. *Protein Science and Engineering* 978-1-61668-615-4
- Frolich L, Blum-Degen D, Bernstein HG, Egelsberger S, Humrich J, Laufer S, et al (1998). Brain insulin and insulin receptors in aging and sporadic Alzheimer's disease. *J Neural Transm* 105: 423-438.
- Frolich L, Blum-Degen D, Riederer P and Hoyer S (1999). A disturbance in the neuronal insulin receptor signal transduction in sporadic Alzheimer's disease. *Ann N Y Acad Sci* 893: 290-293.
- Fruman DA, Meyers RE and Cantley LC (1998). Phosphoinositide kinases. *Annu. Rev. Biochem.* 67:481-507.
- Fruman DA, Rameh LE and Cantley LC (1999). Phosphoinositide binding domains: embracing 3-phosphate. *Cell* 97:817-820.
- Fu W, Ma Q, Chen L, Li P, Zhang M, Ramamoorthy S, Nawaz Z, Shimojima T, Wang H, Yang Y, Shen Z, Zhang Y, Zhang X, Nicosia SV, Pledger JW, Chen J and Bai W (2009). MDM2 acts downstream of p53 as an E3 ligase to promote FOXO ubiquitination and degradation. *J. Biol. Chem.* 284(21):13987-14000.
- Furayama T, Nakazawa T, Nakano I and Mori N (2000). Identification of the differential distribution patterns of mRNAs and consensus binding sequences for mouse DAF-16 homologues. *Biochem. J.* 349:629-634.
- Furuyama T, Kitayama K, Shimoda Y, Ogawa M, Sone K, Yoshida-Araki K, Hisatsune H, Nishikawa S, Nakayama K, Ikeda K, Motoyama N and Mori N (2004). Abnormal angiogenesis in Foxo1 (Fkhr)-deficient mice. *J Biol Chem* 279:34741-34749.
- Gallili N, Davis RJ, Fredericks WJ, Mukhopadhyay S, Rauscher FJ 3rd, Emanuel BS, Rovera G and Barr FG (1993). Fusion of a fork domain gene of PAX3 in solid tumour alveolar rhabdomyosarcoma. *Nat. Genet.* 5:230-235.
- Georganopoulou DG, Chang L, Man JM, Thaxton CS, Mufson EJ, Klein WL and Mirkin A (2005). Nanoparticle-based detection in cerebral spinal fluid of a soluble pathogenic biomarker for Alzheimer's disease. *Proc Natl Acad Sci USA* 102(7):2273-2276.
- Giannakou ME, Goss M, Jacobson J, Vinti G, Leivers SJ, and Partridge L (2007). Dynamics of the action of dFOXO on adult mortality in *Drosophila*. *Aging Cell* 6:429–438.

- Gilley J, Coffey PJ and Ham J (2003). FOXO transcription factors directly activate bcl-2 gene expression and promote apoptosis in sympathetic neurons. *J. Cell. Biol.* 162:613-622.
- Giovannone B, Scialfaferri ML, Federici M, Porzio O, Lauro D, Fusco A, *et al* (2000). Insulin receptor substrate (IRS) transduction system: distinct and overlapping signaling potential. *Diabetes Metab. Res. Rev.* 16:434-441.
- Goate AM (1997). Molecular genetics of Alzheimer's disease. *Geriatrics* 52:S9-17.
- Goedert M. and Spillantini M.G. (2006). A century of Alzheimer's disease. *Science* 314: 777-781.
- Götz J., Ittner L.M. and Kins S (2006). Do axonal defects in tau and amyloid precursor protein transgenic animals model axonopathy in Alzheimer's disease? *J. Neurochem.* 98: 993-1006.
- Goldgaber D, Lerman MI, McBride OW, Saffiotti U and Gajdusek DC (1987). Characterization and chromosomal localization of the cDNA encoding brain amyloid of Alzheimer's disease. *Science* 235: 877-880.
- Goldstein BJ and Kahn CR (1989). Analysis of mRNA heterogeneity by ribonuclease H mapping: application of the insulin receptor. *Biochem. Biophys. Res. Commun.* 159:664-669.
- Gual P, Le Marchand-Brustel Y and Tanti JF (2005). Positive and negative regulation of insulin signaling through IRS-1 phosphorylation. *Biochimie* 87:99-109.
- Gual P, Gremeaux T, Gonzales T, Le Marchand-Brustel Y and Tanti JF (2003). MAP kinases and mTOR mediate insulin-induced phosphorylation of insulin receptor substrate-1 on serine residues 307, 612 and 632. *Diabetologia* 46:1532-1542.
- Guillozet-Bongaarts AL, Cahill ME, Cryns VL, Reynolds MR, Berry RW and Binder LI (2006). Pseudophosphorylation of tau at serine 422 inhibits caspase cleavage: in vitro evidence and implications for tangle formation in vivo. *J. Neurochem.* 97: 1005-1014.
- Haass C and Selkoe DJ (2007). Soluble protein oligomers in neurodegeneration: lessons from Alzheimer's amyloid beta-peptide. *Nat. Rev. Mol. Cell. Biol.* 8:101-112.
- Hanger DP, Hughes K, Woodgett JR, Brion JP and Anderton BH (1992). Glycogen synthase kinase-3 induces Alzheimer's disease-like phosphorylation of tau: generation of helical filament epitopes and neuronal localization of the kinase. *Neurosci. Lett.* 147: 58-62.
- Harada H, Becknell B, Wilm M, Mann M, Huang LJ, Taylor SS, Scott JD and Korsmeyer SJ (1999). Phosphorylation and inactivation of BAD by mitochondria-anchored protein kinase A. *Mol. Cell* 3:413-422.
- Harada H, Tamaoka A, Ishii K, Shoji S, Kametaka S, Kametani F, *et al* (2006). Beta-site APP cleaving enzyme 1 (BACE1) is increased in remaining neurons in Alzheimer's disease brains. *Neurosci. Res.* 54: 24-29.
- Hardy J and Selkoe DJ (2002). The amyloid hypothesis of Alzheimer's disease: progress and problems on the road to therapeutics. *Science* 297: 353-356.
- Harper JD and Lansbury PT Jr (1997). Models of amyloid seeding in Alzheimer's disease and scrapie: mechanistic triads and physiological consequences of the time-dependent solubility of amyloid proteins. *Annu. Rev. Biochem.* 66:385-407.
- Harper JD, Wong SS, Lieber CM and Lansbury PT Jr (1999). Assembly of A beta amyloid protofibrils: an in vitro model for possible early event in Alzheimer's disease. *Biochemistry* 38: 8972-8980.
- Hay N and Sonenberg N (2004). Upstream and downstream of mTOR. *Genes Dev.* 18:1926-1945.
- Henderson ST and Johnson TE (2001). *daf-16* integrates developmental and environmental inputs to mediate aging in the nematode *Caenorhabditis elegans*. *Curr. Biol.* 11:1975-1980.
- Herschkovitz A, Liu Y-F, Ilan E, Ronen D, Boura-Halfon S and Zick Y (2007). Common inhibitory serine sites phosphorylated by IRS-1 kinases, triggered by insulin and inducers of insulin resistance. *J. Biol. Chem.* 282:18018-18027.
- Hideshima T, Nakamura N, Chauhan D, and Anderson KC (2001). Biologic sequelae of interleukin-6 induced PI3-K=Akt signaling in multiple myeloma. *Oncogene* 20: 5991-6000.
- Hillion J, Le Coniat M, Jonveaux P, Berger R and Bernard OA (1997). AF6q21, a novel partner of the MLL gene t(6;11)(q21;q23), defines a forkhead transcription factor subfamily. *Blood* 90:3714-3719.
- Hirokawa N, Funakoshi T, Sato-Harada R and Kanai Y (1996). Selective stabilization of tau in axons and microtubule-associated protein 2C in cell bodies and dendrites contributes to polarized localization of cytoskeletal proteins in mature neurons. *J. Cell. Biol.* 132: 667-679.
- Ho KK, Myatt SS, and Lam EW (2008). Many forks in the path: cycling with FoxO. *Oncogene* 27:2300-2311.
- Hoekman MF, Jacobs FM, Smidt MP and Burbach JP (2006). Spatial and temporal expression of FoxO transcription factors in the developing and adult murine brain. *Gene Expr. Patterns* 6:134-140.
- Holsinger RM, McLean CA, Beyreuther K, Masters CL and Evin G (2002). Increased expression of the amyloid precursor beta-secretase in Alzheimer's disease. *Ann. Neurol.* 51: 783-786.

- Holzenberger M, et al (2003). IGF-1 receptor regulates lifespan and resistance to oxidative stress in mice. *Nature* 421:182–187.
- Holtzman DM (2001). Role of apoe/Abeta interactions in the pathogenesis of Alzheimer's disease and cerebral amyloid angiopathy. *J. Mol. Neurosci.* 17:147-155.
- Hoogeboom D, Essers MAG, Polderman PE, Voets E, Smits LMM and Burgering BMT (2008). Interaction of FOXO with {beta}-catenin inhibits {beta}-catenin/T cell factor activity. *J. Biol. Chem.* 283:9224–9230.
- Hosaka T, Biggs WH, Tieu D, Boyer AD, Varki NM, Cavenee WK and Arden KC (2004). Disruption of forkhead transcription factor (FOXO) family members in mice reveals their functional diversification. *Proc. Natl. Acad. Sci USA* 101:2975-2980.
- Hresko RC, Murata H and Mueckler M (2003). Phosphoinositide-dependent kinase-2 is a distinct protein kinase enriched in a novel cytoskeletal fraction associated with adipocyte plasma membrane. *J. of Biol. Chem. USA* 24:21615-21622.
- Hsiao K, Chapman P, Nilsen S, Eckman C, Harigaya Y, Younkin S, Yang F, Cole G (1996). Correlative memory deficits, A β elevation and amyloid plaques in transgenic mice. *Science* 274, 99–102.
- Hsu AL, Murphy CT and Kenyon C (2003). Regulation of aging and age-related diseases by DAF-16 and heat-shock factor. *Science* 300: 1142-1145.
- Huang H, Regan KM, Wang F, Wang D, Smith DI, van Deursen JM and Tindall DJ (2005). Skp2 inhibits FOXO1 in tumor suppression through ubiquitin-mediated degradation. *Proc. Natl. Acad. Sci. USA* 102:1649-1654
- Huang H and Tindall DJ (2007). Dynamic FoxO transcription factors. *J. Cell Science* 120:2479-2487.
- Irizarry MC, McNamara M, Fedorchak K, Hsiao KK and Hyman BT (1997). APPSW transgenic mice develop age-related A β deposits and neuropil abnormalities, but no neuronal loss in CA1. *J. Neuropathol. Exp. Neurol.* 56, 965–973.
- Isakoff SJ, Cardozo T, Andreev J, Liz Z, Ferguson KM, Abagyan R, Lemmon MA, Aronheim A and Skolnik EY (1998). Identification and analysis of PH-domain containing targets of phosphatidylinositol 3-kinase using a novel in vivo assay in yeast. *EMBO J.* 17:5374-5387.
- Ittner LM et al. (2010). Dendritic function of tau mediates amyloid- β toxicity in Alzheimer's disease mouse model. *Cell* 142: 387-397.
- Iwatsubo T, Odaka A, Suzuki N, Mizusawa H, Nukina N and Ihara Y (1994). Visualization of A β 42(43) and A β 40 in senile plaques with end-specific A β monoclonals: evidence that an initially deposited species is A β 42(43). *Neuron* 13:45-53.
- Jacobs S, Kull FC Jr, Earp HS, Svoboda ME, Van Wyk JJ and Cuatrecasas P (1983). Somatomedin-C stimulates the phosphorylation of the beta-subunit of its own receptor. *J. Biol. Chem.* 258:9581-9584.
- Jacobs FM, van der Heide LP, Wijchers PJ, Burbach JP, Hoekman MF and Smidt MP (2003). FoxO6, a Novel Member of the FoxO Class of Transcription Factors with Distinct Shuttling Dynamics. *J. Biol. Chem.* 278(38):35959-35967.
- Jankowsky JL, Slunt HH, Ratovitski T, Jenkins NA, Copeland NG, Borchelt DR (2001). Co-expression of multiple transgenes in mouse CNS: a comparison of strategies. *Biomolecular engineering* 17:157–165.
- Jankowsky JL, Fadale DJ, Anderson J, Xu GM, Gonzales V, Jenkins NA, Copeland NG, Lee MK, Younkin LH, Wagner SL, et al (2004). Mutant presenilins specifically elevate the levels of the 42 residue beta-amyloid peptide in vivo: evidence for augmentation of a 42-specific gamma secretase. *Human molecular genetics* 13:159–170.
- Janson J, Laedtke T, Parisi JE, O'Brien P, Petersen RC, Butler PC (2004). Increased risk of type 2 diabetes in Alzheimer disease. *Diabetes* 53: 474-481.
- Jansson JO, Eden S and Isaksson O (1985). Sexual dimorphism in the control of growth hormone secretion. *Endocr. Rev.* 6(2):128-50.
- Jarrett JT, Berger EP and Lansbury PT (1993). The carboxy terminus of the beta-amyloid protein is critical for the seeding of amyloid formation—implications for the pathogenesis of Alzheimer's disease. *Biochemistry* 32:4693–4697.
- Kahn CR, Baird KL, Jarrett DB and Flier JS (1978). Direct demonstration that receptor crosslinking or aggregation is important in insulin action. *Proc. Natl. Acad. Sci. USA* 75: 4209-4213.
- Kanazawa I, Yamaguchi T, Yamamoto M, et al (2009). Serum osteocalcin level is associated with glucose metabolism and atherosclerosis parameters in type 2 diabetes mellitus. *J. Clin. Endocrinol. Metab.* 94:45–49.
- Kang J, Lemaire HG, Unterbeck A, Salbaum JM, Masters CL, Grzeschik KH, et al (1987). The precursor of Alzheimer's disease amyloid A β protein resembles a cell-surface receptor. *Nature* 325: 733-736.

- Kang J and Muller-Hill B (1990). Differential splicing of Alzheimer's disease amyloid A4 precursor RNA in rat tissues: PreA4(695) mRNA is predominantly produced in rat and human brain. *Biochem. Biophys. Res. Commun.* 166: 1192-11200.
- Kappeler L, De Magalhaes Filho CM, Dupont J, Leneuve P, et al. (2008). Brain IGF-1 receptors control mammalian growth and lifespan through a neuroendocrine mechanism. *PLoS. Biol.* ;6(10).e254.
- Kasuga M, Zick Y, Blith DL, Karlsson FA, Häring HU, Kahn CR (1982). Insulin stimulation of phosphorylation of the beta subunit of the insulin receptor. Formation of both phosphoserine and phosphotyrosine. *J Biol Chem* 257(17):9891-9894.
- Kasuga M, Karlsson FA and Kahn CR (1982). Insulin stimulates the phosphorylation of the 95,000-dalton subunit of its own receptor. *Science* 215:185-187.
- Kasuga M, Zick Y, Blithe DL, Crettaz M and Kahn CR (1982). Insulin stimulates tyrosine phosphorylation of the insulin receptor in a cell-free system. *Nature* 298: 667-669.
- Katayama K, Nakamura A, Sugimoto Y, Tsuruo T and Fujita N (2008). FOXO transcription factor-dependent p15(INK4b) and p19(INK4d) expression. *Oncogene* 27:1677–1686.
- Kawazoe, Y., et al. 2001. Signal transducer and activator of transcription (STAT)-induced STAT inhibitor 1 (SSI-1)/suppressor of cytokine signaling 1 (SOCS1) inhibits insulin signal transduction pathway through modulating insulin receptor substrate 1 (IRS-1) phosphorylation. *J. Exp. Med.* 193:263–269.
- Kenyon C, Chang J, Gensch E, Rudner A and Tabtiang R (1993). A *C. elegans* mutant that lives twice as long as wild type. *Nature* 366:461–464.
- Kenyon C (2005). The plasticity of aging: insights from long-lived mutants. *Cell* 120:449–460.
- Kheterpal I, Lashuel HA, Hartley DM, Walz T, Lansbury PT Jr and Wetzel R (2003). Abeta protofibrils possess a stable core structure resistant to hydrogen exchange. *Biochemistry* 42: 14092-14098.
- Kilgour E, Gout I and Anderson NG (1996). Requirement for phosphoinositide 3-OH kinase in growth hormone signaling to the mitogen-activated protein kinase and p70s6k pathways. *Biochem. J.* 315:517–522.
- Kimura KD, Tissenbaum HA, Liu Y and Ruvkun G (1997). *daf-2*, an insulin receptor-like gene that regulates longevity and diapause in *Caenorhabditis elegans*. *Science* 277:942–946.
- Kitamura T, Nakae J, Kitamura Y, Kido Y, Biggs WH III, Wright CV, White MF, Arden KC, and Accili D (2002). The forkhead transcription factor Foxo1 links insulin signaling to pdx1 regulation of pancreatic beta cell growth. *J. Clin. Invest.* 110:1839-1847.
- Kitamura T, Kahn CR, Accili D (2003). Insulin receptor knockout mice. *Annu. Rev. Physiol.* 65:313-32.
- Kitamura YI, Kitamura T, Kruse JP, Raum JC, Stein R, Gu W and Accili D (2005). FoxO1 protects against pancreatic beta cell failure through NeuroD and Mafa induction. *Cell Metab.* 2:153-163
- Klein WL, Stine WB Jr, Teplow DB (2004). Small assemblies of unmodified amyloid beta-protein are the proximate neurotoxin in Alzheimer's disease. *Neurobiol. Aging* 25: 569-580.
- Kolch W (2000). Meaningful relationships: the regulation of the Ras/Raf/MEK/ERK pathway by protein interaction. *Biochem. J.* 315: 289-305.
- Kops G, de Ruiter ND, De Vries-Smits AM, Powell DR, Bos JL and Burgering BM (1999). Direct control of the Forkhead transcription factor AFX by protein kinase B. *Nature* 398:630-634.
- Kops GJ, Dansen TB, Polderman PE, Saarloos I, Wirtz KW, Coffey PJ, Huang TT, Bos JL, Medema RH, Burgering BM (2002). Forkhead transcription factor FOXO3a protects quiescent cells from oxidative stress. *Nature* 419:316-321.
- Kops GJ, Medema RH, Glassford J, Essers MA, Dijkers PF, Coffey PJ, Lam EW, Burgering BM (2002). Control of cell cycle exit and entry by protein kinase B-regulated forkhead transcription factors. *Mol. Cell Biol.* 22:2025-2036.
- Lambert MP, Barlow AK, Chromy BA, Edwards C, Freed R, Liosatos M, Morgan TE, Rozovski I, Trommer B, Viola KL, et al (1998). Diffusible, nonfibrillar ligands derived from Abeta1-42 are potent central nervous system neurotoxins. *Proc Natl Acad Sci USA* 95: 6448-6453.
- Lalonde R, Lewis TL, Strazielle C, Kim H, Fukuchi K. (2003) Transgenic mice expressing the betaAPP695SWE mutation: effects on exploratory activity, anxiety, and motor coordination. *Brain Res.* 977(1):38-45.
- Large V, Peroni O, Letexier D, Ray H and Beylot M (2004). Metabolism of lipids in human white adipocyte. *Diabetes Metab.* 30:294-309.
- Lavan BE, Fantin VR, Chang ET, Lane WS, Keller SR and Lienhard GE (1997). A novel 160-kDa phosphotyrosine protein in insulin-treated embryonic kidney cells is a new member of the insulin receptor substrate family. *J. Biol. Chem.* 272: 21403-21407.
- Lavan BE, Lane WS and Lienhard GE (1997). The 60-kDa phosphotyrosine protein in insulin-treated adipocytes is a new member of the insulin receptor substrate family. *J. Biol. Chem.* 272: 11439-11443.
- Lawlor MA and Alessi DR (2001). PKB/Akt: a key mediator of cell proliferation, survival and insulin responses? *J. Cell Sci.* 114:2903-2910.

- Lee RY, Hench J and Ruvkun G (2001). Regulation of *C. elegans* DAF-16 and its human ortholog FKHRL1 by the *daf-2* insulin-like signaling pathway. *Curr. Biol.* 11:1950–1957.
- Lehtinen MK, Yuan Z, Boag PR, Yang Y, Villen J, Becker EB, DiBacco S, de la Iglesia N, Gygi S, Blackwell TK et al. (2006). A conserved MST-FOXO signaling pathway mediates oxidative-stress responses and extends life span. *Cell* 125, 987-1001.
- Leissring MA, Farris W, Chang AY, Walsh DM, Wu X, Sun X, Frosch MP and Selkoe DJ (2003). Enhanced proteolysis of beta-amyloid in APP transgenic mice prevents plaque formation, secondary pathology, and premature death. *Neuron* 40:1087–1093.
- Lesne S, Koh MT, Kotilinek L, Kaye R, Glabe CG, Yang A, Gallagher M and Ashe KH (2006). A specific amyloid-beta protein assembly in the brain impairs memory. 440:352-357.
- Levitan D and Greenwald I (1995). Facilitation of lin-12-mediated signaling by Sel-12, a *Caenorhabditis elegans* S182 Alzheimer's-disease gene. *Nature* 377:351–354.
- Levy-Lahad E, Wasco W, Poorkaj P, et al (1995). Candidate gene for the chromosome-1 familial Alzheimer's-disease locus. *Science* 269:973–977.
- Lewis J, Dickson DW, Lin WL, Chisholm L, Corral A, Jones G, et al. (2001). Enhanced neurofibrillary degeneration in transgenic mice expressing mutant tau and APP. *Science* 293(5534):1487 – 1491.
- Li M, Luo J, Brooks CL and Gu W (2002). Acetylation of p53 inhibits its ubiquitination by Mdm2. *J. Biol. Chem.* 277:50607-50611.
- Lin K, Dorman JB, Rodan A and Kenyon C (1997). Daf-16: An HNF-3/forkhead family member that can function to double the life-span of *Caenorhabditis elegans*. *Science* 278, 1319-1322.
- Lin X, Taguchi A, Park S, Kushner JA, Li F, Li Y, White MF (2004). Dysregulation of insulin receptor substrate 2 in beta cells and brain causes obesity and diabetes. *J. Clin. Invest.* 114(7):908-16.
- Liu R, Zhou XW, Tanila H, Bjorkdahl C, Wang JZ, Guan ZZ, et al (2008). Phosphorylated PP2A (tyrosine 307) is associated with Alzheimer neurofibrillary pathology. *J. Cell. Mol. Med.* 12: 241-257.
- Lizcano JM, Morrice N and Cohen P (2000). Regulation of BAD by cAMP-dependent protein kinase is mediated via phosphorylation of a novel site, Ser¹⁵⁵. *Biochem. J.* 349:547-557.
- Lovestone S (1999). Diabetes and dementia: is the brain another site of end-organ damage? *Neurology* 53: 1907-1909.
- Louvi A, Accili D and Efstratiadis A (1997). Growth-promoting interaction of IGF-II with the insulin receptor during mouse embryonic development. *Dev. Biol.* 189: 33-48.
- Lu B, Greengard P and Poo MM (1992). Exogenous synapsin I promotes functional maturation of developing neuromuscular synapses. *Neuron* 8, 521-529.
- Luchsinger JA, Tang MX, Shea S and Mayeux R (2004). Hyperinsulinemia and risk of Alzheimer disease. *Neurology* 63: 1187-1192.
- Luo M, Reyna S, Wang L, Yi Z, Carroll C, Dong LQ, Langlais P, Weintraub ST and Mandarino LJ (2005). Identification of insulin receptor substrate 1 serine/threonine phosphorylation sites using mass spectroscopy analysis, regulatory role of serine 1223. *Endocrinology* 146:4410-4416.
- Luo M, Langlais P, Yi Z, Lefort N, De Filippis EA, Hwang H, Christ-Robert CY and Mandarino LJ (2007). Phosphorylation of human insulin receptor substrate-1 at serine 629 plays a positive role in insulin signaling. *Endocrinology* 148:4895-4905.
- Manolagas SC and Almeida M (2007). Gone with the Wnts: beta-catenin, T-cell factor, forkhead box O, and oxidative stress in agedependent diseases of bone, lipid, and glucose metabolism. *Mol. Endocrinol.* 21:2605–2614.
- Markesbery WR and Carney JM (1999). Oxidative alterations in Alzheimer's disease. *Brain Pathol.* 9: 133–146.
- Marr RA, Rockenstein E, Mukherjee A, Kindy MS, Hersh LB, et al. (2003). Neprilysin gene transfer reduces human amyloid pathology in transgenic mice. *J. Neurosci.* 23:1992–1996.
- Martinez SC, Tanabe K, Cras-Meneur C, Abumrad NA, Bernal-Mizrachi E and Permutt MA (2008). Inhibition of Foxo1 protects pancreatic islet beta-cells against fatty acid and endoplasmic reticulum stress-induced apoptosis. *Diabetes* 57:846–859.
- Martinez-Gac L, Marques M, Garcia Z, Campanero MR and Carrera AC (2004). Control of cyclin G2 mRNA expression by forkhead transcription factors: novel mechanism for cell cycle control by phosphoinositide 3-kinase and forkhead. *Mol. Cell Biol.* 24:2181-2189.
- Masaki T, Chiba S, Noguchi H, Yasuda T, Tobe K, Suzuki R, Kadowaki T, Yoshimatsu H (2004). Obesity in insulin receptor substrate-2-deficient mice: disrupted control of arcuate nucleus neuropeptides. *Obes. Res.* 12(5):878-85.
- Masters CL, Simmins G, Weinman NA, Multhaup G, et al. (1985). Amyloid plaque core protein in Alzheimer disease and Down syndrome. *Proc. Natl. Acad. USA.* 82: 4245-4249.

- Matsuzaki H, Daitoku H, Hatta M, Aoyama H, Yoshimochi K and Fukamizu A (2005). Acetylation of Foxo1 alters DNA-binding ability and sensitivity to phosphorylation. *Proc. Natl. Acad. Sci. USA* 102: 11278-11283.
- McClain DA (1991). Different ligand binding affinities of the two human insulin receptor splice variants are reflected in parallel changes in sensitivity for insulin action. *Mol. Endocrinol.* 5:734-739.
- McLean CA, Cherny RA, Fraser FW, Fuller SJ, Smith MJ, Beyreuther K, Bush AI and Masters CL (1999). Soluble pool of Abeta amyloid as a determinant of severity of neurodegeneration in Alzheimer's disease. *Ann. Neurol.* 46:860-866.
- Medema RH, Kops GJ, Bos JL and Burgering BM (2000). AFX-like Forkhead transcription factors mediate cell-cycle regulation by Ras and PKB through p27^{kip1}. *Nature* 404:782-787.
- Megyesi K, Kahn CR, Roth J, Froesch ER, Humbel RE, Zapf J and Neville DM Jr (1974). Insulin and non-suppressible insulin-like activity (NSILA-s): evidence for separate plasma membrane receptor sites. *Biochem. Biophys. Res. Commun.* 57:307-315.
- Meilandt WJ, Cisse M, Ho K, Wu T, Esposito L, et al. (2009). Neprilysin Overexpression Inhibits Plaque Formation But Fails to Reduce Pathogenic A{beta} Oligomers and Associated Cognitive Deficits in Human Amyloid Precursor Protein Transgenic Mice. *J. Neurosci.* 29, 1977-1986.
- Millward TA, Tolniewicz S and Hemmings BA (1999). Regulation of protein kinase cascades by protein phosphatase 2A. *Trends Biochem Sci* 24: 186-191.
- Min KJ, Yamamoto R, Buch S, Pankratz M, and Tatar M (2008). Drosophila lifespan control by dietary restriction independent of insulin-like signaling. *Aging Cell* 7:199-206.
- Moll L, Zemva J, Schubert M (2011). Role of Central Insulin-Like growth Factor-1 Receptor Signaling in Ageing and Endocrine Regulation. *Basic and Clinical Endocrinology Up-to-Date*. s.l.: InTech.
- Moller DE, Yokota A, Caro JF and Flier JS (1989). Tissue-specific expression of two alternatively spliced insulin receptor mRNAs in man. *Mol. Endocrinol.* 3:1263-1269.
- Moloney AM, Griffin RJ, Timmons S, O'Connors R, Ravid R, O'Neill C (2010). Defects in IGF-1 receptor, insulin receptor and IRS-1/2 in Alzheimer's disease indicate possible resistance to IGF-1 and insulin signalling. *Neurobiol Aging* 31: 224-243.
- Montine TJ, Neely MD, Quinn JF, Beal MF, Markesbery WR, Roberts LJ et al (2002). Lipid peroxidation in aging brain and Alzheimer's disease. *Free Radic. Biol. Med.* 33: 620-626.
- Mooney RA, et al. (2001). Suppressors of cytokine signaling-1 and -6 associate with and inhibit the insulin receptor. A potential mechanism for cytokine-mediated insulin resistance. *J. Biol. Chem.* 276:25889-25893.
- Morris JZ, Tissenbaum HA and Ruvkun G (1996). A phosphatidylinositol-3-OH kinase family member regulating longevity and diapause in *Caenorhabditis elegans*. *Nature* 382:536-539.
- Mosthaf L, Grako K, Dull TJ, Coussens L, Ullrich A and McClain DA (1990). Functionally distinct insulin receptors generated by tissue-specific alternative splicing. *EMBO J.* 9:2401-2413.
- Muller-Hill B and Beyreuther K (1989). Molecular biology of Alzheimer's disease. *Annu. Rev. Biochem.* 58:287-307.
- Murphy CT, et al (2003). Genes that act downstream of DAF-16 to influence the lifespan of *Caenorhabditis elegans*. *Nature* 424:277-283.
- Naïmi M, Gautier N, Chaussade C, Valverde AM, Accili D, Van Obberghen E (2007). Nuclear forkhead box O1 controls and integrates key signaling pathways in hepatocytes. *Endocrinology* 148(5):2424-34
- Nakae J, Kitamura T, Silver DL and Accili D (2001). The forkhead transcription factor FOXO1 (Fkhr) confers insulin sensitivity onto glucose-6-phosphatase expression. *J. Clin. Invest.* 108: 1359-1367.
- Nakae J, Biggs WH III, Kitamura T, et al (2002). Regulation of insulin action and pancreatic beta-cell function by mutated alleles of the gene encoding forkhead transcription factor Foxo1. *Nat. Genet.* 32:245-253.
- Nakae J, Kitamura T, Kitamura Y, Biggs III WH, Arden KC and Accili D (2003). The forkhead transcription factor Foxo1 regulates adipocyte differentiation. *Dev. Cell* 4:119-129.
- Nakagawa T, Zhu H, Morishima N, Li E, Xu J, Yankner BA, Yuan J (2000): Caspase-12 mediates endoplasmic-reticulum-specific apoptosis and cytotoxicity by amyloid-beta. *Nature* 403: 98-103.
- Nemoto S and Finkel T (2002). Redox regulation of forkhead proteins through a p66shc-dependent signaling pathway. *Science* 295:2450-2452.
- Nojima H, Tokunaga C, Eguchi S, Oshiro N, Hidayat S, Yoshino K, Hara K, Tanaka N, Avruch J and Yonezawa K (2003). The mammalian target of rapamycin (mTOR) partner, raptor, binds the mTOR substrate p70 S6 kinase and 4E-BP1 through their TOR signaling (TOS) motif. *J. Biol. Chem.* 278:15461-15464.
- Numan S and Russell DS (1999). Discrete expression of insulin receptor substrate-4 mRNA in adult rat brain. *Brain Res. Mol. Brain Res.* 72:97-102.

- Ogg S, Paradis S, Gottlieb S, Patterson GI, Lee L, Tissenbaum HA and Ruvkun G (1997). The Fork head transcription factor DAF-16 transduces insulinlike metabolic and longevity signals in *C. elegans*. *Nature* 389, 994-999.
- Oshiro N, Yoshino K, Hidayat S, Tokunaga C, Hara K, Eguchi S, Avruch J and Yonezawa K (2004). Dissociation of raptor from mTOR is a mechanism of rapamycin-induced inhibition of mTOR function. *Genes Cells* 9:359-366.
- Ott A, Stolk RP, van Harskamp F, Pols HA, Hofman A, Breteler MM (1999). Diabetes mellitus and the risk of dementia: The Rotterdam Study. *Neurology* 53:1937-1942.
- Ott A, Stolk RP, Hofman A, van Harskamp F, Grobbee DE, Breteler MM (1996). Association of diabetes mellitus and dementia: the Rotterdam Study. *Diabetologia* 39: 1392-1397.
- Ozcan U, Cao Q, Yilmaz E, Lee AH, Iwakoshi NN, Ozdelen E et al (2004). Endoplasmic reticulum stress links obesity, insulin action, and type 2 diabetes. *Science* 306: 457-461.
- Pandini G, Frasca F, Mineo R, Sciacca L, Vigneri R and Berliore A (2002). Insulin/insulin-like growth factor I hybrid receptors have different biological characteristics dependent on the insulin receptor isoform involved. *J. Biol. Chem.* 277:39684-39695.
- Paradis S and Ruvkun G (1999). *Caenorhabditis elegans* Akt/PKB transduces insulin receptor-like signals from AGE-1 PI3 kinase to the DAF-16 transcription factor. *Genes Dev.* 12:2488-2498.
- Parry P, Wei Y and Evans G (1994). Cloning and characterization of the t(X;11) breakpoint from a leukemic stem cell line identify a new member of the forkhead gene family. *Genes Chromosomes Cancer* 11:79-84.
- Pastorino JG, Tafani M and Farber JL (1999). Tumor necrosis factor induces phosphorylation and translocation of BAD through a phosphatidylinositide-3-OH kinase-dependent pathway. *J. Biol. Chem.* 274:19411-19416.
- Partridge L and Brüning JC (2008). Forkhead transcription factors and ageing. *Oncogene* 27:2351-2363.
- Peraldi P, Filloux C, Emanuelli B, Hilton DJ and Van Obberghen E (2001). Insulin induces suppressor of cytokine signaling-3 tyrosine phosphorylation through Janus-activated kinase. *J. Biol. Chem.* 276:24614-24620.
- Pletcher SD, Macdonald SJ, Marguerie R, Certa U, Stearns SC, Goldstein DB, and Partridge L (2002). Genome-wide transcript profiles in aging and calorically restricted *Drosophila melanogaster*. *Curr. Biol.* 12:712-723.
- Puig O and Tjian R (2005). Transcriptional feedback control of insulin receptor by dFOXO/FOXO1. *Genes. Dev.* 19:2435-2446.
- Qian W, Shi J, Yin X, Iqbal K, Grundke-Iqbal I, Gong CX and Liu F (2010). PP2A regulates tau phosphorylation directly and also indirectly via activating GSK-3 β . *Neurosci.* 19: 1221-1229.
- Qin W, Zhaoa W, Hoa L, Wanga J, Walshe K, Gandyc S and Pasinettia GM (2008). Regulation of forkhead transcription factor FoxO3a contributes to calorie restriction-induced prevention of Alzheimer's disease-type amyloid neuropathology and spatial memory deterioration. *Ann. N. Y. Acad. Sci.* 1147: 335-347.
- Reif K, Burgering BM and Cantrell DA (1997). Phosphatidylinositol 3-kinase links the interleukin-2 receptor to protein kinase B and p70 S6kinase. *J. Biol. Chem.* 272: 14426-14433.
- Reiserer RS, Harrison FE, Syverud DC and McDonald MP (2007). Impaired spatial learning in the APPSwe + PSEN1DeltaE9 bigenic mouse model of Alzheimer's disease. *Genes, brain, and behavior* 6:54-65.
- Rempe D, Vangeison G, Hamilton J, Li Y, Jepson M, Federoff HJ (2006). Synapsin I Cre transgene expression in male mice produces germline recombination in progeny. *Genesis* 44 (1): 44-49.
- Rena G, Guo S, Cichy SC, Unterman TG and Cohen P (1999). Phosphorylation of the transcription factor forkhead family member FKHR by protein kinase B. *J. Biol. Chem.* 274:17179-17183.
- Rivera EJ, Goldin A, Fulmer N, Tavares R, Wands JR and de la Monte SM (2005). Insulin and insulin-like growth factor expression and function deteriorate with progression of Alzheimer's disease: link to brain reductions in acetylcholine. *J. Alzheimers Dis.* 8:247-268.
- Robakis NK, Wisniewski HM, Jenkins EC, Devine-Gage EA, Houck GE, et al (1987). Chromosome 21q21 sublocalisation of gene encoding beta-amyloid peptide in cerebral vessels and neuritic (senile) plaques of people with Alzheimer disease and Down syndrome. *Lancet* 1: 384-385.
- Robertson J, Loviny TL, Goedeert M, Jakes R, Murray KJ, Anderton BH and Hanger DP (1993): Phosphorylation of tau by cyclic-AMP-dependent protein kinase. *Dementia* 4: 256-263.
- Roberson ED and Mucke L (2006). 100 years and counting: prospects for defeating Alzheimer's disease. *Science* 314: 781-784.
- Rocca WA, Hofman A, Brayne C, Breteler MM, et al (1991). Frequency and distribution of Alzheimer's disease in Europe: a collaborative study of 1980 -1990 prevalence findings. The EURODEM-Prevalence Research Group. *Ann Neurol* 30:381-390.

- Roher AE, Chaney MO, Kuo YM, Webster SD, Stine WB, Haverkamp LJ, Woods AS, Cotter RJ, Tuohy JM, Krafft GA, et al (1996). Morphology and toxicity of Abeta(1-42) dimer derived from neuritic and vascular amyloid deposits of Alzheimer's disease. *J. Biol. Chem.* 271:20631-20635.
- Rogaev EI, Sherrington R, Rogaeva EA, et al (1995). Familial Alzheimer's disease in kindred with missense in a gene on chromosome 1 related to the Alzheimer's disease type 3 gene. *Nature* 376: 775-778.
- Ronnemaa E, Zethelius B, Sundelof J, Sundstrom J, et al. (2008). Impaired insulin secretion increases the risk of Alzheimer disease. *Neurology* (2008) [Epub ahead print].
- Ross CA and Poirier MA (2005). Opinion: what is the role of protein aggregation in neurodegeneration? *Nat. Rev. Mol. Cell. Biol.* 6: 891-898.
- Rovelet-Lecrux A, Hannequin D, Raux G, Le Meur N, Laquerriere A, Vital A, et al (2006). APP locus duplication causes autosomal dominant early-onset Alzheimer disease with cerebral amyloid angiopathy. *Nat Genet* 38: 24-6.
- Rubin JB, Shia MA and Pilch PF (1983). Stimulation of tyrosine-specific phosphorylation in vitro by insulin-like growth factor I. *Nature* 305: 438-440.
- Rui L, Yuan M, Frantz D, Shoelson S and White MF (2002). SOCS-1 and SOCS-3 block insulin signaling by ubiquitin-mediated degradation of IRS1 and IRS2. *J. Biol. Chem.* 277:42394-42398.
- Saleem U, Mosley TH Jr and Kullo IJ (2010). Serum osteocalcin is associated with measures of insulin resistance, adipokine levels, and the presence of metabolic syndrome. *Arterioscler. Thromb. Vasc. Biol.* 30:1474-1478.
- Sato M, Chihara K, Kita T, Kashio Y, Okimura Y, Kitajima N and Fujita T (1989). Physiological role of somatostatin-mediated autocrine regulation for growth hormone: importance of growth hormone in triggering somatostatin release during a trough period of pulsatile growth hormone release in conscious male rats. *Neuroendocrinology* 50 (2):139-51.
- Sawka-Verhelle D, Tartare-Deckert S, White MF and Van Obberghen E (1996). Insulin receptor substrate-2 binds to the insulin receptor through its phosphotyrosine-binding domain and through a newly identified domain comprising amino acids. *J. Biol. Chem.* 271:5980-5983.
- Sawka-Verhelle D, Baron V, Mothe I, Filloux C, White MF and Van Obberghen E (1997). Tyr624 and Tyr628 in insulin receptor substrate-2 mediate its association with the insulin receptor. *J. Biol. Chem.* 272:16414-16420.
- Schellenberg GD, Bird TD, Wijsman EM, et al (1992). Genetic linkage evidence for a familial Alzheimer's disease locus on chromosome 14. *Science* 258:668-671.
- Scheuner D, Eckman C, Jensen M, et al (1996). Secreted amyloid beta-protein similar to that in the senile plaques of Alzheimer's-disease is increased in-vivo by the presenilin-1 and presenilin-2 and APP mutations linked to familial Alzheimer's-disease. *Nat. Med.* 2:864-870.
- Schmidt M, Fernandez de Mattos S, van der Horst A, Klompmaaker R, Kops GJ, Lam EW, Burgering BM, Medema RH (2002). Cell cycle inhibition by FoxO forkhead transcription factors involves downregulation of cyclin D. *Mol. Cell Biol.* 22: 7842-7852.
- Schubert M, Brazil DP, Burks DJ, Kushner JA, Ye J, Flint CL, et al (2003). Insulin receptor substrate-2 deficiency impairs brain growth and promotes tau phosphorylation. *J. Neurosci.* 23:7084-7092.
- Schubert M, Gautam D, Surjo D, Ueki K, Baudler S, Schubert D, et al. (2004) Role for neuronal insulin resistance in neurodegenerative diseases. *Proc. Natl. Acad. Sci. USA* 101:3100-3105.
- Seino S, Seino M, Nishi S and Bell GI (1989). Structure of the human insulin receptor gene and characterization of its promoter. *Proc. Natl. Acad. Sci. USA* 86:114-118.
- Seino S and Bell GI (1989). Alternative Splicing of human insulin receptor messenger RNA. *Biochem. Biophys. Res. Commun.* 159: 312-316.
- Selkoe DJ (2001). Clearing the brain's amyloid cobwebs. *Neuron* 32:177-180.
- Selkoe DJ (2004). Cell biology of protein misfolding: the examples of Alzheimer's and Parkinson's disease. *Nat Cell Biol* 6: 1054-1061.
- Selman C, Lingard S, Choudhury AI, Batterham RL, Claret M, Clements M et al. (2008). Evidence for lifespan extension and delayed age-related biomarkers in insulin receptor substrate 1 null mice. *FASEB J.* 22;807-818.
- Seoane J, Le HV, Shen L, Anderson SA, and Massague J (2004). Integration of Smad and forkhead pathways in the control of neuroepithelial and glioblastoma cell proliferation. *Cell* 117:211-223.
- Sharfi H and Eldar-Finkelman H (2008). Sequential phosphorylation of insulin receptor substrate-2 by glycogen synthase kinase-3 and c-Jun NH2-terminal kinase plays a role in hepatic insulin signaling. *Am. J. Physiol. Endocrinol. Metab.* 294:E307-E315.
- Shen J, Bronson RT, Chen DF, et al (1997). Skeletal and CNS defects in presenilin-1-deficient mice. *Cell* 89:629- 39.

- Shen C, Chen Y, Liu H, Zhang K, Zhang T, Lin A et al (2008). Hydrogen peroxide promotes Abeta production through JNK-dependent activation of gamma-secretase. *J. Biol. Chem.* 283:17721–17730.
- Sherrington R, Froelich S, Sorbi E et al (1996). Alzheimer's disease associated with mutations in presenilin 2 is rare and variably penetrant. *Hum. Mol. Genet.* 5: 985-988.
- Sinha S, Anderson JP, Barbour R, Basi GS, Caccavello R, Davis D, et al. (1999). Purification and cloning of amyloid precursor protein beta-secretase from human brain. *Nature* 402: 537-540.
- Skovronsky DM, Moore DB, Milla ME, Doms RW and Lee VM (2000). Protein kinase C-dependent alpha-secretase competes with beta-secretase for cleavage of amyloid-beta precursor protein in the trans-golgi network. *J. Biol. Chem.* 275: 2568-2575.
- Sleegers K, Brouwers N, Gijselink I, Theuns J, Goossens D, Wauters J, Del-Favero J, et al. (2006). APP duplication is sufficient to cause early onset Alzheimer's dementia with cerebral amyloid angiopathy. *Brain* 129:2977-2983.
- Small SA and Gandy S (2006). Sorting through the cell biology of Alzheimer's disease: intracellular pathways to pathogenesis. *Neuron* 52, 15–31.
- Solinas G, Naugler W, Galimi F, Lee MS and Karin M (2006). Saturated fatty acids inhibit induction of insulin gene transcription by JNK-mediated phosphorylation of the insulin-receptor substrates. *Proc. Natl. Acad. Sci. USA* 103:16454-16459.
- Song G, Ouyang G and Bao S (2005). The activation of the Akt/PKB signaling pathway and cell survival. *J. Cell. Mol. Med.* 9:59-71.
- Sontag E, Nunbhakdi-Craig V, Lee G, Bloom GS and Mumby MC (1996). Regulation of the phosphorylation state and microtubule-binding activity of Tau by protein phosphatase 2A. *Neuron.* 17, 1201–1207.
- Soto C (2003). Unfolding the role of protein misfolding in neurodegenerative diseases. *Nat Rev Neurosci* 4: 49-60.
- Stahl M, Dijkers PF, Kops GJ, Lens SM, Coffey PJ, Burgering BM et al (2002). The forkhead transcription factor FoxO regulates transcription of p27Kip1 and Bim in response to IL-2. *J. Immunol.* 168:5024–5031.
- Stewart R and Liolitsa D (1999). Type 2 diabetes mellitus, cognitive impairment and dementia. *Diabet Med* 16: 93-112.
- St George-Hyslop P, Haines J, Rogaev E, et al (1992). Genetic evidence for a novel familial Alzheimer's disease locus on chromosome 14. *Nat. Genet.* 2:330-334.
- Stöhr O, Schilbach K, Moll L, Hettich MM, Freude S, Wunderlich FT, Ernst M, Zemva J, Brüning JC, Krone W, Udelhoven M, Schubert M (2011). Insulin receptor signaling mediates APP processing and β -amyloid accumulation without altering survival in a transgenic mouse model of Alzheimer's disease. *AGE (Dordr.)* DOI 10.1007/s11357-011-9333-2.
- Stokoe D, Stephens LR, Copeland T, Gaffney PR, Reese CB, Painter GF, Holmes AB, McCormick F and Hawkins PT (1997). Dual role of phosphoinositol-3,4,5-triphosphate in the activation of protein kinase B. *Science* 277:567-570.
- Stoothoff WH and Johnson GV (2005). Tau phosphorylation: physiological and pathological consequences. *Biochim. Biophys. Acta.* 1739: 280-297.
- Sturchler-Pierrat C, Abramowski D, Duke M, et al. Two amyloid precursor protein transgenic mouse models with Alzheimer disease-like pathology. *Proc Natl Acad Sci U S A.* 94:13287-13292.
- Sudhof TC, Czernik AJ, Kao H, Takei K, Johnston PA, Horiuchi A, Wagner M, Kanazir SD, Perin MS, De Camilli P and Greengard P (1989). Synapsins: mosaics of shared and individual domains in a family of synaptic vesicle phosphoproteins. *Science* 245, 1474-1480.
- Sun XJ, Rothenberg P, Kahn CR, Backer JM, Araki E, Wilden PA, Cahill DA; Goldenstein BJ and White MF (1991). Structure of the insulin receptor substrate IRS-1 defines a unique signal transduction protein. *Nature* 352:73-77.
- Sun XJ, Wang LM, Zhang Y, Yenush L, Meyers MG Jr, Glasheen E, Lane WS, Pierce JH and White MF (1995). Role of IRS-2 in insulin and cytokine signaling. *Nature* 377:173-177.
- Sunayama J, Tsuruta F, Masuyama N and Gotoh Y (2005). JNK antagonizes Akt mediated survival signals by phosphorylating 14-3-3. *J. Cell Biol.* 170, 295-304.
- Sutterly H, Chatelain E, Marti A, Wirbelauer C, Senften M, Muller C and Krek (1999). P45SSKP2 promotes p27Kip1 degradation and induces S phase in quiescent cells. *Nat. Cell Biol.* 1:207-214
- Sweatt JD (2001). The neuronal MAP kinase cascade: a biochemical signal integration system subserving synaptic plasticity and memory. *J. Neurochem.* 76:1-10.
- Tabaton M and Tamagno E (2007). The molecular link between beta- and gamma secretase activity on the amyloid beta precursor protein. *Cell. Mol. Life Sci.* 64:2211-2218.
- Tabner BJ, El-Agnaf OM, Turnbull S, German MJ, Paleologou KE, Hayashi Y et al (2005). Hydrogen peroxide is generated during the very early stages of aggregation of the amyloid peptides implicated in Alzheimer disease and familial British dementia. *J. Biol. Chem.* 280:35789–35792.

- Taguchi A, Wartschow LM and White MF (2007) Brain IRS2 signaling coordinates life span and nutrient homeostasis. *Science* 317:369–372.
- Tan Y, Demeter MR, Ruan H and Comb MJ (2000). BAD Ser-155 phosphorylation regulates BAD/Bcl-XL interaction and cell survival. *J. Biol. Chem.* 275:25865-25869.
- Tang ED, Nunez G, Barr FG and Guan KL (1999). Negative regulation of the forkhead transcription factor FKHR by Akt. *J. Biol. Chem.* 274:16741-16746.
- Tanzi RE, Gusella JF, Watkins PC, et al (1987). Amyloid beta-protein gene—cDNA, messenger-RNA distribution, and genetic-linkage near the Alzheimer locus. *Science* 235:880–884.
- Tanzi RE, Moir RD and Wagner SL (2004). Clearance of Alzheimer's Abeta peptide: the many roads to perdition. *Neuron* 43: 605-608.
- Thirone AC, Carvalho CR and Saad MJ (1999). Growth hormone stimulates the tyrosine kinase activity of JAK2 and induces tyrosine phosphorylation of insulin receptor substrates and Shc in rat tissues. *Endocrinology.* 140:55–62.
- Tomita S, Kirino Y and Suzuki T (1998). Cleavage of Alzheimer's amyloid precursor protein (APP) by secretases occurs after O-glycosylation of APP in the protein secretory pathway. Identification of intracellular compartments in which APP cleavage occurs without using toxic agents that interfere with protein metabolism. *J. Biol. Chem.* 273, 6277–6284.
- Toyama H, Ye D, Ichise M, Liow JS, Cai L, Jacobowitz D, Musachio JL, Hong J, Crescenzo M, Tiple D, Lu Q, Zoghbi S, Vines DC, Seidel J, Katada K, Green MV, Pike VW,
- Turner AJ, Isaac RE and Coates D (2001). The neprilysin (NEP) family of zinc metalloendopeptidases: genomics and function. *Bioessays* 23:261–269.
- Ulrich A, Gray A, Tam AW, Yang-Feng T, Tsubokawa M, Collins C, et al (1986). Insulin-like growth factor I receptor primary structure: comparison with insulin receptor suggests structural determinants that define functional specificity. *EMBO J.* 5:2503-2512.
- Van Broeckhoven C, Backhovens H, Cruts M, et al (1992). Mapping of gene predisposing to early-onset Alzheimer's disease to chromosome 14q24.3. *Nat. Genet.* 2: 335-339.
- Van Broeckhoven C (1995). Presenilins and Alzheimer-disease. *Nat. Genet.* 11:230–232.
- Van der Horst A, de Vries-Smiths AM, Brenkman AB, van Triest MH, van den Broek N, et al. (2006). FOXO4 transcriptional activity is regulated by monoubiquitylation and USP7/HAUSP. *Natl. Cell Biol.* 8:1064-1073.
- Van der Horts A and Burgering BMT (2007). Stressing the role of FoxO proteins in lifespan and disease. *Nature* 8:440-450.
- Vanderkuur J, Allevato G, Billestrup N, Norstedt G and Carter-Su C (1995). Growth hormone-promoted tyrosyl phosphorylation of SHC proteins and SHC association with Grb2. *J. Biol. Chem.* 270:7587–7593.
- Vanderkuur, J.A., et al. (1997). Signaling molecules involved in coupling growth hormone receptor to mitogen-activated protein kinase activation. *Endocrinology.* 138:4301–4307.
- Van der Vos KE and Coffey PJ (2010). The Extending Network of FOXO Transcriptional Target Genes. *ANTIOXID REDOX SIGNAL.* 14(4): 579-592
- Vanhaesebroeck B, Ali K, Bilancio A, Geering B and Foukas LC (2005). Signaling by PI3K isoforms: insights from gene-targeted mice. *Trend Biochem. Sci.* 30:194-204.
- Van Obberghen E, Ksauga M, Le Cam A, Hedo JA, Itin A and Harrison LC (1981). Biosynthetic labelling of insulin receptor: studies of subunits in cultured human IM-9 lymphocytes. *Proc. Natl. Acad. Sci. USA* 78:1052-1056.
- Valtorta F, Iezzi N, Benfenati F, Lu B, Poo MM and Greengard P (1995) Accelerated structural maturation induced by synapsin I at developing neuromuscular synapses of *Xenopus laevis*. *Eur. J. Neurosci.* 7, 261-270.
- Vardy ER, Rice PJ, Bowie PC, Holmes JD, Grant PJ and Hooper NM (2007). Increased circulating insulin-like growth factor-1 in late-onset Alzheimer's disease. *J. Alzheimers Dis.* 12:285–290.
- Vassar R, Bennett BD, Babu-Khan S, Mendiaz EA, Denis P, et al. (1999). Beta-secretase cleavage of Alzheimer's amyloid precursor protein by the transmembrane aspartic protease BACE. *Science* 286: 735-741.
- Vassar R (2004). BACE1: the beta-secretase enzyme in Alzheimer's disease. *J. Mol. Neurosci.* 23:105-114.
- Vloeberghs E, Van Dam D, Franck F, Serroyen J, Geert M, Staufenbiel M, De Deyn PP (2008) Altered ingestive behavior, weight changes, and intact olfactory sense in an APP overexpression model. *Behav. Neurosci.* 122(3):730-2.
- Walsh DM, Lomakin A, Benedek GB, Condron MM and Teplow DB (1997). Amyloid beta-protein fibrillogenesis: detection of a protofibrillar intermediate. *J. Biol. Chem.* 272: 22364-22372.
- Walsh DM and Selkoe DJ (2007). Abeta Oligomers- a decade of discovery, *J. Neurochem.* 101:1172-1184.

- Watson GS and Craft S (2003). The role of insulin resistance in the pathogenesis of Alzheimer's disease: implications for treatment. *CNS Drug* 17:27-45.
- Weigert C, Henning AM, Brischmann T, Beck A, Moeschel K, et al.(2005). The phosphorylation of Ser318 of insulin receptor substrate 1 is not per se inhibitory in skeletal muscle cells but is necessary to trigger the attenuation of the insulin-stimulated signal. *J. Biol. Chem.* 280:37393-37399.
- Weigert C, Kron M, Kalbacher H, Pohl AK, Runge H, et al. (2008). Interplay and effects of temporal changes in the phosphorylation state of serine-302, -307, and -318 of insulin receptor substrate-1 on insulin action in skeletal muscle cells. *Mol. Endocrinol.* 22:2729-2740.
- White MF, Maron R and Kahn CR (1985). Insulin rapidly stimulates tyrosine phosphorylation of a Mr-185,000 protein in intact cells. *Nature* 352:183-186.
- White MF and Kahn CR (1994). The insulin signaling system. *J. Biol. Chem.* 269:1-4.
- White MF (1998). The IRS-signaling system: a network of docking proteins that mediate insulin action. *Mol. Cell Biochem.* 182:3-11.
- White MF (2002). IRS proteins and the common path to diabetes. *Am. J. Physiol. Endocrinol. Metab.* 283:E413-E422.
- White MF (2003). Insulin signaling in health and disease. *Science* 302:1710-1711.
- Williams AD, Segal M, Chen M, Kheterpal I, et al. (2005). Structural properties of Abeta protofibrils stabilized by a small molecule. *Proc. Natl. Acad. Sci. USA* 102: 7115-7120.
- Withers DJ, Gutierrez JS, Towery H, et al (1998). Disruption of IRS-2 causes type 2 diabetes in mice. *Nature* 391:900-904
- Wolkow CA, Kimura KD, Lee MS and Ruvkun G (2000). Regulation of *C. elegans* life-span by insulin like signaling in the nervous system. *Science* 290, 147-150.
- Wong PC, Zheng H, Chen H, et al (1997). Presenilin 1 is required for Notch1 Dll1 expression in the paraxial mesoderm. *Nature* 387:288-292.
- Woods YL, Rena G, Morrice N, Barthel A, Becker W, Guo S, Unterman TG and Cohen P (2001). The kinase DYRK1A phosphorylates the transcription factor FKHR at Ser329 in vitro, a novel in vivo phosphorylation site. *Biochem J.* 355:597-607
- Yakar S, Setser J, Zhao H, Stannard B, Haluzik M, Glatt V, Bouxsein ML, Kopchick JJ and LeRoith D (2004). Inhibition of growth hormone action improves insulin sensitivity in liver IGF-1-deficient mice. *J. Clin. Invest.* 113(1):96-105.
- Yamaga K, Daitoku H, Takahashi Y, Namiki K, Hisatake K, Kako K, Mukai H, Kasuya Y and Fakamizu A (2008). Arginine methylation of FOXO transcription factors inhibits their phosphorylation by Akt. *Mol. Cell.* 32: 221-231.
- Yamaguchi Y, Flier JS, Yokota A, Benecke H, Backer JM and Moller DE (1991). Functional properties of two naturally occurring isoforms of the human insulin receptor in Chinese hamster ovary cells. *Endocrinology* 129:2058-2066.
- Yang E, Zha J, Jockel J, Boise LH, Thompson CB and Korsmeyer SJ (1995). Bad, a heterodimeric partner of Bcl-X_L and Bcl-2, displays Bax and promotes cell death. *Cell* 80:285-291.
- Yang JY, Zong CS, Xia W, Yamaguchi H, et al. (2008). ERK promotes tumorigenesis by inhibiting FOXO3a via MDM2-mediated degradation. *Nat. Cell Biol.* 10:138-148.
- Yang W, Dolloff NG and El-Deiry WS (2008). ERK and MDM2 prey on FOXO3a. *Nat. Cell Biol.* 10:125-126.
- Yenush L and White MF (1997). The IRS-signaling system during insulin and cytokine action. *Bioessays* 19:491-500.
- Zha J, Harada H, Yang E, Jockel J and Korsmeyer SJ (1996). Serine phosphorylation of death agonist BAD in response to survival factor results in binding to 14-3-3 not BCL-X_L. *Cell* 87:619-628.
- Zha J, Harada H, Osipov K, Jockel J, Waksman G and Korsmeyer SJ (1997). BH3 domain of BAD is required for heterodimerization with BCL-X_L and pro-apoptotic activity. *J. Biol. Chem.* 272:24101-24104.
- Zhang W, Patil S, Chauhan B, Guo S, et al. (2006). FOXO1 regulates multiple metabolic pathways in the liver: effects on gluconeogenic, glycolytic, and lipogenic gene expression. *J. Biol. Chem.* 281:10105-10117.
- Zhao L, Teter B, Morihara T, Lim GP, Ambegaokar SS, Ubeda OJ, et al (2004). Insulin-degrading enzyme as a downstream target of insulin receptor signaling cascade: implications for Alzheimer's disease intervention. *J. Neurosci.* 24:11120-11126.
- Zheng H and Koo EH (2006). The amyloid precursor protein: beyond amyloid. *Mol. Neurodegen.* 1:5.
- Zhu Y, Romero MI, Ghosh P, Ye Z, Charnay P, Rushing EJ, Marth JD, Parada LF (2001). Ablation of NF1 function in neurons induces abnormal development of cerebral cortex and reactive gliosis in the brain. *Genes Dev.* 15(7):859-76.
- Zlokovic BV (2004). Clearing amyloid through the blood-brain barrier. *J. Neurochem.* 89:807-811.

8. Supplementary

8.1. Acknowledgement

First I would like to thank PD Dr. Schubert for providing me with this interesting project. I appreciate the support and advice for me and my work as well as the possibility to learn and work in his lab.

I would like to thank Prof. Dr. Jens Brüning, Prof. Dr. Wilhelm Krone, Prof. Dr. Peter Kloppenburg and Dr. Debora Grosskopf-Kroiher to form my thesis committee.

Furthermore, I would like to thank my present and former colleagues for their help, advice and the nice atmosphere in the lab. Especially I would like to thank Dr. Michael Udelhoven, Dr. Katharina Schilbach, Dr. Susanna Freude and Dr. Oliver Stöhr for their advice.

Additionally I would like to thank my family for their support.

8.2. Erklärung

Ich versichere, dass ich die von mir vorgelegte Dissertation selbständig angefertigt, die benutzten Quellen und Hilfsmittel vollständig angegeben und die Stellen der Arbeit – einschließlich Tabellen, Karten und Abbildungen –, die anderen Werken im Wortlaut oder dem Sinn nach entnommen sind, in jedem Einzelfall als Entlehnung kenntlich gemacht habe; dass diese Dissertation noch keiner anderen Fakultät oder Universität zur Prüfung vorgelegen hat; dass sie – abgesehen von unten angegebenen Teilpublikationen – noch nicht veröffentlicht worden ist sowie, dass ich eine solche Veröffentlichung vor Abschluss des Promotionsverfahrens nicht vornehmen werde. Die Bestimmungen der Promotionsordnung sind mir bekannt. Die von mir vorgelegte Dissertation ist von Prof. Dr. Jens C. Brüning betreut worden.

Köln, den 5.12.11

Lorna Moll

Teilpublikation:

Stöhr O*, Schilbach K*, Moll L*, Hettich MM, Freude S, Wunderlich FT, Ernst M, Zemva J, Brüning JC, Krone W, Udelhoven M, Schubert M (2011). Insulin receptor signaling mediates APP processing and β -amyloid accumulation without altering survival in a transgenic mouse model of Alzheimer's disease. *AGE (Dordr.)* DOI 10.1007/s11357-011-9333-2.

* Authors contribute equally.

8.3. Curriculum vitae

Persönliche Daten

Name, Vorname: Moll, Lorna
Adresse: Max-Reger-Str. 2
50931 Köln
Tel.-Nr: 01777911971
E-Mail: lorna.moll@uk-koeln.de
Geburtstag: 02.10.1983
Familienstand: Ledig
Nationalität: Deutsch

Schulbildung

1990-1994 Grundschole am Schwarzwasser, Ahe
1994-2003 Gutenberg-Gymnasium, Bergheim
2003 Abitur

Hochschulausbildung

2003-2006 Bachelor of Science in Biology, Universität zu Köln
2006 Bachelor thesis: „Zur Regulation des yjjP-yjjQ-bglJ Locus von Escherichia coli durch H-NS und LeuO“
2006-2008 Master of Science in biology, Universität zu Köln
2008 Master thesis: „Transcriptional analysis of Dictyostelium discoideum after infection with Mycobacterium marinum via cDNA Microarrays“
8/2008-1/2009 Wissenschaftliche Hilfskraft, Institut für Biochemie I, PD Dr. Eichinger, Universitätsklinikum Köln
Seit 2/2009 Promotion
Zentrum für Endokrinologie, Diabetologie und Präventivmedizin, Universitätsklinikum Köln

Publikationen

Lucas J, Bilzer A, **Moll L**, Zündorf I, Dingermann T, Eichinger L, Soil O and Winckler T (2009). Regulation of gene expression by the carboxy-terminal domain of C-module-binding factor. *PLoS One* 4(4):5012 doi:10.1371/journal.pone.0005012

Stöhr O, Hahn J, **Moll L**, Leeser U, Freude S, Bernard C, Schilbach K, Markl A, Udelhoven M, Krone W and Schubert M (2011). Insulin receptor substrate-1 and -2 mediate resistance to glucose-induced caspase-3 activation in human neuroblastoma cells. *Biochim. Biophys. Acta*.1812(5):573-580.